

BULGARIAN CHEMICAL COMMUNICATIONS

2022 Volume 54 / Special Issue B1

Selected papers presented on the Ninth International Conference
“Modern Trends in Science”, 15-19 September 2021, Blagoevgrad, Bulgaria

*Journal of the Chemical Institutes
of the Bulgarian Academy of Sciences
and of the Union of Chemists in Bulgaria*

EDITORIAL

**Ninth International Conference
“Modern Trends in Science” - FMNS-2021
15-19 September 2021, Blagoevgrad,
BULGARIA**



Dear Reader,

This special issue of the *Bulgarian Chemical Communications* contains selected papers, reported as oral or poster presentations at the Ninth International Conference „Modern Trends in Science” (FMNS-2021), organized by the Faculty of Mathematics and Natural Sciences of the South-West University “Neofit Rilski”, Blagoevgrad, Bulgaria. Because of the COVID-19 pandemic situation, the conference was held online from the 15th to the 19th of September 2021.

Despite the unpredictable change in the conference format at the very last moment, more than 180 scientists from Albania, Bulgaria, Germany, Italy, Kazakhstan, Macedonia, Mexico, Poland, Russia, and the Czech Republic reported their latest scientific achievements in various fields of natural and technical sciences.

Plenary lectures were presented by prominent Bulgarian and foreign scientists:

- Prof. Toni Spasov – Dean of the Faculty of Chemistry and Pharmacy at Sofia University "St. Kliment Ohridski", Bulgaria;
- Prof. Carlo Santoro - University of Milano-Bicocca, Milan, Italy;
- Dr. Manfred Schütze - Institut für Automation und Kommunikation, Magdeburg, Germany.

Within the framework of the conference a Special Scientific Session was held, at which participants in the National Scientific Program "Low-Carbon Energy for Transport and Household - EPLUS" presented the scientific achievements of the program.

On behalf of the Organizing committee of the Ninth International Conference „Modern Trends in Science” I would like to express our gratitude to the National Science Fund of Bulgaria for the provided financial support through a Contract KP-06-MNF/25/2020.

We would also like to express our gratitude to all FMNS-2021 participants for their contribution to the conference. We gratefully thank the Editorial Board of the *Bulgarian Chemical Communications* for the opportunity to disseminate a part of the papers reported at the conference to the audience of the journal.

*Prof. Mario Mitov, DSc, PhD
Chairman of the Organizing
Committee of FMNS-2021*

Section
Chemistry

Obtaining granular activated carbon using a binder gelatin in the joint processing of rice and oil waste

N. O. Appazov^{1,2*}, B. M. Diyarova³, B. M. Bazarbayev¹, B. Zh. Dzhiembaev³, O. Lygina⁴

¹Korkyt Ata Kyzylorda University, Kyzylorda, Kazakhstan

²I. Zhakhaev Kazakh Scientific Research Institute of Rice Growing, Kyzylorda, Kazakhstan

³Kazakh National Women's Teacher Training University, Almaty, Kazakhstan

⁴Universidade Nova de Lisboa, Lisbon, Portugal

Received: October 27, 2021; Accepted: November 12, 2021

In this article, the effect of gelatin as a binder to obtain granular activated carbon by joint processing of rice waste (husk and straw) and oil sludge was studied. Carbonation and activation of the granules were carried out in a high-temperature vacuum tube furnace of the BR-12 NFT series with a length of 200 mm, in a heating tube made of quartz glass with a length of 300 mm and a diameter of 60 mm. Carbonation was carried out at a temperature of 500°C, activation-by water vapor at a temperature of 850°C, at a ratio of water and carbonizate 2:1. The effect of the ratio of gelatin binder, rice waste and oil sludge on the properties of the activated carbon was studied. The optimal ratio of the joint processing of the mixture is rice husk: oil sludge: gelatin = 9:1:2 (by weight). The studies were carried out according to the following indicators: adsorption activity for iodine, total pore volume for water, mass fraction of moisture, adsorption activity for methylene blue, and bulk density. Granulated activated carbon corresponds to the BAU-MF brand.

Keywords: activated carbon, rice husk, rice straw, oil sludge, gelatin, granules.

INTRODUCTION

The adsorption process is widely used as an effective physical method to eliminate or reduce the concentration of dissolved pollutants (organic and inorganic) in wastewater. Adsorption is recognized as a more advanced method compared to other methods due to its simplicity, cost-effectiveness and wide application. Granular activated carbon, powdered activated carbon, carbon fiber, black coal, and other activated carbon materials are widely used as adsorbents in water treatment [1, 2].

Activated carbon is the best adsorbent that is effectively used to remove a wide range of pollutants from air, soil, and liquids [3, 4]. The resource base of activated carbon is diverse - from plant residues to brown carbon and carbon. Activated carbon is obtained from chestnut peels, watermelon peels, rice peels, mango seeds, banana peels, orange peels, bean peels, nut shells, and agricultural waste [5, 6]. These agricultural waste products are relatively cheap, affordable, biodegradable, environmentally friendly, and contain lignocellulosic material that can improve the adsorption properties of activated carbon.

The characteristics of activated carbon depend on the physical and chemical properties of the raw material, as well as on the activation methods [7, 8]. For the production of activated carbon, in most

cases, two approaches are chosen. The first is grinding of the initial lignite, followed by carbonation and activation. By the second method, after the process of carbonization, granulation, and grinding of raw materials, an activation process is carried out.

Granulation is an effective method of recycling waste from carbon-containing chemical industries [9, 10]. The use of this processing method in theory allows you to obtain activated carbon of high strength and density. In addition, some sources use the co-thermolysis process to produce activated carbon.

Co-thermolysis is a process in which two or more raw materials are processed in one operating system of conventional thermolysis [11, 12]. Thus, it can effectively combine the favorable properties of the raw materials and improve the characteristics of activated carbon [13, 14]. In our research works, the optimal ratios for obtaining activated carbon by carrying out the processes of co-thermolization of rice straw and oil sludge, oil sludge with rice husk have been determined [15-17].

The purpose of this experimental research work is to determine the optimal ratio for obtaining granular activated carbon by adding a binder gelatin in oil sludge with rice waste to increase the sorption and mechanical strength of activated carbon.

* To whom all correspondence should be sent.
E-mail: nurasar.82@mail.ru

EXPERIMENTAL

Rice waste was ground in a laboratory mill to a size of 0.25 mm. The granules were obtained by adding a binder to crushed rice waste (husk and straw) and oil sludge in the proportions indicated in Table 1. Carbonization was carried out in nitrogen atmosphere at a temperature of 500°C, and activation in a high-temperature vacuum tube furnace of the BR-12 NFT series with water vapor at a temperature of 850°C.

To determine the mass fraction of moisture, 1 g of granular activated carbon was weighed and was placed in a pre-weighed bottle. The latter was placed with an open lid in an oven for 1 h at a temperature of 105-110°C. After the specified time had elapsed, the weighing bottle was removed from the drying cabinet and cooled in a desiccator for 15 minutes. Then the mass of the dried granular activated carbon was measured and calculations were made [18].

To determine the adsorption activity for iodine, a solution of iodine in potassium iodide at a concentration of 0.1 mol/dm³ was added to the suspended part of the granular activated carbon and shaken in a shaking unit for 15 min at an intensity of 100-125 vibrations/min. Then the mixture was

titrated with 0.1 mol/dm³ sodium thiosulfate solution until the blue color disappeared using starch as an indicator [19].

To determine the total pore volume with respect to water, the pores were studied in the range of 0.5-104 nm by boiling in water for 15 minutes and weighing on an analytical balance after the excess amount of water was separated by a pump under a pressure of 8 kPa. Determination of the bulk density of the granular activated carbon was carried out by standardizing and measuring the mass of activated carbon of a certain volume [20, 21].

RESULTS AND DISCUSSION

From rice waste (husk and straw) and oil sludge, granules were obtained by adding a gelatin binder. The resulting granules were placed in a tubular furnace which was hermetically closed, filled with gaseous nitrogen, and the carbonization process was carried out at a rate of temperature rise of 10 °C per minute to 500 °C and kept at this temperature for 100 min. The activation was carried out at a temperature of 850 °C. The effect of the ratio of the binder on the yield and physicochemical properties of granular activated carbon was investigated.

Table 1. Properties of granular activated carbon obtained with the addition of gelatin as a binder in the processing of rice straw and oil sludge

Indicator name	Results of experimental studies							
	Rice straw: gelatin	Rice straw: gelatin	oil sludge: gelatin	oil sludge: gelatin	Rice husk: gelatin	Rice husk: gelatin	oil sludge: gelatin	oil sludge: gelatin
Ratio (by weight)	10:1	9:1:1.1	9:1:1.25	9:1:2	10:1	9:1:1.1	9:1:1.25	9:1:2
Carbonation temperature, °C					500			
Carbonization yield, wt. %	78.86	71.28	70.56	80.53	70.3	76.28	69.8	62.86
Activation temperature, °C					850			
Water:carbonization (mass ratio)					2:1			
Activated carbon yield, wt. %	25.06	30.07	26.07	27.41	35.9	34.23	33.8	37.08
Iodine absorption activity,%	32.8	51.5	59.9	71.2	72.24	87.63	88.45	89.72
Water total pore volume, cm ³ /g	0.94	0.99	0.99	0.91	0.50	0.42	0.49	0.56
Mass fraction of moisture, %	0.70	1.09	0.50	2.30	2.65	1.99	2.18	2.21
Bulk density, g/dm ³	241.36	232.73	201.12	201.52	463.19	458.45	459.06	433.99
Adsorption activity of methylene blue, mg/g	372.29	370.12	378.78	380.74	335.82	341.56	345.51	356.01

Table 1 shows the data of granulated activated carbon obtained by adding rice waste, oil sludge and gelatin in a ratio of 10:1, 9:1:1.1, 9:1:1.25, and 9:1:2. Granulated activated carbon from rice husk: oil sludge: gelatin in a ratio of 9: 1:2 showed the highest values for the following indicators: adsorption activity for iodine – 89.72%, total pore volume for water-0.56 cm³/g, bulk density-433.99 g/dm³ and adsorption activity for methylene blue-356.01 mg/g.

According to the results of the research, it was found that the optimal ratio for the production of granular activated carbon is the ratio of rice husk: oil sludge: gelatin = 9:1:2. At the optimal ratio, granulated activated carbon corresponds to the BAU – MF brand. Figure 1 shows the granulated activated carbon obtained at the ratio of 9:1:2 rice husk: oil sludge: gelatin.



Figure 1. Granulated activated carbon obtained from rice husk, oil sludge and gelatin at a ratio of 9: 1: 2.

CONCLUSIONS

In conclusion, granular activated carbon was obtained with the addition of gelatin at various ratios to rice and oil waste. The physicochemical properties of the granular activated carbons were investigated and their optimal ratio was determined. Based on the adsorption activity of activated carbon at the optimal ratio, the resulting adsorbent allows water purification from inorganic and organic impurities.

Acknowledgement: The work was carried out with the financial support of the Committee of Science of the Ministry of Education and Science of the Republic of Kazakhstan at the expense of grant funding AR 05134356.

REFERENCES

1. T. Ahmad, M. Rafatullah, A. Ghazali, O. Sulaiman, R. Hashim, A. Ahmad, *J. Environ. Sci. Health*, **28** (4), 231 (2010).
2. H. A. Suerbaev, E. G. Chepajkin, B. Z. Dzhiembaev, N. O. Appazov, G. M. Abyzbekova, *Petroleum Chemistry*, **47**(5), 345 (2007). <https://doi.org/10.1134/s0965544107050064>.
3. H. Zhonghuo, M. P. Srinivasan, N. Yaming, *Carbon*, **39**, 877 (2001).
4. T. V. Arutyunyan, A. F. Korystova, L. N. Kublik, M. K. Levitman, V. V. Shaposhnikova, N. O. Appazov, R. A. Narmanova, S. Z. Ibadullayeva, Y. N. Korystov, *Bulletin of Experimental Biology and Medicine*, **158**(2), 222 (2014). <https://doi.org/10.1007/s10517-014-2727-2>.
5. B. Srivastava, V. Jhelum, D. D. Basu, P. K. Patanjali, *J. Sci. Ind. Res. (India)*, **68**, 839 (2009).
6. N. O. Appazov, S. S. Seitzhanov, A. T. Zhunissof, R. A. Narmanova, *Russian Journal of Organic Chemistry*, **53**(10), 1596 (2017), ISSN: 1608-3393 (Online), ISSN: 1070-4280. doi: 10.1134/S1070428017100189.
7. A. C. Lua, J. Guo, *Lagmuir*, **17**, 7112 (2001).
8. S. Lyubchik, O. Shapovalova, O. Lygina, M. C. Oliveira, N. Appazov, A. Lyubchik, A. J. Charmier, S. Lyubchik, A. J. L. Pombeiro, *Scientific Reports*, **9**, 12, Article 18171 (2019), <https://doi.org/10.1038/s41598-019-53817-8>
9. V. N. Piyalkin, A. A. Leonovich, V. I. Shirshikov, *Izvestiya Sankt-Peterburgskoy Lesotekhnicheskoy Akademii*, **198**, 201 (2012) [in Russian].
10. K.A. Suerbaev, E.G. Chepajkin, N.O. Appazov, B.Z. Dzhiembaev, *Petroleum Chemistry*, **52**(3), 189 (2012). ISSN: 1555-6239 (Online), ISSN: 0965-5441. doi: 10.1134/S0965544112030127.
11. H., Hassan, J. K. Lim, B. H. Hameed, *Bioresour. Technol.*, **221**, 645 (2016).
12. K. A. Suerbaev, N. Z. Kudaibergenov, N. O. Appazov, G. Z. Zhaksylykova, *Russian Journal of Organic Chemistry*, **52**(4), 585 (2016), <https://doi.org/10.1134/s1070428016040205>.
13. S. Fan, H. Li, Y. Wang, Z. Wang, J. Tang, J. Tang, X. Li, *Res. Chem. Intermed.*, **44**, 135 (2018).
14. H. A. Suerbaev, E. G. Chepajkin, B. Z. Dzhiembaev, N. O. Appazov, G. M. Abyzbekova, *Petroleum Chemistry*, **47**(5), 345 (2007), <https://doi.org/10.1134/s0965544107050064>
15. S. R. Bainazarova, B. M. Diyarova, O. Lygina, A. T. Shuragazyeva, A. S. Tapalova, L. A. Zhusupova, N. O. Appazov, *Chemical Journal of Kazakhstan*, **4**(64), 259 (2018).
16. N. O. Appazov, B. M. Bazarbayev, B. M. Diyarova, O. S. Lygina, A. T. Shuragazyeva, N. I. Akyzbekov, *Chemical Journal of Kazakhstan*, **4**(68), 46 (2019) [in Russian].
17. N. O. Appazov, R. A. Turmanov, R. U. Zhapparbergenov, B. M. Diyarova, O. S. Lygina, A. T. Shuragazyeva, N. I. Akyzbekov, *Chemical Journal of Kazakhstan*, **4**(68), 77 (2019) [in Russian].
18. GOST 12597. Sorbenty. Metod opredeleniya massovoj doli vody v aktivnyh ugljah i katalizatorakh na ih osnove, M., Izdatel'stvo standartov, 1989, [in Russian].
19. GOST 6217. Ugol' aktivnyy drevesnny droblenny. Tekhnicheskiye usloviya, M.: Izdatel'stvo standartov, 2003, [in Russian].

20. GOST 17219. Ugli aktivnye. Metod opredelenija summarnogo ob'ema por po vode, M., Izdatel'stvo standartov, 1988, [in Russian].
21. GOST 16190. Sorbenty. Metod opredelenija nasypnoj plotnosti, M., Izdatel'stvo standartov, 1970, [in Russian].

Factors influencing the tautomeric form stabilization and spectral characteristics of 1-phenyl substituted pyrazol-5-ones

A. G. Chapkanov^{1*}, T. G. Dzimbova^{1,2}

¹South-West University "Neofit Rilski", 66 Ivan Mihailov str., 2700 Blagoevgrad, Bulgaria

²Institute of Molecular Biology "Rumen Tsanev", 21 Acad. Georgi Bonchev str., 1311 Sofia, Bulgaria

Received: November 25, 2021; Revised: February 24, 2022

The tautomerism of pyrazolone derivatives is a challenging field of study with importance for chemical and biological systems. Spectral analysis of different stabilized tautomeric forms of 1-phenyl-substituted pyrazolones and their photochemical behavior was conducted in different conditions. The experimental UV-spectral data in solvents have been compared with those after UV-light irradiation. The obtained results showed the presence of the photoisomerization process between the tautomeric forms of the compounds depending on the structure substituents at 3- and 4-position, polarity effect of the solvents, time of irradiation, temperature and concentration.

Keywords: 1-phenyl-substituted pyrazole-5-ones, spectral analysis, photoinduced tautomeric forms

INTRODUCTION

Pyrazoles and their derivatives are attractive compounds, because they have a wide variety of biological activities [1, 2] and different drugs possess a pyrazole ring as the key structural unit [3]. Some pyrazole derivatives have been proved to be cytotoxic on human cells lines [4-7] and at the same time, several drugs containing pyrazoles in their structure have been approved for the treatment of several types of cancer and amyotrophic lateral sclerosis (ALS) [8]. The phenyl-pyrazolone structural unit can be found in a large diversity of compounds with medicinal application [9]. On the other hand, the tautomerism of pyrazolone derivatives is a challenging field of study with importance for chemical and biological systems. The 1-phenyl substituted pyrazol-5-ones exist as three possible tautomeric forms: CH (a), OH (b) and NH (c) (Scheme 1), where relative proportions in the established equilibrium depends on the structure of the compounds, medium effects and possibilities for inter- and intramolecular interactions [10-13].

In the literature there are not enough data about the photochemical behavior of 1-substituted pyrazol-5-ones and especially for the compounds, which we studied. The UV-light influence is important from therapy point of view and initial research has been conducted already [14, 15]. After UV-irradiation the N-N bond is easier to break and photochemical cleavage of pyrazolone ring between nitrogen atoms in protic solvents is observed [16]. Under influence of light and atmospheric oxygen, the pyrazolone derivatives became yellow,

possessing lower biological activity and higher toxicity [17, 18]. The kinetic investigations and photochemical rearrangement showed that their photostability depends in different factors and conditions [19].

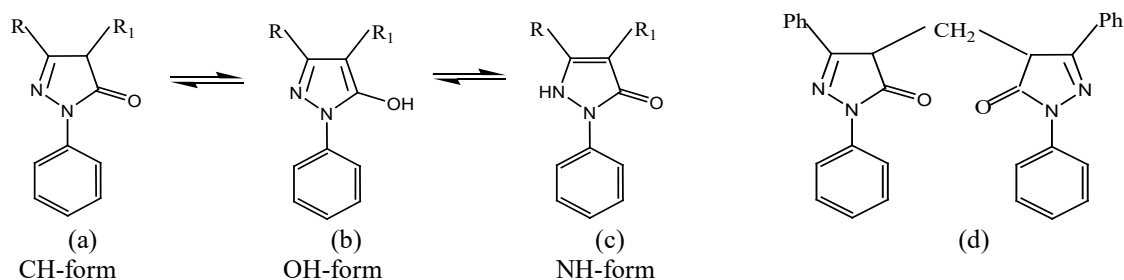
In this work we continued our investigations on the photochemical behavior and the spectral elucidation of the possible tautomeric forms in different solvents of 3-methyl-1-phenyl pyrazole-5-one (MPhP), 1,3-diphenyl pyrazole-5-one (DPhP), 4-benzyl-3-methyl-1-phenyl pyrazole-5-one (4-BMPhP), 3,4-dimethyl pyrazole-5-one (3,4-di-MPhP) and 4,4'-methylidene-bis-(1,3-diphenyl pyrazole-5-one) (4,4'-MBDPhP) shown in Scheme 1.

Structural characterization of the CH-tautomers of two derivatives as MPhP and DPhP, has been carried out by IR-spectroscopic study using linear-dichroic (IR-LD) analysis [20, 22]. By reducing-difference procedure the NH-tautomeric form of DPhP was established in the polymer film after UV-light irradiation [23-25].

EXPERIMENTAL

The synthesis of the studied compounds is described elsewhere [26, 27]. The solvents used were Uvasol (Merck) products. The UV-absorption spectra in different solvents ($1 \cdot 10^{-4}$ mol/l solution, quartz cell of 1 cm) as isoctane, n-hexane, methanol, ethanol, acetonitrile and H₂O were recorded on an Agilent 8453 UV-VIS spectrometer with ± 3 nm resolution. The sample solution was irradiated from a distance of 15 cm using a medium pressure mercury vapor lamp and a system of liquid filters (310 nm). The irradiation intensity was $1.29 \cdot 10^{16}$ quant s⁻¹.cm³.

* To whom all correspondence should be sent:
E-mail: chapkanov@swu.bg



Scheme 1. Tautomeric forms of 1-phenyl-3, 4-substituted pyrazole-5-ones: R = -CH₃, R₁= H (MPhP); R = -C₆H₅, R₁= H (DPhP); R = -CH₃, R₁ = -CH₂C₆H₅(4-BMPhP); R = -CH₃, R₁ = -CH₃ (3,4-di-MPhP); R = Ph, R₁ = -CH₂-DPhP) - 4,4'-methylidene-bis-(1,3-diphenyl pyrazole-5-ones), (4,4'-MBDPhP) (d)

Table 1. UV-spectral data in different solvents for studied compounds

Compound	Solvent, λ [nm]					
	n-Hexane	Isooctane	EtOH	MeOH	H ₂ O	CH ₃ CN
MPhP*	246, 270-330sh	248	244	246	240, 275sh	243, 270 sh
DPhP*	264, 322	265, 325	268	270	264	266
3,4-di-MPhP	236	246	243	251, 286sh	262	254
4-BMPhP	245	248	250, 278sh	248, 270sh	248, 270	247, 272sh
4,4'-MBDPhP	265, 325	252, 315	263	258	256	267

* According to [20, 24, 25]

RESULTS AND DISCUSSION

Although the application of UV-spectroscopy is complicated by overlapping of the broad absorption maxima [10, 11], we studied the compounds mentioned above and the corresponding tautomeric forms in solution for spectral elucidation and explanation of photochemical relations. The obtained results could be used for establishing of some correlations connected to compounds structure influence, medium effect, UV-light irradiation, as well as and other factors concerning spectral characteristics and stabilization of the corresponding tautomeric forms.

UV-spectral analysis

The UV-spectral data of the investigated compounds in different solvents before irradiation are presented in Table 1. According to previous results in some nonpolar solvents (chloroform) DPhP and MPhP stabilized the CH-form [23]. In solvents as n-hexane, isooctane, DPhP stabilized the CH-form too, with charge transfer (CT) origin of the band at longer wavelengths [23, 27, 28], while MPhP preferred the HO-tautomeric form [24, 25]. The latter is in contradiction with literature data for nonpolar solvents [11, 12]. For the other compounds, some results in the used solvents are similar to those of MPhP (4-BMPhP, 3,4-di-MPhP in isooctane and n-hexane) stabilizing the HO-form and DPhP (4,4'-MBDPhP in n-hexane) stabilizing

CH-form) (see Table 1).

In polar solvents (MeOH, EtOH) MPhP and DPhP stabilized the OH-tautomer [8, 21, 23, 27]. But for 4-BMPhP and MPhP in water and acetonitrile, the bands are at 240-250 nm (OH-form) with a shoulder at 270-280 nm (Table 1). The second maximum should be considered as a characteristic of a third NH-tautomeric form, i.e., in these solvents a mixture between the two OH- and NH-forms is available. Similar bands have been observed for 2,3-dimethyl-1-phenyl pyrazol-5-one (which is a model compound for NH-form) in different solvents [24]. The experimental results for 4,4'-MBDPhP suggest a domination of HO-tautomer, confirming its stabilization in polar solvents. The observed differences in the spectral characteristics can be additionally explained in different degree by compounds structure influence, polarity effects of solvents and specific interactions between solvent and dissolved molecules.

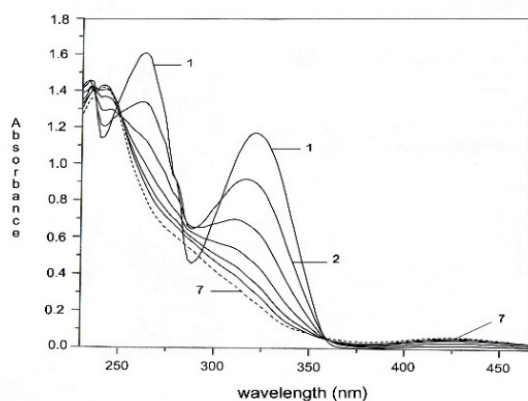
UV-spectral analysis of irradiated compounds in solution

As was stated above, there are not enough data in the literature about the photochemical behavior of 1-substituted pyrazolones. We investigated our compounds after irradiation with UV-light ($\lambda=310$ nm) in different solvents and the experimental results are presented below.

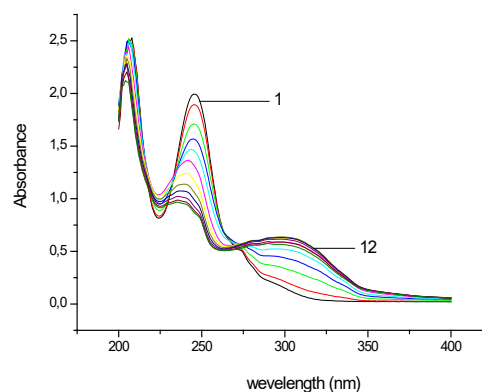
Irradiation in non-polar solvents

The data for DPhP in nonpolar solvents indicate stabilization of the CH-tautomer [17, 19]. However, the irradiation in other solvents, such as n-hexane leads to disappearance of the band at 325 nm and appearance of a new one at 245-250 nm, which is a hypsochromic shift (Fig.1(1)). The latter single

band characterizes the HO-form [21, 24] and the available isosbestic points (260 and 350 nm) in the spectrum assume a photo-transformation process between the tautomeric forms, i.e. CH→OH photo-isomerization is realized. The data for MPhP in nonpolar solvents are discussed in [25] showing OH→CH photo isomerization only in isooctane.

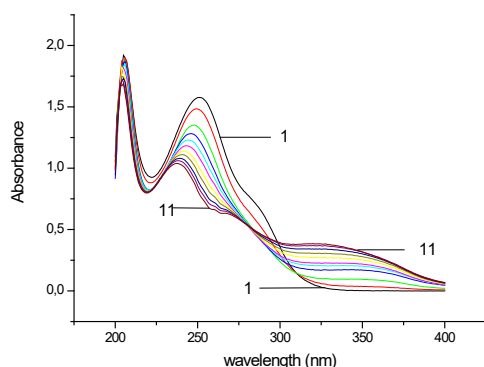


(1)

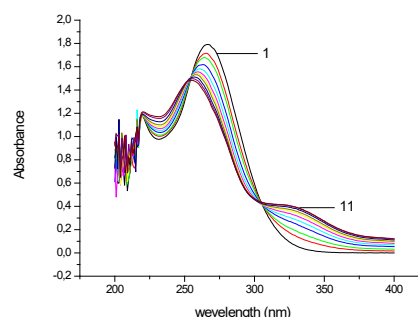


(2)

Fig. 1. UV-spectra of DPhP (1) and 4-BMPPhP (2) in n-hexane: 1- before irradiation. 2 - 7, 12- after irradiation for 30 sec.



(1)



(2)

Fig. 2. UV-spectra of 3,4-di-MPhP in MeOH (1) and 4,4-BMDPhP in CH₃CN (2): 1-before irradiation; 9-11 after irradiation for 30 sec.

A similar result we obtained also for 4-BMPPhP in n-hexane (Fig. 1(2)) and isooctane, where irradiation leads to the same spectral changes and photo transformation. For the compound 4,4'-BMDPhP after irradiation only decreasing intensity of the absorption bands is observed, i.e. no photo isomerization is realized, which means that the used solvents are not appropriate for photochemical isomerization, which depends on their polarity and specific inter- and intramolecular interaction. Moreover, the obtained experimental results reveal a different photochemical behavior of the compounds

at the identical spectral and experimental conditions. The observed reversible $\text{OH} \rightleftharpoons \text{CH}$ isomerization after irradiation of some of compounds is analogous to the keto-enol tautomerism of β -dicarbonyl compounds after irradiation [29-31].

Irradiation in polar solvents

Experimental results for MPhP and DPhP in polar solvents are already discussed [17, 19-21], where the HO-form is stabilized with a single absorption maximum in the UV-spectrum.

However, after irradiation of MPhP in these solvents the spectra are practically not changed, which means more stability and different behavior toward UV-light irradiation. The experimentally observed data for the other compounds after irradiation correlate well with some established above dependences.

Concerning 3,4-diMPhP and 4,4-BMDPhP in MeOH and CH₃CN solutions, new bands (240-252, 320-330 nm) appeared and the presence of isosbestic points at 245 and 320 nm assumes OH → CH photoisomerization (Fig. 2). In EtOH and CH₃CN, 4-BMPhP stabilize the NH-tautomer and UV-irradiation leads to disappearance of the second maximum at 270 nm and shift to 250 nm, furthermore a new band at 320 nm appears (Fig. 3). The latter two bands belong to the CH-tautomer, which corresponds to tautomeric transition from the NH, OH into the CH form, i.e. a process of photoisomerization NH, OH → CH form. Such kind of photo transformation in solution is not established till now in our investigations of 1-phenyl substituted pyrazol-5-ones.

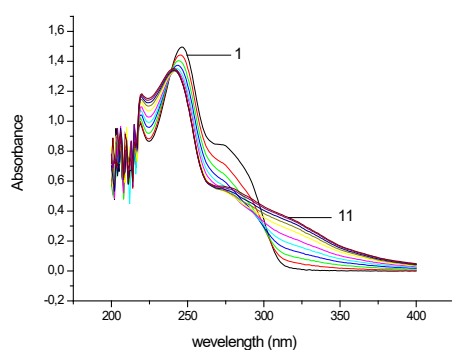
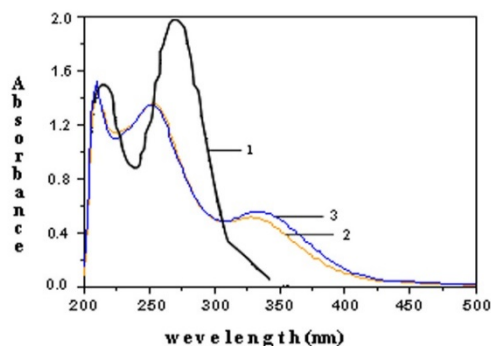
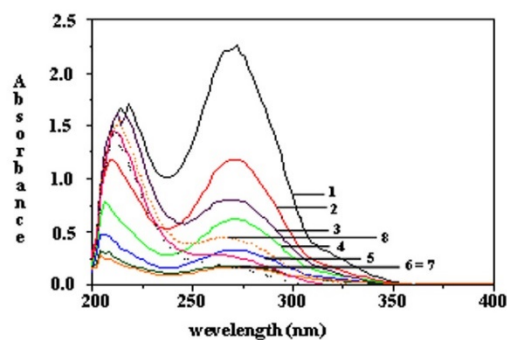


Fig. 3. UV-spectra of 4-BMPhP (1) in CH₃CN:1- before irradiation; 9-11 after irradiation for 30 sec.

These results show the significant influence of



(1)



(2)

Fig. 4. UV spectra of DPhP: (1) in EtOH: 1-at room temperature; 2-at room temperature after 12 min irradiation; 3-at 60° after 12 min irradiation; (2) in EtOH at different concentrations; 1- 1×10^{-4} M; 3- 2.5×10^{-5} M; 6- 6.25×10^{-6} M.

the substituents' structure at 3-and 4-position on the spectral characteristics and photochemical behavior of the compounds. Another explanation of these facts probably consists in the different steric disposition of the substituents at 1,3 and 4- position toward pyrazolone ring plane in the corresponding tautomeric forms [19, 21]. We have studied the influence of other factors such as temperature, concentration, and UV-light irradiation on the spectra, but only for DPhP in EtOH. The obtained results showed insignificant temperature and concentration dependence of the spectral characteristics (Figs. 4(1) and 4(2)) for the investigated compound. From the obtained experimental data the following could be said: i) a structure influence of the substituents in the pyrazole ring (3- and 4-position) on the spectral characteristics and photochemical behavior of the investigated compounds is established, which can be explained with specific disposition of the different substituents at 3-position toward the pyrazole ring plane in the tautomeric forms, as well as the substituents structure at 4-position; ii) some of the solvents (mainly polar) are more appropriate for transformation or photochemical isomerization; iii) the influence of other factors as temperature and concentration is insignificant.

CONCLUSION

The obtained results revealed that the specific spectral and photochemical behavior of the investigated compounds depends on their structure, kind of solvent, and irradiation with UV-light. Furthermore, DPhP showed a higher activity and lower stability in solution than MPhP, while for 4BMPhP another kind of photo transformation was established.

In the other cases the photoisomerization is very specific. No correlations for the investigated compounds were established between structure, spectral characteristics, stability of tautomeric forms and their photo transformation, because of the very specific behavior of the compounds.

REFERENCES

1. A. Pandey, D. Dewangan, S. Verma, A. Mishra, R. D. Dubey, *Int J. Chem. Tech. Res.*, **3**, 178 (2011).
2. K. Halim, S. Ramadan, S. Rizk, M. El-Hashash, *Synth. Commun.*, **50**, 1159 (2020).
3. M. Naim, O. Alam, F. Nawaz, Md. J. Alam, P. Alam, *J. Pharm. Bioallied Sci.*, **8**, 2 (2016)
4. M. Mohamed, A. Abdelhamid, F. Almutairi A. Ali, M. Bashr, *Bioorg. Med. Chem.*, **26**, 623 (2018).
5. S. Ramadan, K. Halim, S. Rizk, M. El-Hashash, *J. Iran Chem. Soc.*, **17**, 1575 (2020).
6. S. Ramadan, A. El-Ziaty, R. Ali, *J. Heterocycl. Chem.*, **58**, 290 (2021).
7. K. Halim, S. Rizk, M. El-Hashash, S. Ramadan, *J. Heterocycl. Chem.*, **58**, 636 (2021)
8. C. Bailly, P. Hecquet, M. Kouach, X. Thuru, J. Goossens *Bioorganic Med. Chem.*, **28**, 1 (2020).
9. Y. Higashi, D. Jitsuiki, K. Chayama, M. Yoshizumi, *Recent Pat Cardiovasc. Drug Discov.*, **1**, 85 (2006).
10. A. Katritzky, F.M. Maine, *Tetrahedron*, **20**, 299 (1964).
11. J. Elguero, C. Marzin, A. Katritzky, P. Linda, *Adv. Heterocyclic Chem.*, Suppl. **1** (1976).
12. J. Elguero, *Comprehensive Heterocyclic Chemistry*, Pergamon Press, Oxford, 1984, p. 5.
13. A. Katritzky, *Chemistry of Heterocyclic Compounds*, 1992, p. 291.
14. J. Reisch, A. Fitzek, *Tetrahedron Letters*, 4513 (1967).
15. J. Reisch, *Bull. Chim. Therap.*, 335 (1966).
16. M. Nicolics H. Denes, N. Nicolics, *Gyogyszereszet*, **8**, 13 (1953).
17. W. Awe, B. Stoy, *Arch. Pharm. (Weinheim, Ger)*, **293**, 489 (1960).
18. H. Cardy, E. Poquet, *Tetrahedron*, **37**, 2279 (1981).
19. N. Y. Kovalenko, Yu. A. Ershov, S. F. Orlova, *J. Photochem.*, **31**, 289 (1985).
20. A. Chapkanov, I. Petkov, *Anal. Labor.*, **7(3)**, 143 (1998).
21. B. Ivanova, A. Chapkanov, M. Arnaudov, I. Petkov, *Struct. Chem.*, **16(1)**, 47 (2005).
22. B. Ivanova, A. Chapkanov, M. Arnaudov, I. Petkov, *Spectr. Lett.*, **39**, 1 (2006).
23. B. Ivanova, A. Chapkanov, M. Arnaudov, I. Petkov, *Central Europ. J. Chem.*, **4**, 356 (2003).
24. A. Chapkanov, B. Koleva, M. Arnaudov, I. Petkov, *Chem. Papers*, **62(3)**, 294 (2008).
25. A. Chapkanov, I. Petkov, *Annual-Science-Education-Art.*, SWU "N. Rilski"-Publ. **2**, 349 (2008).
26. A. Katritzky, D. Ostercamp, T. Yousaf, *Tetrahedron*, **43**, 5171 (1987).
27. F. Marchetti, R. Pettinari, A. Cingolani, M. Rossi, F. Caruso, *J. Organomet. Chem.*, **645**, 134 (2002).
28. J. Mistol, N. Grossmann, H. Piesch, *J. Pract. Chemie*, **327(3)**, 371 (1985).
29. P. Markov, I. Petkov, *Tetrahedron*, **33**, 1013 (1977).
30. I. Petkov, N. Dodov, P. Markov, *J. Photoch. Photobiol., A: Chem.*, **54**, 119 (1990).
31. I. Petkov, S. Masuda, N. Sertova, L. Grigorov, *J. Photoch. Photobiol. A: Chemistry*, **95**, 189 (1996).

Combined action of His-Leu analogues on angiotensin converting enzyme (ACE) and angiotensin receptor (AR)

T. Dzimbova^{1,2*}, A. Chapkanov¹

¹ South-West University "Neofit Rilski", 66 Ivan Mihailov str., 2700 Blagoevgrad, Bulgaria

² Institute of Molecular Biology "Roumen Tsanev", 21 Acad. Georgi Bonchev str., 1311 Sofia, Bulgaria

Received: November 17, 2021; Accepted: May 20, 2022

Classically, the renin-angiotensin system (RAS) has been viewed solely as a hormonal circulating system involved in the regulation of blood pressure and salt and fluid homeostasis. According to this view, liver-derived circulating angiotensinogen (Aogen) is acting by renin released from the kidney forming the decapeptide angiotensin (Ang) I. Finally, angiotensin converting enzyme (ACE) present on the luminal surface of vascular endothelium converts Ang I to the biologically active end product Ang II by cleavage of the Phe⁸-His⁹-bond. This traditional concept has undergone several and important changes in recent years [1]. It has become clear that various fragments of the peptide can act on the receptor. Therefore, the purpose of the present study is to determine by docking whether His-Leu analogues, which act as ACE inhibitors, will have an effect on AR. The compounds were modelled with Avogadro software, the structure of the receptor was obtained from RCSB (PDB id: 4zud), and docking was performed with GOLD 5.2 software. The visualization of the obtained results was performed with a Molegro molecular view, where the energies of the ligand-receptor complexes were determined. The results of the docking indicate that all tested analogues bind to the receptor in an appropriate manner. Three of them – His-sLeu, His-sNle and His-sNle3, have the potential to act as its antagonists, as the formed ligand-receptor complexes have low enough energies to be stable over a long period of time. The test compounds can have a complex effect on RAS, on the one hand by inhibiting ACE and on the other hand by blocking AR.

Key words: renin-angiotensin system, angiotensin converting enzyme, angiotensin receptor, docking, GOLD 5.2

INTRODUCTION

The relatively simple "classical" concept of "circulating RAS (Fig. 1) involves angiotensinogen (AGT) produced in the liver, renin formed in the kidneys, the major effector peptide angiotensin II (Ang II) formed in blood vessels under the action of ACE, and angiotensin receptors of type 1 and 2 (AR1 and AR2) [2].

The renin-angiotensin system (RAS) is a hormonal system that regulates blood pressure and fluid balance. Agents acting on RAS act by blocking

various stages of the renin-angiotensin system by lowering blood pressure and their use in the treatment of hypertension and its complications (including acute myocardial infarction, congestive heart failure and chronic renal failure) is recommended in many of the current clinical guidelines. Agents acting on RAS include angiotensin-converting enzyme inhibitors (ACE inhibitors), angiotensin receptor blockers (ARBs), as well as direct renin inhibitors.

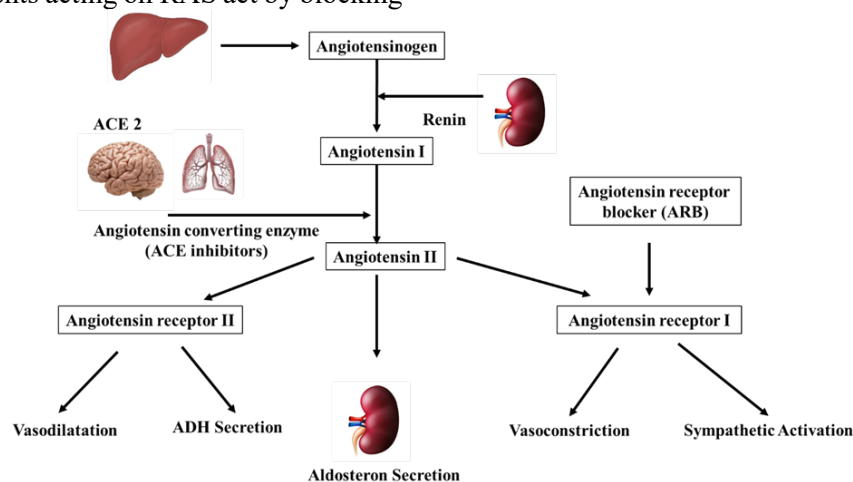


Fig. 1. A simplified model of the "classical" circulating renin-angiotensin system.

* To whom all correspondence should be sent:
E-mail: tania_dzimbova@abv.bg

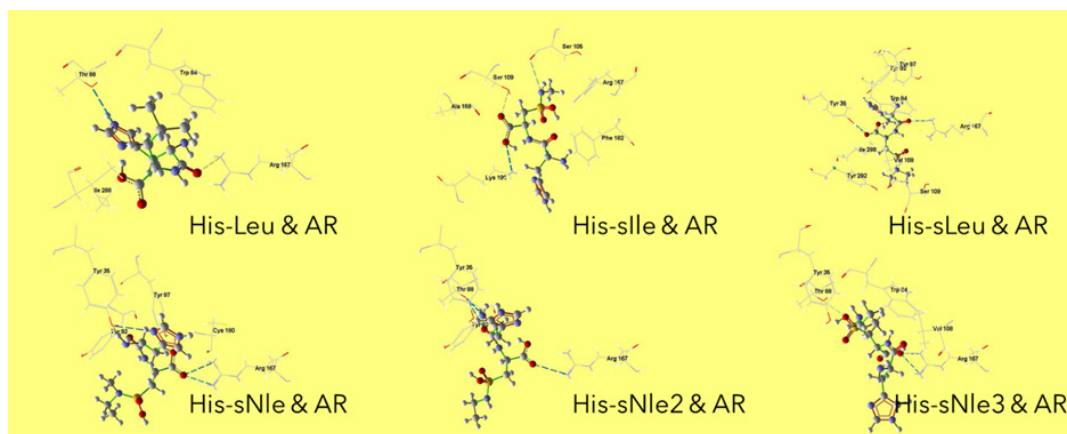


Fig. 2. Binding of the ligand with AR.

MATERIALS AND METHODS

Ligands

Ligands used in this work were previously used [6]: His-sLeu, His-sNle and His-sNle3.

Computational tools

In order to perform computational studies, different software was used in the present work. Ligand preparation was done with Avogadro [7]. Docking studies were performed by using GOLD 5.2 (Genetic Optimization for Ligand Docking) [8], run on Scientific LINUX 5.5 operating system. Molegro Molecular Viewer [9] was used for generating figures.

Docking of ligands

Six ligands, investigated for their binding to AR, were selected for docking studies. 3D structures of the ligands were modeled in Avogadro. Ligands were protonated at the physiological pH 7.4. Docking was carried out with GOLD 5.2 software. It uses a generic algorithm and considers full ligand conformational flexibility and partial protein flexibility. The binding site for AR (PDB id: 4zud), we assumed that like in all G-protein couple receptors, it was on the third transmembrane helix (TM). For the docking we used Arg167 residue from the TM and the space within 10 Å radius of them. GoldScore scoring function of GOLD was used. The conformations of the ligands with best scoring functions were selected and the total energies of the complexes with AR were used for analysis.

RESULTS AND DISCUSSION

The residues from TM helix 3 are important residues for ligand recognition. The binding site was defined as residues within 10 Å radius of Arg167 on TM3. Docking was performed with AR (PDB id: 4zud) and 6 ligands.

The results from docking were analyzed in Molegro Molecular Viewer, where total energies of the obtained ligand-receptor complexes were calculated (Table 1).

Table 1. Total energies of the complexes between ligands and the model of AR

Ligand	Total energies of complexes with AR
His-Leu	-34.27
His-sIle	-25.08
His-sLeu	-49.05
His-sNle	-82.91
His-sNle2	-55.45
His-sNle3	-85.72

Total energies show how strong the ligand binds the receptor. We could assume that they represent the affinity of the compound to the respective receptor type. The table shows that all analogues bind strongly to AR, but three of them – His-sLeu, His-sNle and His-sNle3, have the potential to act as its antagonists, as the formed ligand-receptor complexes have low enough energies to be stable over a long period of time. The same can be seen in the way they bind to the receptors (Fig. 2). The ligand His-sNle3 forms a larger number of hydrogen bonds, and interactions (electrostatic, hydrophobic) with the AR than the other.

All of the peptides interacted with the crucial amino acid residue of the receptor sequence Arg167. The most potent ligands had an additional interaction with Tyr35 which stabilizes the complex. Our previous study showed that the same ligands His-sLeu, His-sNle and His-sNle3 bound strongly ACE [6]. So, these three compounds have the potential to block RAS by inhibiting both ACE and AR.

CONCLUSION

The test compounds can have a complex effect on RAS, on the one hand by inhibiting ACE and on the other hand by blocking AR. Compounds His-sLeu, His-sNle and His-sNle3 bind strongly not only with the AR, but also with ACE as we reported previously. This study shows once again the possibilities of docking studies for prediction of the biological effect in a faster way. Computer-aided drug design is a useful approach in the modern design of new compounds with a desired biological effect. It could shorten the process by calculating different constants thus helping in improving structure and properties of a compound.

REFERENCES

1. R. A. S. Santos, M. J. Campagnole-Santos, S. P. Andrade, *Regulatory Peptides*, **91**, 45 (2000).
2. P. B. Timmermans, P. C. Wong, A. T. Chiu, W. F. Herblin, P. Benfield, D. J. Carini, R. J. Lee, R. R. Wexler, A. J. Saye, R. D. Smith, *Pharmacol Rev.*, **45**, 205 (1993).
3. M. Mei, Z. Zhou, Q. Zhang, Y. Chen, H. Zhao, B. Shen, *Nephron*, **145**, 99 (2021).
4. C. E. Mogensen, S. Neldam, I. Tikkanen, S. Oren, R. Viskoper, R. W. Watts, M. E. Cooper, *BMJ*, **321**, 1440 (2000).
5. D. Z. Cherney, J. W. Scholey, S. Jiang, R. Har, V. Lai, E. B. Sochett, H. N. Reich, *Diabetes Care*, **35**, 2324 (2012).
6. R. Georgiev, T. Dzimbova, A. Chapkanov, *Chemistry: Bulgarian Journal*, **27**, 864 (2018).
7. M. D. Hanwell, D. E. Curtis, D. C. Lonie, T. Vandermeersch, E. Zurek, G. R. Hutchison, *J. Cheminformatics*, **4**, art. 17 (2012).
8. G. Jones, P. Willett, R. C. Glen, A. R. Leach, R. Taylor, *J. Mol. Biol.*, **267**, 727 (1997).
9. R. Thomsen, M. H. Christensen, *J. Med. Chem.*, **49**, 3315 (2006).

Durability of porous anodic alumina layers on AA1050 modified by incorporation of Cu, Ni and Cu/Ni

Ch. Girginov^{1*}, St. Kozhukharov², B. Tzaneva³

¹Department of Physical Chemistry, Faculty of Chemical Technologies, University of Chemical Technology and Metallurgy, Sofia, Bulgaria

²LAMAR Laboratory, University of Chemical Technology and Metallurgy, Sofia, Bulgaria

³Department of Chemistry, Faculty of Electronic Engineering and Technologies, Technical University of Sofia, Sofia, Bulgaria

Received: November 17, 2021; Revised: March 03, 2022

The resistance of referent porous AAO (anodic aluminum oxide) layers and such modified by incorporation of Cu, Ni and both Cu and Ni was evaluated by performing electrochemical measurements using electrochemical impedance spectroscopy (EIS) and linear sweep voltammetry (LSV). The reported results are obtained after 168 hours of exposure to a 3.5% NaCl model corrosive medium. The acquired EIS spectra were analyzed by fitting to a suitable model equivalent circuit (MEC). Further, the estimated impedance values, acquired by the performed EIS data evaluation were further verified by Tafel slope analysis of the respective LSV curves. The results have shown that the elaborated films are sufficiently durable and can successfully be employed as primers for the deposition of other types of advanced coating layers.

Keywords: AAO layers; Ni, Cu and Cu/Ni incorporation; Electrochemical characterization methods

INTRODUCTION

Low-doped Al alloys, such as AA1050, find various applications in both mass production and high-tech industries. One of the widest fields of use of these materials is the packaging of various nutrition products and soft drinks [1, 2]. However, reliable packaging requires additional protection of the surface of Al-based packaging materials before they come into contact with any food product. This requirement has arisen because the resorption of Al-ions from such packaging products was recently demonstrated [3, 4], which is dangerous to human health [5, 6]. The specific connection between electrical conductivity and the strength-to-weight ratio [7, 8] makes aluminum an indispensable material for high-voltage, long-distance electricity distribution [9, 10] as well. Among the most notable advantages of aluminum is its ability to form a highly ordered self-assembled porous surface by means of anodizing under certain conditions [11, 12]. The surfaces of the obtained textured *anodic aluminum oxide* (AAO) films are widely used for ink-printing on paper and plastic packaging materials [13, 14]. Also, anodized pure aluminum is used for manufacturing metal-oxide-semiconductor electronic components [15, 16], sensors [17, 18] and biosensors [19]. Other recently proposed important applications are for alternative energy sources, such as production of flexible solar cells [20] and fuel cell electrodes by anodization [21]. Recently, the

obvious advances of the multilayer coating systems elaborated by various electrochemical methods have been outlined in an extended review [22]. In this sense, AAO layers additionally modified by incorporation of Ce [23], Ag [24], and Cu and Ni [25] have shown superior corrosion-protective properties. In addition, these electrochemical modifications provide additional benefits, such as decorative color effects and even bactericidal ability. Undoubtedly, these modified AAO layers enable the deposition of other types of advanced coating layers, in order to produce various hi-tech components and multifunctional devices.

In this sense, the aim of the present research work is the performance of systematic comparative electrochemical measurements on porous AAO layers, after their modification by incorporation of Cu, Ni, and both Cu and Ni in their pores. The measurements were performed on two samples from each set: (i) reference AAO, (ii) AAO with incorporated Cu, (iii) AAO with incorporated Ni and (iv) AAO with incorporated Cu and Ni. All measurements were performed after 168 hours of exposure to a model corrosive medium (aqueous solution of 3.5% NaCl).

EXPERIMENTAL

Electrochemical elaboration of the investigated films

Eight square-shaped specimens (2 × 2 cm) of the low-doped AA 1050 alloy were cut in order to

* To whom all correspondence should be sent:
E-mail: girginov@uctm.edu

perform the planned systematic comparative study. The preliminary surface treatment was performed by etching in a NaOH solution (50 g dm^{-3}) for 2 minutes at $60 \text{ }^\circ\text{C}$ and subsequent activation in dilute nitric acid ($\text{HNO}_3:\text{H}_2\text{O} - 1:1$) for 2 minutes at room temperature, followed by a final vigorous washing with both tap and double-distilled water.

The specimens were then anodized in a 15 wt.% solution of H_2SO_4 under galvanostatic conditions (15 mA cm^{-2}) for 50 min at room temperature. The formed porous AAO layers were electrochemically modified by incorporation of Cu and/or Ni. This process was performed at the following conditions: AC-polarization at a constant voltage of 20 V and applied frequency of 60 Hz, for 15 min at $20 \text{ }^\circ\text{C}$. Both Cu- and Ni-containing electrolytes were composed by CuSO_4 or NiSO_4 (0.4 mol dm^{-3}), respectively. The combined Cu/Ni electrolyte was prepared by mixing these solutions in a volume ratio of 1:1. Each of these deposition electrolytes contained also $(\text{NH}_4)_2\text{SO}_4$ (30 g dm^{-3}) and H_3BO_3 (50 g dm^{-3}).

As a result, a set of: (i) reference AAO, (ii) AAO with incorporated Cu, (iii) AAO with incorporated Ni and (iv) AAO with incorporated Cu and Ni was prepared. In order to assess the repeatability of the results, each of these types of coatings was represented by two samples.

Electrochemical characterization of the obtained films

All samples were subjected to comparative electrochemical measurements after 168 hours of exposure to the model corrosive medium (MCM), which is essentially a 3.5 % aqueous NaCl solution. The electrochemical film characterizations were performed using an Autolab PGStat 30 potentiostat/galvanostat of Metrohm (Netherlands), equipped with FRA-2 frequency response analyzer. The measurements were performed in a standard, three-electrode flat cell (ISO 16773-2), equipped with a cylindrical platinum mesh as a counter-electrode and an Ag/AgCl/3M KCl reference electrode. Test areas of 2 cm^2 from the specimens served as working electrodes. The measurements included electrochemical impedance spectroscopy (EIS) and linear sweep voltammetry (LSV). The EIS spectra were acquired in the frequency range from 10 kHz to 0.01 Hz, distributed in 50 measurement points. The amplitude of the excitation signal was up to 35 mV in relation to the open circuit potential (OCP), in order to acquire

readable spectra. The linear sweep voltammetry (LSV) curve acquisitions were performed in the potential range from -150 to 550 mV. OCP, at a sweep rate of 10 mV s^{-1} .

RESULTS AND DISCUSSION

EIS data acquisition

The electrochemical impedance spectra were acquired from all samples after 168 hours of exposure to the model corrosive medium, in order to obtain comparable results for all specimens. Figure 1 presents averaged EIS spectra plotted in Bode (a) and Nyquist (b) coordinates. The spectra resemble this of a capacitor, due to the excellent insulation properties of the elaborated AAO layers on the metallic surfaces. Only the phase shift of the reference AAO layers can be distinguished from those of the modified ones. Consequently, their modification by means of incorporation of Cu and/or Ni obviously results in further improvement of the formed AAO layers.

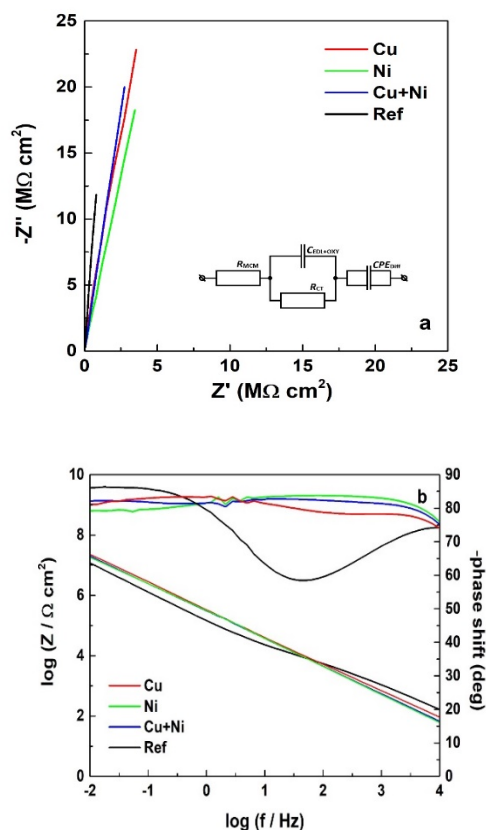


Fig. 1. Averaged EIS spectra of the investigated specimens, acquired after 168 hours of exposure to the 3.5% NaCl model corrosive medium.

Table 1. Results of the numerical analysis of the EIS spectra

Group	Sample	R_{MCM}		$C_{EDL OXY}$		R_{CT}		CPE_{diff}		n	
		cm^2	cm^2	$F \cdot \text{cm}^{-2}$	$F \cdot \text{cm}^{-2}$	k	cm^2	$(10^{-7})s^n$	cm^{-2}		
G1 – Ref	S1	90.40	28.02	0.12	0.01	6.590	0.66	12.20	0.63	0.88	0.01
	S2	34.90	8.49	0.36	0.01	1.820	0.22	11.56	0.30	0.91	0.01
G2 – Cu	S1	8.87	1.40	1.22	0.07	0.297	0.030	5.53	0.02	0.91	0.01
	S2	5.79	1.33	9.07	1.27	0.219	0.035	5.47	0.01	0.93	0.01
G3 – Ni	S1	8.73	1.00	4.73	0.46	275.184	33.732	7.36	0.05	0.91	0.01
	S2	7.38	1.05	3.47	0.26	260.900	37.332	6.73	0.08	0.93	0.01
G4 – Cu/Ni	S1	8.21	0.85	7.65	0.13	23.79	6.13	6.47	0.03	0.92	0.01
		9.68	0.58	5.02	0.43	33.90	10.70	6.08	0.02	0.91	0.01

The obtained spectra were further submitted to analysis using a suitable model equivalent circuit (MEC), illustrated in Fig. 1a. It is composed of resistance of the model corrosive medium R_{MCM} , connected to the capacitance of the electric double layer and the oxide film $C_{EDL OXY}$ and the charge transfer resistance R_{ct} . Finally, a constant phase element CPE_{diff} was required in order to describe the diffusion of the electrolyte inside the pores of the AAO.

The results of the numerical analysis of the EIS spectra with the used MEC are presented in Table 1.

The comparative analysis of the data in Table 1 has revealed several obvious trends. The values of R_{MCM} , for the reference AAO layers are by entire order of magnitude higher than those of the modified layers. At the same time, there are no obvious differences between the R_{MCM} values of the AAO layers modified with incorporation of Cu and/or Ni. The capacitance $C_{EDL OXY}$ of the reference samples is also lower than this of the modified layers by at least one order of magnitude. The biggest differences are in the charge transfer resistance R_{ct} . The electrochemical modification with Cu has led to a decrease by an entire order of magnitude, compared to the R_{ct} of the reference AAO layers. In contrast, the incorporation of Ni resulted in a sharp rise of R_{ct} by three orders of magnitude.

In the case of the AAO layer modified with both Cu and Ni, the R_{ct} values are with an entire order of magnitude higher than those of the reference AAO layers. Consequently, the beneficial effect of the Ni-incorporation is compensated by the weak detrimental effect of the Cu deposition. Both these effects are probable, because on one hand, the Cu and/or Ni incorporation enhances the barrier properties of the AAO layer by sealing the pore walls and bottoms. However, on the other hand, the AC-polarization during the electrochemical Cu and/or Ni incorporation results in pore widening, due to the cathodic dissolution commented elsewhere [26].

An additional analysis of the EIS spectra was performed, following the general concepts of Zheludkevich *et al.* [27]. It was performed by determination of the $\log Z$ values, acquired at 0.01 Hz (i.e., the last impedance data points). The corresponding values of the impedance modulus Z (Table 2) should approximate those of the polarization resistance (R_p), commented in the next paragraph.

According to this parameter (i.e., Z), the AAO layers modified with Cu possess similar barrier properties to the reference ones. However, the other two trends commented above, regarding the obvious beneficial effect of the modification of the AAO layer with Ni and the weakening of this effect, are confirmed by the values of Z presented in Table 2. Indeed, these values, estimated for the AAO layers with incorporated Ni are about three times higher, whereas the AAO modified with Cu and Ni have almost the same Z -values as those of the other groups.

A rather interesting fact is that the Z -values are by more than three orders of magnitude higher than those of R_{ct} . The discrepancy between the values of these parameters is a result of the fact that the value of Z comprises the capacitive reactance, unlike R_{ct} .

Analysis of the data acquired by linear sweep voltammetry (LSV)

The EIS spectra, commented in the previous paragraph, were followed by recording of LSV curves, under the conditions described in the experimental section. The averaged LSV curves are presented in Fig. 2.

The anodic branches of all LSV curves are almost horizontal, revealing the lack of any corrosion processes. Consequently, the formation of the AAO layer results in efficient passivation of the surfaces of the AA1050 samples and serves as efficient barrier against access of corrosive species to the metallic surface.

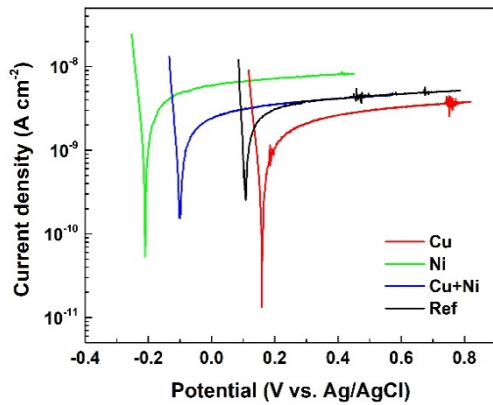


Fig. 2. Averaged LSV curves, acquired after 168 hours of exposure to 3.5% NaCl model corrosive medium

Again, the averaged LSV curve for the Ni-AAO samples falls below those of the other types of coatings, due to the already mentioned beneficial effect of the electrochemical treatment of the AAO layers in the electrolyte containing NiSO₄. This curve is followed by the curves for Cu/Ni-AAO and for Cu-AAO. The LSV curves of the reference AAO layers are at the highest current. Besides, both modified with Ni and Cu AAO layers are shifted to more negative potentials, whereas the combined Cu and Ni AAO approaches the potential of the reference AAO layer. The LSV curves were submitted to further Tafel slope analysis, in order to acquire a clearer image regarding the corrosion characteristics of the investigated layers. The respective numerical data for the corrosion potential (calculated vs. SHE) and the polarization resistance are summarized in Table 3. The data for the corrosion potential in Table 3 reveal that the additional Cu and/or Ni modifications result in its shifting towards more negative values. Nevertheless, this shift is rather weaker for the combined Cu and Ni AAO layers.

The data for the polarization resistance (R_p) represented in Table 3 almost coincide with those for $|Z|$ in Table 2. Indeed, the data from both tables reveal the remarkable beneficial effect of the AC assisted electrochemical modification of the AAO

layers. Indeed, the average value for $|Z|^{av} = 27.00 \text{ M}\Omega\cdot\text{cm}^2$ approaches the average value for $R_p^{av} = 27.55 \text{ M}\Omega\cdot\text{cm}^2$, and both of them are three times higher than these of the other types of coatings.

CONCLUSIONS

The data, acquired from the electrochemical impedance spectroscopy (EIS), were fitted to appropriate model equivalent circuit (MEC). It was evinced that the main impedance components of the spectra are: resistance of the model corrosive medium (R_{MCM}), capacitance of the electric double layer and the oxide film ($C_{EDL+OXY}$), the charge transfer resistance (R_{ct}) and diffusion constant phase element CPE_{diff} . Further analysis was performed of the EIS spectra in order to acquire the values of the impedance modulus $|Z|$ at 0.01 Hz. It was established that these values are higher than those of R_{ct} by more than three orders of magnitude. The found discrepancy between the values of these parameters is a result from the fact that the value of $|Z|$ comprises the capacitive reactance as well.

Afterwards, linear sweep voltammetry (LSV) was applied, in order to determine the values of the corrosion potential and the polarization resistance (R_p).

The present research is based on the comparative analysis of data, acquired from systematic electrochemical measurements on AAO layers, after modification with Cu, Ni, and combination of them. Two independent electrochemical analytical methods were applied for data acquisition, after 168 hours of exposure of the specimens to 3.5% NaCl model corrosive medium.

Both analytical methods have revealed that the basic AAO layer behaves as almost perfect insulator. Further, the analysis of the obtained data has shown superior behavior of the AAO layers modified with Ni, compared to the other types. Besides, a weak deterioration of this behavior was registered for the AAO films modified with both Cu and Ni. As a main achievement of the present research could be pointed out the clear correspondence between $|Z|$ at the lowest frequency and the R_p from the LSV curves.

Table 2. Values of the total impedance modulus, acquired at 0.01 Hz.

Sample No.	S1		S2	
Unit	Log $ Z $	$ Z $ ($\text{M}\Omega\cdot\text{cm}^2$)	Log $ Z $	$ Z $ ($\text{M}\Omega\cdot\text{cm}^2$)
G1-Ref	7.118	13.12	7.066	11.65
G2-Cu	7.161	14.49	7.168	14.71
G3-Ni	7.454	28.42	7.408	25.58
G4-Cu/Ni	7.253	17.91	7.242	17.46

Table 3. Numerical data of the corrosion potential and the polarization resistance

Sample No.	S1		S2	
	Corrosion potential (mV versus Ag/AgCl)	Polarization resistance (MΩ.cm ²)	Corrosion potential (mV versus Ag/AgCl)	Polarization resistance (MΩ.cm ²)
G1-Ref	-102	13.79	-103	11.50
G2-Cu	-312	14.84	-332	15.56
G3-Ni	-293	29.06	-328	26.04
G4-Cu/Ni	-176	17.44	-125	17.55

In general, the Cu- and/or Ni-modified AAO layers, elaborated during the present research activities, can be efficiently used as a basis for deposition of other types of advanced coating systems. In particular, the approaches described here enable the elaboration of entire new generations of metal/dielectric/metal systems.

Acknowledgements: The authors gratefully acknowledge the financial support of the Bulgarian National Science Fund, under project 06- 29/1.

REFERENCES

- M. Lamberti, F. Escher, *Food Rev. Internat.*, **23**, 407 (2007).
- O. Ayalon, Y. Avnimelech, M. Shechter, *Envir. Sci. Pol.*, **3**, 135 (2000).
- S. P. Joshi, R. B. Toma, N. Medora, K. O'Connor, *Food Chemistry*, **83**, 383 (2003).
- F. Bianchi, M. Careri, M. Maffini, A. Mangia, C. Mucchino, *Rapid Commun. Mass Spectr.*, **17**, 251 (2003).
- A. Becaria, A. Campbell, S. C. Bondy, *Toxicology and Industrial Health*, **18**, 309 (2002).
- J. Kandiah, C. Kies, *Biometals*, **7**, 57 (1994).
- S. S. Golru, M. M. Attar, B. Ramezanzadeh, *Appl. Surf. Sci.*, **345**, 360 (2015).
- R. Lukauskaitė, A. V. Valiulis, O. Černašėjus, J. Škamat, J. A. Rębiś, *J. Mater. Eng. Perform.*, **25**, 3493 (2016).
- D. E. Johnson, T. L. Anderson, US patent, US 6559385 B1 (2003).
- C. Hiel, G. Korzeniowski, D. Bryant, US patent, US 7179522 B2 (2004).
- Ch. A. Girginov, S. V. Kozhukharov, Chapter 1. Theoretical Bases and Mechanisms of the Electrochemical Alumina Films Formation, in: Aluminium Oxide. Structure Production and Application, A. Hermansen (ed.), NOVA Sci. Publ., 2020, p. 3.
- W. Stępniewski, J. M. Salerno, Chapter 12. Fabrication of nanowires and nanotubes by anodic alumina template-assisted electrodeposition, Manufacturing Nanostructures, in: Manufacturing Nanostructures, W. Ahmed, N. Ali (eds.), One Central Press –ISBN: 9781910086070, 2014, p. 321.
- R. E. Cleveland, US patent, US 2114072 A (1938).
- J. Curt, US patent, US 2780253 A (2008).
- P. Vachkov, D. Ivanov, Powerful MOS transistors and their application, Gov. Ed. "Tekhnicka", Sofia, 1990, p. 15.
- S. Iwauchi, T. Tanaka, *Jpn. J. Appl. Phys.*, **10**, 260 (1971).
- T. Kumeria, A. Santos, D. Losic, *Sensors*, **14**, 11878 (2014).
- I. Abrego, A. Campos, G. Bethencourt, E. Ching-Prado, *Mater. Proceed. Res. Soc. Symp.*, **1449**, 73 (2012).
- A. Santos, T. Kumeria, D. Losic, *Materials*, **7**, 4297 (2014).
- F.-C. Chen, M.-K. Chuang, S.-C. Chien, J.-H. Fang, C.-W. Chu, *J. Mater. Chem.*, **21**, 11378 (2011).
- P. Bocchetta, M. Santamaria, F. Di Quarto, *J. Mater. Sci. Nanotechnol.*, **1**, 1 (2014).
- M. Aliofkhaezrai, F. C. Walsh, G. Zangari, H. Koçkar, M. Alper, C. Rizal, L. Magagnin, V. Protsenko, R. Arunachalam, A. Rezvanian, A. Moein, S. Assareh, M. H. Allahyarzadeh, *Appl. Surf. Sci. Adv.*, **6**, 100141 (2021).
- S. Kozhukharov, Ch. Girginov, *J. Electrochem. Sci. Eng.*, **8**, 113 (2018).
- S. V. Kozhukharov, Ch. Girginov, D. Kiradzhyska, A. Tsanev, G. Avdeev, *J. Electrochem. Sci. Eng.*, **10**, 317 (2020).
- Ch. Girginov, S. Kozhukharov, A. Tsanev, A. Dishliev, *J. Electrochem. Sci. Technol.*, **12**, 188 (2021).
- T. T. M. Tran, B. Tribollet, E. M. M. Sutter, *Electrochim. Acta*, **216**, 58 (2016).
- M. L. Zheludkevich, I. M. Salvado, M. G. Ferreira, *J. Mater. Chem.*, **15**, 5099 (2005).

Assessment of the elemental composition, antioxidant activity, and optical properties of non-traditional Bulgarian fruit wines

S. Minkova¹, I. Vlaeva², Kr. Nikolova^{1*}, N. Petkova², G. Gentscheva^{3,4}, Ch. Tzvetkova⁴

¹Medical University, Varna, Bulgaria

²University of Food Technologies, Plovdiv, Bulgaria

³Medical University-Pleven, Bulgaria

⁴Institute of General and Inorganic Chemistry, Bulgarian Academy of Sciences, Sofia, Bulgaria

Received: November 17, 2021; Revised: May 19, 2022

Melon wine and white cherry wines purchased from the commercial market were studied. The aim of the present work is to evaluate the elemental composition, antioxidant activity and optical properties of these fruit wines. The concentrations of certain elements in wines are of interest because some of them are regulated, others affect the organoleptic properties of wine, and some elements are essential to the human body. Organic chemicals that contribute to the taste and color of wine are also of healthy interest. For this purpose, the total phenolic content (TPC), the total flavonoid content, the total monomeric and antioxidant activity were determined by four different methods (ABTS, DPPH, FRAP and CUPRAC). A correlation between these parameters and the emission maxima of the fluorescence spectra was obtained for the wavelengths of light excitation 245 nm and 285 nm.

Keywords: fluorescence, antioxidant activity, white wines from melon, white wines with cherry, chemical elements

INTRODUCTION

Fruit wines are made from a variety of fruits, including watermelon and melon. The preparation of these wines has its own peculiarities, but in all other respects they are produced on the same principle as these from grapes, following certain rules. Practically fruit wine can be obtained from almost all fruits, and the color obtained is considered white, red or rosé. In addition to pure fruit wines, wines can be made from various combinations with classic grape wines. Fruit wines or combinations of wines and fruits of apple, blueberry, raspberry, black currant, watermelon, plum, fig, as well as non-traditional for our latitudes tropical fruits such as mango, lemon, pomegranate, lime, passion fruit, kiwi and others can be found on the Bulgarian market. Interest in the production of this type of wine is growing due to the rich aroma and taste qualities that the fruits transmit to the wine [1]. The production of fruit wines from black currant, blueberry, strawberry, raspberry and apricot is already a tradition in many countries of the European Union and the United States [2]. The total phenolic content of wines from raspberries, black currant, blueberries, elderberries, buckwheat, etc. has been studied. Their phenol content is comparable to or higher than that of red grape wines [3 4]. The existence of a positive relationship between the total antioxidant activity of fruit wines and the total phenolic content [5, 6] is confirmed. Last but not least, it is important to

determine the mineral content of fruit wines, related to their ecological purity and health safety. Prolonged contact of the product with the facilities in which the various stages of technological processing take place and the use of bentonites may lead to an increase in the content of some elements [7, 8]. Other metals are able to influence the organoleptic properties of fruit wines and are the basis of sensory evaluation of such products.

Although fruit wines are rich in antioxidants and minerals, there are still insufficient data on their chemical composition and physical properties. The aim of the present study is to investigate the optical properties of melon and white cherry wine in combination with Chardonnay. Additionally, the contents of Cu and Pd against their allowable reference values, as well as the concentrations of some elements with potential biological role with health benefits, such as Mg, Zn, Mn and Fe, have also been evaluated.

MATERIALS AND METHODS

Materials

In the present study, two wines were chosen for analysis with the composition:

- a) 40% cherry & 60% Chardonnay wine – 3 bottles;
- b) 100% melon wine– 3 bottles.

All samples were purchased from the local market and are from the same manufacturer.

* To whom all correspondence should be sent.

Determination of total phenolic content (TPC)

The total phenolic content in the fruit wines was determined using the Folin–Ciocalteu's reagent [9]. The analysis was performed as 0.2 mL 70 % ethanol extract was mixed with 1 mL of Folin–Ciocalteu reagent diluted five times and then 0.8 mL of 7.5% Na₂CO₃ was added. After 20 min, the absorption was measured at 765 nm against a blank sample. The results were expressed in mg equivalent of gallic acid (GAE) per ml using the calibration curve $Y = 12.557x - 0.0871$ [10].

Determination of total flavonoids content

The total flavonoids content was determined by Al(NO₃)₃ reagent. The absorbance was measured at 415 nm. The results were presented as mg equivalents quercetin (QE) per ml according to the calibration curve $Y = 0.0119x - 0.0467$ with quercetin as a standard [10].

Total monomeric anthocyanins content (TMA)

Total anthocyanins content was determined using the pH differential method [11] at two wavelengths 520 and 700 nm. The results were presented as cyanidin-3-glycoside per ml.

Antioxidant activity

DPPH radical-scavenging ability. Wine sample (0.15 ml) was added to 2.85 ml of freshly prepared 0.1mM methanol solution of DPPH. The reduction of absorbance at 517 nm was measured by spectrophotometer against blank containing methanol. The percent inhibition was also calculated. The results were expressed in mM Trolox® equivalents (TE)/ml [10].

ABTS+ radical scavenging ability. The ABTS+ solution (2.85 ml) was mixed with 0.15 ml of fruit wine sample. After 15 min at 37°C in darkness, the absorbance was measured at 734 nm against ethanol. The percent inhibition was also calculated. The results were expressed in mM Trolox® equivalents (TE)/g dw [10].

FRAP assay. The FRAP reagent was prepared before analysis by mixing 10 parts of 0.3M acetate buffer (pH 3.6), 1 part of 10 mM 2,4,6-tri(2-pyridyl)-s-triazine (TPTZ) in 40 mM HCl and 1 part of 20 mM FeCl₃×6H₂O in distilled water. FRAP reagent (3.0 ml) was mixed with 0.1 ml of wine extract. After 10 min at 37°C in darkness, the absorbance of the sample was measured at 593 nm [12].

CUPRAC assay. Wine extract (0.1 ml) was mixed with 1 ml of CuCl₂×2H₂O, 1 ml of methanol

solution of neocuproine, 1 ml of 0.1M ammonium acetate buffer and 1 ml of distilled H₂O. After 20 min at 50°C in darkness, the samples were cooled to room temperature and the absorbance was measured at 450 nm. The results were expressed in mM Trolox® equivalents (TE)/g dw [10].

Fluorescence spectra

Fluorescence spectra were measured with an optical spectrometer (AvaSpec-2048, Avantes) with an operating range from 200 nm to 1100 nm. The used sources are LEDs operating at wavelengths of 245 nm, 265 nm, 275 nm and 295 nm. The resolution of the spectrometer is 8 nm for an input slit of 200 μm. An optical fiber with a diameter of 200 μm is used to bring the light to the probe and to measure the scattered and fluorescent light. A collimator with a lens with an aperture of D=5 mm is used to collect more light and send it to the receiver.

For each wine, three fluorescence spectra were recorded for three different bottles, purchased from the market. During the investigation the average spectra are presented for each excitation wavelength of the sample.

Determination of elements

A sample of about 5 g was weighed on an analytical balance and treated with 3-4 mL of HNO₃ (65%, Suprapur®, Merck) on a hot plate to remove the organic part. The residue was transferred into a 25-ml flask and diluted with distilled water [13]. Multielement standard solution 5 for ICP (TraceCERT®, Merck) was used for the preparation of working standard solutions for calibration for ICP-OES iCAP 7000 SERIES (Thermo Fisher Scientific, USA).

Statistical analysis:

The ANOVA single factor analysis and descriptive statistic methods are used. Each parameter was measured in triplicate and the average results and standard deviation are presented in the experimental results.

RESULTS AND DISCUSSION

The fluorescence spectra were obtained by excitation of melon and cherry&Chardonnay wines by light with wavelength 245 nm, 285 nm, 370 nm, 380 nm, 390 nm, 400 nm and 420 nm. The best ratio between the intensity of excitation and intensity of emission was found for excitation light from the UV region. For that reason only these spectra are given in figures 1a and 1b.

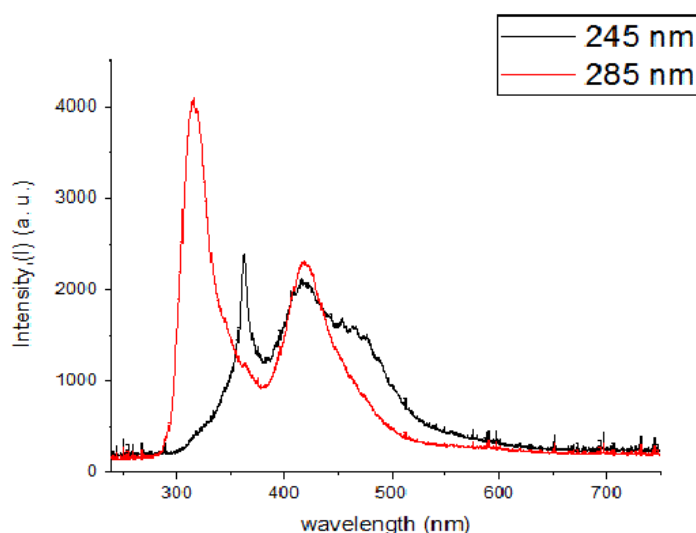


Figure 1a. Fluorescence spectra of melon wine, obtained by using excitation light in the UV-VIS region

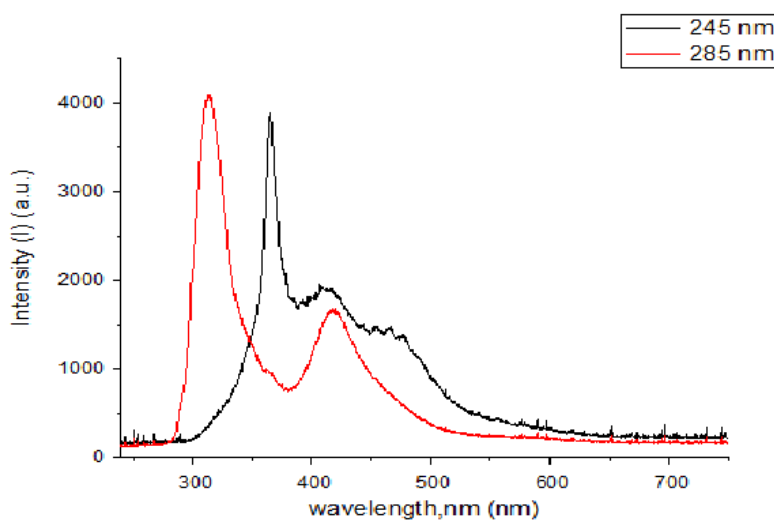


Figure 1b. Fluorescence spectra of cherry&Chardonnay wine, obtained by using excitation light in the UV-VIS region.

The spectra are characterized with two maxima:

- The first one is between 320 and 365 nm;
- The second one is between 420 and 427 nm.

The similar wavelength for fluorescence maximum of wine are reported by Dufour *et al.* of French and German grape wines [14]. According to Rodríguez-Delgado the fluorescence maximum in the region (320 - 426) nm for excitation wavelength (262 - 285) nm is connected with the presence of caffeic acid in the wine [15]. The fluorescence maximum in the region (320-366) nm for excitation wavelength (278 – 285) nm is connected with gallic acid [16].

The difference between the fluorescence maxima for cherry&Chardonnay and melon wine was in the shape and in the maximum values of the fluorescence intensity. This can be explained with the different content of phenolic components in

these fruits and the different technology of production of the wine.

Total phenolic content and total flavonoids content were evaluated (Table 1). The cherry&Chardonnay wine and melon wine possessed similar total phenolic contents. However, flavonoids content of white cherry wine is slightly higher than that of melon wine.

Various authors [17-20] reported that the highest total phenolic content (TPC) is demonstrated by the fruit wines from red cherry (1.081-2.711) mg GAE/ml, black currant (0.941-3.086) mg GAE/ml and blackberry (1.055-2.705) mg GAE/ml. Apple wine possesses the lowest TPC (0.244-0.644) mg GAE/ml [20]. In our case the results for TPC white cherry wine are lower than those reported by Brat *et al.* [21] – 0.94 mg GAE/g, but they are close to those reported for apple wines.

Table 1. Phenolic content and antioxidant activity in the fruit wine samples

	TPC, mg GAE/ml	Total flavonoids, mg QE/ml	TMA, mg cyanidin-3-glycoside/ml	Antioxidant activity, mM TE/ml			
				DPPH	ABTS	FRAP	CUPRAC
Cherry& Chardonnay	0.34±0.02	6.61±0.01	N.D.	1.25±0.01	1.98±0.03	1.11±0.01	3.38±0.05
Melon	0.35±0.01	5.86±0.03	N.D.	1.35±0.02	2.02±0.02	1.22±0.01	3.61±0.06

Table 2. Content of Mg, Fe, Cu, Zn, and Mn in fruit wine samples (RSD varied between 2–5%)

	Mg, mg kg ⁻¹	Fe, mg kg ⁻¹	Cu, mg kg ⁻¹	Zn, mg kg ⁻¹	Mn, mg kg ⁻¹
Cherry& Chardonnay*	46.8	0.68	0.11	0.18	0.24
Melon*	50.6	0.62	0.09	0.13	0.25

* Pb<0.17 mg kg⁻¹ and Cd<0.01 mg kg⁻¹

The total phenolic content in melon wine is similar to that for grapefruit (0.39 mg GAE/g and 0.47 mg GAE/g) [21]. Total phenolic content in both wines under study is similar to that in white wine. TPC in cherry wine is equal to those in white wine from Dimyat and Mavrud (0.33 mg GAE/ml) [22] and from Chardonnay (0.29 mg GAE/ml) [19]. TPC in melon wine is higher than that of some rose wine. It is reported that Grenache and Souvingnon blanc types of rosé wine have TPC 0.257 mg GAE/ml and 0.255 mg GAE/ml, respectively [22].

As expected, anthocyanins were not detected in the investigated wines. Similar results are reported for apple wine [20].

The antioxidant and pharmacological effects of fruit wines are due to the phenolic compounds - anthocyanins, flavanols and other flavonoids. These compounds also improve the sensory characteristics of wines such as color and astringency [16]. The most studied phenolic compounds in fruit wines are flavonoids, because they are widely present in the plants and they possess antioxidant properties. The important class of flavonoids is flavanols such as myricetin and quercetin, which are spread in red berry wines [23]. Czyzowska reported that flavanols' content of cherry wines is 10 times higher than that of grape wine [24]. In our case cherry wine (6.61 mg QE/ml) is superior to melon wine (5.86 mg QE/ml) in total flavonoids.

The main compounds with antioxidant activity are flavonoids and phenolic acids, carotenoids and vitamins. The order of antioxidant activity (AOA) in the fruit wines is reported in [19] – AOA decreases from bilberry, blackberry, black mulberry, sour cherry, strawberry, raspberry, apricot, quince, apple and melon. Kalkan Yildirim [19] reported AOA of fruit wines in the following decreasing rank: bilberry > blackberry > black mulberry > sour cherry > strawberry > raspberry >

apricot > quince, apple > melon. AOA is determined by us using 4 different methods: ABTS, DPPH, FRAP and CUPRAC. All methods revealed a higher AOA of melon wine compared with the white cherry wine. The highest antioxidant activity in our case was found by CUPRAC assay, where the antioxidant potential was twice higher in comparison with the radical scavenging capacity determined by DPPH method. Therefore, the investigated wines demonstrated better antioxidant potential by using the principle of metal-reducing activity.

The concentrations of Cu, Cd, Mg, Mn, Fe, Zn and Pb in the fruit wine samples were determined (Table 2). The analyzed elements belong to three groups in terms of human health: main elements such as Mg (essential in amount > 50 mg/day), trace elements Fe, Cu, Zn and Mn (essential in concentrations < 50 mg/day) and toxic elements Pb and Cd [25]. The content of metals in grape wines is regulated by the legislation of the European Union – 0.20 mg kg⁻¹ for Pb and 1 mg L⁻¹ for Cu [26]; additionally the OIV recommends up to 5 mg L⁻¹ Zn content [27]. The concentrations of all three elements in the studied fruit wines remain below the normative/ recommended values. Cd concentrations are extremely low and below detection limits.

The mineral composition of wines is determined by many factors: type of fruit, climatic conditions, soil characteristics, cultivation methods, technological procedures and equipment, fermentation, bottling, etc. According to Pohl [28], who summarizes the research of a number of authors on the mineral composition of different types of wine from different regions of the world, the content of Mg, Fe and Mn varies widely (7.8–718 mg L⁻¹ for Mg, 0.06–23.7 mg L⁻¹ for Fe, 0.1–5.5 mg L⁻¹ for Mn). As can be seen from Table 2, both wines fit perfectly within the specified limits.

A comparison with blackberry wines from Croatia [29] and sour cherry wine from Serbia [30] shows that the wines we studied are more than 3 times poorer in iron and manganese, while in magnesium there is no significant difference.

As can be seen, the content of the elements can vary widely due to the great variety of fruits and grapes, which leads to their difficulty in comparison, and it can be concluded that Mg > Fe > Mn > Zn > Cu > Cd.

CONCLUSIONS

- There are no significant differences in the elemental composition of the two studied fruit wines.

- The difference between the fluorescence maxima for cherry&Chardonnay and melon wine is in the form and in the maximum values of the fluorescence intensity. This can be explained by the different content of phenolic components in these fruits and the different technology of wine production.

- Melon wine demonstrates slightly higher AOA than cherry&Chardonnay wine for each method used. A positive correlation can be established between the antioxidant activity of AOA and the total phenolic content, but not between AOA and flavonoids content. The highest antioxidant activity was found by CUPRAC analysis, where the antioxidant potential was twice as high as DPPH radical scavenging methods. Therefore, the studied wines demonstrate better antioxidant potential by using the principle of metal-reducing activity.

REFERENCES

1. J. A. Pino, O. Queris, *Food Chemistry*, **125**, 1141 (2011).
2. M. Heinonen, P. J. Lehtonen, A. I. Hopia, *J. Agric. Food Chem.*, **46**, 25 (1998),
3. G. Dey, B. Negi, A. Gandhi, *Indian Journal of Natural Products and Resources*, **8(4)**, 314 (2009).
4. H. P. V. Rupasinghe, S. Clegg, *Journal of Food Composition and Analysis*, **20(2)**, 133 (2007).
5. R. G. C. Barros, J. K. S. Andrade, M. Denadai, M. L. Nunes, N. Narain, *Food Research International*, **102**, 84 (2017).
6. L. Jakobek, M. Šeruga, M. Medvidović-Kosanović, I. Novak, *Deutsche Lebensmittel Rundschau*, **103(2)**, 58 (2007).
7. P. Kment, M. Mihaljevič, V. Ettler, O. Šebek, L. Strnad, L. Rohlova, *Food Chemistry*, **91(1)**, 157 (2005).
8. C. Díaz, J. E. Conde, D. Estévez, S. J. P. Olivero, J. P. P. Trujillo, *Agriculture and Food Chemistry*, **51**, 4303 (2003).
9. F. C. Stintzing, K. M. Nerbach, M. Mosshammer, R. Carle, W. Yi, S. Sellappan, C. C. Acoh, R. Bunch, P. Felker, *J. Agric. Food Chem.*, **53**, 442 (2005).
10. I. Ivanov, R. Vrancheva, A. Marchev, N. Petkova, I. Aneva, P. Denev, V. Georgiev, A. Pavlov, *Int. J. Curr. Microbiol. Appl. Sci.*, **3**, 296 (2014).
11. J. Lee, R. W. Durst, R. E. Wrolstad, *J AOAC Int.*, **88**, 1269 (2005).
12. F. Benzie, J. Srain, *Anal. Biochem.*, **70**, 239 (1996).
13. St. Minkova, G. Gentscheva, Kr. Nikolova, Chr. Tzvetkova, *IOP Science Conference series*, in press.
14. E. Dufour, A. Letort, A. Laguet, A. Lebecque, J. N. Serra, *Analytica Chimica Acta*, **563**, 292 (2006).
15. M. A. Rodríguez-Delgado, S. Malovaná, J. P. Pérez, T. Borges, F. J. García Montelongo, *Journal of Chromatography A*, **912**, 249 (2001).
16. A. Rodríguez-Bernaldo de Quirós, J. López-Hernández, P. Ferraces-Casais, M. A. Lage-Yusty, *Journal of Separation Science*, **30**, 1262 (2007).
17. H. P. V. Rupasinghe, S. Clegg, *J. Food Compos. Anal.*, **20**, 133 (2007).
18. I. M. Heinonen, P. J. Lehtonen, A. I. Hopia, *J. Agric. Food Chem.*, **46**, 25 (1998).
19. H. Kalkan Yildirim, *Int. J. Food Sci. Nutr.*, **57**, 47 (2006).
20. A. Ljevar, N. Čurko, M. Tomašević, Kr. Radošević, V. Gaurina Srček, K. Kovačević Ganić, *Food Technol. Biotechnol.*, **54 (2)**, 145 (2016).
21. M. N. Todorova, M. G. Pasheva, Y. D. Kiselova-Kaneva, *Bulg. Chem. Commun.*, **50**, 164 (2018).
22. P. Brat, S. George, A. Bellamy, L. D. Chaffaut, A. Scalbert, L. Mennen, et al., *Journal of Nutrition*, **136**, 2368 (2006).
23. H. Vuorinen, K. Määttä, R. Törrönen, *Journal of Agricultural and Food Chemistry*, **48(7)**, 2675 (2000).
24. A. Czyzowska, E. Pogorzelski, *European Food Research and Technology*, **218 (4)**, 355 (2004).
25. H. D. Belitz, W. Grosch, P. Schieberle, *Food Chemistry*. 4th revised and extended edn., Springer, Berlin, Heidelberg, 2009.
26. Commission Regulation (EC) No 1881/2006; Commission Regulation (EC) No 1410/2003 amending Regulation (EC) No 1622/2000 implementing Council Regulation (EC) No 1493/1999.
27. International Code of Oenological Practices (OIV), Annex maximum acceptable limits, 2015.
28. P. Pohl, *Analyt. Chem.*, **26**, 941 (2007).
29. D. Klaric, Il. Klaric, A. Mornar, D. Velic, N. Velic, *International Journal of Food Sciences and Nutrition*, (2016).
30. M. Pantelić, Dr. Dabić, S. Matijašević et al., *Scientific World Journal*, 454797, (2014).

Influence of electrolyte additives on the performance of the positive plates of lead batteries

A. Aleksandrova*, M. Matrakova, P. Nikolov

Institute of Electrochemistry and Energy Systems "Acad. Evgeni Budevski", Bulgarian Academy of Sciences, Acad. Georgi Bonchev Str., 1113 Sofia, Bulgaria

Received: November 17, 2021; Revised: February 28, 2022

In this work, different concentrations of sodium dodecyl sulfate (SDS) or cetyltrimethylammonium bromide (CTAB) were used as electrolyte additives in flooded laboratory test lead acid cells with 2 positive and 3 negative plates to evaluate the influence of the selected additives on the cycling performance of the positive plates at 17.5% DoD (depth-of-discharge) employing PSoC (partial state-of-charge) cycling protocol for automotive applications. On the basis of the obtained results the optimal concentrations of the tested surfactants SDS or CTAB in the electrolyte were established as follows: 600 ppm SDS and 100 ppm CTAB. These concentrations of the additives under test exert strong influence on the size of the individual PbO_2 particles, the volume of pores and the pore surface area. The experimental results demonstrate that the selected organic substances are promising for use as electrolyte additives for lead batteries that operate under partial-state-of-charge conditions.

Keywords: lead acid battery, positive electrode, positive active mass, surfactant, PSoC cycling, electrolyte additive

INTRODUCTION

New applications such as micro-hybrid cars, remote telecommunications and energy storage for renewables are placing strong demands upon lead acid batteries for improved charge-acceptance and extended service life under partial state-of-charge (PSoC) conditions. The main processes that lead to decline of the capacity and the cycle endurance of lead acid batteries are irreversible formation of PbSO_4 in the negative active mass (NAM), corrosion of positive electrode grids, positive active mass (PAM) degradation, loss of adherence to the grid and shedding, hydrogen and oxygen evolution reactions, etc. [1]. In the past decade the problems of NAM performance under PSoC cycling conditions were largely overcome by addition of carbon materials in the negative electrodes. Hence, the positive electrodes could become the limiting factor for further improvement of the cycling endurance of lead batteries. PAM has a complex structural organization – the very fine individual PbO_2 particles are interconnected into agglomerates which in turn are organized in aggregates. These structural elements form the pore system of PAM – comprising reaction and transport pores. The individual PbO_2 particles themselves have a complex structure consisting of gel and crystalline zones ensuring proton and electron conductivity, respectively. The equilibrium between the gel and crystalline zones is one of the key factors determining the discharge performance of PAM. In addition, the PbO_2 phase in PAM is present in two

polymorphic forms, alpha- and beta- PbO_2 , which in turn have different crystal morphology and electrochemical behavior [2]. One successful approach employed in lead battery science and technology to improve the capacity and cycle life or suppress the gas evolution reactions is the application of a variety of organic or inorganic substances as additives to the sulfuric acid electrolyte [3–16].

Surfactants are substances that modify the morphology and surface of crystals and can suppress gas evolution, and are widely used in different types of batteries. The influence of surfactants in an electrolyte on the structure and performance of PbO_2 electrodes for wastewater treatment has been extensively investigated in the literature [17–21]. Xiaoliang *et al.* studied the impact of sodium dodecyl sulfate (SDS) on the electro-catalytic performance and the stability of PbO_2 electrode and reported its beneficial effect [20]. Xiaoyue and co-workers used cetyltrimethylammonium bromide (CTAB) or lauryl benzene sulfonic acid sodium into the electrodeposition solution to prevent the aggregation of CNT and assist the doping of CNT into the PbO_2 film [22]. Ghavami *et al.* investigated the effect of surfactants on the sulfation of lead acid cell negative electrodes in high-rate-partial-state-of-charge (HRPSoC) duty and reported that SDS improved the cycle life and fine PbSO_4 crystals were formed, while CTAB surfactant exerted the opposite effect on the crystal morphology of the negative active mass [23]. Nikolov *et al.* [24]

* To whom all correspondence should be sent:
E-mail: albena.aleksandrova@iees.bas.bg

discussed the structural changes in the positive active mass during PSoC operation and the influence of electrolyte additives on the cycling endurance of lead batteries in automotive applications.

In our previous work [25, 26] we presented the obtained results about the effect of SDS or CTAB on the electrochemical behavior of lead acid battery alloys.

The focus of the present study is to evaluate the structural changes of the positive active mass during partial state-of-charge operation of lead batteries for automotive applications and to explore the effect of SDS or CTAB as additives to the sulfuric acid electrolyte solution aimed to improve the cycling performance of PAM.

EXPERIMENTAL

Materials

In this work, two types of surfactants, anionic sodium dodecyl sulphate (SDS) and cationic cetyltrimethylammonium bromide (CTAB), were used as electrolyte additives in lead test cells. Sulfuric acid (95-98%), SDS (> 98.5%) and CTAB (> 99%) were supplied by Sigma-Aldrich. Three concentrations of the additives in $1.28 \text{ cm}^3 \cdot \text{g}^{-1}$ H_2SO_4 aqueous solution were tested, as follows: 240 ppm, 600 ppm and 1200 ppm of SDS; and 100 ppm, 240 ppm and 500 ppm of CTAB, respectively.

Electrodes manufacture and test cell design

Positive and negative paste batches were produced using ball mill type leady oxide. The negative paste composition was as follows: 0.5 wt.% carbon material (PBX51, Cabot Corp. (USA)), 0.2 wt.% lignosulfonate additive (Vanisperse-A, Borregaard LignoTech (USA)) and 0.8 wt.% BaSO_4 (Blank Fixe N, Solvay, (Belgium)) The positive paste contained no additives. The thus produced positive and negative pastes were used for pasting small Pb-0.06Ca-1.25Sn alloy grids marked as PbCa grids. The positive plates were wrapped in polyethylene separator (Daramic (USA)) with ribs facing the negative plates. Flooded laboratory test cells with 2 positive and 3 negative plates per cell were used to evaluate the influence of the selected electrolyte additives on the electrochemical performance of the positive plates. The obtained plates were subjected to standard and widely accepted by the industry curing, drying and formation processes suitable for 3BS paste technology.

Performance tests and characterization

Testing was conducted using 2V flooded test cells with 2 positive and 3 negative plates per cell and rated (nominal) capacity of 4.0 Ah at 20 h rate of discharge and 50% utilization of the positive active mass (PAM). Thus, the performance parameters of the cells were limited by the positive plates. Each investigated surfactant was dissolved in $1.28 \text{ cm}^3 \cdot \text{g}^{-1}$ H_2SO_4 solution and after complete formation of both the positive and negative electrodes, the cells were refilled with doped solutions. Control cells (blank) with no additives to the electrolyte were also assembled. Initial capacity tests comprising three consecutive C_{20} (the energy a battery can deliver continuously for 20 hours) discharge-charge cycles were performed and after that the test cells were subjected to cycling endurance test at 17.5% DoD (depth-of-discharge) according to the EN 50324-6 protocol, but without capacity checks after every 85 cycles. All above mentioned tests were performed at a temperature of 25°C . At the end-of-life of each of test cells, the cell was disassembled and the positive and negative plates were washed under running water. The positive plates were dried in a thermo-chamber, while the negative plates were immediately put in and dried in thermo-chamber under nitrogen atmosphere in order to avoid oxidation of the negative active mass (NAM).

The powder X-ray diffraction patterns of the tested active masses were recorded on an X-ray diffractometer APD 15 Philips 2134 (Cu $K\alpha$ radiation). The structure and crystal morphology of the active masses was observed on a JEOL 200 CX scanning electron microscope. The samples taken from the cells under test were set also to Hg porosimetry (MICROMERITICS AutoPore 9200) to estimate the pore volume distribution by pore radius of the positive active masses.

RESULTS AND DISCUSSION

Figure 1 presents the results of the initial C_{20} capacity tests of lead cells with different concentrations of the tested surfactants in the electrolyte. The obtained results indicate that, in the case of cells with SDS doped electrolyte, increase of SDS concentration results in reduction of C_{20} discharge capacity by about 15%. Addition of CTAB to the electrolyte has a negligible effect on C_{20} discharge capacity. All tested cells exhibit a progressive decline in C_{20} discharge capacity from cycle to cycle, except the blank cell. Yet, all tested cells have higher initial capacities than the rated values and exhibit C_{20} capacity performance better than 120% of the nominal capacity value.

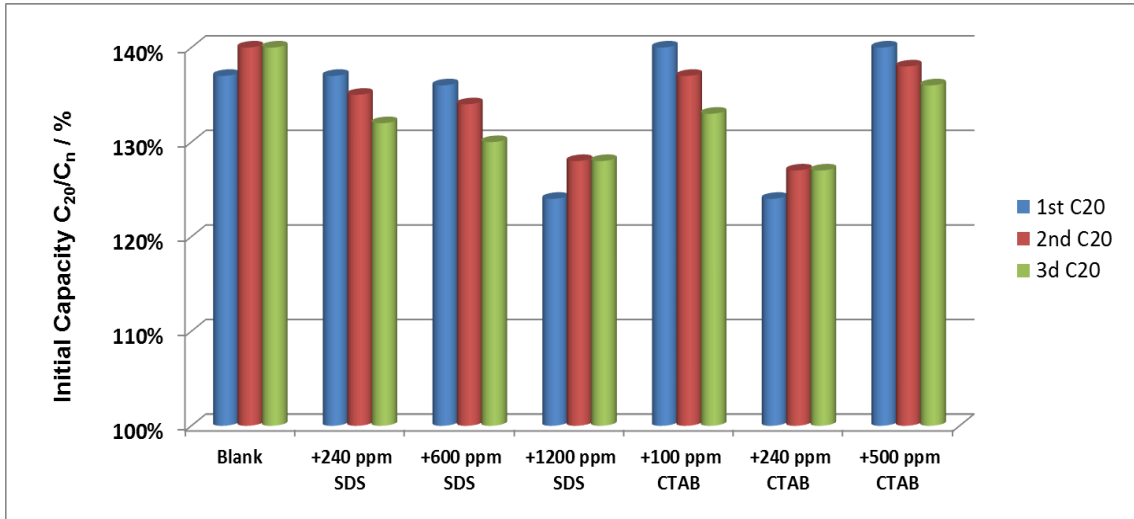


Figure 1. Initial C₂₀ capacities of test cells with blank or surfactant-doped solutions. Values are reported as percent of actual versus rated discharge capacity.

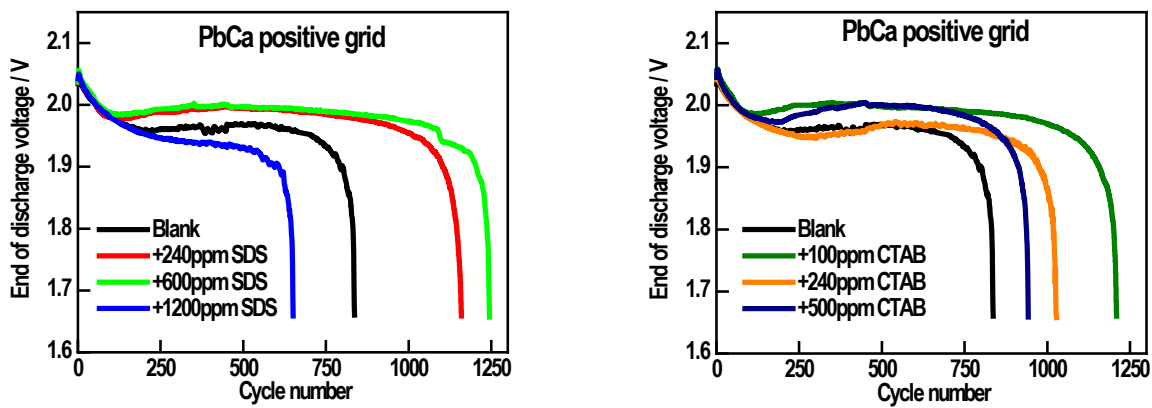


Figure 2. Changes in end-of-discharge voltage of test cells with different electrolyte additives cycled continuously with 17.5% DoD.

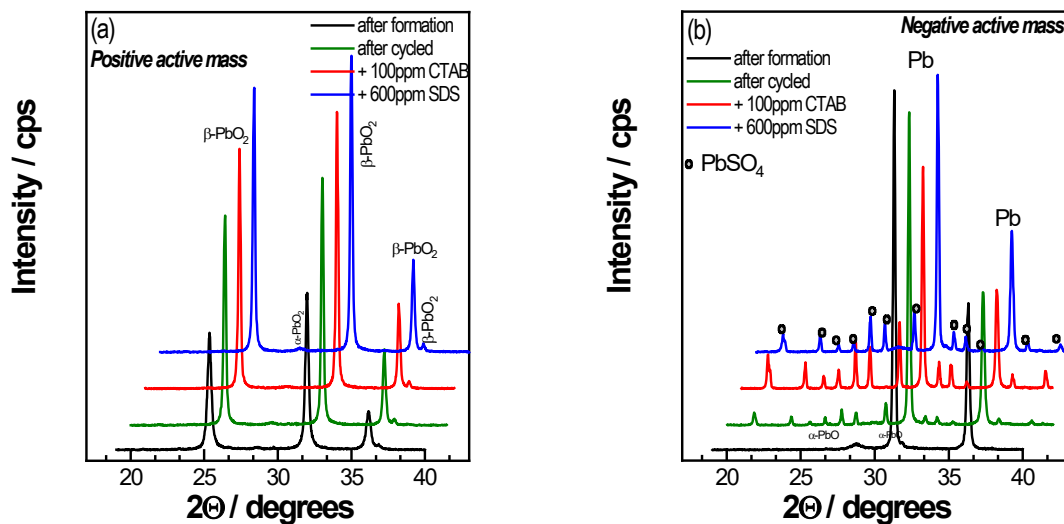


Figure 3. XRD patterns of different active mass samples after the cycling test: (a) PAM and (b) NAM.

Figure 2 illustrates the end-of-discharge voltage course during the cycling test of the cells containing the studied additives in the electrolyte. The cut-off voltage limit of the test was 1.65V.

The experimental results evidence that the cell with blank electrolyte endures 800 cycles. The differences in end-of-discharge voltage course during PSoC cycling suggest that SDS and CTAB

and their loading concentrations have their own specific effect on the processes in PAM. The left-hand figure shows that the dependence of the number of completed PSoC cycles as a function of dosage levels of SDS in the electrolyte passes through a maximum at 600 ppm additive load. Increase of CTAB concentration in the cell electrolyte above 100 ppm has negative impact on PSoC cycling endurance.

The phase composition of freshly formed and cycled PAM and NAM samples was determined by X-ray diffraction analysis. Figure 3 summarizes the XRD patterns recorded for NAM and PAM samples taken from the blank and the best performed doped test cells.

The intensity of the beta-PbO₂ [1 1 0] and [0 1 1] peaks is affected by both, the number of completed cycles and the type of studied electrolyte additives. The obtained XRD patterns of the cycled PAM samples taken from different test cells evidence that these peaks have twice higher

intensity than that of the freshly formed PAM sample.

As can be seen from the data in Fig.3b, the NAM sample taken from the cycled blank cell contains the lowest amount of PbSO₄. This finding is related to the smallest number of completed cycles during the PSoC cycling test. The XRD peaks of lead sulfate phase for NAM samples cycled in the presence of 100 ppm CTAB or 600 ppm SDS have more than twice higher intensity. Yet, these are the cells that endure the highest number of PSoC cycles. As is well known, in battery applications under PSoC conditions, insoluble PbSO₄ crystals accumulate on the surface of the negative electrodes.

The effect of number of completed PSoC cycles and studied electrolyte additives on PAM and NAM morphology was observed by scanning electron microscopy. Figure 4 compares the microstructure of the positive plate interior of freshly formed and cycled PAM samples at two different magnifications.

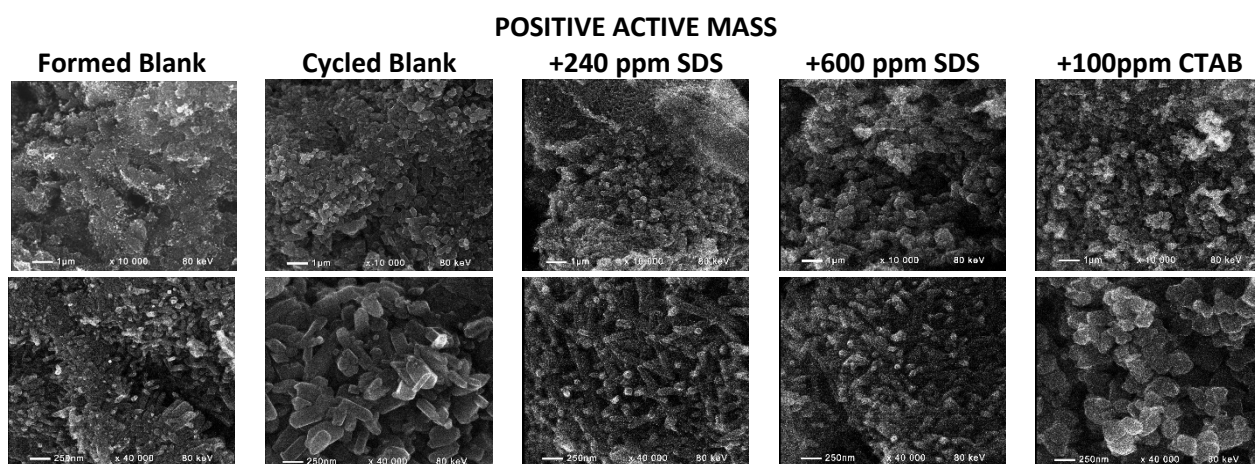


Figure 4. Scanning electron microscopy images of freshly formed and cycled PAM samples taken from different test cells.

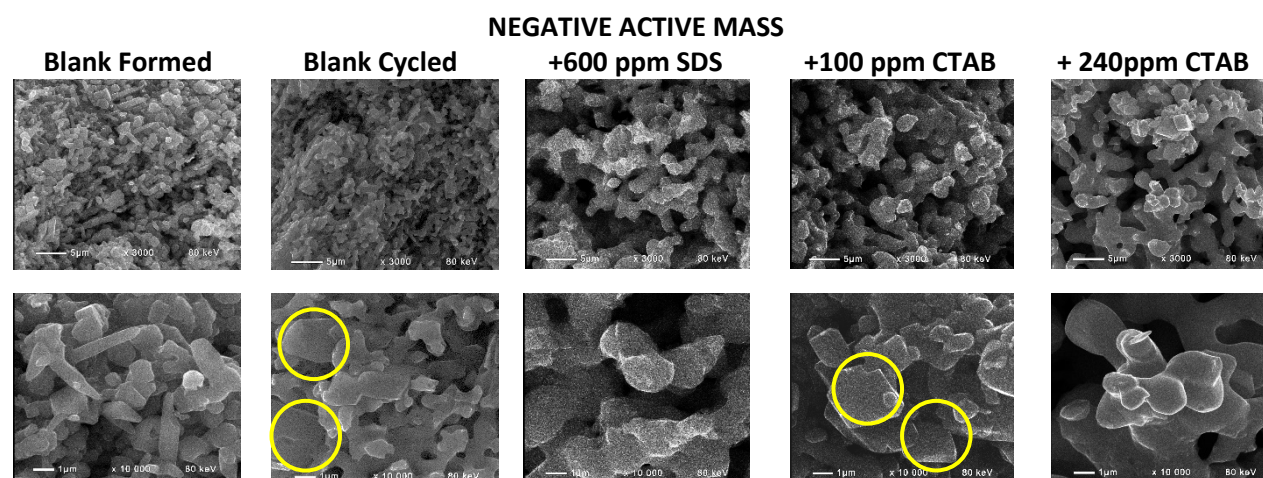


Figure 5. Scanning electron microscopy images of freshly formed and cycled NAM samples taken from different test cells. The yellow circles on the images mark PbSO₄ crystals in the NAM interior.

The SEM images of the freshly formed PAM sample feature very fine individual needle-like PbO_2 particles (about few nm in size), tightly interconnected in agglomerates (1-2 μm in size), which in turn are grouped together into aggregates (10-20 μm in size). The morphology of the cycled blank PAM samples differs completely. The individual PbO_2 particles are rounded in shape and much bigger in size (100-500 nm) and the connection between the particles is loose. The crystal morphology of PAM samples cycled in the presence of 240 ppm CTAB or 600 ppm of SDS features fine individual stick-like PbO_2 particles (200-250 nm in length). Analogous effect of SDS on the microstructure of PbO_2 crystals was mentioned by Xiaoliang *et al.* and Amadelli *et al.* when modified PbO_2 electrode was synthesized by electro-deposition method. [20, 27]. O. Shmychkova *et al.* and R. Munoz-Espi *et al.* have explained that surfactant additives selectively adsorb on the surface and reduce the growth of crystals and thereby alter their shape and size [28, 29].

The morphology of PbO_2 crystals of the 100 ppm CTAB PAM sample (Fig. 4) is similar to that of the cycled blank sample. The most significant visible difference is the presence of well-formed pores between the aggregates in the interior of the 100 ppm CTAB PAM sample. The sample doped with 240 ppm SDS is characterized by compact structure. The SEM images of PAM samples cycled in the presence of 1200 ppm of SDS or 500 ppm of CTAB feature structures similar to that of the cycled blank sample. Probably, at these higher concentration levels of the additives in H_2SO_4 aqueous solution, the molecules of the tested surfactants self-organize in a supramolecular assembly, as a result of which their influence on the processes of PbO_2 crystallization weakens.

Figure 5 presents scanning electron microphotographs of freshly formed and cycled NAM samples at two different magnifications. The SEM images indicate that, despite the considerable amount of PbSO_4 phase detected in the negative plates by XRD, the NAM interior contains predominantly Pb phase. Hence, it can be assumed that the PbSO_4 crystals are concentrated mainly in regions close to the surface of the negative plate, which is a typical failure mode for lead batteries operated at PSoC conditions. Normally, PbSO_4 crystals are about 5 μm big in size and have well shaped walls, edges, and apexes and sometimes are incorporated in the network structure of Pb. The cycled black NAM sample features very compact structure built of irregularly shaped Pb crystals. The

studied electrolyte additives have similar effect on the morphology of the Pb crystals. Both SDS and CTAB surfactants provoke a change of the typical NAM energetic structure to a more skeleton-like one as observed in the SEM images of the electrolyte doped samples. It is clearly evident that, in the presence of surfactant, the NAM microstructure features significantly higher open porosity as compared to the blank NAM sample.

Hg porosimetry was employed to evaluate the combined effect of the studied additives and the ageing processes due to the employed cycling profile on the characteristics of the PAM pore system. The graphic plots in Figure 6 summarize the cumulative pore volume as a function of the pore radius for PAM samples from the cells with different concentrations of the studied surfactants in the electrolyte.

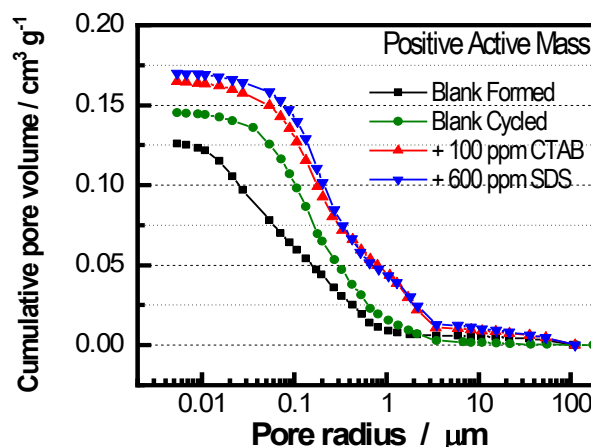


Figure 6. Cumulative pore volume and pore size distribution of different PAM samples obtained by Hg porosimetry.

PSoC cycling with 17.5% DoD has a notable effect on the characteristics of the PAM pore system. The total pore volume of the cycled blank PAM sample increases because of opening of new pores with radii in the range of 0.1 to 1.0 μm as compared to the freshly formed sample. Thus, the ratio of submicron to micron sized pores decreases. This observation is more pronounced for PAM samples cycled in the electrolyte doped with 100 ppm CTAB or 600 ppm SDS.

CONCLUSIONS

On grounds of the obtained results of the present study, it can be concluded that the optimal concentrations of the tested surfactants SDS or CTAB in the electrolyte of lead cells are 600 ppm of SDS and 100 ppm of CTAB. The cells doped with 600 ppm of SDS or 100 ppm of CTAB exhibit an improvement by more than 25% in initial

capacity and cycle life performance vs. the blank electrolyte cell.

Both CTAB and SDS additives exert strong influence on the size of the individual PbO₂ particles. The studied surfactants are promising for use as electrolyte additives for lead batteries that operate under partial-state-of-charge conditions.

REFERENCES

1. P. Ruetschi, *J. Power Sources*, **127**, 33 (2004).
2. D. Pavlov, *Lead-Acid Batteries: Science and Technology*, 2nd edn., Elsevier, 2017.
3. S. Tudor, A. Weisstuch, S. H. Davang, *Electrochem. Technol.*, **5**, 21 (1967).
4. J. Burbank, *J. Electrochem. Soc.*, **111**, 1112 (1964).
5. B. K. Mahato, *J. Electrochem. Soc.*, **126**, 369 (1979).
6. E. Voss, *J. Power Sources*, **24**, 171 (1988).
7. H. A. Laitinen, N. Walkins, *Anal. Chem.*, **47**, 1353 (1975).
8. K. R. Bullock, *J. Electrochem. Soc.*, **126**, 1848 (1979).
9. E. Meissner, *J. Power Sources*, **67**, 135 (1997).
10. K. Saminathan, N. Jayaprakash, B. Rajeswari, T. Vasudevan, *J. Power Sources*, **160**, 1410 (2006).
11. C. Bemelmans, T. O'Keefe, E. Cole, *Bull. Electrochem.*, **12**, 591 (1996).
12. T. C. Wen, M. G. Wei, K. L. Lin, *J. Electrochem. Soc.*, **137**, 2700 (1990).
13. Y. Sato, K. Hishimoto, K. Togashi, H. Yanagawa, K. Kobayakawa, *J. Power Sources*, **39**, 43 (1992).
14. Z. Shi, Y.-H. Zhou, C.-S. Cha, *J. Power Sources*, **70**, 205 (1998).
15. L. Torcheux, C. Rouvet, J. P. Vaurijoux, *J. Power Sources*, **78**, 147 (1999).
16. A. Tizpar, Z. Ghasemi, *Appl. Surface Science*, **252**, 8630 (2006).
17. C. Comninellis, *Electrochim. Acta*, **39**, 1857 (1994).
18. M. Panizza, G. Cerisola, *Chem. Rev.*, **109**, 6541 (2009).
19. J. Niu, Y. Li, E. Shang, Z. Xu, J. Liu, *Chemosphere*, **146**, 526 (2016).
20. L. Xiaoliang, X. Hao, Y. Wei, *J. Alloy. Compd.*, **718**, 386 (2017).
21. N. Boudieb, M. Bounoughaz, A. Bouklachi, *Proc.-Soc. Behav. Sci.*, **195**, 1618 (2015).
22. Xiaoyue D., Fang M., Zhongxin Y., Limin C, Xintong J., *J. Electroanalytical Chemistry*, **677–680**, 90 (2012).
23. R. K. Ghavami, F. Kameli, A. Shirojan, A. Azizi, *J. Energy Storage*, **17**, 170 (2018).
24. P. Nikolov, M. Matrakova, A. Aleksandrova, *Proc. 11th Int. Conference on Lead-Acid Batteries - LABAT'2021(Extended Abstracts)*, 8-11 June, Virtual Conference, 63 (2021).
25. M. Matrakova, A. Aleksandrova, P. Nikolov, O. Saoudi, L. Zerroual, *Bulgarian Chemical Communications*, **52 A**, 74 (2020).
26. O. Saoudi, M. Matrakova, A. Aleksandrova, L. Zerroual, *Arabian Journal of Chemistry*, **13**, 5326 (2020).
27. R. Amadelli, L. Samiolo, A. B. Velichenko, V. A. Knysh, T. V. Luk'yanenko, F. I. Danilov, *Electrochimica Acta*, **54**, 5239 (2009).
28. O. Shmychkova, T. Luk'yanenko, A. Velichenko, *ECS Trans.*, **77**, 1617 (2017).
29. R. Munoz-Espi, Y. Mastai, S. Gross, K. Landfester, *Cryst. Eng. Comm.*, **15**, 2175 (2013).

Absorption-adsorption method for waste-free decontamination of gases from SO₂

P. G. Popova-Krumova*, Chr. B. Boyadjiev, B. Chr. Boyadjiev

Institute of Chemical Engineering, Bulgarian Academy of Sciences, Acad. St. Angelov Str. 103, 1113 Sofia, Bulgaria

Received: November 11, 2021; Revised: April 20, 2022

In the paper a theoretical approach to model the absorption-adsorption processes for waste-free decontamination of gases from SO₂ is presented. A new method for waste gas purification is realized in two steps: physical absorption of SO₂ with water and chemical adsorption of HSO₃⁻ from the water solution by synthetic anionite particles. The adsorbent regeneration is made with NH₄OH solution. The obtained (NH₄)₂SO₃ (NH₄HSO₃) is used (after reaction with HNO₃) for production of concentrated SO₂ (gas) and NH₄NO₃ (solution). Convection-diffusion and average concentration models of the absorption and adsorption processes are presented.

Keywords: Absorption, adsorption, average concentration model, convection-diffusion model, gas purification, SO₂.

INTRODUCTION

One of the main pollutants in the atmosphere is SO₂. Fossil fuel thermal power plants are considered to be the main source of SO₂ emissions. In industry, the sources are metallurgy, chemical industry and others. In recent years, the increased content of SO₂ in the atmosphere has led to the search for new engineering solutions and cost-effective methods to reduce it. The problem of purification of waste gases from SO₂ focuses the interest of researchers, as its relevance increases over time, changing from technical and economic to environmental.

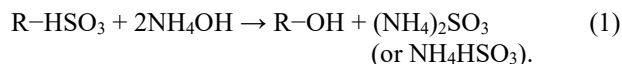
Different companies (Babcock & Wilcox Power Generation Group, Inc., Alstom Power Italy, Idreco-Insigma-Consortium) propose methods and apparatuses for waste gases purification from SO₂ using a two-phase absorbent (CaCO₃ suspension). The adsorption (absorption) of SO₂ on materials derived from natural carbonates [1–3] has the drawback of waste accumulation. The basic problem of the carbonate absorbents is that its chemical reaction with SO₂ leads to CO₂ emission (every molecule of SO₂ absorbed from the air is equivalent to a molecule of CO₂ emitted in the air), because the ecological problems (greenhouse effects) of SO₂ and CO₂ are similar. The large quantity of by-products is a problem, too. Another drawback of these methods is the impossibility for regeneration of the absorbents.

The theoretical analysis [4–10] of the method and apparatus for waste gases purification from SO₂ using a two-phase absorbent (CaCO₃ suspension) shows that the process in the absorption column in the gas-liquid drops flow is practically physical absorption as a result of the low concentration of the dissolved CaCO₃ and SO₂ in the drops and its brief existence in the gas-liquid dispersion. An increase of

the process efficiency is proposed in the patent [11], where an absorption column with two absorption zones (lower liquid-gas bubbles zone and upper gas-liquid drops zone) is used. This creates a possibility to increase the absorption degree or to lower the column height. Many developments are dedicated to improving the design of the apparatuses for obtaining products and quality control to expand their application [12–15].

The difficulties in the purification of SO₂ gases in the energy sector stem from its low concentration (0.1 - 0.5% vol.) and high waste gas flows. One of the possibilities for their solution is the use of regenerable sorbents. The use of synthetic anionites (basic anion-exchange resins - R-OH form of Amberlite, Duolite, Kastel, Varion, Wofatit) as adsorbents [16–18] for gas purification from SO₂ provides possibilities for adsorbent regeneration. The chemical reaction of SO₂ with the synthetic anionites can be presented by the stoichiometric equation: SO₂ + R-OH → R-HSO₃.

After saturation of the synthetic anionite particles with sulfur dioxide, the adsorbent regeneration can be carried out with a water solution of NH₄OH:



In the presented method [19] the adsorption is realized in the gas phase, while the adsorbent regeneration is realized in the liquid phase.

In this scientific research, a theoretical absorption-adsorption approach is proposed to solve the problem of waste gases purification from SO₂.

Absorption-adsorption approach

The main disadvantages of the CaCO₃ suspension method – CO₂ emission, gypsum accumulation and

* To whom all correspondence should be sent.
E-mail: petyabs@yahoo.com

The main processes in the absorption-adsorption method are the physical absorption of SO₂ by H₂O in a counter-current gas-liquid drops system and a chemical adsorption of SO₂ by synthetic anionite particles in a liquid-solid system.

Absorption-adsorption modeling

The modeling of a non-stationary (as a result of the adsorbent saturation) absorption-adsorption cycle of the method for gas purification from SO₂ uses a combination of the physical absorption and chemical adsorption models [20]:

$$\begin{aligned} \frac{\partial c_1}{\partial t} + u_1 \frac{\partial c_1}{\partial z_1} &= D_1 \left(\frac{\partial^2 c_1}{\partial z_1^2} + \frac{1}{r_1} \frac{\partial c_1}{\partial r_1} + \frac{\partial^2 c_1}{\partial r_1^2} \right) - k_0 (c_1 - \chi c_2); \\ \frac{\partial c_2}{\partial t} + u_2 \frac{\partial c_2}{\partial z_2} &= D_2 \left(\frac{\partial^2 c_2}{\partial z_2^2} + \frac{1}{r_1} \frac{\partial c_2}{\partial r_1} + \frac{\partial^2 c_2}{\partial r_1^2} \right) + k_0 (c_1 - \chi c_2); \\ t = 0, \quad c_1 &\equiv c_1^0, \quad c_2 \equiv 0; \\ r_1 = 0, \quad \frac{\partial c_1}{\partial r_1} &= \frac{\partial c_2}{\partial r_1} \equiv 0; \quad r_1 = r_{10}, \quad \frac{\partial c_1}{\partial r_1} = \frac{\partial c_2}{\partial r_1} \equiv 0; \\ z_1 = 0, \quad c_1(r_1, 0) &\equiv c_1^0, \quad u_1^0 c_1^0 \equiv u_1(r_1) c_1^0 - D_1 \left(\frac{\partial c_1}{\partial z_1} \right)_{z_1=0}; \\ z_2 = 0, \quad c_2(r_1, 0) &\equiv \bar{c}_2(l_2), \\ u_2^0 \bar{c}_2(l_2) &\equiv u_2(r_1) \bar{c}_2(l_2) - D_2 \left(\frac{\partial c_2}{\partial z_2} \right)_{z_2=0}. \end{aligned} \quad (4)$$

$$\begin{aligned} \frac{\partial c_{12}}{\partial t} + u \frac{\partial c_{12}}{\partial z} &= D_{12} \left(\frac{\partial^2 c_{12}}{\partial z^2} + \frac{1}{r} \frac{\partial c_{12}}{\partial r_2} + \frac{\partial^2 c_{12}}{\partial r_2^2} \right) - k_1 (c_{12} - c_{13}); \\ \frac{dc_{13}}{dt} &= k_1 (c_{12} - c_{13}) - kc_{13}c_{23} = 0; \quad \frac{dc_{23}}{dt} = -kc_{13}c_{23}; \\ t = 0, \quad c_{12} &\equiv 0, \quad c_{13} \equiv 0, \quad c_{23} \equiv c_{23}^0; \\ r_2 = 0, \quad \frac{\partial c_{12}}{\partial r_2} &\equiv 0; \quad r_2 = r_{20}, \quad \frac{\partial c_{12}}{\partial r_2} \equiv 0; \\ z = 0, \quad c_{12}(r_2, 0) &\equiv \bar{c}_2(l_1), \\ u^0 \bar{c}_2(l_1) &\equiv u(r_2) \bar{c}_2(l_1) - D_{12} \left(\frac{\partial c_{12}}{\partial z} \right)_{z=0}. \end{aligned} \quad (5)$$

In the absorber model (4) c_1, c_2, D_1, D_2 are the concentrations and diffusivities of SO₂ in the gas and liquid phases, u_1, u_2 – the velocities in the gas and liquid phases, r_1, l_1 – the radius and height of the working zone of the column, t – the time. In the adsorber model (5) c_{12}, D_{12} are the concentration and diffusivity of SO₂ in the liquid phase in the adsorber, c_{13}, c_{23} – the concentrations of SO₂ and active sides in the adsorbent, u – the velocity in the liquid phases, r_2, l_2 – the radius and height of the working zone of the column, t – the time. In the absorption-adsorption cycle the average outlet concentration of

SO₂ in the liquid phase of the absorber is the inlet concentration of SO₂ in the liquid phase of the adsorber ($c_{12}(r_2, 0) \equiv \bar{c}_2(l_1)$), while the average outlet concentration of SO₂ in the liquid phase of the adsorber is the inlet concentration of SO₂ in the liquid phase of the absorber ($c_2(r_1, 0) \equiv \bar{c}_2(l_2)$).

Generalized analysis

The use of dimensionless (generalized) variables [20-22] allows to make a qualitative analysis of the models (4, 5), whereas characteristic scales are used for the average velocity, the inlet and initial concentrations, the characteristic time t_0 (saturation time of the adsorbent) and the column's dimensions (r_1, r_2, l_1, l_2):

$$\begin{aligned} T &= \frac{t}{t_0}, \quad R_1 = \frac{r_1}{r_{10}}, \quad R_2 = \frac{r_2}{r_{20}}, \\ Z &= \frac{z}{l_2}, \quad Z_1 = \frac{z_1}{l_1}, \quad Z_2 = \frac{z_2}{l_1}, \\ U &= \frac{u}{u^0}, \quad U_1 = \frac{u_1}{u_1^0}, \quad U_2 = \frac{u_2}{u_2^0}, \quad C_1 = \frac{c_1}{c_1^0}, \quad C_2 = \frac{c_2}{c_1^0}, \\ C_{12} &= \frac{c_{12}}{c_1^0}, \quad C_{13} = \frac{c_{13}}{c_1^0}, \quad C_{23} = \frac{c_{23}}{c_{23}^0}. \end{aligned} \quad (6)$$

When (6) is put into (4) and (5), the models in generalized variables take the form:

$$\begin{aligned} \gamma_1 \frac{\partial C_1}{\partial T} + U_1 \frac{\partial C_1}{\partial Z_1} &= \\ &= \text{Fo}_1 \left(\beta_1 \frac{\partial^2 C_1}{\partial Z_1^2} + \frac{1}{R_1} \frac{\partial C_1}{\partial R_1} + \frac{\partial^2 C_1}{\partial R_1^2} \right) - K_1 (C_1 - C_2); \\ \gamma_2 \frac{\partial C_2}{\partial T} + U_2 \frac{\partial C_2}{\partial Z_2} &= \\ &= \text{Fo}_2 \left(\beta_1 \frac{\partial^2 C_2}{\partial Z_2^2} + \frac{1}{R_1} \frac{\partial C_2}{\partial R_1} + \frac{\partial^2 C_2}{\partial R_1^2} \right) + K_2 (C_1 - C_2); \\ T = 0, \quad C_1 &\equiv 1, \quad C_2 \equiv 0; \\ R_1 = 0, \quad \frac{\partial C_1}{\partial R_1} &= \frac{\partial C_2}{\partial R_1} \equiv 0; \\ R_1 = 1, \quad \frac{\partial C_1}{\partial R_1} &= \frac{\partial C_2}{\partial R_1} \equiv 0; \\ Z_1 = 0, \quad C_1(R_1, 0) &\equiv 1, \quad 1 \equiv U_1(R_1) - \text{Pe}_1^{-1} \left(\frac{\partial C_1}{\partial Z_1} \right)_{Z_1=0}; \\ Z_2 = 0, \quad C_2(R_1, 0) &\equiv \bar{C}_2(1), \\ 1 \equiv U_2(R_1) - \frac{\text{Pe}_2^{-1}}{C_{12}(1)} D_2 \left(\frac{\partial C_2}{\partial Z_2} \right)_{Z_2=0}. \end{aligned} \quad (7)$$

$$\begin{aligned}
 & \gamma_0 \frac{\partial C_{12}}{\partial T} + U \frac{\partial C_{12}}{\partial Z} = \\
 & = \text{Fo}_0 \left(\beta_0 \frac{\partial^2 C_{12}}{\partial Z^2} + \frac{1}{R_2} \frac{\partial C_{12}}{\partial R_2} + \frac{\partial^2 C_{12}}{\partial R_2^2} \right) - K_0 (C_{12} - C_{13}); \\
 & \frac{dC_{13}}{dT} = K_3 (C_{12} - C_{13}) - K_4 C_{13} C_{23} = 0; \\
 & \frac{dC_{23}}{dT} = -K_5 C_{13} C_{23}; \\
 & T = 0, \quad C_{12} \equiv 0, \quad C_{13} \equiv 0, \quad C_{23} \equiv 1; \\
 & R_2 = 0, \quad \frac{\partial C_{12}}{\partial R_2} \equiv 0; \quad R_2 = 1, \quad \frac{\partial C_{12}}{\partial R_2} \equiv 0; \\
 & Z = 0, \quad C_{12}(R_2, 0) \equiv \bar{C}_2(1), \\
 & 1 \equiv U(R_2) - \frac{\text{Pe}_0^{-1}}{C_2(1)} \left(\frac{\partial C_{12}}{\partial Z} \right)_{Z=0}.
 \end{aligned} \tag{8}$$

The following parameters are used in (7), (8):

$$\begin{aligned}
 K_0 &= \frac{k_1 l_2}{u^0}, \quad K_1 = \frac{k_0 l_1}{u_1^0}, \quad K_2 = \frac{k_0 l_1 \chi}{u_2^0}, \quad K_3 = k_1 t_0, \\
 K_4 &= k t_0 c_{23}^0, \quad K_5 = k t_0 \frac{c_1^0}{\chi}, \quad \beta_0 = \frac{r_{20}^2}{l_2^2}, \quad \beta_1 = \frac{r_{10}^2}{l_1^2}, \\
 \gamma_0 &= \frac{l_2}{t_0 u^0}, \quad \gamma_1 = \frac{l_1}{t_0 u_1^0}, \quad \gamma_2 = \frac{l_1}{t_0 u_2^0}, \\
 \text{Fo}_0 &= \frac{D_2 l_2}{u^0 r_{20}^2}, \quad \text{Fo}_1 = \frac{D_1 l_1}{u_1^0 r_{10}^2}, \quad \text{Fo}_2 = \frac{D_2 l_1}{u_2^0 r_{10}^2}, \\
 \bar{C}_2(1) &= 2 \int_0^1 R_1 C_2(R_1, 1) dR_1, \quad \bar{C}_{12}(1) = 2 \int_0^1 R_2 C_{12}(R_2, 1) dR_2.
 \end{aligned} \tag{9}$$

For lengthy processes ($0 = \gamma_0 \sim \gamma_1 \sim \gamma_2 \leq 10^{-2}$), high columns ($0 = \beta_0 \sim \beta_1 \leq 10^{-2}$) and typical fluid velocities ($0 = \text{Fo}_0 \sim \text{Fo}_1 \sim \text{Fo}_2 \leq 10^{-2}$) the model has the form:

$$\begin{aligned}
 U_1 \frac{dC_1}{dZ_1} &= -K_1 (C_1 - C_2); \quad Z_1 = 0, \quad C_1(R_1, 0) \equiv 1; \\
 U_2 \frac{dC_2}{dZ_2} &= K_2 (C_1 - C_2); \quad Z_2 = 0, \quad C_2(R_1, 0) \equiv \bar{C}_{12}(1). \\
 U \frac{dC_{12}}{dZ} &= -K_0 (C_{12} - C_{13}); \\
 \frac{dC_{13}}{dT} &= K_3 (C_{12} - C_{13}) - K_4 C_{13} C_{23} = 0; \\
 \frac{dC_{23}}{dT} &= -K_5 C_{13} C_{23}; \\
 Z = 0, \quad C_{12}(R_2, 0) &\equiv \bar{C}_2(1); \\
 T = 0, \quad C_{13} \equiv 0, \quad C_{23} &\equiv 1.
 \end{aligned} \tag{10}$$

Average-concentration model

The presented models (10, 11) show that in the practical cases convective type of models have to be used:

$$\begin{aligned}
 u_1 \frac{dc_1}{dz_1} &= -k_0 (c_1 - \chi c_2); \quad z_1 = 0, \quad c_1(t, r_1, 0) \equiv c_1^0; \\
 u_2 \frac{dc_2}{dz_2} &= k_0 (c_1 - \chi c_2); \quad z_2 = 0, \quad c_2(t, r_1, 0) \equiv \bar{c}_{12}(t, l_2). \\
 u \frac{dc_{12}}{dz} &= -k_1 (c_{12} - c_{13}); \\
 \frac{dc_{13}}{dt} &= k_1 (c_{12} - c_{13}) - k c_{13} c_{23} = 0; \\
 \frac{dc_{23}}{dt} &= -k c_{13} c_{23}; \\
 z = 0, \quad c_{12}(t, r_2, 0) &\equiv \bar{c}_2(t, l_1); \\
 t = 0, \quad c_{13}(0, r_2, z) &\equiv 0, \quad c_{23}(0, r_2, z) \equiv c_{23}^0.
 \end{aligned} \tag{11}$$

The average values of the velocities and concentrations in the column's cross-sectional area can be obtained [20-22] using the expressions:

$$\begin{aligned}
 \bar{u} &= \frac{2}{r_{20}^2} \int_0^{r_{20}} r_2 u(r_2) dr_2 = u^0, \\
 \bar{u}_1 &= \frac{2}{r_{10}^2} \int_0^{r_{10}} r_1 u_1(r_1) dr_1 = u_1^0, \\
 \bar{u}_2 &= \frac{2}{r_{10}^2} \int_0^{r_{10}} r_1 u_2(r_1) dr_1 = u_2^0, \\
 \bar{c}_1(t, z_1) &= \frac{2}{r_{10}^2} \int_0^{r_{10}} r_1 c_1(t, r_1, z_1) dr_1, \\
 \bar{c}_2(t, z_2) &= \frac{2}{r_{10}^2} \int_0^{r_{10}} r_1 c_2(t, r_1, z_2) dr_1, \\
 \bar{c}_{12}(t, z) &= \frac{2}{r_{20}^2} \int_0^{r_{20}} r_2 c_{12}(t, r_2, z) dr_2, \\
 c_{13}(t, z) &= \frac{2}{r_{20}^2} \int_0^{r_{20}} r_2 c_{13}(t, r_2, z) dr_2, \\
 \bar{c}_{23}(t, z) &= \frac{2}{r_{20}^2} \int_0^{r_{20}} r_2 c_{23}(t, r_2, z) dr_2.
 \end{aligned} \tag{12}$$

The velocities and concentration distributions in (12) and (13) can be presented with the help of the average functions (14):

$$\begin{aligned}
 u(r_2) &= \bar{u} \bar{u}(r_2), \quad u_1(r_1) = \bar{u}_1 \bar{u}_1(r_1), \\
 u_2(r_1) &= \bar{u}_2 \bar{u}_2(r_1), \\
 c_1(t, r_1, z_1) &= \bar{c}_1(t, z_1) \tilde{c}_1(t, r_1, z_1), \\
 c_2(t, r_1, z_2) &= \bar{c}_2(t, z_2) \tilde{c}_2(t, r_1, z_2), \\
 c_{12}(t, r_2, z) &= \bar{c}_{12}(t, z) \tilde{c}_{12}(t, r_2, z), \\
 c_{13}(t, r_2, z) &= \bar{c}_{13}(t, z) \tilde{c}_{13}(t, r_2, z), \\
 c_{23}(t, r_2, z) &= \bar{c}_{23}(t, z) \tilde{c}_{23}(t, r_2, z).
 \end{aligned} \tag{13}$$

Here $\tilde{u}(r_2)$, $\tilde{u}_1(r_1)$, $\tilde{u}_2(r_1)$, $\tilde{c}_1(t, r_1, z_1)$, $\tilde{c}_2(t, r_1, z_2)$, $\tilde{c}_{12}(t, r_2, z)$, $\tilde{c}_{13}(t, r_2, z)$, $\tilde{c}_{23}(t, r_2, z)$ present the radial non-uniformity of the velocity and the concentration distributions satisfying the conditions:

$$\begin{aligned} \frac{2}{r_{20}^2} \int_0^{r_{20}} r_2 \tilde{u}(r_2) dr_2 &= 1, & \frac{2}{r_{10}^2} \int_0^{r_{10}} r_1 \tilde{u}_1(r_1) dr_1 &= 1, \\ \frac{2}{r_{10}^2} \int_0^{r_{10}} r_1 \tilde{u}_2(r_1) dr_1 &= 1, & \int_0^{r_{10}} r_1 \tilde{c}_1(t, r_1, z_1) dr_1 &= 1, \\ \frac{2}{r_{10}^2} \int_0^{r_{10}} r_1 \tilde{c}_2(t, r_1, z_2) dr_1 &= 1, & \frac{2}{r_{20}^2} \int_0^{r_{20}} r_2 \tilde{c}_{12}(t, r_2, z) dr_2 &= 1, \\ \frac{2}{r_{20}^2} \int_0^{r_{20}} r_2 \tilde{c}_{13}(t, r_2, z) dr_2 &= 1, & \frac{2}{r_{20}^2} \int_0^{r_{20}} r_2 \tilde{c}_{23}(t, r_2, z) dr_2 &= 1. \end{aligned} \quad (16)$$

The use of the averaging procedure [20] leads to:

$$\begin{aligned} \alpha_1 \bar{u}_1 \frac{d\bar{c}_1}{dz_1} + \frac{d\alpha_1}{dz_1} \bar{u}_1 \bar{c}_1 &= -k_0 (\bar{c}_1 - \chi \bar{c}_2); \\ \alpha_2 \bar{u}_2 \frac{d\bar{c}_2}{dz_2} + \frac{d\alpha_2}{dz_2} \bar{u}_2 \bar{c}_2 &= k_0 (\bar{c}_1 - \chi \bar{c}_2); \\ z_1 = 0, \quad \bar{c}_1(t, 0) &\equiv c_1^0; \\ z_2 = 0, \quad \bar{c}_2(t, 0) &\equiv \bar{c}_2(t, l_2); \\ \alpha \bar{u} \frac{d\bar{c}_{12}}{dz} + \frac{d\alpha}{dz} \bar{u} \bar{c}_{12} &= -k_1 (\bar{c}_{12} - \bar{c}_{13}); \\ \frac{d\bar{c}_{13}}{dt} &= k_1 (\bar{c}_{12} - \bar{c}_{13}) - \beta k \bar{c}_{13} \bar{c}_{23} = 0; \\ \frac{d\bar{c}_{23}}{dt} &= -\beta k \bar{c}_{13} \bar{c}_{23}; \\ z = 0, \quad \bar{c}_{12}(t, 0) &\equiv \bar{c}_2(t, l_1); \\ t = 0, \quad \bar{c}_{13}(0, z) &\equiv 0, \quad \bar{c}_{23}(0, z) \equiv c_{23}^0. \end{aligned} \quad (17)$$

The following functions are used in (17) and (18):

$$\begin{aligned} \alpha(t, z) &= \frac{2}{r_{20}^2} \int_0^{r_{20}} r_2 \tilde{u}(r_2) \tilde{c}_{12}(t, r_2, z) dr_2, \\ \alpha_1(t, z_1) &= \frac{2}{r_{10}^2} \int_0^{r_{10}} r_1 \tilde{u}_1(r_1) \tilde{c}_1(t, r_1, z_1) dr_1, \\ \alpha_2(t, z_2) &= \frac{2}{r_{10}^2} \int_0^{r_{10}} r_1 \tilde{u}_2(r_1) \tilde{c}_2(t, r_1, z_2) dr_1, \\ \beta(t, z) &= \frac{2}{r_{20}^2} \int_0^{r_{20}} r_2 \tilde{c}_{13}(t, r_2, z) \tilde{c}_{23}(t, r_2, z) dr_2. \end{aligned} \quad (19)$$

Generalized analysis

The use of the dimensionless (generalized) variables

$$\begin{aligned} T &= \frac{t}{t_0}, \quad Z = \frac{z}{l_2}, \\ Z_1 &= \frac{z_1}{l_1}, \quad Z_2 = \frac{z_2}{l_1}, \\ \bar{C}_1 &= \frac{\bar{c}_1}{c_1^0}, \quad \bar{C}_2 = \frac{\bar{c}_2 \chi}{c_1^0}, \\ \bar{C}_{12} &= \frac{\bar{c}_{12} \chi}{c_1^0}, \quad \bar{C}_{13} = \frac{\bar{c}_{13} \chi}{c_1^0}, \quad \bar{C}_{23} = \frac{\bar{c}_{23}}{c_{23}^0}. \end{aligned} \quad (20)$$

leads to:

$$\begin{aligned} A_1 \frac{d\bar{C}_1}{dZ_1} + \frac{dA_1}{dZ_1} \bar{C}_1 &= -K_1 (\bar{C}_1 - \bar{C}_2); \\ A_2 \frac{d\bar{C}_2}{dZ_2} + \frac{dA_2}{dZ_2} \bar{C}_2 &= K_2 (\bar{C}_1 - \bar{C}_2); \\ Z_1 = 0, \quad \bar{C}_1(T, 0) &\equiv 1; \\ Z_2 = 0, \quad \bar{C}_2(T, 0) &\equiv \bar{C}_{12}(T, 1). \end{aligned} \quad (21)$$

$$\begin{aligned} A \frac{d\bar{C}_{12}}{dZ} + \frac{dA}{dZ} \bar{C}_{12} &= -K_0 (\bar{C}_{12} - \bar{C}_{13}); \\ \frac{d\bar{C}_{13}}{dT} &= K_3 (\bar{C}_{12} - \bar{C}_{13}) - BK_4 \bar{C}_{13} \bar{C}_{23} = 0; \\ \frac{d\bar{C}_{23}}{dT} &= -BK_5 \bar{C}_{13} \bar{C}_{23}; \\ Z = 0, \quad \bar{C}_{12}(T, 0) &\equiv \bar{C}_2(T, 1); \\ T = 0, \quad \bar{C}_{13}(0, Z) &\equiv 0, \quad \bar{C}_{23}(0, Z) \equiv 1. \end{aligned} \quad (22)$$

The following functions are used in (21) and (22):

$$\begin{aligned} \bar{C}_1(T, Z_1) &= 2 \int_0^1 R_1 C_1(T, R_1, Z_1) dR_1, \\ \bar{C}_2(T, Z_2) &= 2 \int_0^1 R_1 C_2(T, R_1, Z_2) dR_1, \\ \bar{C}_{13}(T, Z) &= 2 \int_0^1 R_2 C_{13}(T, R_2, Z) dR_2, \\ \bar{C}_{23}(T, Z) &= 2 \int_0^1 R_2 C_{23}(T, R_2, Z) dR_2. \\ A(T, Z) &= \alpha(t_0 T, l_2 Z) = \alpha(t, z) = \\ &= 2 \int_0^1 R U(R_2) \frac{C_{12}(T, R_2, Z)}{\bar{C}_{12}(T, Z)} dR_2 \\ A_1(T, Z_1) &= \alpha_1(t_0 T, l_1 Z_1) = \alpha_1(t, z_1) = \\ &= 2 \int_0^1 R_1 U_1(R_1) \frac{C_1(T, R_1, Z_1)}{\bar{C}_1(T, Z_1)} dR_1 \end{aligned}$$

$$\begin{aligned}
 A_2(T, Z_2) &= \alpha_2(t_0 T, l_1 Z_2) = \alpha_2(t, z_2) = \\
 &= 2 \int_0^1 R_1 U_2(R_1) \frac{C_2(T, R_1, Z_2)}{\bar{C}_2(T, Z_2)} dR_1 \\
 B(T, Z) &= \beta(t_0 T, l_2 Z) = \beta(t, z) = \\
 &= 2 \int_0^1 R_2 \frac{C_{13}(T, R_2, Z)}{\bar{C}_{13}(T, Z)} \frac{C_{23}(T, R_2, Z)}{\bar{C}_{23}(T, Z)} dR_2
 \end{aligned} \tag{23}$$

In [20] it was shown that $B(T, Z) \equiv 1$ and $A(T, Z), A_1(T, Z_1), A_2(T, Z_2)$ can be presented as linear approximations:

$$\begin{aligned}
 A &= 1 + a_z Z + a_t T, \\
 A_1 &= 1 + a_z^1 Z_1 + a_t^1 T, \\
 A_2 &= 1 + a_z^2 Z_2 + a_t^2 T.
 \end{aligned} \tag{24}$$

As a result, the model of the absorption-desorption process has the form:

$$\begin{aligned}
 (1 + a_z^1 Z_1 + a_t^1 T) \frac{d\bar{C}_1}{dZ_1} + a_z^1 \bar{C}_1 &= -K_1 (\bar{C}_1 - \bar{C}_2); \\
 (1 + a_z^2 Z_2 + a_t^2 T) \frac{d\bar{C}_2}{dZ_2} + a_z^2 \bar{C}_2 &= K_2 (\bar{C}_1 - \bar{C}_2); \\
 Z_1 = 0, \quad \bar{C}_1(T, 0) &\equiv 1; \quad Z_2 = 0, \quad \bar{C}_2(T, 0) \equiv \bar{C}_{12}(T, 1). \\
 (1 + a_z Z + a_t T) \frac{d\bar{C}_{12}}{dZ} + a_z \bar{C}_{12} &= -K_0 (\bar{C}_{12} - \bar{C}_{13}); \\
 \frac{d\bar{C}_{13}}{dT} &= K_3 (\bar{C}_{12} - \bar{C}_{13}) - K_4 \bar{C}_{13} \bar{C}_{23} = 0; \\
 \frac{d\bar{C}_{23}}{dT} &= -K_5 \bar{C}_{13} \bar{C}_{23}; \\
 Z = 0, \quad \bar{C}_{12}(T, 0) &\equiv \bar{C}_2(T, 1); \\
 T = 0, \quad \bar{C}_{13}(0, Z) &\equiv 0, \quad \bar{C}_{23}(0, Z) \equiv 1.
 \end{aligned} \tag{25}$$

Algorithm of the solution

The solution of (25) and (26) can be obtained as five matrix forms:

$$\begin{aligned}
 \bar{C}_1(T, Z) &= \|C_{(1)\tau\zeta}\|, \quad \bar{C}_2(T, Z) = \|C_{(2)\tau\zeta}\|, \\
 \bar{C}_{12}(T, Z) &= \|C_{(12)\tau\zeta}\|, \quad \bar{C}_{13}(T, Z) = \|C_{(13)\tau\zeta}\|, \\
 \bar{C}_{23}(T, Z) &= \|C_{(23)\tau\zeta}\|; \\
 0 \leq T \leq 1, \quad T &= \frac{\tau - 1}{\tau^0 - 1}, \quad \tau = 1, 2, \dots, \tau^0; \\
 0 \leq Z \leq 1, \quad Z &= \frac{\zeta - 1}{\zeta^0 - 1}, \quad \zeta = 1, 2, \dots, \zeta^0; \quad \tau^0 = \zeta^0.
 \end{aligned} \tag{27}$$

A multi-step approach may be used. At each step the problems (25) and (26) have to be solved consecutively, where T is a parameter in (25), Z is a parameter in (26), $\bar{C}_2^{(s)}(T, 0) \equiv \bar{C}_{12}^{(s-1)}(T, 1), \bar{C}_{13}^{(0)}(T, 1) \equiv 0$,

where the superscript values ($s = 0, 1, 2, \dots$) are the step numbers.

Parameters identification

The availability of experimental data for the SO₂ concentrations in the gas and liquid phases at the absorber and adsorber outlets ($\bar{C}_1^{\text{exp}}(T_n, 1), \bar{C}_{12}^{\text{exp}}(T_n, 1), T_n = 0.05n, n = 1, 2, \dots, 20$) permits to use the following algorithm for the parameters identification in the model (25), (26):

1. Put $a_z = a_t = a_z^1 = a_t^1 = a_z^2 = a_t^2 = 0$ in (25), (26) and minimize the least squares functions:

$$F_1(K_1, K_2) = \sum_{n=1}^{20} [\bar{C}_1(T_n, 1) - \bar{C}_1^{\text{exp}}(T_n, 1)]^2, \tag{28}$$

$$F_2(K_0, K_3, K_4, K_5) = \sum_{n=1}^{20} [\bar{C}_{12}(T_n, 1) - \bar{C}_{12}^{\text{exp}}(T_n, 1)]^2,$$

where $\bar{C}_1(T_n, 1), \bar{C}_{12}(T_n, 1)$ are obtained as a solution of (25), (26) for $T_n = 0.05n, n = 1, 2, \dots, 20$.

2. Enter the obtained parameter values ($K_p, p = 0, 1, \dots, 5$) in (25), (26) and minimize the least squares functions:

$$F_3(a_z^1, a_t^1, a_z^2, a_t^2) = \sum_{n=1}^{20} [\bar{C}_1(T_n, 1) - \bar{C}_1^{\text{exp}}(T_n, 1)]^2, \tag{29}$$

$$F_4(a_z, a_t) = \sum_{n=1}^{20} [\bar{C}_{12}(T_n, 1) - \bar{C}_{12}^{\text{exp}}(T_n, 1)]^2,$$

where $\bar{C}_1(T_n, 1), \bar{C}_{12}(T_n, 1)$ are obtained as a solution of (25), (26) for $T_n = 0.05n, n = 1, 2, \dots, 20$.

3. Enter the calculated values of the parameters $a_z, a_t, a_z^1, a_t^1, a_z^2, a_t^2$ in (25), (26) and minimize the least squares functions (29), etc.

CONCLUSION

The emphasis of the presented research is on eco-technologies and waste-free production. The proposed patent [19] makes it possible to create a waste-free technology for waste gases purification from SO₂ by means of regenerable absorbent and adsorbent. Convection-diffusion and average concentration models of the absorption and adsorption processes permit to model the patent processes.

The new technology will help to solve the problems faced by entrepreneurs in implementing innovations and compliance with environmental standards. Obtaining valuable products according to the proposed technology will allow for cost-effective purification of SO₂ gases.

Acknowledgement: This work has received funding from the National Research und project No -06-37/11/ 06.12.2019 Integrated absorption-adsorption process for waste-free decontamination of gases from sulfur dioxide”.

REFERENCES

- 1 K. R. Bruce, *AIChE J.*, **35(1)**, 37 (1989).
- 2 H. Fahlenkamp, *Vortagsveröff. HausTech. Essen*, **490**, 9 (1985).
- 3 W Jozewicz, D. A. Kirchgessner, *Powder Technol.*, **58(3)**, 221 (1989).
- 4 Chr. Boyadjiev, *Int. J. Heat Mass Transfer*, **54**, 3004 (2011).
- 5 Chr. Boyadjiev, Proc. Energy Forum, Bulgaria, 2011, p. 114.
- 6 Chr. Boyadjiev, Proc. Asia-Pacific Power and Energy Engineering Conf. (APPEEC), Shanghai, China, 2012, vol. 1.
- 7 Chr. Boyadjiev, Proc. VIII All-Russian Conf. "Solid Fuel Combustion", Novosibirsk, Russia, 2012, p. 1.
- 8 Chr. Boyadjiev, M. Doichinova, P. Popova, Proc. 15th Workshop on Transport Phenomena in Two-Phase Flow, Sunny Beach Resort, Bulgaria, 2011, p. 94.
- 9 Chr. Boyadjiev, P. Popova, M. Doichinova, Proc. 15th Workshop on Transport Phenomena in Two-Phase Flow, Sunny Beach Resort, Bulgaria, 2011, p. 104.
- 10 Chr. Boyadjiev, M. Doichinova, P. Popova, *Trans. of Academenergo*, **1**, 44 (2012).
- 11 Chr. Boyadjiev, B. Boyadjiev, M. Doichinova, P. Popova-Krumova, *BG Patent* 111168 (2013).
- 12 D. Dzhonova-Atanasova, E. Razkazova-Velkova, L. Ljutzkanov, N. Kolev, D. Kolev, *Journal of Chemical Technology and Metallurgy*, **48 (5)**, 457 (2013).
- 13 N. Kolev, L. Ljutzkanov, D. Kolev, D. Dzhonova-Atanasova, E. Razkazova-Velkova, *Journal of International Scientific Publications, Materials, Methods and Technologies*, **5 (1)**, 375 (2011).
- 14 D. Dzhonova-Atanasova, E. Razkazova-Velkova, L. Ljutzkanov, *Journal of International Scientific Publications, Materials, Methods and Technologies*, **5 (1)**, 74 (2011).
- 15 L. Ljutzkanov, E. Razkazova-Velkova, N. Kolev, D. Dzhonova-Atanasova, D. Kolev, *Journal of International Scientific Publications, Materials, Methods and Technologies*, **5 (1)**, 304 (2011).
- 16 L. Pantofchieva, Chr. Boyadjiev, *Bulg. Chem. Commun.*, **28**, 780 (1995).
- 17 Chr. Boyadjiev, L. Pantofchieva, J. Hristov, *Theor. Found. Chem. Eng.*, **34(2)**, 141 (2000).
- 18 J. Hristov, Chr. Boyadjiev, L. Pantofchieva, *Theor. Found. Chem. Eng.*, **34(5)**, 489 (2000).
- 19 Chr. Boyadjiev, B. Boyadjiev, M. Doichinova, P. Popova-Krumova, *BG Patent* 111398 (2014).
- 20 Chr. Boyadjiev, M. Doichinova, B. Boyadjiev, P. Popova-Krumova, Modeling of Column Apparatus Processes, Springer-Verlag, Berlin, Heidelberg, 2016.
- 21 Chr. Boyadjiev, Theoretical Chemical Engineering. Modeling and Simulation, Springer-Verlag, Berlin, Heidelberg, 2010.
- 22 M. Doichinova, Chr. Boyadjiev, *Int. J. Heat Mass Transfer*, **55**, 6705 (2012).

Section
Physics

Impact of physical and chemical modification on the immobilization of β -galactosidase in poly-lactic acid multilayer structures

A. V. Grigorov^{1*}, T. Yovcheva¹, I. Iliev¹, I. Vlaeva², A. Viraneva¹

¹University of Plovdiv "Paisii Hilendarski", Plovdiv, Bulgaria

²University of Food Technology, Plovdiv, Bulgaria

Received: November 17, 2021; Revised: May 8, 2022

The present paper investigated the effects of a combination of two different techniques for modification of poly(D-lactic acid) (PDLA) films on the creation of polyelectrolyte multilayers of chitosan and xanthan, used for enzyme immobilization. PDLA films were modified both physically under negative corona discharge (NCD) and chemically with N-ethyl-N'-(3-dimethylaminopropyl) carbodiimide hydrochloride (EDAC) in four configurations (only NCD, only EDAC, EDAC followed by NCD, NCD followed by EDAC). Negative corona was chosen in combination with the chemical modification as it activates the carboxyl groups of the modified PDLA surface. Before EDAC treatment, substrates were first hydrolyzed with NaOH. The surface contact angle for all samples was measured and their surface energy was determined. The enzymatic activity of the immobilized enzyme (β -galactosidase) was investigated using the ONPG method. The modified multilayer structures retain up to half of the initial enzymatic activity up to one month after immobilization.

Keywords: modification, EDAC, poly(D-lactic acid), enzyme immobilization, polyelectrolyte multilayers

INTRODUCTION

In the last few decades the increased demand for biodegradable and renewable alternatives of the widest spread oil-based synthetic polymers has led to an increased interest in the field of biopolymers. One such biopolymer, poly-lactic acid (PLA) has become one of the most popular natural polymers for different applications from biomedicine to packaging and tissue engineering [1, 2]. As a biodegradable polymer PLA possesses several advantages such as high biocompatibility and processability, however due to several drawbacks, such as hydrophobicity and lack of reactive side-chain groups, its practical implementation has been limited. [3] One of the most popular methods to reduce the drawbacks of PLA is surface modification. This modification can be performed using different methods, physical and chemical modification being two of the most popular ones [4, 5]. Physical modification can be performed using corona discharge and offers an easy and reliable method for surface modification. Chemical modification is often achieved using hydrolysis. This modification creates reactive side-chain groups that can be further activated with the use of the reagent N-ethyl-N'-(3-dimethyl aminopropyl) carbodiimide hydrochloride (EDAC). The modified PLA substrates can be used for the

creation of different multilayer composites with the use of a layer-by-layer deposition technique, thus further increasing the potential applications of this biopolymer [6].

In our study we investigated the effects of two different types of surface modification of PDLA on the immobilization of a chosen enzyme β -galactosidase within multilayers of chitosan and xanthan, deposited on the modified polymer substrates.

The purpose of this study is to examine the effects of the combination of two different modification techniques (physical and chemical) on the level of immobilization and activity retention of a chosen enzyme (β -galactosidase) within biodegradable multilayers, and to compare those values with the ones obtained by using only one of the aforementioned modification techniques.

EXPERIMENTAL

Substrate formation. The poly (D-lactic) acid (PDLA) used for the creation of the substrates was purchased from Lactel Absorbable Polymers (USA). The substrates were prepared by dissolving 1 g of PDLA in 50 ml of chloroform. The chloroform solution was then casted in a round metal dish and left to dry at room temperature until the complete evaporation of the solvent. The resulting film was kept in a desiccator, at room temperature, and 54 % relative humidity (RH).

* To whom all correspondence should be sent.

E-mail: aleksandar.grigorov@abv.bg

Surface modification. Two types of surface modification (physical and chemical) were used for this study. A standard system of a corona discharge was utilized for the physical modification. This system consists of a corona electrode (needle), a grounded plate electrode and a grid placed between the two. All substrates were charged for 1 minute at 5 kV of negative voltage, 1 kV of the same polarity being supplied to the grid. The chemical modification was carried out in two steps. First the surface of the substrates was hydrolyzed in a 0.3 M solution of aqueous sodium hydroxide (NaOH) at 45° C for 15 minutes. The samples were then washed in dilute HCL (0.1 N) and deionized water three times to remove any residual NaOH. Finally, the hydrolyzed samples were submerged in a methanol solution, containing 75 mg of EDAC for 4 hours. This was done to activate and condense the free carboxyl (-COOH) groups, created during the hydrolysis. After activation all samples were rinsed three times in methanol to remove any residual EDAC. Four different modification combinations were investigated in this study – two of them being pure modifications (only chemical or purely physical) and two combinations of both modifications (chemical followed by physical and physical followed by chemical). After modifications the surface potential of all of the studied samples was measured with the use of the vibrating electrode method with compensation, like the one described in [7].

Multilayers creation. The creation of the multilayers on the modified surface of the substrates was carried out with the use of a layer-by-layer (LbL) deposition technique in a MSM SLEE automatic carousel stainer. The multilayers were formed by consecutive dipping in two acetate buffer (pH 5) solutions – one containing 0.1 % chitosan and another containing 0.05 % xanthan and 0,05 % locust bean gum (LBG). The enzyme β -galactosidase, used in this study, was included in the xanthan solution. Each dipping step lasted 15 minutes and was followed by an acetate buffer (pH 5) wash for 5 minutes to remove any residual solution before the next dipping step. This procedure was repeated until the creation of 8 layers on the surface of the modified substrates.

Water contact angle measurement. All water contact angle measurements were performed under standard conditions (at room temperature and normal air pressure). Five measurements were performed for each type of modification on different places of the surface of the multilayer films. The average of those five results was used for determination of the hydrophobicity of the

modified samples. Tiny droplets of 2 μ l were used in order to reduce the effect of surface roughness on the water contact angle. The drops were deposited on the surface with the use of a precise 10 μ l microsyringe (Innovative Labor System GmbH, Germany). Contact angles were obtained by using the tangent of the drop profile from pictures captured with an USB microscope. Image processing was performed using public domain ImageJ software (ImageJ v1.51k software).

Determination of enzyme activity. The enzymatic activity of the immobilized enzyme was determined with the use of the ONPG method. This method utilizes the reaction between the immobilized enzyme β -galactosidase and O-nitrophenyl- β -D-galactopyranoside (ONPG). The multilayer samples were submerged in a mixture of 1500 μ l of ONPG solution (ionic strength 2.0 mM) and 900 μ l of deionized water for 60 minutes at 37 °C. At the 30th and 60th minute 800 μ l were taken from the reaction liquid and 4 ml of sodium carbonate solution (with ionic strength 1 M) was added to stop the reaction. Through hydrolysis the enzyme reacts with the ONPG solution and produces two byproducts - β -D-galactose and o-nitrophenol. The amount of reaction is then determined by measuring the amount of o-nitrophenol (colored yellow) produced during the reaction by measuring the absorption of the reacted liquid at 405 nm with the use of a spectrophotometer. This test was repeated several times at 24 hour increments to determine the amount of immobilized enzyme after repeated use.

RESULTS AND DISCUSSION

Time storage influence on the electrets surface potential decay

Dependences of the normalized surface potential on the storage time for negatively charged PDLA substrates (PDLA NCD), PDLA substrates chemically modified with EDAC (PDLA EDAC) and substrates modified with combinations of a negative corona and EDAC (PDLA NCD EDAC or PDLA EDAC NCD) were studied for 360 minutes. The surface potential was measured once of 5 minutes for the first 60 minutes when the charge was rapidly decaying. After this period, steady state values of the surface potential at a time of 360 minutes were established for all investigated samples. Each point in the figure is a mean value from 6 samples. The calculated standard deviation was better than 5 % from the mean value with confidence level 95 %.

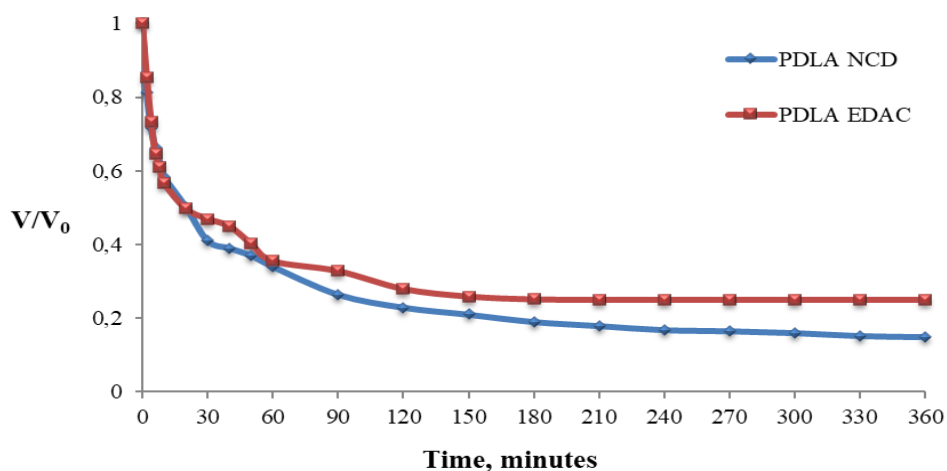


Figure 1. Normalized surface potential time dependences for modified PDLA substrates

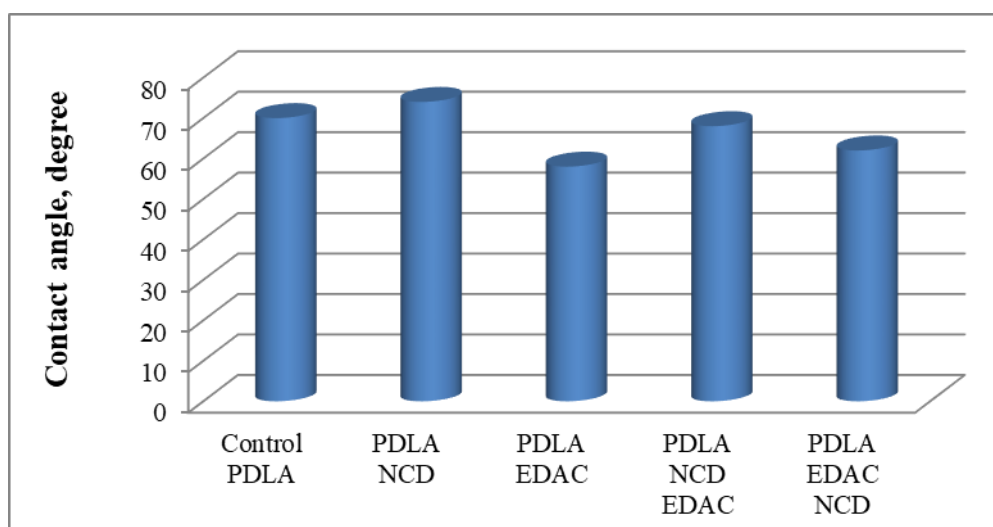


Figure 2. Water contact angles for different PDLA modification combinations

It was found that for the substrates obtained by combination of chemical and physical modification, the surface potential decreases very rapidly and time dependences cannot be constructed. Therefore, only time dependences of the normalized surface potential for negatively charged PDLA substrates and PDLA substrates chemically modified with EDAC were obtained (Fig. 1).

The experimental data presented in Figure 1 demonstrate that:

✓ There is an initial fast decay of the normalized surface potential that occurs in the first 60 minutes after the initial charging. After this initial period the rate of charge decay slows down and the remaining surface charge decreases at a slower rate and then becomes practically stable after at the 360th minute. The initial rapid decrease in the surface charge density can be explained with the release of weakly captured charges from the shallow energy traps. The steady state value is achieved due to the remaining charge consisting of mostly tightly captured charges in the deep energy traps.

The exponential decay of the electrets charge is consistent with the one measured by Sessler [8].

✓ The values for the physically modified PDLA samples (PDLA NCD) are lower than those for the chemically modified samples (PDLA EDAC). This can be caused by the difference in the type of dominant ions on the surface. The different types of dominant ions can be bounded in traps of varying depths and then released depending on the surrounding conditions.

Water contact angle measurements

Surface wettability of the film coatings is directly governed by their chemical composition. Thus, it is of importance to measure contact angles in order to calculate the values of surface free energy. The surface contact angle for all samples was measured and their surface energy was determined. The results for surface contact angles are presented in Figure 2.

The surface of PDLA is hydrophobic and when water was used as test liquid and PDLA as target

surface, high values of water contact angle were expected because water is hydrophilic in nature whereas PDLA surface is hydrophobic in nature. If by chemical reaction PDLA surface was modified and polar groups are inserted on the surface, then a decrease of values of contact angle is expected. This decrease will be different for different polar functional groups.

Our research shows that the negative corona loading increases the value of the contact angle for PDLA samples. For PDLA modified with EDAC, lower contact angle values were observed compared to those loaded in corona discharge. The contact angle values of the two modification combinations are between those of PDLA NCD and PDLA EDAC. The results obtained show that the values of free surface energy of the PDLA EDAC are the highest comparing with values of other investigated samples (Figure 3).

A higher surface energy will cause good wetting and has respectively a lower contact angle. Therefore, we can conclude that the modification with the test substances in this article leads to better wettability of their surface.

Enzyme activity

The activity of the immobilized enzyme was used to determine the effect of the different modification combinations. The amount of enzyme activity was measured at the 30th and 60th minute of the reaction on four consecutive days and one

further measurement was performed after 20 days to determine the long-term retention of activity.

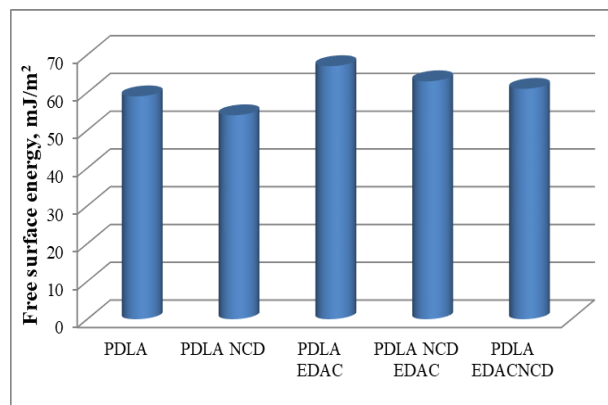


Figure 3. Free surface energy for different PDLA modification combinations.

After the end of the activity test all samples were removed from the reactive fluid and left to dry in normal atmospheric conditions and the assay was repeated with fresh reactive solution on the following day. Three samples of each type of modification were tested and the average values of the activity were calculated. The amounts of enzyme activity for each type of modification at the 30th and 60th minute of the reactions are displayed on Figures 4 and 5, respectively.

Table 1 presents the average values of the measured activity for all modification types for the entire duration of the enzymatic assay measurements.

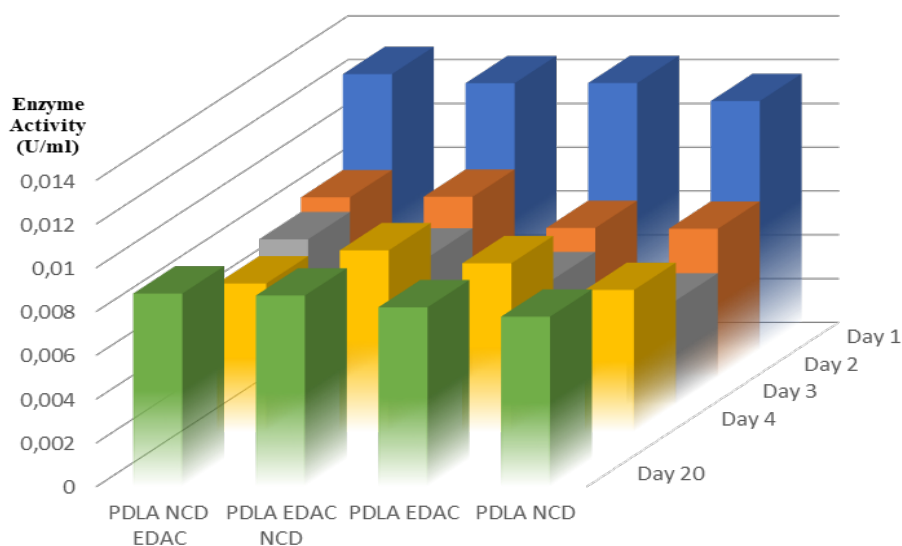


Figure 4. Enzyme activity of immobilized β – galactosidase at the 30th minute of the assay*

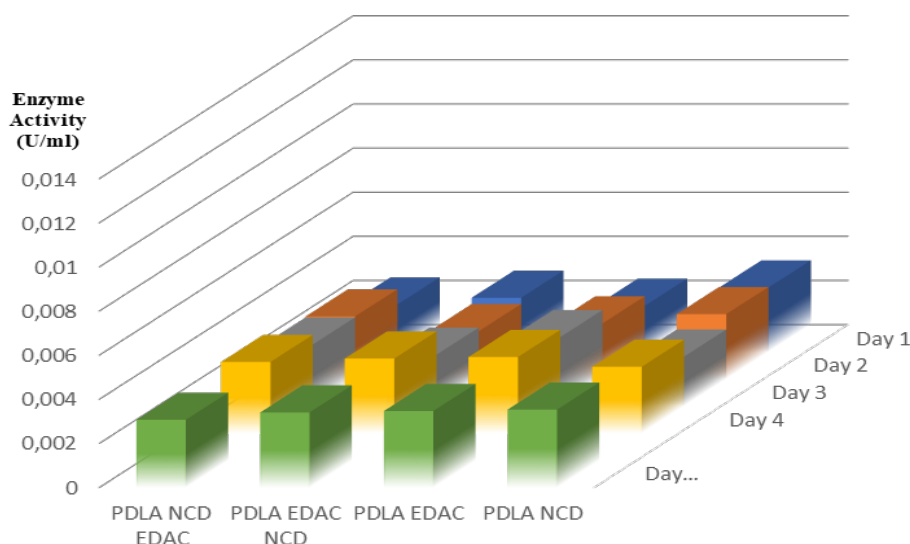


Figure 5. Enzyme activity of immobilized β – galactosidase at the 60th minute of the assay

Table 1. Average enzyme activity of immobilized β – galactosidase

Enzyme (U/ml)		PDLA NCD	PDLA EDAC	PDLA EDAC NCD	PDLA NCD EDAC
Day 1	30 min	0.0111 0.0004	0.0122 0.0003	0.0122 0.0004	0.0126 0.0006
	60 min	0.0029 0.0002	0.0022 0.0001	0.0024 0.0001	0.0021 0.0001
Day 2	30 min	0.0067 0.0003	0.0068 0.0002	0.0084 0.0003	0.0081 0.0002
	60 min	0.0028 0.0001	0.0025 0.0001	0.0022 0.0001	0.0030 0.0002
Day 3	30 min	0.0065 0.0001	0.0067 0.0003	0.0068 0.0005	0.0074 0.0003
	60 min	0.0025 0.0001	0.0031 0.0002	0.0026 0.0001	0.0028 0.0001
Day 4	30 min	0.0065 0.0002	0.0077 0.0004	0.0078 0.0004	0.0068 0.0003
	60 min	0.0030 0.0002	0.0034 0.0002	0.0034 0.0002	0.0032 0.0001
Day 20	30 min	0.0077 0.0004	0.0082 0.0003	0.0075 0.0002	0.0076 0.0004
	60 min	0.0034 0.0002	0.0032 0.0001	0.0030 0.0002	0.0031 0.0001

The results displayed in Figures 4 and 5 and Table 1 show that the chemical modification with EDAC improves the level of retention of the enzyme activity in all cases, with both combinations of the two modification types providing higher values than any of the single

modifications. The data also demonstrate that the level of activity decreases by around 40 % after the first day and remains stable for prolonged periods of time (up to 20 days).

The increase in enzymatic activity of the chemically modified samples can be explained with the higher amount of reactive side chains created on

the surface of the polymer substrate during hydrolysis when compared to the surface degradation from the plasma treatment. These reactive carboxyl chains are then further activated by the EDAC treatment which changes the type of crosslinking between the surface of the polymer and the two polysaccharides used in the creation of the multilayers. As both the physical and chemical modification increase the amount of side chains on the surface, their combinations display the expected higher level of activity when compared with single modifications.

The results obtained in this study demonstrate the suitability of both chemical and physical modification methods for the improvement of the properties of PDLA substrates. The collected data also show that any of the two investigated types and combinations of modifications can produce multilayer films that can maintain a stable level of enzyme activity for a prolonged period of time.

CONCLUSION

The results obtained in this paper demonstrate that both the physical and chemical modifications of the surface of a PDLA substrate can improve its properties and assist in immobilization of bioactive materials on its surface through the creation of multilayer structures. The collected data also indicate that combinations of different modification techniques are superior to any single modification, as utilizing a second modification method can mitigate some of the drawbacks of the first modification. These results can assist in widening of the field of potential applications of different biopolymers. The results of this study can assist the

development of different biomedical products and applications. The level of control, provided by the combination of different types of surface modifications can lead to the creation of two different biomedical applications: the development of drug carrying biodegradable multilayers with controlled drug release rate and the development of multiuse biodegradable sensors.

Acknowledgement: This work was supported by Project "Green Technologies GT-1/2020", Scientific Found of Plovdiv University "Paisii Hilendarski", Bulgaria, and by the operational program "Science and education for smart growth" 2014-2020, grant number BG05M20P001-1.002-0005-C01, Personalized Innovative Medicine Competence Centre (PERIMED).

REFERENCES

1. I. A. Zagidullina, M. F. Galikhanov, R. I. Kamalova, G. F. Sharipova, R. Z. Khairullin, *AIP Conference Proceedings*, **2313**, 050048 (2020).
2. D. Muenprasat, S. Suttireungwon, C. Tongpin, *J. Met., Mater. Minerals*, **20(3)**, 189 (2010).
3. R. M. Rasal, A. V. Janorkar, D. E. Hirt, *Progress in Polymer Science*, **35**, 338 (2010).
4. Tr. I. Croll, A. J. O'Connor, G. W. Stevens, J. J. Cooper-White, *Biomacromolecules*, **5**, 463 (2004).
5. K. Ozaltin, A. Di Martino, Z. Capakova, M. Lehocky, P. Humpolicek, T. Saha, D. Vesela, M. Mozetic, P. Saha, *Polymers*, **13**, 1201 (2021).
6. M. M. Wang, H. L. Li, M. R. Liu, *EXPRESS Polymer Letters*, **13(7)**, 673 (2019).
7. C. Reedyk, M. Perlman, *Journal of Electrochemical Society*, **115(1)**, 49 (1968).
8. G. Sessler, *Journal of Electrostatics*, **51-52**, 137 (2001).

On matrices of coefficients of electromagnetic and elastic waves propagating in anisotropic media

N. A. Ispulov, A. Zh. Zhumabekov, K. R. Dossumbekov, A. K. Bektazinova

Toraighyrov University, Pavlodar 140008, Kazakhstan

Received: November 02, 2021; Accepted: May 25, 2022

Thermoelasticity describes a wide range of phenomena and generalizes the classical theory of elasticity and the theory of heat conductivity. Thermoelastic and electromagnetic waves propagation in anisotropic media is of the most interest at present. Within the bounds of this area, based on the use of physical-mechanical properties of anisotropic media bound heat and mechanical fields are being studied.

The article is devoted to the study of thermoelastic wave propagation in anisotropic media of hexagonal systems in the case of the second order axis symmetry and heterogeneity along X-axis. In the article, by means of analytical matricant method, a set of motion equations of thermoelastic media is reduced to an equivalent set of first-order differential equations.

The structures of the matrices of the coefficients of the constitutive equations and the structure of the matrix for waves of an acoustic and electromagnetic coupled field in thermoelastic, piezoelectric, piezomagnetic and magnetoelectric anisotropic media are presented.

Keywords: Anisotropic medium, thermoelastic and electromagnetic waves, matricant.

INTRODUCTION

The dynamical theory of thermoelasticity is the study of dynamical interaction between thermal and mechanical fields in solid bodies and is of high importance in various engineering fields such as earthquake engineering, soil dynamics, aeronautics, nuclear reactors, etc. It is well known that the classical theory of thermoelasticity [1, 2] rests upon the hypothesis of the Fourier law of heat conduction, in which the temperature propagation is governed by a parabolic-type partial differential equation. The theory predicts that a thermal signal is felt instantaneously everywhere in a body. This is unrealistic from the physical point of view, especially for short-time responses. To account for the effect of thermal relaxation, generalized thermoelasticity has been formulated on the basis of a modified Fourier law such that the temperature propagation is governed by a hyperbolic-type equation. Accordingly, heat transport in solids is regarded as a wave phenomenon rather than a diffusion phenomenon.

In the paper [3], waves propagating along an arbitrary direction in a heat-conducting orthotropic thermoelastic plate are presented by utilizing the normal mode expansion method in the generalized theory of thermoelasticity with one thermal relaxation time. In the paper [4], the author studied the interaction of free harmonic waves with a multilayered medium in generalized thermoelasticity by utilizing the combination of the linear

transformation formation and transfer matrix method approach. Solutions obtained are general and pertain to several special cases. Of these mention the dispersion characteristics for a multilayered medium.

The wave propagation in an anisotropic inhomogeneous medium is considered. A new method of matricant has been developed. Based on the method matricant [5] treated wave processes in elastic and thermoelastic anisotropic media in anisotropic dielectric media, the waves in anisotropic plates, electromagnetic waves in media with magnetoelectric effect [6-8], the waves in liquid crystals, wave propagation in thermoelastic media [9-12].

The structure of matricant for the equation motion elastic medium equations, equations of thermo-mechanical medium has been established. Wave propagation in infinite and finite periodical inhomogeneous media are studied.

Research method

The research method is the matricant method [5] which allows to obtain accurate analytical solutions of differential equations describing the related processes in media with piezoelectric, piezomagnetic, thermoelastic and thermo-piezoelectric properties.

The method of study is analytical and is based on the development of matrix methods for studying the dynamics of elastic stratified media.

The method is about reducing the initial motion equations based on the variable separation method

* To whom all correspondence should be sent:
E-mail: nurlybek_79@mail.ru

(representation of the solution in the form of plane waves) to the equivalent system of ordinary differential equations of the first order with variable coefficients and the construction of the matrix structure (normalized matrix of fundamental solutions).

In the case of the consistent approach, the matrix method allows considering the propagation of waves in a wide class of media. Another advantage of this method is that the expressions obtained by the matrix method have a very compact form, which proves to be convenient both for analytical studies and for numerical calculations.

The matrix method has been tested and the results obtained are consistent with previously known ones. This is confirmed by the presence of a large number of publications based on the above method.

Matrix formulation of the propagation of thermoelastic waves

Propagation of thermoelastic waves in anisotropic medium is described by the equations of motion to be solved together with the Fourier heat equation and the equation of heat flow, which have the form [1]:

$$\begin{aligned} \frac{\partial \sigma_{XX}}{\partial X} + \frac{\partial \sigma_{XY}}{\partial Y} + \frac{\partial \sigma_{XZ}}{\partial Z} &= \rho \frac{\partial^2 U_X}{\partial t^2} \\ \frac{\partial \sigma_{XY}}{\partial X} + \frac{\partial \sigma_{YY}}{\partial Y} + \frac{\partial \sigma_{YZ}}{\partial Z} &= \rho \frac{\partial^2 U_Y}{\partial t^2} \end{aligned} \quad (1)$$

$$\begin{aligned} \frac{\partial \sigma_{XZ}}{\partial X} + \frac{\partial \sigma_{YZ}}{\partial Y} + \frac{\partial \sigma_{ZZ}}{\partial Z} &= \rho \frac{\partial^2 U_Z}{\partial t^2} \\ \lambda_{ij} \frac{\partial \theta}{\partial x_j} &= -q_i \end{aligned} \quad (2)$$

$$\frac{\partial q_i}{\partial x_i} = -i\omega \beta_{ij} \varepsilon_{ij} - i\omega \frac{c_\varepsilon}{T_0} \theta \quad (3)$$

where σ_{ij} - stress tensor, ρ - density of the medium, λ_{ij} - thermal conductivity tensor, q_i - the vector of heat, ω - the angular frequency, β_{ij} - thermomechanical constants, $\beta_{ij} = \beta_{ji}$, ε_{ij} - the strain tensor, c_ε - specific heat at constant strain, θ - temperature increase compared with the temperature of the natural state θ_0 , $\left| \frac{\theta}{\theta_0} \right| \ll 1$ for small deformations.

Physical and mechanical quantities are related by the relation of Duhamel-Neumann [2]:

$$\sigma_{ij} = c_{ijkl} \varepsilon_{kl} - \beta_{ij} \theta \quad (4)$$

Here c_{ij} - elastic parameters, $c_{ijkl} = c_{jikl} = c_{ijlk} = c_{klij}$; ε_{kl} - the tensor Cauchy for small deformations.

For crystals of a hexagonal system as coordinate three orthogonal axes of symmetry or inversion axes of the second order get out.

For a hexagonal class of crystals, the ratio of Duhamel - Neumann looks like:

$$\begin{aligned} \begin{pmatrix} \sigma_{xx} \\ \sigma_{yy} \\ \sigma_{zz} \end{pmatrix} &= \begin{pmatrix} c_{11} & c_{12} & c_{13} \\ c_{12} & c_{11} & c_{13} \\ c_{13} & c_{13} & c_{33} \end{pmatrix} \begin{pmatrix} \varepsilon_1 \\ \varepsilon_2 \\ \varepsilon_3 \end{pmatrix} - \begin{pmatrix} \beta_{11} & 0 & 0 \\ 0 & \beta_{11} & 0 \\ 0 & 0 & \beta_{33} \end{pmatrix} \theta \quad (4a) \\ \begin{pmatrix} \sigma_{yz} \\ \sigma_{xz} \\ \sigma_{xy} \end{pmatrix} &= \begin{pmatrix} 44 & 0 & 0 \\ 0 & 44 & 0 \\ 0 & 0 & \frac{c_{11} - c_{12}}{2} \end{pmatrix} \begin{pmatrix} \varepsilon_4 \\ \varepsilon_5 \\ \varepsilon_6 \end{pmatrix} \end{aligned}$$

Equations (1), (2), (3), (4) and (4a) determine the relationship of mechanical stress and temperature as a function of the independent variables - the thermal field and deformation.

Thus, the relations (1) - (4) constitute a closed system of thermoelasticity equations, which describes the propagation of thermoelastic waves.

Based on the method of separation of variables in the case of a harmonic function of time [5]:

$$\left[U_i(x, y, z, t); \sigma_{ij}(x, y, z, t); \theta; q_z \right] = \left[U_i(x), \sigma_{ij}(x), \theta; q_z \right] e^{i(\omega t - m y - l z)} \quad (5)$$

the system of equations (1) -- (4) reduces to a system of differential equations of first order with variable coefficients which describes the propagation of harmonic waves:

$$\frac{d\vec{W}}{dx} = B\vec{W} \quad (6)$$

where: \vec{W} is a column vector, $u_x(x)$, $u_y(x)$, $u_z(x)$ represent the projection of the displacement vector on the corresponding coordinates, and m k_x , n k_y , l k_z , show the x , y and z components of a wave vector k , respectively; $B = B[c_{ijkl}(x), \beta_{ij}(x), \theta, \omega, m, n, l]$ - coefficient matrix which elements contain the parameters of the medium in which thermoelastic waves propagate.

The vector \vec{W} has the form:

$$\vec{W}(x, y, z, t) = [u_x(x), \sigma_{xx}, u_y(x), \sigma_{yy}, u_z(x), \sigma_{zz}, \theta, q_z]^T \exp(i\omega t - imy - ilz) \quad (7)$$

The symbol t indicates the transpose of the vector - a vector of strings - column.

The system of differential equations (6) for an anisotropic medium of a hexagonal system looks like:

$$\frac{dU_x}{dx} = \frac{1}{c_{11}} \sigma_{xx} + \frac{c_{12}}{c_{11}} in U_y + \frac{c_{13}}{c_{11}} il U_z + \frac{\beta_{11}}{c_{11}} \theta$$

$$\begin{aligned}
 \frac{d\sigma_{xx}}{dx} &= -\rho\omega^2 U_x + in\sigma_{xy} + il\sigma_{xz} \\
 \frac{dU_y}{dx} &= \frac{2}{c_{11}-c_{12}}\sigma_{xy} + inU_x \\
 \frac{d\sigma_{xy}}{dx} &= in\frac{c_{12}}{c_{11}}\sigma_{xx} + \left[-\rho\omega^2 + n^2\left(c_{11}-\frac{c_{12}^2}{c_{11}}\right) + c_{44}l^2\right]U_y + nl\left(c_{13}-\frac{c_{12}c_{13}}{c_{11}} + c_{44}\right)U_z + \left(\frac{c_{12}}{c_{11}}\beta_{11} - \beta_{11}\right)in\theta \\
 \frac{dU_z}{dx} &= \frac{1}{c_{44}}\sigma_{xz} + iU_x \quad (6a) \\
 \frac{d\sigma_{xz}}{dx} &= il\frac{c_{13}}{c_{11}}\sigma_{xx} + nl\left[c_{44}-\frac{13c_{12}}{c_{11}} + c_{13}\right]U_y + \left(-\rho\omega^2 + n^2c_{44} - l^2\frac{c_{13}^2}{c_{11}} + c_{33}l^2\right)U_z + \\
 &+ \left[\frac{c_{13}}{c_{11}}\beta_{11} - \beta_{33}\right]il\theta \\
 \frac{d\theta}{dx} &= -\frac{1}{\lambda_{11}}q_x \\
 \frac{dq_z}{dx} &= i\omega\frac{\beta_{11}}{c_{11}}\sigma_{xx} + i\omega n\left(\frac{c_{12}}{c_{11}} - 1\right)\beta_{11}U_y + i\omega l\left[\frac{c_{13}}{c_{11}}\beta_{11} - \beta_{33}\right]U_z + i\omega\left(\frac{\beta_{11} + c_\varepsilon}{c_{11} T_0}\right)\theta
 \end{aligned}$$

The heterogeneity of the medium is assumed along X. In constructing the coefficient matrix B is used as a representation of the solution (5), the system of equations (1) - (4) are in the derivatives along the coordinate X and the excluded components of the stress tensor are not included in the boundary conditions. The multiplier $\exp(i\omega t - iny - ilz)$ is omitted throughout.

In the structure of the matrix and vector - column boundary conditions in the bulk case for the hexagonal crystal system in the case of the symmetry axis of the second order and heterogeneity along the X axis are given by:

$$B = \begin{pmatrix} 0 & b_{12} & b_{13} & 0 & b_{15} & 0 & b_{17} & 0 \\ b_{21} & 0 & 0 & b_{24} & 0 & b_{26} & 0 & 0 \\ b_{24} & 0 & 0 & b_{34} & 0 & 0 & 0 & 0 \\ 0 & b_{13} & b_{43} & 0 & b_{45} & 0 & b_{47} & 0 \\ b_{26} & 0 & 0 & 0 & 0 & b_{56} & 0 & 0 \\ 0 & b_{15} & b_{45} & 0 & b_{65} & 0 & b_{67} & 0 \\ 0 & 0 & 0 & 0 & 0 & 0 & 0 & b_{78} \\ 0 & i\omega b_{17} & i\omega b_{47} & 0 & i\omega b_{67} & 0 & b_{87} & 0 \end{pmatrix}; \quad (8)$$

$$\vec{W} = \begin{pmatrix} u_x \\ \sigma_{xx} \\ u_y \\ \sigma_{xy} \\ u_z \\ \sigma_{xz} \\ \theta \\ q_x \end{pmatrix}$$

From the structure of the coefficient matrix (8) that is in the spatial case, the elastic waves of different polarization and the heat wave are interrelated.

The b_{ij} elements of the coefficient matrix B for a hexagonal system in a volume case look like:

$$\begin{aligned}
 b_{12} &= \frac{1}{c_{11}}; b_{13} = \frac{c_{12}}{c_{11}}in; b_{15} = \frac{c_{13}}{c_{11}}il; b_{17} = \frac{\beta_{11}}{c_{11}}; \\
 b_{21} &= -\omega^2\rho; b_{24} = in; b_{26} = il \\
 b_{34} &= \frac{2}{c_{11}-c_{12}}; b_{43} = \left(c_{11}-\frac{c_{12}^2}{c_{11}}\right)n^2 + c_{44}l^2 - \omega^2\rho; b_{45} = \left(c_{44} + c_{13} - \frac{c_{12}c_{13}}{c_{11}}\right)nl; \\
 b_{47} &= \left(\frac{c_{12}}{c_{11}} - 1\right)\beta_{11}in \\
 b_{56} &= \frac{1}{c_{44}}; b_{65} = \left(c_{33} - \frac{c_{13}^2}{c_{11}}\right)l^2 + c_{44}n^2 - \omega^2\rho; b_{67} = \left(\frac{c_{13}}{c_{11}}\beta_{11} - \beta_{33}\right)il; \\
 b_{87} &= -i\omega\left(-\frac{\beta_{11}}{c_{11}} + \frac{c_\varepsilon}{0}\right); b_{78} = -\frac{1}{\lambda_{11}}
 \end{aligned}$$

The nonzero elements of the matrix of coefficients B b_{13} , b_{24} determine the mutual transformation of longitudinal and transverse X - polarized waves. Elements of b_{15} , b_{26} describe the relationship of transverse X-polarization with the longitudinal wave. Nonzero element b_{45} defines the mutual transformation between the waves of transverse polarization.

The fact that the coefficient b_{17} :

$$b_{17} = \frac{\beta_{11}}{c_{11}}$$

means that the longitudinal wave is propagated by the thermoelastic effect.

Non-zero elements b_{47} and b_{67} :

$$b_{47} = \left(\frac{c_{12}}{c_{11}} - 1\right)\beta_{11}in; b_{67} = \left(\frac{c_{13}}{c_{11}}\beta_{11} - \beta_{33}\right)il;$$

indicate the effect on the elastic wave transverse polarizations thermoelastic effect. At the same time. it describes the b_{47} thermoelastic effect on the elastic shear wave of the Y-polarization, and the b_{67} thermoelastic effect on the transverse wave Z-polarization.

Similarly, for the thermoelastic waves propagating in an anisotropic medium of hexagonal symmetry the coefficient matrix is constructed in the bulk case and the analysis of matrix coefficients is performed. We also obtained that the structure of the matrix of coefficients in the propagation of thermoelastic waves in an anisotropic medium of hexagonal crystal systems in the planes XY and XZ, defines the types of waves and the mutual transformation of waves of different polarizations.

Piezoelastic waves

The existence of direct and reverse piezoelectric effects in a dielectric medium leads to the mutual

generation of elastic and electromagnetic waves. A complete description of the processes of propagation of elastic and electromagnetic waves is based on the analysis of joint solutions of the equations of motion of an elastic anisotropic medium (1) and Maxwell's equations [13]. Electromagnetic wave processes are considered on the basis of Maxwell's equations in the absence of free charges and currents in the medium:

$$\begin{cases} \text{rot } \vec{E} = -\frac{\partial \vec{B}}{\partial t} \\ \text{rot } \vec{H} = \frac{\partial \vec{D}}{\partial t} \end{cases} \begin{cases} \text{div } \vec{B} = 0 \\ \text{div } \vec{D} = 0 \end{cases} \quad (9)$$

$$D_i = \epsilon_{ij} E_j; \quad B_i = \mu_{ij} H_j$$

where: E_i are the components of the electric field strength vector, D_i are the components of the electric displacement vector, B_i are the components of the magnetic induction vector, and H_i are the components of the magnetic field strength vector. The coefficients ϵ_{ij} , μ_{ij} are dielectric and magnetic parameters of the medium, which included ϵ_0 , μ_0 are the magnetic and dielectric permeability of free space, respectively.

System of Eqs. (1), (9) coupled with material equations:

$$\begin{cases} \sigma_{ij} = c_{ijkl} \epsilon_{kl} - e_{ijk} E_k \\ D_i = \epsilon_{ik} E_k + e_{ikl} \epsilon_{kl} \end{cases} \quad (10)$$

where e_{ikl} is the piezoelectric tensor, which determines the interaction of elastic and electromagnetic fields and can be represented as a (3 6) matrix. Application of the representation of solutions for the desired function in the form (5) reduces the system of Eqs. (9) and equations of motion (1) with (10) to a system of first-order equations [14]:

$$\frac{d\vec{W}}{dz} = \mathbf{B}\vec{W}; \quad \vec{W} = (u_z, \sigma_{zz}, u_x, \sigma_{xz}, u_y, \sigma_{yz}, E_y, H_x, H_y, E_x)^t \quad (11)$$

As a result, the matrix of coefficients \mathbf{B} has (10 10) order. For example, when we consider waves in orthorhombic media of class 222, when the projection of the wave vector $k_y = 0$ (the plane xz), the matrix is divided into a (6 6) and a (4 4) matrix. The (4 4) matrix describes propagation of coupled shear elastic waves with Y-polarization and TM electromagnetic waves. The structure of the matrix of coefficients \mathbf{B} has the form [14]:

$$\mathbf{B} = \begin{pmatrix} 0 & b_{12} & 0 & b_{14} \\ b_{21} & 0 & b_{23} & 0 \\ 0 & -i\omega b_{14} & 0 & b_{34} \\ -i\omega b_{23} & 0 & b_{43} & 0 \end{pmatrix};$$

$$\vec{W} = (u_y, \sigma_{zz}, H_y, E_x)^t \quad (12)$$

$$\text{where: } b_{21} = k_x^2 (C_{66} + \frac{e_{36}^2}{\epsilon_{33}}) - \rho\omega^2;$$

$$b_{12} = \frac{1}{C_{44}};$$

$$b_{23} = \frac{im^2 e_{36}}{\omega \epsilon_{33}};$$

$$b_{14} = \frac{e_{14}}{C_{44}};$$

$$b_{34} = -i\omega (\mu_{11} + \frac{e_{14}^2}{C_{44}});$$

$$b_{43} = i\omega (\frac{m^2}{\omega^2 \epsilon_{33}} - \mu_{22}).$$

Piezomagnetic media

Previously, the paper [15] considered physical models describing piezomagnetic media coupled by elastic and electromagnetic fields, based on the system of equations (1), (9) in combination with material equations for piezomagnetic media:

$$\sigma_{ij} = c_{ijkl} \epsilon_{kl} - Q_{ijk} H_k \quad (13)$$

$$B_i = \mu_{ik} H_k + Q_{ikl} \epsilon_{kl}$$

where Q_{ijk} are piezomagnetic modules of the anisotropic media. Application of the representation solution (5) allows Eqs. (1), (9), and (12) to give a system of first-order ODEs:

$$\frac{d\vec{W}}{dz} = \mathbf{B}\vec{W}; \quad \vec{W} = (u_z, \sigma_{zz}, u_y, \sigma_{yz}, u_x, \sigma_{xz}, E_y, H_x, H_y, E_x)^t \quad (14)$$

The matrix of coefficients \mathbf{B} in the general case has order (10 10). The structure of this matrix coefficients is obtained for orthorhombic media [15].

Magnetolectric media

In the work [16], Maxwell's system of equations and constitutive equations describing the propagation of electromagnetic waves in an anisotropic magnetolectric medium are equated to an equivalent system of differential equations of first order. This gives an opportunity to analyze magnetolectric effect on electromagnetic wave propagation along axes planes and in bulk case.

Under absence of volume charge density, current density vectors and harmonic dependence of the wave fields solutions on time Maxwell's equations take following form:

$$\text{rot } \vec{H} = \frac{\partial \vec{D}}{\partial t} = i\omega \vec{D}; \quad (15)$$

$$\operatorname{div} \vec{B} = 0; \quad \operatorname{div} \vec{D} = 0;$$

The dependence of \vec{D} and \vec{B} on \vec{E} and \vec{H} in presence of magnetoelectric effect has the following form:

$$\begin{cases} D_i = \varepsilon_0 \varepsilon_{ij} E_j - \alpha_{ij} H_j \\ B_i = \mu_0 \mu_{ij} H_j - \alpha_{ij} E_j \end{cases} \quad (16)$$

where: ε_0 , μ_0 - absolute dielectric permeability of vacuum; ε_{ij} , μ_{ij} - components of relative dielectric and magnetic permeability of medium. α_{ij} - components of the tensor that describe the influence of the magnetoelectric effect.

In general, the matrix of B coefficients has the following structure:

$$B = \begin{pmatrix} b_{11} & b_{12} & b_{13} & b_{14} \\ b_{21} & b_{11} & b_{23} & b_{24} \\ -b_{24} & -b_{14} & -b_{11} & b_{34} \\ -b_{23} & -b_{13} & b_{43} & -b_{11} \end{pmatrix} \quad (17)$$

For the antiferromagnetic Cr_2O_3 that is being considered in this article tensor α has the following form:

$$\alpha = \begin{pmatrix} \alpha_{\parallel} & 0 & 0 \\ 0 & \alpha_{\parallel} & 0 \\ 0 & 0 & \alpha_{\perp} \end{pmatrix} \quad (18)$$

CONCLUSION

This paper is devoted to the research of thermoelastic wave propagation in anisotropic media of hexagonal systems in the case of a second-order axis symmetry and heterogeneity along the axis. Differential equations system of the first order with variable coefficients that are made by means of the variable separation method are obtained (solution is presented as a plane harmonic wave). Coefficients matrices for anisotropic medium of a hexagonal system for three-, two-, and one-dimensional cases were obtained. The structures of the matrices of the coefficients of the constitutive equations and the structure of the matrix for waves of an elastic and electromagnetic coupled field in thermoelastic, piezoelectric, piezomagnetic and magnetoelectric anisotropic media are presented.

Acknowledgement: This research has been funded by the Science Committee of the Ministry of Education and Science of the Republic of Kazakhstan (Grant No. AP08856290).

REFERENCES

1. W. Nowacki, Dynamic Problems of Thermoelasticity, Noordhoff, The Netherlands, 1975.
2. W. Nowacki, Thermoelasticity. 2nd edn. Pergamon Press, Oxford, 1986.
3. K. L. Verma, *International Journal of Aerospace and Mechanical Engineering* **2** (2), 86 (2008).
4. K. L. Verma, *International Journal of Applied Engineering Research, Dindigul*, **1** (4), 908 (2011).
5. S. Tleukenov, Matricant method, Pavlodar, PSU after S. Toraihyrov, 2004 (in Russian).
6. S. K. Tleukenov, M. K. Zhukonov, Materials of the IIIrd International Scientific-Practical Conference Mathematical modeling of mechanical systems and physical processes - Almaty, 2016, p. 174 (in Russian).
7. S. K. Tleukenov, T. S. Dossanov, N. A. Ispulov, A. D. Gutenko, K. R. Dossumbekov, Proceedings of the International Conference Innovative approaches to solving technical and economic problems, Moscow, 2019, p. 104 (in Russian).
8. S. K. Tleukenov, M. K. Zhukonov, N. A. Ispulov, *Bulletin of the University of Karaganda-Physics*, **2** (94) (2019).
9. N. A. Ispulov, A. adir, M. A. Shah, *Chinese Physics B*, **25** (3), article ID 038102, (2016).
10. N. A. Ispulov, A. adir, M. K. Zhukonov, E. Arinov, *Advances in Mathematical Physics*, article No 4898467, DOI: 1155/2017/4898467 (2017).
11. N. A. Ispulov, A. adir, M. K. Zhukonov, T. S. Dossanov, T. G. Kissikov, *Advances in Mathematical Physics*, article No 5236898, DOI: 10.1155/2017/5236898 (2017).
12. A. A. Kurmanov, N. A. Ispulov, A. adir, A. Zh. Zhumabekov, Sh. N. Sarymova, K. R. Dossumbekov, *Physica Scripta*, **96**, article No 085505, DOI: 10.1088/1402-4896/abfe87 (2021).
13. S. K. Tleukenov, *Acta Mechanica*, **225**, 3535 (2014).
14. S.K. Tleukenov, N.K. Zhakiyev, L. Yeltinova, IEEE Joint UFFC, EFTF and PFM Symp. Proc., 2013, p. 1025.
15. S.K. Tleukenov, T.S. Dossanov, *KazNPU*, **2** (18), 229 (2007) (in Russian).
16. . Zhukonov, T. Dossanov, N. Ispulov, A. adir, *Bulletin of S. Toraihyrov Pavlodar State University, Physics and Mathematics series*, **1**, p. 82, 2018.

Material and optomechanical characteristics of polymers in optical design

R. K. Kasarov¹, S. N. Kasarova^{2*}, N. G. Sultanova²

¹Department of Electronics and ²Department of Mathematics and Physics,
"Prof. Dr. Assen Zlatarov" University, 1 Prof. Yakimov Str., 8010 Burgas, Bulgaria

Received: November 02, 2021; Revised: May 10, 2022

In addition to the optical requirements, polymers should be selected in the design on the basis of their material and mechanical properties. Stress-strain analysis requires knowledge of elastic moduli at static or dynamic loading. In this report results of acoustic measurements of different types of optical polymers are presented. Dynamic Young's, shear and volume moduli, as well as Poisson's ratio were determined on base of ultrasonic investigations. Some optomechanical, thermo-optical, and thermo-mechanical parameters were calculated which characterise deflection at constant thickness and constant mass, resonant frequency, linear thermal expansion coefficients, as well as thermal stress due to temperature differences. Presented results were compared to literature data for principal polymers and optical glass types.

Keywords: optical polymers, dynamic elastic moduli, optomechanical parameters, ultrasound velocities

INTRODUCTION

Polymers are preferred materials not only in consumer but in high quality optics for their excellent transparency in visible (VIS) and near-infrared (NIR) region, much lower weight in comparison to glass, high impact resistance, configuration flexibility, safety and low production costs because of the injection moulding technology [1]. Most important optical characteristics of plastics are their refractive indices at selected wavelengths, spectral transmission, as well as the consequent dispersive parameters. Precise refractometric data of various types of polymers have been obtained by means of different measuring techniques at many wavelengths between 406 and 1320 nm [2, 3]. Polymer properties are substantially influenced by temperature variations. Refractive indices (RIs) have been measured in the diapason 0 ÷ 50 °C and the thermo-optic coefficients have been estimated. On base of experimental RIs linear and volume thermal expansion coefficients are then calculated.

Rigidity of solids ensures their impact and shatter resistance and is a factor that determines safety in applications. Usually elastic moduli are reported to characterise rigidity. In [4] we have reported measured velocities of longitudinal ultrasonic waves but elastic moduli were estimated on base of literature data for Poisson's ratio. Velocities of shear waves are very difficult to be measured and there are some materials for which they are not reported due to high attenuations of the shear mode [5]. In this report a special emitter-

receiver was used to measure velocities of shear acoustic waves and obtained values were compared to literature data. On base of the ultrasonic results the dynamic Poisson's ratio was determined and Young's, shear and volume elastic moduli are reported. Some optomechanical and thermo-mechanical characteristics are calculated.

EXPERIMENTAL

Refractive index measurements

We have studied various types of American, German and Japanese optical plastics including principal polymers as polymethyl methacrylate (PMMA), polystyrene (PS), polycarbonate (PC), copolymers styrene acrylonitrile (SAN) and methyl methacrylate styrene (NAS), many trademarks as CTE-Richardson, Zeonex E48R, Optorez 1330, NAS 21 Novacor, Bayer, and some development materials, produced by the USA Eastman Chemical Company (ECC). Bulk samples were measured by means of an one-arc second goniometric set-up with a lighting module consisting of 250 W halogen lamp, condenser system and Carl Zeiss metal interference filters for VIS and NIR spectrum. Laser illumination was used, too. RIs in the VIS and NIR region were obtained within accuracy of $\pm 3.9 \times 10^{-4}$ for goniometric measurements and $\pm 3.6 \times 10^{-4}$ in case of laser illumination [6]. In the VIS area results were compared to RI values obtained by the classical Pulfrich refractometer with its V-shaped prism and coincidence better than 0.001 was obtained. Influence of temperature on refraction and dispersion was investigated on base

* To whom all correspondence should be sent.
E-mail: kasarova_st@yahoo.com

of Pulfrich refractometric measurements in the range 0÷50 °C with a step of 2 degrees below 10 °C and 5 degrees at higher temperatures at the wavelengths of the spectral lamps of the instrument. The measuring accuracy was $\pm 2 \times 10^{-5}$. Thin polymer films were measured by means of a three- and four-wavelength laser microrefractometer. RI values of films differ in respect to layer thickness and bulk sample results.

Ultrasonic measurements

Velocities of longitudinal and shear waves with magnitudes higher than 1000 m/s were determined by means of a Krautkramer flaw detector USM 35XS. For lower values of velocities, a Panametrics apparatus was used. A pulse-echo contact method with a Krautkramer CLF5 transducer (10 MHz) for longitudinal waves and a specially designed sensor Sonic (5 MHz) for shear waves was applied. Thicknesses of the samples were measured by a Mitutoyo caliper with an accuracy of 0.01 mm. Single or multiple reflected echoes were registered to determine time propagation of sound waves and then velocities were automatically calculated. The receiver filtering was adusted to pass the broadband frequency range and the attenuation was adusted to produce a non-saturating signal on the A-scan display. Different values of input electrical impedance and pulse power were used to increase the resolution.

RESULTS AND DISCUSSION

Optical characteristics

Selection of polymeric materials (PMs) in lens design is based on knowledge of their optical and material properties. Most important optical characteristics are spectral transmission, refractive index and dispersion. We have measured spectra of many thin thermoplastic polymer films and the results show transmittance better than 85 % in the range 400 – 2000 nm [7]. Some weak absorption bands between 1660 and 1700 nm have been registered and a considerable transmission decrease has been found beyond 2200 nm due to the absorption of the functional groups.

Obtained refractive data are substantial. Refractive indices of polymer bulk samples and thin films were measured at 22 wavelengths in the interval of 406 ÷ 1320 nm. Usually RIs at the d-line of the helium source ($\lambda_d = 587.6$ nm) at standard temperature of 22 °C according to the USA standard are reported and RI values at the mercury e-line ($\lambda_e = 546.1$ nm) at 20 °C are used in the continental European standard. Many laser

emission wavelengths have been used not only in VIS but in NIR range, too. Abbe number is another important input parameter in lens design which characterises dispersion properties of optical materials in the applied spectral range. In Table 1 RIs and Abbe numbers of several polymers at d-line in VIS and the middle wavelength 879 nm of the measuring NIR range are presented. Values of v_{879} are determined by the equation:

$$v_{879} = \frac{n_{879} - 1}{n_{703} - n_{1052}} \tag{1}$$

and are used in case of the goniometric RI measurements of bulk samples. When laser microrefractometers were applied to measure thin polymer films the Abbe number at mean value of 1010 nm for the measuring range from 700 to 1320 nm was calculated as: $v_{1010} = (n_{1010} - 1)/(n_{700} - n_{1320})$. Random RIs at any wavelength can be computed by means of the Cauchy-Schott approximation [2].

Table 1. Refractive indices and Abbe numbers of PMs.

Polymer	n_d	n_{879}	v_d	v_{879}
PMMA	1.4914	1.4835	59.2	96.7
PS	1.5917	1.5756	30.5	55.9
PC	1.5849	1.5683	29.1	54.6
SAN	1.5667	1.5526	35.4	66.6
Zeonex E48R	1.5309	1.5224	56.5	100.5
Optorez 1330	1.5094	1.5017	52.0	71.7
Bayer	1.5857	1.5698	30.0	54.8

As seen, low-refractive polymers have higher values of Abbe numbers. Dispersion in NIR spectrum is not essential in comparison to VIS light. Relative partial dispersions are maximal in the short-range diapason [6].

RIs for all of the studied polymers decrease with increasing temperature which is opposite to the behaviour of most glass types. Our results show nearly linear dependence $n(T)$ in the regarded interval 0 ÷ 50 °C. There are some slight variations in respect to the wavelength and the measuring temperature. On base of our refractometric results, the thermo-optic coefficient dn/dT (TOC) for each polymer was determined at the respective wavelength. TOCs at d-line for some of the PMs are included in Table 2. As seen, polycarbonate materials as PC of ECC and Bayer show highest thermal stability in respect to the values of TOC and linear thermal expansion coefficient α . Thermo-optic coefficients are related to the thermal linear expansion coefficients by the Lorentz-Lorenz equation and α values in the second column of

Table 2 are determined on base of measured RIs by the equation:

$$\alpha \approx \frac{2n}{(n^2 - 1)(n^2 + 2)} \frac{dn}{dT} \quad (2)$$

Thermal linear coefficient α is related to the volume expansion coefficient as $\beta \approx 3\alpha$ which plays an important role for the dimensional stability of optical elements.

Table 2. Thermal parameters of PMs.

Polymer	dn/dT , 10^{-4} K^{-1}	α , 10^{-4} K^{-1}	α_{lit} , 10^{-4} K^{-1}	S , 10^{-4} K^{-1}
PMMA	-1.2	0.7	0.5 0.9	-0.86
PS	-1.3	0.6	0.6 0.8	-0.95
PC	-1.0	0.5	0.6 0.7	-0.73
SAN	-1.1	0.5	0.65 0.67	-0.80
Zeonex E48R	-1.2	0.6	0.6	-0.87
Optorez 1330	-1.1	0.6	0.7	-0.79
Bayer	-1.1	0.5	0.65	-0.80

Calculated expansion coefficients are compared in the table to literature data α_{lit} [1, 8]. Good coincidence can be established. Slight variations are noticed for each thermoplastic brand which may be due not only to measuring accuracy but to polymerization and moulding conditions, additives as plasticisers, mould release agents, etc. The expansion coefficients α of optical glasses for the internationally used temperature range for comparison purposes (-20 °C; 300 °C) are rather small and vary from 4 to 16 10^{-6} K^{-1} [9]. This fact explicitly confirms that temperature aberrations arising from geometrical alteration of plastic elements is a significant problem in the design. Hybrid glass-plastic optics should be applied to increase temperature stability of the systems [7].

Another thermal parameter is the thermo-optical constant defined as:

$$S = \alpha(n - 1) + \frac{dn}{dT} \quad (3)$$

in case of a plane-parallel plate which is an approximate measure of the sensitivity of the material to radial gradients and quantifies the optical path difference with temperature. Negative values of S show the same tendency as TOCs. In comparison to most glass types [9], TOCs of polymer materials are negative and their absolute values are with about two orders of magnitude larger. Thus, maintaining focus over a large range of temperature is a significant problem in plastic optics.

Acoustic and optomechanical characteristics

Low weight of polymer elements is a great priority in comparison to optical glass types. In Table 3 results for obtained densities ρ of studied polymers measured by the hydrostatic weighing method are presented. Density values are from 2 to 6 times smaller than those of glasses.

As known, dynamic elastic moduli of materials are related to sound velocities in solid bodies. In Table 3 measured values of velocities of longitudinal c_l , and transverse c_t waves are given. A comparison to velocities published by other sources [5] is presented. As seen, there can be significant differences for one and the same named material in respect to the measuring method, as well as to the processing conditions of the polymeric brand. Literature data were found only for basic polymer types. Velocities of shear waves are difficult to be measured and are rarely cited. Results show that longitudinal waves travel faster than shear waves and velocities of longitudinal waves are approximately twice the value of shear waves. Given values of densities and velocities of longitudinal waves determine the material acoustic impedance which is defined as the product of both quantities. Knowledge of material impedances enables the study of propagation of sound waves and phenomena at sample interfaces.

Table 3. Densities and ultrasound velocities of PMs.

Polymer	ρ , kg/m^3	c_l , m/s		c_t , m/s	
		meas.	lit.	meas.	lit.
PMMA	1187	2745	2724 2730	1356	1377 1430
PS	1040	2388	2346 2340	1152	1157 1143
PC	1195	2234	2250 2268	906	948
SAN	1160	2561	–	1176	–
Zeonex E48R	1007	2535	–	1035	–
Optorez 1330	1202	2648	–	1209	–
Bayer	1204	2221	–	824	–

Propagation of sound waves in isotropic solid bodies is determined by the material elasticity moduli. In case of samples which transverse dimensions are much greater than the sound wavelength, there are simple relations between sound velocities and the material elastic parameters:

$$c_l = \sqrt{\frac{E(1 - \mu)}{\rho(1 + \mu)(1 - 2\mu)}} \quad (4)$$

$$c_t = \sqrt{\frac{G}{\rho}} \quad (5)$$

As it can be seen, the velocity of the longitudinal wave depends on Young's modulus E , also known as tensile modulus, and it is a measure of the stiffness of an isotropic material. Velocity of shear (transverse) wave is related to shear modulus G in Eq. (5). Static and dynamic methods are applied for determination of elastic moduli of solids but they differ substantially. Experimental conditions such as magnitude of the external load, as well as of loading rate significantly affect measuring accuracy of the results obtained by static stress – strain measurements. The dynamic methods with a sinusoidal load are also applicable and they have a relatively high accuracy. According to the frequency range, the dynamic methods are classified as: acoustic for frequencies below 10^4 Hz and ultrasonic for frequencies between 10^4 and 10^8 Hz. The dynamic methods are widely applied to study elastic properties and determine the elastic moduli of glasses and glass-forming liquids [9]. Young's modulus of optical glass ranges from 51 GPa (SF66) to 126 GPa (N-LASF21). As seen from Table 4, tensile moduli of PMs vary between 2.3 and 5.8 GPa and their elastic properties are rather different. Large values of E for glasses and glass-ceramics correspond to their ideal brittleness and are matched by an equally ideal elastic behaviour up to the breaking point.

In Eq. (4) μ is the Poisson's ratio which is another important material characteristic used in elastic analysis. It is calculated by:

$$\mu = \frac{1 - 2(c_t / c_l)^2}{2 - 2(c_t / c_l)^2}. \quad (6)$$

Generally, stiffer materials have lower Poisson's ratio than softer materials. According to the results in Table 4, Poisson's ratio of PMs varies between 0.34 and 0.42 while for glasses is in the range 0.21 to 0.25.

There are also some other useful relations – shear modulus G and bulk modulus K depend on μ and tensile modulus E by the expressions:

$$G = \frac{E}{2(1 + \mu)}, \quad (7)$$

$$K = \frac{E}{3(1 - 2\mu)}. \quad (8)$$

The bulk modulus can be determined by static compression experiments but also and more easily by measuring the velocity of longitudinal sound waves. Different models are applied and K is the only mechanical quantity that can be calculated by means of additive quantities according to the group contribution theory [10].

Table 4. Elastic characteristics of PMs.

Polymer	μ	E , GPa	G , GPa	K , GPa
PMMA	0.34	5.8	2.2	6.0
PS	0.35	3.7	1.4	4.1
PC	0.40	2.7	1.0	4.7
SAN	0.37	4.4	1.6	5.5
Zeonex E48R	0.40	3.0	1.1	5.0
Optorez 1330	0.37	4.8	1.8	6.1
Bayer	0.42	2.3	0.8	4.8

Dimensional stability of optical components is influenced by many factors as varying temperature, moisture, pressure, stress, etc. Low values of Young's moduli of PMs confirm easy deflection of plastic elements by external loading or intrinsic mass. Structural stability in respect to both static and dynamic load is a basic requirement for most optical systems and can be characterised by the following parameters: resonant frequency, deflection at constant thickness, deflection at constant mass and mass at constant deflection [8]. All these quantities are functions of density and Young's modulus and are used to compare structural efficiency of materials [11]. Results for these characteristics are presented in Table 5. Deflection at constant thickness indicates the self-weight deflections of plastic elements with identical geometry and equal thickness. The figure of merit of this parameter is the specific stiffness E/ρ . Lowest possible ratio of ρ/E is preferred in order to minimize deflection. In the case where the deflections of components of equal mass but independent thickness are to be compared, deflection at constant mass, characterised by the ratio ρ^3/E , serves as an appropriate parameter and small values are preferred. This factor should be compared if mass is a specified parameter of the optical element and minimum self-weight deflection is desired [11].

Table 5. Optomechanical parameters of PMs.

Polymer	$\rho/E, \times 10^{-7}$ kg/(N.m)	ρ^3/E kg ³ /(N.m ⁷)	$(E/\rho)^{1/2}$ $\times 10^3$ m/s	σ , MPa
PMMA	2.0	0.3	2.2	30.9
PS	2.8	0.3	1.9	17.1
PC	4.3	0.6	1.5	11.5
SAN	2.6	0.4	2.0	17.3
Zeonex E48R	3.3	0.3	1.7	15.1
Optorez 1330	2.5	0.4	2.0	22.8
Bayer	5.2	0.7	1.4	10.0

For most applications, the resonant frequency of the optical element is an important figure of merit and is characterised by $(E/\rho)^{1/2}$ since natural frequency is proportional to the square root of the specific stiffness. High values of this parameter are appropriate for large plastic optical components with protruding parts, in order to get high resonant frequencies [8].

Thermal stress σ is another quantity used in polymer optics which combines mechanical and thermal properties of materials. This is the internal stress generated in a plastic piece due to a specified temperature difference ΔT . It can be estimated in first approximation using the following formula:

$$\sigma = \frac{E\alpha\Delta T}{1 - \mu} \quad (9)$$

The values in Table 5 represent the thermal stress factor, indicating stress over a temperature change ΔT of 50 °C which corresponds to usual variations of service temperatures in respect to environmental conditions. Results for PC and Bayer confirm their greatest stability in respect to temperature. Polycarbonate materials also have broadest service interval from -137 to 130 °C and possess more stable thermo-mechanical and physical-chemical properties in the limits from -30 ° to 125 ° [6]. The Japanese brand Zeonex E48R is a thermally stable polymer, too. Most of PMs, have much lower service temperature limits, in some cases no higher than about 60 °C. The maximal limit may approach 250 °C for some of the fluoropolymers.

As seen from Eq. (9), thermal stress is proportional to Youngs modulus and to the coefficient of thermal expansion and reciprocal to the Poisson's ratio. Therefore, materials with a large thermal expansion coefficient and Youngs modulus value are very sensitive to thermal shock and have to be processed very carefully. In comparison to glass, thermal stresses in PMs are lower because of

the small values of Youngs modulus and higher Poisson's ratios though thermal expansion coefficient is larger [9]. Generally, the ability of plastics to withstand rapid changes of temperature is better than that of glasses. Thermoplastics allow variation of temperature below melting point without loss of optical quality. All of studied PMs in this report are thermoplastic.

Thermal stress is especially useful in coating of PMs with inorganic layers to compensate their imperfections as low abrasion or chemical resistance, hygroscopicity, etc. Since the temperature rises gradually during film deposition, large differences between the stress levels at the interface between the coating and the polymer occur and generated stress may be as high as 5–20 MPa/K [8].

CONCLUSION

Refractometric and ultrasonic measurements were accomplished to reveal material and optomechanical characteristics of PMs which are important in lens design. Though polymers have excellent transmission in VIS and NIR region, they have a much more restricted range of refractive index values between 1.49 and 1.59 at d-line (Table 1). There are some PMs with RIs of 1.47 (e.g. cellulose) and high refractive polymers of HOYA company and MITSUI Chemicals, etc. with n_d 1.7 [6]. Results of RIs and Abbe numbers in NIR region are useful for the design of night vision optical systems. Presented values show lower dispersion of PMs in comparison to glasses in this part of the spectrum.

Thermal properties of PMs are studied on base of RI measurements in the interval between 0 and 50 °C. Temperature instability of refractive and dispersive properties of polymers should be regarded in the design of optical elements and devices. The large thermo-optic coefficients, linear and volume expansion coefficients and thermo-optical constants (Table 2) as well as thermal stress values (Table 5) result in arising of significant thermo-optical aberrations which should be minimised in the final construction by proper selection of optical glass-plastic and housing materials. On the other hand, thermal sensitivity of PMs may favour their utilization for dynamic control of refractive index in active waveguide components of photonic devices [7].

Dynamic elastic moduli and optomechanical characteristics of PMs are estimated on base of measured velocities of longitudinal and transverse ultrasonic waves. Comparison to literature data shows differences due to measuring method and

technology specifications of the polymer brands. In many cases published values are merely indicative for a given polymer in respect to the sample shape. Material parameters as moduli of elasticity, Poisson's ratio (Table 4), as well as parameters as resonant frequency, deflection at constant thickness, deflection at constant mass and mass at constant deflection which are responsible for structural stability (Table 5) are presented. Comparison to glasses gives higher values for factors of deflection at constant thickness and constant mass of PMs and lower values for the resonant frequency which result in lower structural stability of plastic components. PMs are suitable for optical fiber fabrication, because of their higher flexibility.

REFERENCES

1. J. Lytle, in: Handbook of Optics, M. Bass, E. W. Van Stryland, D. R. Williams, W. L. Wolfe (eds.), vol. II, McGraw-Hill, New York, 1995, p. 34.1.
2. N. G. Sultanova, C. D. Ivanov, I. D. Nikolov, *Opt. Quant. Electron.*, **35**, 21 (2003).
3. N. G. Sultanova, S. N. Kasarova, I. D. Nikolov, *J. Phys. Conf. Ser.*, **356**, 0120409 (2012).
4. S. N. Kasarova, N. G. Sultanova, R. K. Kasarov, I. D. Nikolov, *Proc. SPIE*, **11047**, 104711I (2019).
5. E. Ginzel, B. Turnbull, *NDT.net Journal*, 12 (2016).
6. N. G. Sultanova, C. D. Ivanov, I. D. Nikolov, *Refractive Index Metrology of Optical Polymers*, Lap Lambert Academic Publishing, Saarbrücken, 2014.
7. N. G. Sultanova, S. N. Kasarova, I. D. Nikolov, *Opt. Quant. Electron.*, **45**, 221 (2013).
8. M. Pfeffer, in: Handbook of Plastic Optics, S. Bumer (ed.), Wiley-VCH Verlag GmbH & Co. KGaA, Weinheim, 2005, p.7.
9. SCHOTT AG, <http://www.schott.com>.
10. D. W. Van Krevelen, *Properties of Polymers*, Elsevier, Amsterdam, 1972, p. 151.
11. R. A. Paquin, *Materials for Optical Systems*, in: Handbook of Optomechanical Engineering, A. Ahmad (ed.), CRC Press, Boca Raton, Chapter 3, 1999.

Milk protein-based formulations as controlled delivery systems for tolfenamic acid

S. Milenkova¹, B. Pilicheva^{2,3}, N. Zahariev^{2,3}, B. Shivachev⁴, R. Ivanov Rusev⁴, T. Yovcheva¹, M. Marudova^{1*}

¹University of Plovdiv "Paisii Hilendarski", Faculty of Physics and Technology, 24 Tsar Assen str., 4000 Plovdiv, Bulgaria

²Medical University - Plovdiv, Faculty of Pharmacy, 15A Vassil Aprilov blvd., 4002 Plovdiv, Bulgaria

³Research Institute, Medical University, Plovdiv, Bulgaria

⁴Institute of Mineralogy and Crystallography, Bulgarian Academy of Sciences, Acad. Georgi Bonchev str., 1113 Sofia, Bulgaria

Received: November 15, 2021; Revised: April 20, 2022

Casein-based gels were examined as potential drug carrier for a model drug, namely tolfenamic acid (TA). TA is widely applied as anti-cancer agent along with its ability to induce degradation of specific tumor proteins and decrease metastasis in liver in the case of pancreatic cancer. Casein-based spheres were formulated at high pH by ionotropic gelation in the presence of crosslinker CaCl₂. To optimize their chemical content and structure, casein concentration, TA concentration and casein/crosslinker ratio were varied. Sizes and morphology of casein gels loaded with TA were examined. The structure's phase state was tested by differential scanning calorimetry. ATR-FTIR was used to establish the crosslinking process between casein and CaCl₂. The efficiency of the loading process of drug was calculated. Studies on the drug release kinetics were conducted under simulated physiological conditions.

Keywords: casein, nanoparticles, tolfenamic acid, drug delivery system

INTRODUCTION

Proteins are macromolecules which play significant role in human life. From the nutrition aspect, through their specific functions in the human body all the way to different medical applications, proteins are practically irreplaceable on a daily basis in our life. Some of the most important advantages of the proteins are the facts that depending on the pH conditions they can be both negatively or positively charged, and they are able to interact with both hydrophobic and hydrophilic compounds [1]. Other significant characteristic of proteins is their affinity to bind ligands, hence they can be applied in specific targeted therapies. Proteins are also able to reduce the drug toxicity and extend the drug half-life [1]. These features make them desired potential drug carriers for different non-invasive paths of drug delivery [2]. One of the most examined proteins is the main milk protein, namely casein. It consists of 94% phosphoproteins (S₁-, S₂-, β-, and -casein in different ratios), which contain hydrophilic and hydrophobic domains, and 6% low-molecular weight compounds [3]. Casein is GRAS (generally recognized as safe) and it is quite often used in the preparation of different micro – and nanostructures due to its high stability, low price and low toxicity. Casein possesses other important physicochemical properties such as self-assembly, ability to bind with low-molecular compounds and ions. It is capable to

form stable strong gels and bind large amounts of water. These properties are quite useful when casein-based structures are applied in the food and medical industries. The structures attracting highest interests are pH-responsive gels and particles, result of physical, chemical or even enzymatic crosslinking, that show great potential as sustainable or controlled drug release systems. Casein can screen UV radiation due to its strong adsorption properties in the range between 200 nm and 300 nm [3]. The biggest drawback of this compound is the possible immune or allergic reaction against it in lactose intolerant patients.

Tolfenamic acid is a non-steroidal anti-inflammatory drug acting as an inhibitor of cyclooxygenases (COX) which are primarily involved in inflammation processes. This compound has shown great potential in treatment of different types of cancer by inhibiting their specific proteins leading to shrinkage of the tumor tissue, hindering the synthesis of surviving cancer cells and inducing faster apoptosis with lower chances of metastasis [4]. However, it has two major disadvantages, namely low solubility and causing irritation in the gastrointestinal tract (GIT) after administration for long time [5]. Both of these shortcomings can be overcome with one step – encapsulation the active substance in a drug delivery system. In this way its solubility and bioavailability will be significantly increased and the presence of polymeric package

* To whom all correspondence should be sent.
E-mail: marudova@uni-plovdiv.net

will prevent the irritation of GIT.

In the present study the features of a drug delivery system for tolfenamic acid on the basis of casein were examined. The effect of the concentrations of the protein, the crosslinker and the active compound on the carrier surface morphology, loading efficiency and release rate were investigated.

EXPERIMENTAL

Used material

Sodium caseinate (casein sodium salt from bovine milk) was delivered by Sigma Aldrich. Tolfenamic acid was bought from Cayman Chemical. Calcium dichloride, ethanol and sodium hydroxide used were with analytical grade. Ultra-pure water was obtained with the system Adrona Crystal B30 Bio with conductivity 0.055 S/cm.

Preparation of casein particles loaded with tolfenamic acid

The casein gels are formulated as a result of the electrostatic interactions between the negatively charged parts of the casein micelles and the positive divalent counter-ions of calcium chloride.

The studied systems in the current research were prepared according to the following procedure. Stock solution of sodium caseinate with 2% w/v concentration was prepared. The pH of the stock was adjusted to 11 with 1M NaOH and it was kept the same throughout the whole preparative process. This stock was diluted in a manner that the final concentrations of casein at the end of the mixing process were 0.5% and 1%. Tolfenamic acid was dissolved in pure ethanol at two different concentrations – 8 mg/ml and 4 mg/ml. 1 ml of this solution was added to each 4 ml of casein solution and the protocol was followed for both concentrations of each solution. The resultant mixture was stirred for 30 min at room temperature and after that time the crosslinker was added. 5% w/v CaCl₂ solution in three different ratios with respect to the concentration of the casein, namely 3:1, 5:1 and 10:1 was used as a crosslinker. The crosslinking process was left to be done for 2 hours. Then the reacting solutions were centrifuged for 15 min at 14000 rpm. The precipitate was washed twice and the obtained particles were freeze-dried and stored for further use. The samples were named as follows: Cas concentration (0.5% or 1%), Cas:CaCl₂ ratio (3:1; 5:1 or 10:1), amount of TA (20 mg or 40 mg).

Characterization of non-loaded and loaded casein particles

The size and the size distribution of the particles were examined using a NANOTRAC WAVE Particle Size, Zeta Potential, and Molecular Weight Analyzer (Microtrac). The hydrodynamic diameter of the particles was presented as the z-average size.

The shape, size and aggregation phenomena of both loaded and non-loaded particles were investigated by atomic force microscopy (AFM) AFM NANOSURF FLEX AFM (SWITZERLAND) and scanning electron microscopy (SEM) PRISMA E SEM, Thermo Scientific (USA). The particles, examined by AFM, were redissolved in distilled water and the sample suspension was deposited on a freshly cleaned microscopic glass. One minute after the deposition the surface was rinsed with distilled water. The sample was left to dry for 24 hours. The images were collected in tapping mode of the AFM using standard cantilever Tap190Al-G with 10 nm tip radius. The resultant picture showed 2.5 μm × 2.5 μm area from the sample surface with viewing field of 256 × 256 pixels collected for 1 s scan time. The samples for SEM were deposited onto double-face adhesive carbon tape and left to dry at room temperature (25°C). The SEM images of both non-loaded and loaded particles were obtained at 15 kV and 20 kV acceleration voltage.

In order to confirm both the crosslinking and the encapsulation processes, ATR-FTIR spectra were taken. A comparison between native and crosslinked casein, as well as between empty particles and loaded particles was done. The equipment for this experiment was Nicolet iS 10 FTIR spectrometer (Thermo Fisher Scientific, Pittsburgh, PA, USA), equipped with a diamond attenuated total reflection (ATR) accessory. The operating range for the spectra collection was 600 cm⁻¹ to 4000 cm⁻¹ with a resolution of 4 nm and 64 scans. The obtained spectra were analyzed with OMNIC software package.

Determination of the yield of the gelation process

The yield of the gelation process was estimated as the ratio between the dry mass of the particles (after the freeze-drying) and the total dry mass in the formulation. The calculation was done according to the equation presented below:

$$\text{Yield (\%)} = \frac{\text{dry mass of the particles}}{\text{total dry mass in the formulation}} \cdot 100 \quad (1)$$

Calculation of the loading efficiency of casein particles

To establish the encapsulated amount of tolfenamic acid into the casein structures, their loading efficiency was calculated. After the particle formation process, they were centrifuged at 14000 rpm for 15 min and the resultant supernatant was measured at 287 nm with UV-VIS spectrophotometer. The encapsulated amount of TA was calculated by the following equation:

$$E\% = \frac{(c_0 - c)}{c_0} \cdot 100 \quad (2)$$

where c_0 is the total amount of tolfenamic acid and c is the non-loaded tolfenamic acid.

Investigation of the release kinetics of tolfenamic acid from casein particles

The release kinetics of the active compound from the resultant casein structures was examined on the base of the diffusion method in a dialysis bag. A certain amount of loaded particles (equivalent to 10 mg of tolfenamic acid) was suspended in 1 ml of PBS (pH 7.4) and placed in a dialysis membrane. Then, the membranes were placed in 25 ml of release medium. For the first two hours the pH of the medium was 1.5 (hydrochloric acid buffer), for the next two pH 4 (acetate buffer) and for the next time period the pH was kept at 7.4 (PBS). During the whole process the temperature was kept 37° C and the stirring speed was 100 rpm. For the spectrophotometric analysis, samples at each hour for a consecutive 8-hour period were taken and an aliquot amount of the same buffer was added back to the solution. All the samples were examined in triplicate. The samples were analyzed at 287 nm.

Investigation of the tolfenamic acid physical state

The TA phase state was examined by the method of differential scanning calorimetry. It was performed on a TA Discovery 250 (TA instruments, New Castle, DE, USA) at a heating rate of 10 °C/min for a temperature ranging from 25 to 350 °C in an argon environment with a purging rate of 30 mL/min. Aluminum T-zero containers were used to seal the samples. The onset temperature, peak temperature and normalized enthalpy (calibrated against indium melting enthalpy standard) were analyzed by TA TRIOS software 5.1.1.46572.

RESULTS AND DISCUSSION

In the present research, structures of casein micelles crosslinked with calcium chloride were successfully formulated at different concentrations of the polymer and the crosslinker by the method of

ionotropic gelation. Their size and size distribution were investigated by dynamic light scattering technique. The average sizes of the structures are presented on Figure 1. No sizes were detected for the sample with 0.5% casein concentration and polymer:crosslinker ratio 10:1, possibly due to the low yield and concentrations. In the process of examination, a bimodal distribution was observed for all detected samples. About 70% of the particles possessed sizes in the nano-range - between 140 nm and 370 nm depending on the casein concentration and Cas:CaCl₂ ratio. The other structures were in the m range and were most likely aggregates of nanoparticles.

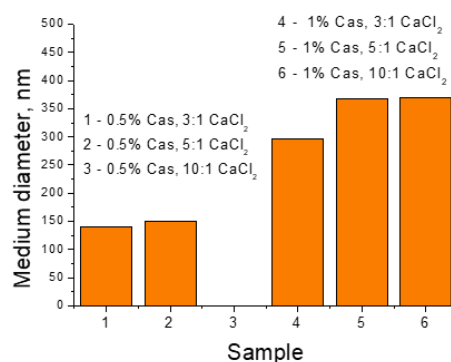


Fig. 1. Medium diameter of the formed casein structures with different concentrations of the polymer and the crosslinker.

The particle sizes strongly depend on both polymer and crosslinker concentrations. They are 140 nm (Cas:CaCl₂ 3:1) and 150 nm (Cas:CaCl₂ 5:1) when 0.5% casein solution is used, and grow to 296 nm (Cas:CaCl₂ 3:1), 368 nm (Cas:CaCl₂ 5:1) and 370 nm (Cas:CaCl₂ 10:1) at polymer concentration of 1.0%. As it is shown on the graph, for the same concentrations of casein, smaller sized particles are formed with the highest amount of CaCl₂. This result is a consequence of the mechanism of micelle crosslinking – the higher the concentration of the crosslinker, the denser micelle structure is formed.

It could be concluded, based on the size examination, that the concentration of casein influences more significantly the size distribution of the particles than the crosslinker concentration.

Couple characteristics of the particles like shape, size, morphology and aggregation were examined with AFM and SEM techniques. A microphotograph of empty casein particles and their cross-section profile is presented on Fig. 2. As can be seen from the figure, some of the particles are stuck together,

resulting in bigger aggregates. This fact, together with the cross-section image, confirms the results from the DLS. The particle's shape is not quite spherical, but closer to irregular oval one. Possible reason for this could be the result of the internal characteristic distances reported from a SAXS experiment. Similar images were observed by other authors [6]. The formed structures are uniformly distributed in the investigated area, suggesting that the particles' solution is homogenous.

Similar irregular oval shape of the empty particles is also observed in the SEM images, which

are shown on Fig. 3. After the encapsulation of tolfenamic acid, there is a variation of the morphology. Probably, as a result of the entrapment of the drug and its crystallinity state, the appearance of the micelles changed from oval to elongated rod-like shape. In addition to this, loaded particles also aggregated into branch-like islands of particles. This turns out to be a common behavior of casein micelles loaded with crystalline drug [7, 8].

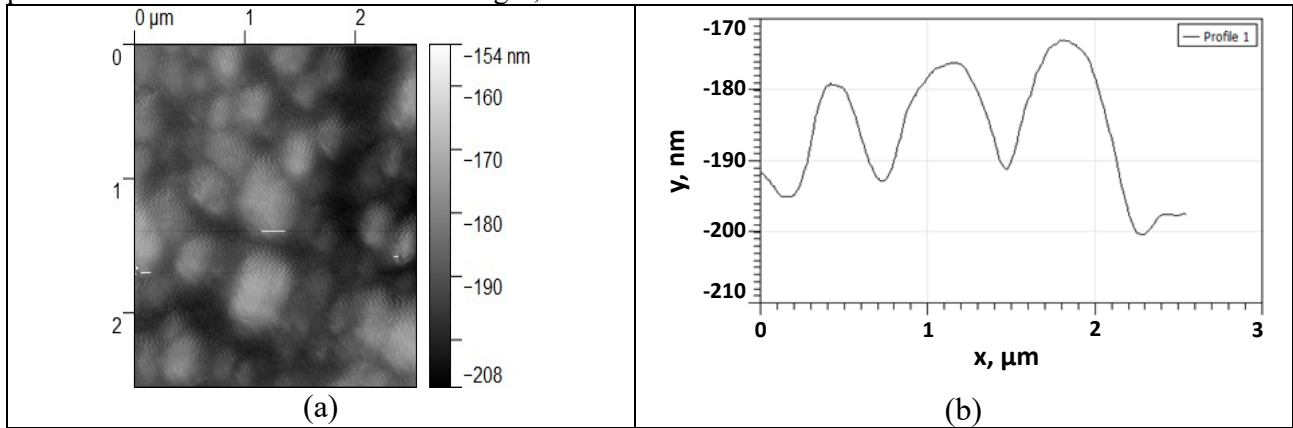


Fig. 2. AFM image of empty casein particles (a) and cross-section (b)

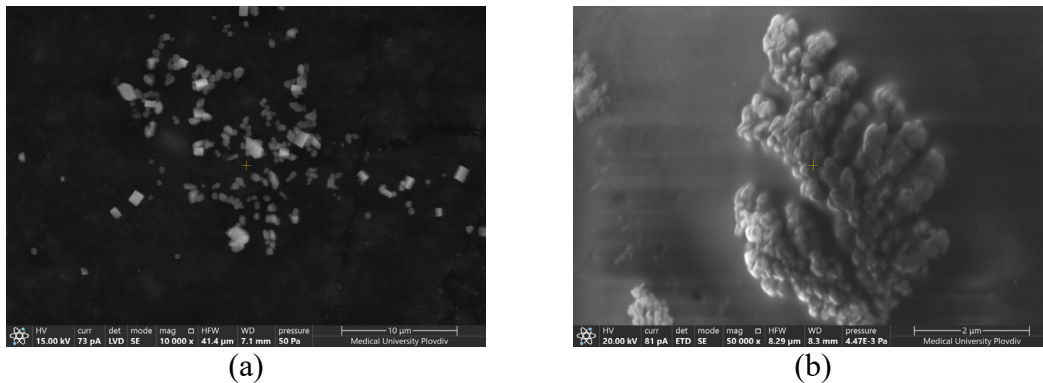


Fig. 3. SEM images of non-loaded (a) and loaded (b) casein particles

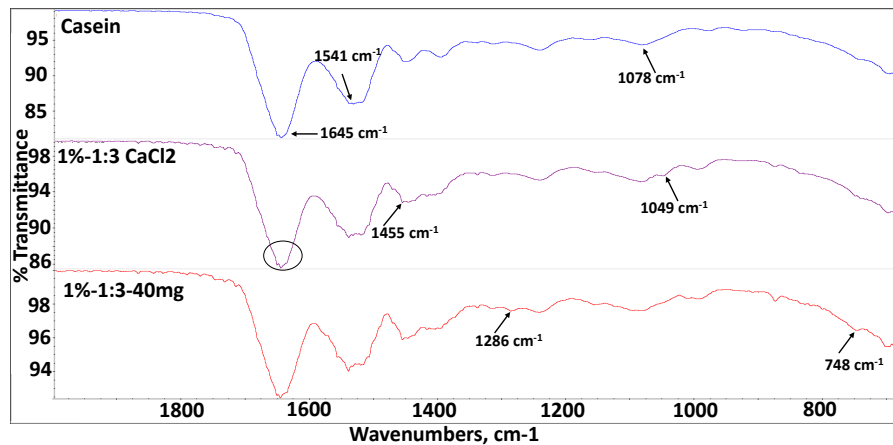


Fig. 4. Characteristic ATR-FTIR spectra of casein (blue line), empty casein particles (purple line) and casein particles, loaded with tolfenamic acid (red line).

Table 1. Particle yields (%) and encapsulation efficiencies (%) of all model samples

Sample name	Yield, %	Loading efficiency, %	Sample name	Yield, %	Loading efficiency, %
0.5%, 3:1, 20 mg	28.39	52.78	1%, 3:1, 20 mg	45.76	71.63
0.5%, 5:1, 20 mg	22.00	52.11	1%, 5:1, 20 mg	44.50	68.55
0.5%, 10:1, 20 mg	6.41	34.22	1%, 10:1, 20 mg	24.54	48.96
0.5%, 3:1, 40 mg	69.92	73.58	1%, 3:1, 40 mg	66.19	86.43
0.5%, 5:1, 40 mg	64.15	83.21	1%, 5:1, 40 mg	59.02	83.41
0.5%, 10:1, 40 mg	8.73	51.48	1%, 10:1, 40 mg	29.20	56.57

The processes of crosslinking of casein micelles by Ca^{2+} ions and the loading of tolfenamic acid into the casein particles are confirmed by ATR-FTIR analysis.

As it is shown in Fig. 4, the characteristic band of amide I at 1645 cm^{-1} (C O stretching vibration coupled with the bending vibration of NH) [9] changes its shape and transforms from doublet to triplet demonstrating that the carbonyl group might be involved in interaction with calcium. The new band at 1455 cm^{-1} that occurs in the particle's spectrum can be associated with the formation of a complex between the carboxylate ion and calcium [10]. A second new band occurs at 1049 cm^{-1} , suggesting that the phosphate group might involve in the calcium binding [9]. These results therefore demonstrated that Ca^{2+} binding to the casein most likely occurred through interaction with the carbonyl group and the phosphate group, and the presence of calcium might induce the conformational change.

The FTIR spectrum of casein particles formulated in the presence of tolfenamic acid in the reacting solution is characterized with two new bands appearing at 1286 cm^{-1} (C-H stretch deformation) and at 750 cm^{-1} (C-N stretch deformation). They indicate that the tolfenamic acid is loaded to the casein particles without presence of chemical interactions [11].

To characterize the potential of casein gels loaded with tolfenamic acid as drug delivery systems, both yield and loading efficiency of all variations of the system were examined (Table 1). The models with the highest loading efficiency and yield are those with casein:crosslinker ratio 3:1. This is a result of the densest packed micelle due to the stabilizing properties of CaCl_2 towards the casein micelles [12]. These two factors correlate with each other, because the increased casein concentration results in higher micelle concentration, which contributes to more hydrophobic interactions. Thus, they have better loading efficiency and inflated yield [13].

The phase state of the drugs (crystal *versus* amorphous) is one of the most important physical parameters which influence their bioavailability. The thermal behavior of TA in pure and in loaded state was studied by the method of DSC (Fig. 5). The melting peak of crystalline TA was observed at $\sim 214^\circ\text{C}$, which is close to the values cited in the literature [14]. No peak is observed for the casein particles with loaded TA except for the sample with 0.5% casein concentration, casein: CaCl_2 ratio 3:1 and 40 mg loaded TA, suggesting the conversion of crystalline TA into amorphous form. The TA loaded in the sample 0.5%. 3:1, 40 mg is partially crystal with degree of crystallinity 12%. In this case, as far as the TA concentration is high, it might migrate to the surface of the nanoparticles and form small irregular crystals, which melt at lower temperature than the crystal of neat TA.

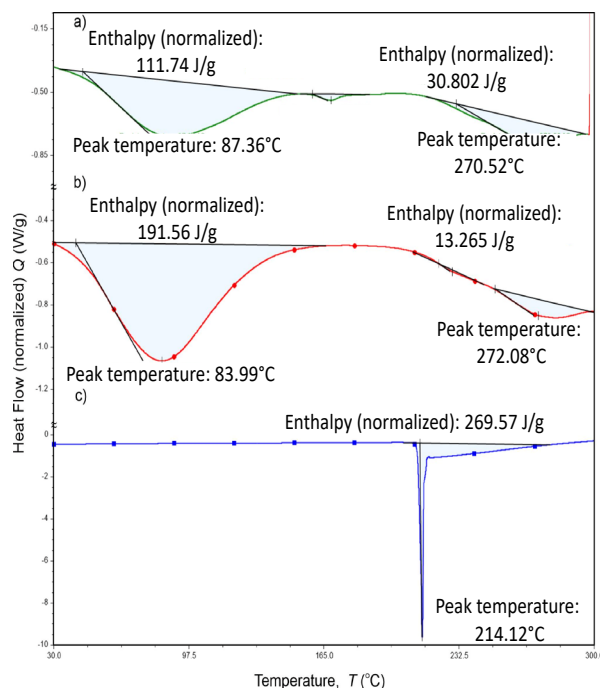


Fig. 5. DSC thermograms of TA (blue line), empty casein particles (red line) and casein particles loaded with TA (green line).

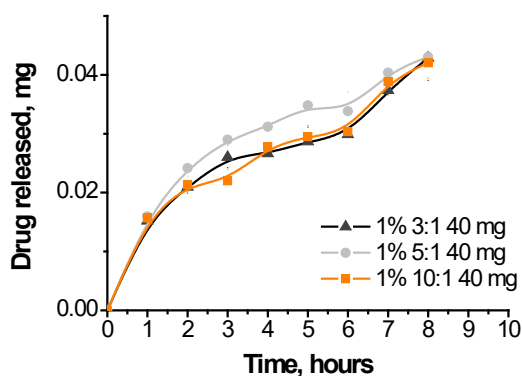


Fig. 6. TA release from casein nanoparticles with different crosslinker concentration

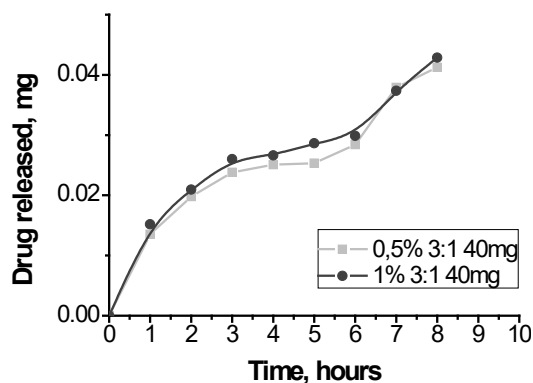


Fig. 7. TA release from casein nanoparticles with different protein concentration

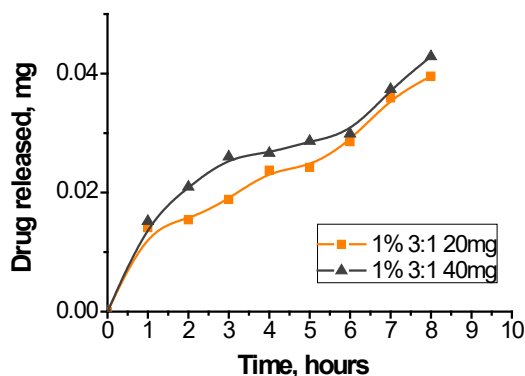


Fig. 8. TA release from casein nanoparticles at different drug concentration

The cumulative release of in different media at pH 7.4 and 37 °C for the first 8 hours is shown in Figures 6-8. The cumulative release is not more than 0.6 % during this period, demonstrating that no burst effect is realized. Hence, is well encapsulated in the casein gels. The slow release of TA could be due to its hydrophobic properties and its difficult dissolution in water media. The slower release is observed between the second and the fourth hour, when the nanoparticles are immersed in acetate buffer at pH 4. This pH is very close to the isoelectric point of casein and in this case the polymer is prone to precipitation [3]. Hence, the matrix is the densest and the drug diffusion is very difficult.

The increase of crosslinker concentration leads to delayed release (Fig. 6). Similar results have been reported by Baimark and Srisuwan [15] who found that the amount of released drug goes down when the concentration of Ca²⁺ crosslinker in alginate gels rose from 5% to 10% due to harder swelling of the alginate network.

Increasing the concentration of the casein solution from which the submicron gel particles were formed from 0.5% to 1% results in an increase in the TA release rate – Fig. 7. These results could be explained with the fact, that at the lower protein concentration the particles are less dense

and part of the drug migrates from the bulk to the surface of the particles. This assumption is confirmed by the DSC experiments. Once the drug has come to the surface, its release is faster.

The dependence of the drug concentration on the release rate is presented in Fig. 8. The increase of the drug concentration leads to faster release as a result of the looser structure of the matrix.

The obtained results demonstrated that the release profile could be controlled by the concentration of casein and crosslinker.

CONCLUSION

TA-loaded casein gels crosslinked with CaCl₂ were investigated in this study. The average size of the gel particles varied from 140 nm to 380 nm, depending on the casein concentration and casein:crosslinker ratio. The loading of TA into the nanospheres did not lead to chemical interactions between the matrix and the drug. The loaded TA was predominantly amorphous, which increased its bioavailability.

Acknowledgements: This work was financially supported by the Bulgarian National Science Fund, Project KP-06-N 38/3. The authors thank the project BG05M20P001-1.002-0005, Personalized

Innovative Medicine Competence Center (PERIMED) for the provided instrumentation used during the study.

REFERENCES

1. D. Verma, N. Gulati, S. Kaul, S. Mukherjee, U. Nagaich, *Journal of Pharmaceutics*, 2018:9285854, (2018), DOI: 10.1155/2018/9285854.
2. L. R. Brown, *Expert Opinion on Drug Delivery*, **2**(1), 29 (2005).
3. A. O. Elzoghby, W. S. A. El-Fotoh, N. A. Elgindy, *Journal of Controlled Release*, **153**(3), 206 (2011).
4. R. Basha, C. H. Baker, U. T. Sankpal, S. Ahmad, S. Safe, J. L. Abbruzzese, M. Abdelrahim, *Front Biosci. (Schol. Ed.)*, **3**(1), 797 (2011).
5. S. Rozou, S. Michaleas, E. Antoniadou Vyza, *Pharmacy and Pharmacology Communications*, **5**(2), 79 (1999).
6. M. Ouanezar, F. Guyomarc'h, A. Bouchoux, *Langmuir*, **28**(11), 4915 (2012).
7. S. Vino, K. R. Lokesh, S. Viayaragavan, G. Jayaraman, A. R. Ghosh, *International Journal of Pharmaceutical Sciences and Research*, **2**(2), 383 (2011).
8. J. Ra, K. B. Uppuluri, *Biomedical and Pharmacology Journal*, **8**(1), 83 (2015).
9. M. Luo, J. Xiao, S. Sun, F. Cui, G. Liu, W. Li, Y. Li, Y. Cao, *Food & Function*, **11**(6), 5284 (2020).
10. D. M. Byler, Jr, H. M. Farrell, *Journal of Dairy Science*, **72**(7), 1719 (1989).
11. S. Ahmed, M. A. Sheraz, I. Ahmad, *Excipients and Related Methodology*, **43**, 255 (2018).
12. A. Tsioulpas, M. J. Lewis, A. S. Grandison, *Journal of Dairy Research*, **74**(2), 167 (2007).
13. A. O. Elzoghby, M. W. Helmy, W. M. Samy, N. A. Elgindy, *European Journal of Pharmaceutics and Biopharmaceutics*, **84**(3), 487 (2013).
14. S. Ahmed, M. A. Sheraz, I. U. Rehman, *AAPS PharmSciTech*, **14**(2), 870 (2013).
15. Y. Baimark, Y. Srisuwan, *Adv. Powder Techn.*, **25**(5), 1541 (2014).

Physicochemical study of bulk Dy-123 doped with nano-Fe₃O₄

A. Stoyanova-Ivanova¹, S. Kolev^{2,3*}, V. Petrova¹, O. Petkov¹, L. M. Tran⁴, M. Babi⁴, A. Zaleski⁴, V. Mikli⁵, D. Kovacheva⁶

¹ G. Nadjakov Institute of Solid State Physics, Bulgarian Academy of Sciences, 72 Tsarigradsko Chaussee, 1784 Sofia, Bulgaria

²Institute of Electronics, Bulgarian Academy of Sciences, 72 Tsarigradsko Chaussee, 1784 Sofia, Bulgaria

³Neofit Rilski South-Western University, 66 Ivan Mihailov Str., 2700 Blagoevgrad, Bulgaria

⁴ Institute of Low Temperature and Structure Research, Polish Academy of Sciences, ul. Okolna 2, 50-422 Wrocław, Poland

⁵ Institute of Materials and Environmental Technology, Tallinn University of Technology, 19086 Tallinn, Estonia

⁶ Institute of General and Inorganic Chemistry, Bulgarian Academy of Sciences, G. Bonchev Str., bl.11, 1113 Sofia, Bulgaria

Received: November 12, 2021; Accepted: April 04, 2022

DyBa₂Cu₃O_{7-β}, or Dy-123, is a superconducting material with a high T_c . We synthesized a bulk ceramic Dy123 composite by a solid-state reaction with a starting stoichiometry of 1:2:3 (Dy:Ba:Cu). The reagents were Dy₂O₃, BaCO₃ and CuO with analytical grade purity and were mixed by grinding in an agate mortar. The resulting mixture was calcined at 900 °C in a flowing oxygen atmosphere for 21 h. The calcined powder was reground and sintered again at 940 °C for 21 h with additional annealing at 450 °C in an oxygen atmosphere for 2 h. Further, the obtained powder was reground, mixed with 2 wt. % of Fe₃O₄ nanopowder, homogenized and then pressed into tablets at 4 MPa. The bulk sample was sintered at 930 °C in a flowing oxygen atmosphere for 24 h and annealed at 450 °C in an oxygen atmosphere for 4 h. The phase composition, the microstructure and the superconducting properties of the sample were investigated.

Keywords: superconductors, nanoparticles, magnetite

INTRODUCTION

ReBa₂Cu₃O_{7-β} or Re-123 (Re rare earth element, such as Y, Eu, Gd, Dy, Nd, Sm, Ho, Er) materials are known as being superconductors with a high T_c [1]. Their properties are suitable for high-field electronic applications, such as magnetic bearings, permanent magnets, power cables, etc. Different theoretical models have been used to explain the varying T_c and the transition superconductor-insulator properties of the compound – hole filling [2], hole localization in the CuO₂ plane [3, 4], oxygen deficiency in the CuO chains leading to orthorhombic-tetragonal phase transition at its critical temperature. The higher the oxygen content, the lower the T_c [5].

The crystal structure of the ReBCO-based compounds is a multilayered perovskite structure. The layers are separated by two different Cu-sites: Cu(1) site in CuO chains and Cu(2) site in CuO₂ planes. The planes are believed to be the reason for the superconductive properties of the compound, while the chains are non-superconductive charge reservoirs introducing holes into the CuO₂ planes [6-8].

The studies carried out so far have shown that Re-123 exhibit better properties (higher transition temperatures, better performance in external magnetic fields, better surface morphology) and are more easily applicable compared to the Y123 system [9-12]. Boonsong *et al.* synthesized DyBCO ceramics under different temperatures and analyzed them, finding that the DyBa₂Cu₃O_{7-β} (Dy123) phase was the main crystalline phase in all samples. An oxygen stoichiometric change has also been observed that seems to largely affect the structural transformation of the material system [13]. On the other hand, another way of influencing the properties of the HTSC ReBCO ceramics is introducing dopants during the ceramic processing. Among the different elements studied as dopants have been Ca, K [14, 15], Ag [16] and Fe [17]. Adding ferrite nanoparticles has been reported to further improve the morphology and the magnetic flux pinning [18]. Abd-Ghani *et al.* studied the influence of Fe₃O₄ magnetic nanoparticles on the properties of YBCO superconductors and proposed that a small amount of this additive acts as effective flux pinning centers and can be applied in order to improve the critical transport current density of the

* To whom all correspondence should be sent:
E-mail: svet_kolev@swu.bg

superconductor [17].

The aim of this study is, therefore, to synthesize and characterize DyBCO ceramic with a nano-Fe₃O₄ additive in terms of identifying the phase and elemental composition, the microstructure and the superconducting transition temperature and follow any changes in the material's properties.

Experimental procedure

A bulk ceramic composite Dy123 was synthesized by a solid-state reaction with a starting stoichiometry of 1:2:3 (Dy:Ba:Cu). The reagents were Dy₂O₃, BaCO₃ and CuO with analytical grade purity mixed by grinding in an agate mortar. The resulting mixture was calcined at 900 °C in a flowing oxygen atmosphere for 21 h. The calcined powder was reground and sintered again at 940 °C for 21 h with additional annealing at 450 °C in an oxygen atmosphere for 2 h. Further, the obtained powder was reground, mixed with 2 wt.% of Fe₃O₄ nanopowder obtained by the microemulsion technique [19], homogenized and then pressed into tablets at 4 MPa. The bulk sample was sintered at 930 °C in a flowing oxygen atmosphere for 24 h and annealed at 450 °C in an oxygen atmosphere for 4 h.

Experimental methods

The X-ray diffraction patterns of the superconducting powder sample were obtained within the range 5.3 – 80°2θ at a constant step of 0.02°2θ on a Bruker D8 Advance diffractometer with Cu Kα radiation and a LynxEye detector. The phase identification was performed by the Diffracplus EVA program using the ICDD-PDF2 (2014) database. The mean crystallite size was determined by the Topas-4.2 software package using the fundamental parameters peak-shape description including appropriate corrections for the instrumental broadening and diffractometer geometry.

The microstructure of the samples was studied by means of a Zeiss EVO MA-15 scanning electron

microscope (SEM) with a LaB6 cathode on the polished cross-section of the samples. The chemical composition was determined by X-ray microanalysis using energy dispersive spectroscopy (EDS) on an Oxford Instruments INCA Energy system. The qualitative and quantitative analyses were carried out at an accelerating voltage of 20 kV.

RESULTS AND DISCUSSION

Fig. 1 shows the XRD patterns of pure Dy123 and Dy123 Fe₃O₄ samples. The high-intensity peaks are assigned to the respective samples. The XRD analysis was conducted on the whole sample surface and did not detect phases with an amount under 4%. Adding such a small amount of Fe₃O₄ nanoparticles does not affect the cell parameters, as the Fe₃O₄ does not enter the DyBCO crystal structure. For the same reason, no peaks are detected assigned to pure nano Fe₃O₄ in the XRD patterns.

The XRD analysis showed that the pure Dy123 and the Dy123 with Fe₃O₄ have the same DyBa₂Cu₃O₇ phase with orthorhombic structure and lattice parameters a 3.887 Å, b 3.825 Å and c 11.686 Å, as well as the same cell volume (V) of 173.745 Å³. The addition of 2 wt. % of nano-Fe₃O₄ to the ceramic sample does not affect the cell lattice parameters. The results thus obtained for the lattice parameters of pure Dy123 correspond to the ones obtained by other authors [13].

To calculate the oxygen content in the investigated HTSC ceramics, we used an equation establishing a correlation between the c lattice parameter and the oxygen coefficient (y) in the ReBa₂Cu₃O _{y} ceramic [21]. The results quoted in Table 2 show that the oxygen content in the sample with Fe₃O₄ is the same as in the pure one. We, therefore, assume that adding 2 wt.% of Fe₃O₄ nanopowder to the DyBCO ceramic investigated did not influence the amount of oxygen, the latter being important for its superconducting properties.

Table 1. Lattice parameters of pure Dy123 and Dy123 Fe₃O₄ samples obtained by XRD analysis

Phase	Type	Lattice parameter			V [Å ³]
		a [Å]	b [Å]	c [Å]	
Sample		Dy123			
DyBa ₂ Cu ₃ O ₇	Orthorhombic	3.887	3.825	11.686	173.745
Sample		Dy123 Fe ₃ O ₄			
DyBa ₂ Cu ₃ O ₇	Orthorhombic	3.887	3.825	11.686	173.745
Sample		Dy123 [20]			
DyBa ₂ Cu ₃ O ₇	Orthorhombic	3.839	3.889	11.687	174.485

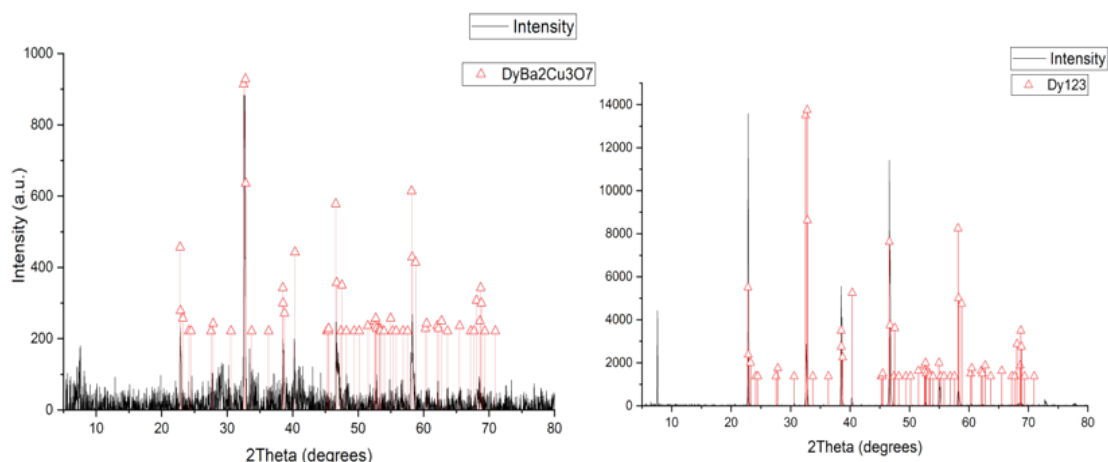


Fig. 1. XRD patterns of pure Dy123 (left) and Dy123 synthesized with Fe₃O₄ (right)

Table 2. Calculation of the oxygen content in the samples studied

Sample	Lattice parameter c [Å]	Equation $y = f(c)$	Calculated oxygen
Dy23	11.686	$y = 74.843 - 5.814 c$	6.901
Dy123 Fe ₃ O ₄	11.686		6.901

Table 3. Elemental composition of the Dy123 Fe₃O₄ sample obtained by EDX analysis

Spectrum Element	Series	1	2	3	4	5	6
		Atom. C. [at. %]	Atom. C. [at. %]	Atom. C. [at. %]	Atom. C. [at. %]	Atom. C. [at. %]	Atom. C. [at. %]
Dysprosium	L	11.65	0.28	0	4.68	4.71	4.30
Barium	L	9.04	0.26	12.59	9.34	9.39	8.52
Copper	K	11.13	44.99	17.70	13.25	13.22	14.61
Oxygen	K	68.19	54.47	57.07	71.57	71.40	71.13
Chlorine	K	0	0	12.33	0	0	0.42
Iron	K	0	0	0.32	1.16	1.29	1.02
Phase		DyBaCu	CuO	BaCuO ₂ Fe	Dy123 Fe	Dy123 Fe	Dy123 Fe

Table 3 summarizes the EDX results. They indicate that the ceramic has a non-monophasic composition. In the Dy123 with Fe₃O₄ sample, the Dy-123, BaCuO₂ and CuO phases are detected. The amount of Fe in the sample is found to be very small located around the main phases.

The EDX mapping analysis of the Dy123 with Fe₃O₄ sample (Fig. 3) confirms the presence of the main elements of the DyBCO ceramic, as well as the presence of Fe from the doping and small quantities of chlorine. We assume that the chlorine originates from the epoxy resin used to hold the sample during the test. Whole crystals of CuO and BaCuO₂ are visible on the surface, with small quantities of Fe also detected scattered around the Dy123, CuO and BaCuO₂ crystals. We believe that Fe does not react with the other elements and does not form phases of its own.

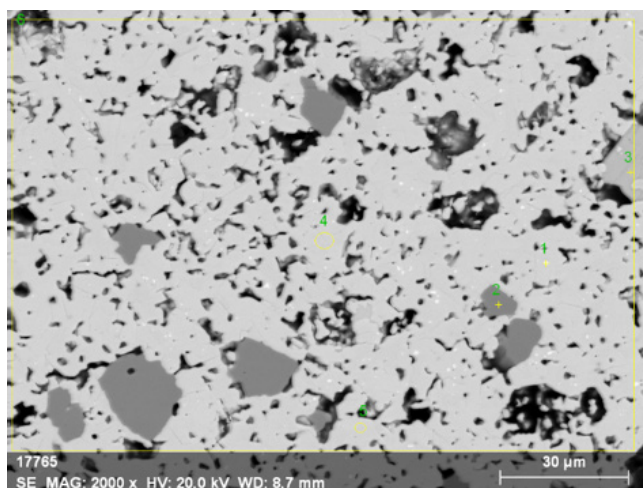


Fig. 2. SEM of Dy123 with Fe₃O₄

Fig. 2 shows a SEM micrograph of the sample Dy123 with Fe₃O₄ exhibiting a multiphase structure. The prevailing Dy123 phase has a typical surface with elongated grains and an average grain size of 3.74 μm.

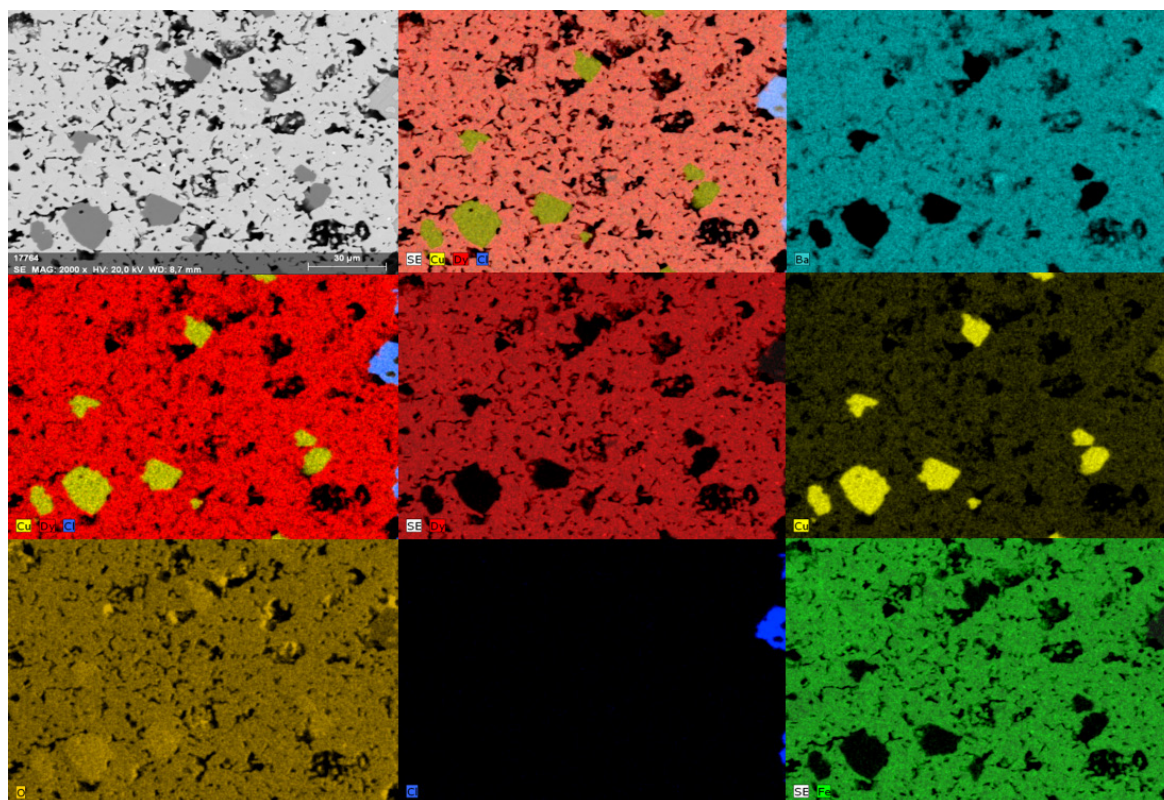


Fig. 3. EDX mapping analysis of Dy123 with Fe₃O₄

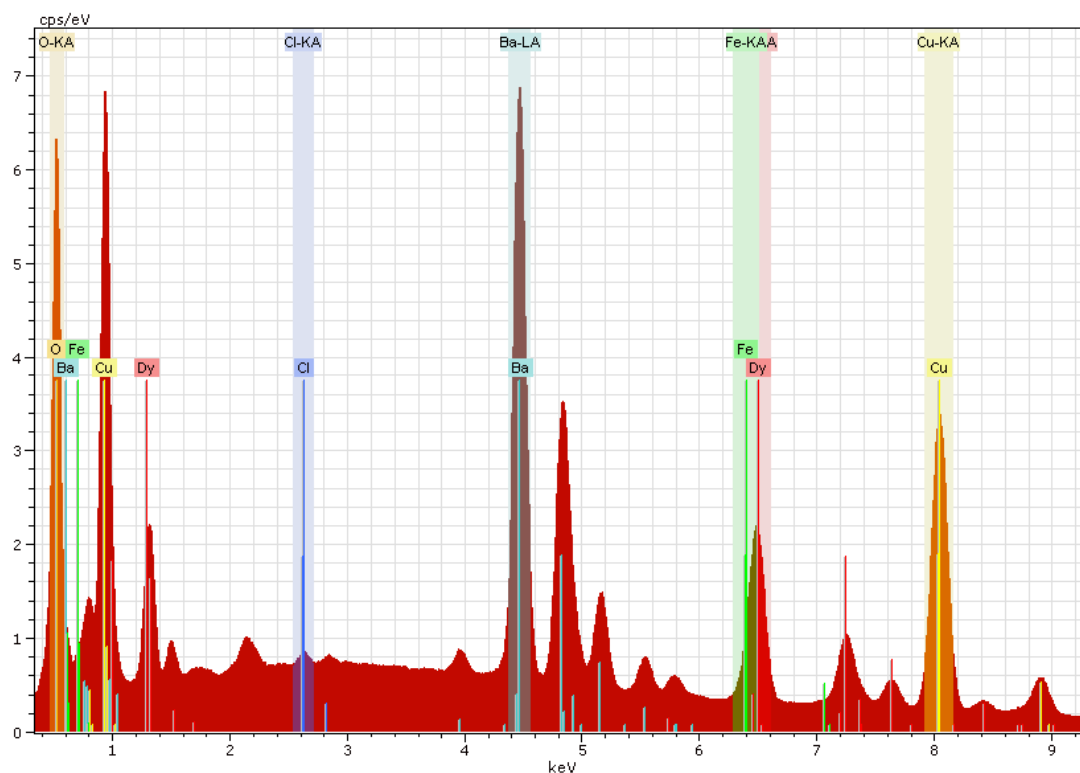


Fig. 4. EDX spectra of the Dy123 sample with Fe₃O₄

The EDX spectra of the Dy123 sample with Fe₃O₄ (Fig. 4) exhibit lines for Dy (red), Ba (light green), Cu (yellow), O (dark yellow), Fe (green) and Cl (dark blue), which correspond to the literature table values for X-ray emission lines [25]

of those elements. Respectively, L₁ 6.50 keV, L₂ 6.46 keV, L_{β1} 7.25 keV, L_{β2} 7.64 keV, L₁ 8.42 keV and M₁ 1.29 keV for Dy; L₁ 4.47 keV, L₂ 4.45 keV, L_{β1} 4.83 keV, L_{β2} 5.16 keV, L₁ 5.53 keV for Ba;

K₁ 8.05 keV, K₂ 8.03 keV, K_{β1} 8.91 keV and L lines in the 0.92 – 0.95 keV range for Cu; K₁ 0.52 keV for O and K₁ 6.40 keV, K₂ 6.39 keV, K_{β1} 7.06 keV and L lines in the 0.70 – 0.72 keV range for Fe. There are also spectral lines for Cl (K₁ 2.62 keV) detected in small quantities on the surface of the sample.

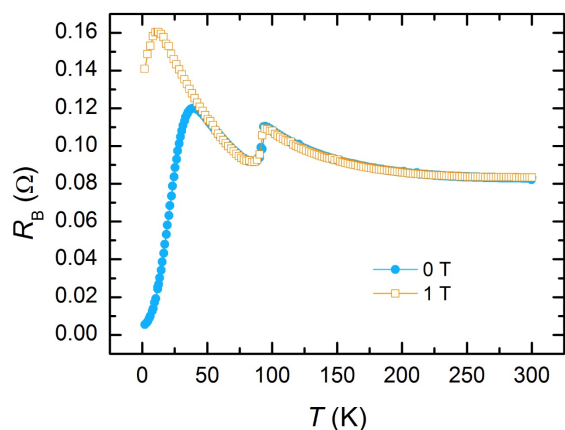


Fig 5. Electrical resistivity *versus* temperature for Dy123 with Fe₃O₄ without and with magnetic field of 1 T.

It has been found that barium cuprate is one of the few copper oxides exhibiting ferromagnetic interactions, so that during T_c measurements it can affect the transition width of the $-T$ curves. Studies have shown that, besides the superconducting properties, a composite ReBCO compound that contains BaCuO₂ exhibits magnetic properties as well [22]. Thus, one can expect that such a diversity in the non-monophasic ReBCO ceramic's property might be useful for future practical application [22-24]. The presence of the magnetic Dy³ cation in the crystal structure of the 123-phase and of the second magnetic phase of Fe₃O₄ provoked us to explore the effect of an external magnetic field on the superconducting transition temperature. Fig. 5 shows the resistivity as a function of the temperature without and with a magnetic field of 1 T. The onset of the resistivity drop is seen at 94 K ($T_{c-onset}$) in both cases, which is typical for intragrain superconductivity. The second maximum at 36 K and 12 K for measurements without and with external magnetic field, respectively, is due to the intragrain superconductivity. The $T_{c-onset}$ is higher compared with the value reported for pure polycrystalline DyBCO [12]. We presume that this is due to the presence of Fe₃O₄ nanoparticles and BaCuO₂ and CuO phases at the grain boundaries that improves the grain connectivity.

CONCLUSIONS

Using XRD analysis, the cell volume (V) of the superconducting phase (Dy123) of bulk samples was calculated.

Its values for a pure Dy123 and Dy123 with Fe₃O₄ additive were found to be the same. XRD analysis was conducted on the entire surface of the samples and did not detect phases whose amount was below 4%. EDX analysis was performed at a specific spot only and thus was able to detect other phases despite their small amounts. SEM micrographs revealed a multiphase structure with elongated grains for the DyBCO ceramic. Introducing Fe₃O₄ to the composition of the multiphase DyBCO sample investigated did not interfere with the formation of the Dy123 superconducting phase, as well as with the formation of the BaCuO₂ and CuO phases. The EDX results and the mapping analyses pointed to the presence of small quantities of Fe on the surface scattered around the Dy123, CuO and BaCuO₂ crystals, which led us to the conclusion that Fe did not react with the other elements and did not form phases of its own, nor did it enter the lattice cells of the other phases. The calculated oxygen content in the samples did not vary significantly between the sample with Fe₃O₄ and the pure one. We, therefore, assumed that adding 2 wt.% of Fe₃O₄ nanopowder to the DyBCO ceramic did not influence the amount of oxygen, its value playing an important role in the material's superconducting properties.

Acknowledgements: This work was supported by a bilateral project between the Bulgarian Academy of Sciences and the Estonian Academy of Science, Tallinn University of Technology, and a bilateral project between the Bulgarian Academy of Sciences and the Polish Academy of Sciences, Institute of Low Temperature and Structure Research, Wroclaw, Poland.

REFERENCES

1. C. Andreouli, A. Tsetsekou, *Journal of the European Ceramic Society*, **20**(12), 2101 (2000).
2. A. Matsuda, K. Kinoshita, T. Ishii, H. Shibata, T. Watanabe, T. Yamada, *Physical Review B*, **38**(4), 2910 (1988).
3. P. Wei, H. W. Ying, Z. . . i, *Physica C: Superconductivity*, **209**(4), 400 (1993).
4. H. C. Kao, F. C. Yu, W. Guan, *Physica C: Superconductivity*, **292**(1-2), 53 (1997).
5. P. Chainok, T. Khuntak, S. Su innapram, S. Tiyasri, W. Wongphakdee, T. Kruaehong, T. Nilkam on, S. Ratreng, P. Udomsamuthirun, *International Journal of Modern Physics B*, **29**(09), 1550060 (2015).
6. W. Brenig, *Physics Reports*, **251**(3-4), 153 (1995).
7. E. Dagotto, *Reviews of Modern Physics*, **66**(3) 763 (1994).
8. M. Karppinen, H. Yamauchi, *International Journal of Inorganic Materials*, **2**(6), 589 (2000).
9. . X. Jia, B. Maiorov, H. Wang, Y. Lin, S. R. Foltyn, L. Civale, J. L. MacManus-Driscoll, *IEEE*

- Transactions on Applied Superconductivity*, **15**(2), 2723 (2005).
10. J. L. MacManus-Driscoll, S. R. Foltyn, . X. Jia, H. Wang, A. Serquis, B. Maiorov, L. Civale, Y. Lin, M. E. Hawley, M. P. Maley, D. E. Peterson, *Applied Physics Letters*, **84**(26), 5329 (2004).
 11. H. Zhou, B. Maiorov, H. Wang, J. L. MacManus-Driscoll, T. G. Holesinger, L. Civale, . X. Jia, S. R. Foltyn, *Superconductor Science and Technology*, **21**(2), 025001 (2007).
 12. T. Koutzarova, I. Nedkov, M. Ausloos, R. Cloots, T. Midlarz, M. Nogues, *Phys. Stat. Sol. (a)*, **191**, 235 (2002).
 13. P. Boonsong, P. Wannasut, A. Rachakom, A. Watcharapasorn, *Chiang Mai Journal of Science*, **45**(4), 1835 (2018).
 14. A. Veneva, I. Iordanov, L. Toshev, A. Stoyanova-Ivanova, D. Gogova, *Physica C: Superconductivity*, **308**(3-4), 175 (1998).
 15. B. Khoshnevisan, M. Mohammadi, *Physica C: Superconductivity and Its Applications*, **523**, 5 (2016).
 16. K. Tantivichitvech, S. Sirininlakul, W. Bunyoprakan, T. Nilkam on, R. Supadanaison, S. Tiyasri, W. Wongphakdee, P. Udomsamuthirun, *Science and Technology RMUTT Journal*, **8** (2), 73 (2018).
 17. S. N. Abd-Ghani, R. Abd-Shukor, W. Kong, *Advanced Materials Research*, **501**, 309 (2012), Trans Tech Publications Ltd.
 18. W. Malaeb, H. Basma, R. Awad, T. Hibino, Y. Kamihara, *Journal of Superconductivity and Novel Magnetism*, **32**(10), 3065 (2019).
 19. T. Koutzarova, S. Kolev, C. Ghelev, D. Paneva, I. Nedkov, *Physica Status Solidi C*, **3**(5), 1302 (2006).
 20. P. Boonsong, P. Wannasut, S. Buntham, A. Rachakom, C. Sriprachuabwong, A. Tuantranont, A. Watcharapasorn, *Chiang Mai Journal of Science*, **45**(7), 2809 (2018).
 21. A. Stoyanova-Ivanova, T. St. Georgieva, L. Dimova, B. Shivachev, *Bulgarian Chemical Communications*, **43**(2), 320 (2011).
 22. A. K. Stoyanova-Ivanova, S. D. Terzieva, S. I. Georgieva, B. S. Blagoev, D. G. Kovacheva, A. Zaleski, V. Mikli, *Romanian Journal of Physics*, **63**(1-2), 1 (2018).
 23. K. Sreedhar, P. Ganguly, *Inorganic Chemistry*, **27**(13), 2261 (1988).
 24. P. Ganguly, K. Sreedhar, A. R. Ra u, G. Demazeau, P. Hagenmuller, *Journal of Physics: Condensed Matter*, **1**(1), 213 (1989).
 25. A. Thompson, D. Attwood, E. Gullikson, M. Howells, K. J. Kim, J. Kirz, J. Kortright, I. Lindau, P. Pianetta, A. Robinson, J. Scofield, X-ray Data Booklet, Lawrence Berkeley National Laboratory, University of California, Berkeley, CA, 94720, 2001.

Opportunities of ecologization of physics course

N. Shuyushbayeva^{1*}, A. Kaliyeva¹, N. Tanasheva², G. Altayeva², M. Talpakova³

¹*Sh.Ualikhanov Kokshetau University, Kokshetau, Kazakhstan*

²*Buketov Kar ganda University, Kar ganda, Kazakhstan*

³*L.N.Gumilyov ENU, Nur-Sultan, Kazakhstan*

Received: November 15, 2021; Revised: May 18, 2022

In the modern educational space, the priority of environmental aspects is based on solving environmental problems as a leading role of education. The article considers and analyzes the possibilities of considering environmental issues in the course of physics - the most common scientific and methodological literature. In addition, the methodological and psychological, as well as pedagogical bases of the conditions of formation of environmental education and upbringing are studied. The main goals, principles, and objectives of environmental education and upbringing in secondary school are given. In the context of the study, the most important areas that link ecology with physics are identified. The content of the course of physics in the environmental direction is marked by optional interpretations of this knowledge in accordance with the issues of environmental education, such as compulsory education. The greening of education allows us to imagine the human activity in the natural environment and to address regional and global environmental issues. The article states that the essence of many environmental laws is that they are realized in connection with the fundamental laws of nature, and the flow of energy and metabolism in ecosystems is governed by general natural laws.

Keywords: physics, ecology, nature, laws, ecological culture, facts.

INTRODUCTION

The main mechanism of formation of ecological culture is the target system of ecological education and training, including pre-school, primary, secondary, higher education, advanced training, retraining, promotion of scientific knowledge.

Environmental issues in the physics course are clearly discussed in scientific and popular literature. Among them are E. A. Turdikulov's Environmental education and upbringing of students in the process of teaching physics, Environmental monitoring of the school, T. Ya. Ashikhmina's publication, A. F. Boriskin, N. A. Ivanova Ecology in school physics; Sh. G. Ziyatdinov Environmental education in the process of teaching physics, Issues of ecology in the teaching of physics and astronomy, D. G. Maslova, . . . Alekseev Physics and Ecology; A. P. Ryzhenkov Physics and Ecology; A. P. Novikov Environmental aspects of cosmonautics; V. A. Nikerov Ecological house. Physics advice; Yu. L. Khotuntsev Man, technology, environment, V. A. Yatskevich Problems of Physics and Ecology and others [1-9].

The formation of the complex of environmental education, which is the basis of the content of environmental education, is most closely linked with physical thinking and knowledge is shown in Table 1. Also, the theoretical and methodological guidelines developed in the learning process are

slowly entering. In physics programs, only individual environmental questions are included in the physics course, and in the problem set only 1-2% of their total number are devoted to environmental issues.

It is known that to date there is no concept of environmental education in the methodological literature and the possibility of its application in the teaching process. In recent years, many researchers have adopted the concept of environmental education as a process aimed at shaping the ecological culture of the individual.

In the concept of environmental culture, it is necessary to create a culture that is the basis for the preservation and development of society-nature. Ecological ethics is a measure of ecological culture.

Methods

Environmental education in the educational process is carried out through the introduction of environmental education and direct environmentalization of the education system.

General environmental education is the direct acquisition of environmental knowledge of different nature and level, which has two main directions:

- education of ideas in the spirit of environmental protection and human health;
- finding special professional knowledge about the general laws of education of natural and anthropogenic systems.

* To whom all correspondence should be sent.
E-mail: nn_shuish@mail.ru

Environmentalization of the education system is a description of the process of penetration of environmental ideas, concepts, principles into other disciplines, as well as the training of environmentally literate professionals of various profiles [10].

Currently, there are three main models of environmental education:

- multidisciplinary model - assumes the greening of disciplines;
- introduction of one-subject - general ecological education;
- combined - in each subject and as a whole - individual disciplines in terms of environmental issues.

Table 1. Conceptual aspects of greening the course of physics in interaction with the system of environmental education in accordance with the concept of environmental education

Substantive ways to consider environmental concepts from a physical point of view	Elements of physical knowledge in the interpretation of environmental concepts
Global megaecology. Object: biosphere. Physical features of construction, life and evolution. The relationship between the biosphere and geosphere, the biosphere and the planet around the world. Physics of biosphere phenomena and processes. Physical pollution of the biosphere.	Planets and their cosmic environment. Day-to-day communications. Outside the planets: atmosphere, hydrosphere, lithosphere, and magnetosphere. Metabolism: geological, biogenic. Energy flow in the biosphere. Heat balance of the atmosphere and the earth's surface. Transformation of energy by living matter in the biosphere. Thermal, electromagnetic, radioactive, pollution. Equilibrium of the biosphere. Targeted values of physical effects on the biosphere and its elements.
Geographical ecology. Object: landscapes. Physical features of landscape formation. Physical bases of climatic processes. Physical parameters of geosystem resilience: physical norms of anthropogenic load on different types of landscapes.	Erosion of mountain seeds and land. Mechanical, thermal, electromagnetic, acoustic, radiation characteristics of the area (local geosystem). Climate is like physical influences. (natural and anthropogenic). Equilibrium of geoecosystems. Load on geoecosystems, load values.

Classical bioecology. Object: Ecosystem (organism level). The influence of physical factors of the environment on the nutrition of the union, the vital activity of various organisms and their ability to adapt. Evolution of physical factors of organisms and the environment. Influence of physical factors of environment on succession rate and characteristics.	Physical factors of the region: light, electromagnetic waves, spectrum, EMV, temperature, humidity, ionizing radiation, field characteristics, etc. (gravitational, electromagnetic) Adaptation of the organism. Heat exchange, heat balance. Metabolism (water and gas exchange). The impact of physical pollution on population health.
Human ecology. Human is a psychobiological system that interacts with the natural and socio-cultural environment. Physical factors of the environment and the human body in different climatic conditions. Human adaptation. Ecology of urban population: the impact of urban environmental factors on human health (noise, lighting, air ionization, ionizing radiation, etc.). Radio ecology: radiation as an anthropogenic factor of the environment, its impact on the gene pool and population of individuals.	Human adaptation. Influence of physical factors of the region on the gene pool. Human health. Physically stable living conditions.
Social ecology. The principles of physical cognition (methodological), as the basis of the scientific paradigm, were translated into the general cultural environment. Improving the means of production and research aimed at engineering and technical optimization of society and nature. Finding an optimal economic and environmental approach, a rational technical and engineering solution to meet the needs of society and man.	The experience of physical recognition of natural systems seems to be a key part of the scientific approach. The physical basis for the improvement of existing technologies and the invention of new technologies.

On the base of our research the following environmental issues in the physics course should be considered:

- methods of physics and scientific cognition: scientific methods of cognition of the environment and their differences from other methods of cognition; the role of experiment and theory in the process of recognizing nature; modeling of physical phenomena and processes; scientific concepts; physical laws; physical theories; boundaries of application of physical laws and theories; principles of conformity; basic elements of the physical image of the world; human development and modern environmental issues; physical ecology;

i) Mechanics: space monitoring of the biosphere; issues of development of environmentally friendly clean energy sources and prospects for their use; wind energy; Efficiency and environmental safety of various mechanisms; hydropower; issues of river energy consumption (loss of fertile lands, pollution of the region, climate change, etc.).

- noise of pollution of the environment; decrease of the natural noise background level or abrupt oscillation and change of such sound characteristics as frequency of sound wave and strength of sound flow; calculate the nature of noise, noise protection structures and sound insulation

ii) Molecular physics and thermal phenomena: energy flows in the biosphere:

- the effect of temperature on the biosphere; water circulation in nature;

- the phenomenon of evaporation on the surface of the seas and oceans and its impact on the Earth's climate;

- formation of acidic precipitates; the effect of water salinity on the freezing point; the importance of air humidity and its impact on ecosystems;

- the effect of air pollution on the condensation of vapor in the atmosphere; the combined effect of temperature and humidity on living organisms;

- the second law of thermodynamics of ecological content; issues of heat engines and air protection; thermal power plants and environmental issues.

iii) Fundamentals of electrodynamics: causal phenomena in nature; effects of magnetic and electric fields on the biosphere; biopotentials; basics of electrocardiography; biological action of static electricity:

- the effect of electric current on living organisms; physical bases of operation of defensive buildings; prospects for the development of electric transport; features of an electric motor, such as an environmentally friendly motor; use of semiconductor devices; environmental converters that convert heat and light energy into electricity; water pollution treatment; (electroflotation method of purification); method for determining soil salinity by its electrical conductivity; environmental aspects of electricity generation; biological effects of heavy and light ions; the concept of electrostatic precipitators; environmental energy converters; the effect of magnetic fields on living organisms; ionization of atmospheric air; ionosphere; biological effects of heavy and light ions;

- the effect of magnetic fields on living organisms; magnetic purification of water from impurities - magnetic separation;

- electromagnetic oscillations and waves: biological effects of high-frequency electromagnetic waves and their protection; ecological examination of various options for remote transmission of electricity;

iv) Optics: differences in reflectivity on different surfaces from an ecological point of view; changes in the purification of the atmosphere under the influence of anthropogenic factors, its environmental consequences; infrared and ultraviolet radiation; environmentally hazardous light factors; biological effects of infrared and ultraviolet radiation and their protection; the result of evaporation.

v) quantum physics: alternative energy; solar energy; photo converters; the effect of laser radiation on the bioplasm:

- noise pollution of the environment; reduction of the natural background noise level or a sharp fluctuation and change in such sound characteristics as the frequency of the sound wave and the strength of the sound stream;

- calculate the nature of noise, noise protection structures and sound insulation.

vi) Radioactivity and ionizing radiation issues of radioactive waste disposal at nuclear power plants; safety at nuclear facilities; biological effects of radioactive radiation; physiological activity of neutrons and methods of protection against neutron radiation.

CONCLUSION

The content of the course of physics in the environmental direction is marked by optional interpretations of this knowledge by the issues of environmental education, such as compulsory

education. In this case, the material is collected to demonstrate the capabilities of the physical aspect in the formation of a set of environmental knowledge. Systematization of knowledge should be based on the structural elements of physical knowledge, taking into account the logic of scientific knowledge (scientific facts, the main components of systems considered from an ecological point of view, as well as the main components of the apparatus of understanding physics; laws; basic laws and theoretical principles.

REFERENCES

1. E. A. Turdykulov, Ecological education and educating schoolchildren in the process of teaching physics. A book for teachers, Moscow, Enlightenment, 1988.
2. T. Ya. Ashikhmina, School environmental monitoring, Moscow, AGAR: Rendezvous-AM, 2000.
3. A. F. Boriskin, N. A. Ivanova, Ecology in the school physics course, Textbook, Nizhnevart. Ped. Inst., Nizhnevartovsk, 1999.
4. Sh. G. Ziyatdinov, Ecological education in the process of teaching physics, Moscow-Birsk: BGSPA, 2005.
5. A. P. Ryzhenkov, Physics and ecology, Kolomen. Ped. Inst. M., Prometheus, 1989.
6. L. C. Novikov Environmental aspects of cosmonautics, Moscow, Knowledge, 1986.
7. V. A. Nikerov, Eco-friendly home: Physics advice, M., Energoatomizdat, 1992.
8. Yu. L. Khotuntsev, Ecology and ecological safety: a textbook for students, 2nd edn., M., Publishing house. Academy, 2007.
9. V. A. Yatskevich, Physics and environmental issues, Vologod. State Ped. Inst., Vologda, 1997.
10. I. T. Suravegina, V. M. Senkevich, V. T. Kucher, Environmental education at school, Soviet pedagogy, 1990.

Possibility of measuring the angular characteristics of the primary and secondary tracks of relativistic nuclear fragmentation by the nuclear track emulsion method

R. Stanoeva^{1,2*}, A. A. Zaitsev^{3,4}, P. I. Zarubin^{3,4}

¹South-West University, Ivan Michailov Str. 66, 2700 Blagoevgrad, Bulgaria

²Institute for Nuclear Research and Nuclear Energy, Bulgarian Academy of Sciences, BG-1784, Sofia, Bulgaria

³Joint Institute for Nuclear Research, Joliot-Curie 6, Dubna, Moscow region, 141980, Russia

⁴P. N. Lebedev Physical Institute of the Russian Academy of Sciences, Leninskij Prospekt 53, Moscow, 119991, Russia

Received: October 27, 2021; Accepted: March 21, 2022

In this study the application of the nuclear track emulsion technique (NTE) in radioactivity and nuclear fission studies is used. As an example, some results for determining the angular characteristics of the primary and secondary tracks of relativistic fragmentation of ^{28}Si nuclei with a momentum of 4.5 A GeV/c are presented. Angular measurements only for fragments are performed. The invariant mass approach based on angular emission measurements of secondary fragments and approximation of the momentum conservation per nucleon of the parent nucleus is applied.

Keywords: nuclear track emulsion technique, relativistic fragmentation, angular measurements.

INTRODUCTION

Providing a record spatial resolution, the nuclear emulsion method makes it possible to very effectively conduct survey studies on newly formed beams. A set of relativistic fragments can be observed entirely in a single emulsion layer with a thickness of only about 500 μm in 3 spatial dimensions with a resolution of better than 0.5 μm [1, 2]. The accuracy of the reconstruction of the vertex makes it possible to get rid of secondary interactions, since the thickness of the substance before the start of observing individual tracks in such a detector does not exceed several mg/cm^2 . The limitation on the analyzed statistics is compensated for by the inaccessibility for complete observation of fragment set composition in other methods. The content in a nuclear emulsion in close concentrations of heavy nuclei Ag and Br, a group of light nuclei C, N, and O, and hydrogen turns out to be useful when comparing peripheral interactions of various types. Under the same conditions, one can observe both the breakup of the nucleus by the electromagnetic field of the heavy target nucleus and in collisions with the target protons. The fragmentation pattern of emulsion nuclei includes a multiplicity of strongly ionizing target fragments, including α -particles, protons with energies below 26 MeV, and light recoil nuclei - n_b (b-particles), as well as non-relativistic protons with energies above 26 MeV - n_g (g-particles). In addition, the reactions are characterized by a multiplicity of produced mesons n_s (s-particles). Using these parameters, one can draw preliminary conclusions on the character of the interaction.

* To whom all correspondence should be sent:
E-mail: rstanoeva@swu.bg

An example of the interaction of pro ectile nuclei in a nuclear track emulsion is shown in Fig. 1.

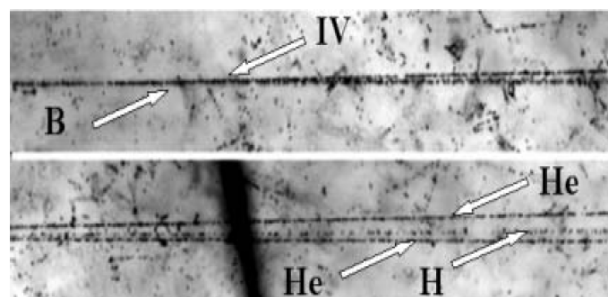


Fig. 1. Example of peripheral interaction of a 1.2 A GeV ^{8}B 2He H in a nuclear track emulsion (white star). The interaction vertex (indicated as IV) and nuclear fragment tracks (H and He) in a narrow angular cone are seen on the upper microphotograph. Following the direction of the fragment set, it is possible to distinguish 1 singly (the central track) and 2 doubly charged fragments on the bottom microphotograph.

Angular measurement conditions

Fragments of the relativistic nucleus fly out in a narrow front cone, the angle of which can be approximately estimated by:

$$\theta \approx \sin^{-1} \frac{P_F}{P_0}$$

where P_F is the average momentum of the Fermi motion of nucleons in the pro ectile nucleus, and P_0 is the momentum per nucleon of the pro ectile nucleus. It can be seen from the above formula that the greater the pro ectile energy, the smaller the emission angles of the pro ectile-nucleus fragments. For a pro ectile-nucleus momentum of 4.5 A GeV/c and a Fermi momentum of $P_F = 200$ MeV/c, we obtain $\theta \approx 2.5^\circ$. Most sensitive to the structural

features of the nuclei under study are the angular distributions of relativistic fragments and their angular correlations.

The search and collection of material in a nuclear photographic emulsion is carried out at the stage of viewing, preceding direct measurements, sometimes with the aim of isolating certain types of events. Analysis of angular distributions plays an important role in describing the physical picture of the reaction under study. The emulsion technique makes it possible to measure the track angles, both of primary particles and those formed with a high accuracy of 10^{-3} radians. Measurements of the angular characteristics of the tracks are carried out in a coordinate system associated with the Cartesian coordinates of the microscope.

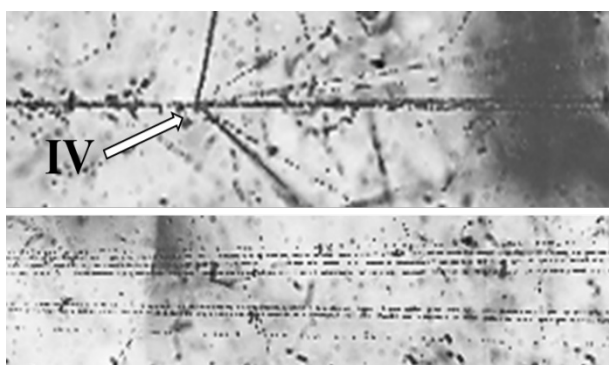


Fig. 2. Example of peripheral interaction of a 4.5 A GeV/c ^{28}Si ^5He ^2H in a nuclear track emulsion. The interaction vertex (indicated as IV) and nuclear fragment tracks (He and H) in a narrow angular cone are seen on the upper microphotograph. Following the direction of the fragment et, it is possible to distinguish 2 singly and 5 doubly charged fragments on the bottom microphotograph.

EXPERIMENTAL

A stack of NTE layers was exposed to a beam of ^{28}Si nuclei with a momentum of 4.5 A GeV/c. An example of the interaction of projectile nuclei in a nuclear track emulsion is shown in Fig. 2.

The NTE layer with the plate number 34 is randomly selected. Viewing the plate was aimed at searching for nuclear interactions of ^{28}Si nuclei with nuclei from the emulsion. We can use three methods for searching for events, including trail, area, and strip. In our study the search was carried out by scanning by stripes with a step of 1 mm.

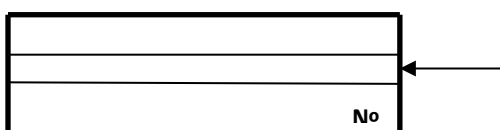


Fig. 3. A schematic representation of the emulsion layer, where No is the plate number.

The NTE layer has a size of 10 × 20 cm², and its primary thickness is 579 μm. During irradiation, the beam was directed as shown in Fig. 3.

To view the emulsion layer, an MBI-9 type microscope was used with a 60 objective lens and 15 eyepieces. In total, about 60 squares were viewed. Eight different types of interactions of beam nuclei were found, in which the formation of more than two α -particles in the fragmentation cone is observed. The fragmentation cone was determined visually.

In our experiment, the coordinate method of angular measurements was used. The emission angles of secondary relativistic particles relative to the primary particle (polar and azimuthal) were measured using a special measuring microscope for nuclear research KSM-1 from Zeiss. Since the microscope is designed to measure momentum of high-energy particles by multiple Coulomb scattering, then the noise of the microscope when measuring the coordinates of the tracks can be ignored. It is worth noting that there are situations where angular measurements cannot be taken. This is most often associated with the location of the event in the emulsion. For example, the star is too close to the edge of the record, etc. Further, we assume that the conditions for the measurement are favorable. The angles of secondary particles measured in emulsions and their designations are shown in Fig. 4.

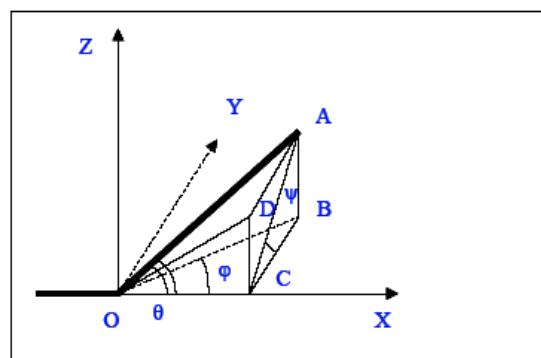


Fig. 4. Determination of the angles of secondary particles: \vec{OY} - direction of the primary particle; \vec{OA} - direction of the secondary (measured) particle; $\angle OAZ$ - polar angle (θ); $\angle AOX$ - azimuth angle (ϕ); $\angle AOB$ - angle in the plane of the emulsion (α); $\angle DOA$ - depth angle (β).

The emulsion layer glued to the glass is fixed on the microscope stage. In this case, the plate is turned in such a way that the direction of the primary particle best coincides with the OX axis of the microscope stage with an accuracy of 0.1–0.2 μm. Before starting measurements, select a rectangular Cartesian coordinate system as follows.

The OX axis is directed along the beam along the projection of the primary track. The OZ axis is perpendicular to the plane of the emulsion and is directed from the glass on which the emulsion is fixed to the surface. The OY axis is directed so that a right-handed coordinate system is obtained. In this coordinate system, it is possible to determine the coordinates of points, both of the track of the primary particle and the tracks of fragments. The coordinate method is based on the measurement of three coordinates (x, y, z) of the track point in the emulsion, on the basis of which the track angles are calculated. The transition to the system associated with the primary particle uses the angular measurement of the primary track.

Angular measurements were performed only for fragments in 6 events with the formation of target fragments. Two of them are ^{28}Si 5 ...,

1- ^{28}Si 6 ..., 1- ^{28}Si 4 ... and 2- ^{28}Si 3 ... The track point coordinates were measured sequentially in one direction (from left to right and from the layer surface to) along the beam starting from the primary track and further for all tracks of fragments simultaneously. To measure the angles of fragments with a narrow angular cone of fragmentation, it was necessary to shift the measurement from the center of the event at a distance 200 μm , since the fragments cannot be distinguished. The offset for each event was selected individually. For all tracks, 10 triplets (x, y, z) of coordinates of points were measured with a step of 100 μm , with a total track length used for measurement of 1 mm. In one event, 15 triplets (x, y, z) with a step of 100 μm were measured for the secondary tracks (Fig. 5). Below are the primary results of angular measurements.

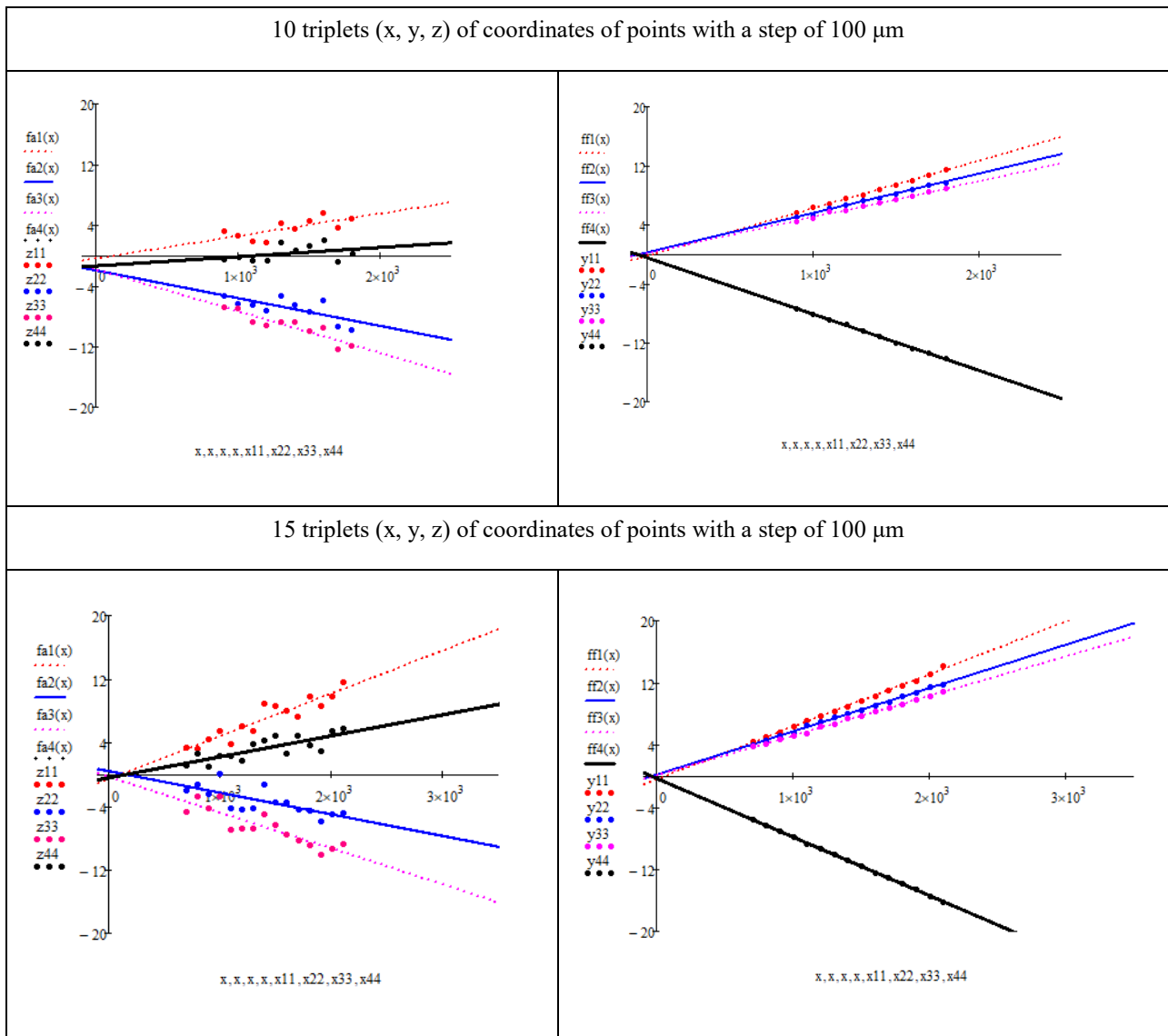


Fig. 5. Examples of observed triplets (x, y, z) of coordinates of points with a step of 100 μm . The left-side pictures are projections of tracks to the XOZ plane, on the right side – to the XOY plane. Dots are the measured points, lines – approximated directions of tracks.

Some results of angular characteristics of fragments of the ^{28}Si nucleus

The emission angles of particles with $Z_{fr} = 2$ (Fig. 6) are measured up to the value 3° with mean value $12 \cdot 10^{-3}$ rad (RMS $9 \cdot 10^{-3}$ rad) for 26 fragments. Measurements of the angle make it possible to calculate the transverse momenta P_T of relativistic fragments with a mass number A_{fr} according to the approximate relation $P_T = A_{fr} P_0 \sin \theta$, where A_{fr} is the mass number of a fragment, θ its emission angle and P_0 the momentum per ^{28}Si nucleon ($P_0 = 4.5 A \text{ GeV}/c$).

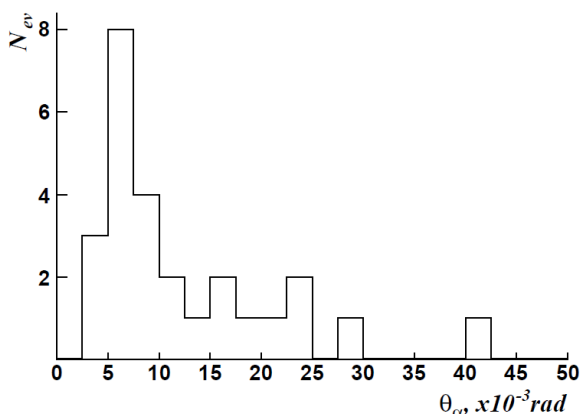


Fig. 6. Distribution of the α -particle polar angle.

As the next step in the analysis of events, the spectrum of pair angles was obtained. Figure 7 shows the opening angle distribution $\Theta_{2\alpha}$ of α -particle pairs with mean value $\Theta_{2\alpha} = 16 \cdot 10^{-3}$ rad (RMS $10 \cdot 10^{-3}$ rad) (47 pairs of alpha particles). Associated with the distribution over the pair angle is the invariant mass of the system of fragments: $M^{*2} = (P_i + P_j)^2 = (P_i^2 + P_j^2 + 2P_i P_j \cos \Theta_{2\alpha})$. Knowing its value allows you to calculate the excitation energy $M^* - M$, where M is the mass of the ground state of the nucleus corresponding to the charge and weight of the analyzed system.

Figure 8 presents the energy distribution $Q_{2\alpha}$ of α -particle pairs with mean value $Q_{2\alpha} = 8 \text{ MeV}$ (RMS 9 MeV) for 47 pairs of α -particles. In the interval $Q_{2\alpha} = 1 \text{ MeV}$, a grouping of events is observed. A more detailed histogram in this interval presented in the inset shows an increased distribution of $Q_{2\alpha} = 1 \text{ MeV}$ of pairs of α -particles, which includes 17% (8 α -particle pairs) of α -particle pairs with an average value $\Theta_{2\alpha} = 3 \cdot 10^{-3}$ rad (RMS $2 \cdot 10^{-3}$ rad). The relativistic fragmentation of the ^{28}Si nuclei in a nuclear track emulsion can help us to identify decays of ^8Be , ^9B nuclei and Hoyle state in the invariant mass distributions of 2α -pairs. As an example, the values of $Q_{2\alpha} = 0.1 \text{ MeV}$ indicate decays of the unstable ^8Be nucleus.

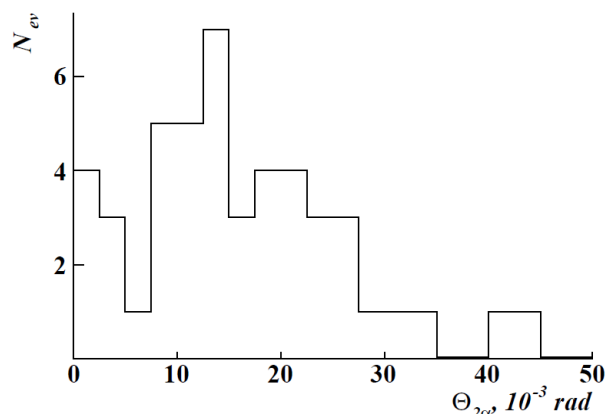


Fig. 7. Distribution over angle $\Theta_{2\alpha}$ of α -particle pairs

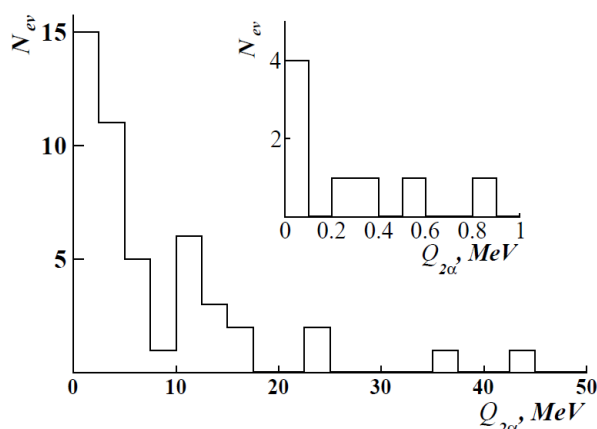


Fig. 8. Energy distribution $Q_{2\alpha}$ of α -particle pairs. The inset shows an increased distribution of $Q_{2\alpha} = 1 \text{ MeV}$ of pairs of α -particles.

CONCLUSIONS

Possessing a record space resolution, the nuclear emulsion method keeps unique possibilities in studying the structure particularities of light nuclei. The traditional task of the nuclear track emulsion method is to outline the nuclear-interaction pattern on the basis of a limited statistical data sample in order to plan better future complicated experiments featuring various detectors. Limitations on the statistics subjected to analysis are compensated to some extent by the impossibility of completely observing the composition of fragments within other methods. The macro photos of the experiments under discussion and the corresponding videos are available on the website of the BEC UEREL project [3].

The results of this work can form the basis for planning future experiments with radioactive relativistic nuclei with higher statistics and detail of fragment identification, as well as higher complexity and variety of detectors. The described option for measuring angles is not the only one.

The choice of technique depends on the specific task and the resources available.

Acknowledgement: *The scientific publication was realized as a result of the provided funding from the Ministry of Education and Science under the project "Joint Institute for Nuclear Research (JINR, Dubna)", object of the National Roadmap for Scientific Infrastructure 2020 – 2027.*

REFERENCES

1. C. F. Powell, P. H. Fowler, D. H. Perkins, The Study of Elementary Particles by the Photographic Method, London - New York, Pergamon Press, 1959.
2. W. H. Barkas, Nuclear Research Emulsions. New York – London, Academic Press, 1963.
3. The BEC UEREL Project, <http://becquerel.inr.ru/>.

Section
Technical Sciences

An Android-based mobile application giving information for weather in real-time

F. I. Sapundzhi*, M. D. Mladenov

¹South-West University "Neofit Rilski", 2700 Blagoevgrad, Bulgaria

Received: November 25, 2021; Accepted: April 08, 2022

Nowadays mobile devices are very popular in the work and life of people. Many software applications of various mobile operating systems like Android, Symbian, and iPhone are available in online software stores. The most widely used mobile operating system is Android. It is a very popular open-source system for mobile phones and tablet personal computers. The Android Studio Integrated Development Environment is used for the development of the Android application. In the present work, we focus on designing a new smart Android-based mobile application giving information for weather in real-time. This application is expected to be useful for customers in terms of time and cost.

Keywords: Android, Mobile operating system, Mobile device, Software

INTRODUCTION

Nowadays, smartphones are some of the most popular devices used by humans, with each user using different types of smartphones with different functions. Mobile operating systems (MOS) are a software interface that is responsible for managing the hardware units and assisting the user in their use. MOS are designed to allow users to use phones as they do personal computers [1, 2]. The most popular MOS are Android, iOS and Windows phone. According to Market Share Worldwide - October 2021 [3] the ratio of these MOS is as follows: Android 71.09%, iOS 28.21%, Samsung 0.38%.

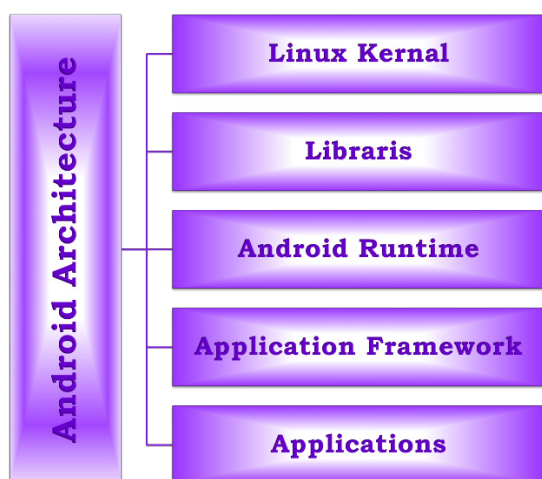


Fig. 1. Android architecture [4].

Android is an open-source mobile OS developed by an Open Handset Alliance consortium and commercially sponsored by Google in 2008. Android source code is known as the Android Open Source Project (AOSP), which is primarily licensed under the Apache license [5-7].

In the present work we focus on designing a new smart Android-based mobile application giving information for weather in real-time. This application is expected to be useful for customers in terms of time and cost.

The aim of this study is to develop a mobile application that will allow the user to check the weather or available restaurants for a city or a specifically populated place.

METHODS

The mobile application which is discussed in the current paper is called COMPASS. The technologies used to develop the mobile application COMPASS are the following:

- ✓ Android Studio version 10.0;
- ✓ Java and XML programming languages;
- ✓ Volley and JSON;
- ✓ AsyncTask Library;
- ✓ OpenWeatherMap and Google API for Restaurant Places.

Today, the most popular and used languages for developing Android applications are Java and Kotlin programming languages [7]. Kotlin is a new programming language representing an alternative to Java. The developed Android application was written in the Java programming language using an IDE called Android Studio version 10.0 and Nexus 5X with API 29. Based on JetBrains IntelliJ IDEA software, Android Studio is an IDE created specifically for Android development.

XML (eXtensible Markup Language) is used for drawing the interfaces of the developed application. Java is used for writing the backend codes while frontend codes are written in XML.

* To whom all correspondence should be sent.
E-mail: sapundzhi@swu.bg

Volley is an HTTP library that makes networking for Android applications easier and faster. It offers automatic scheduling of network requests, multiple concurrent network connections, memory response caching with standard HTTP cache coherence, request prioritization, ease of customization, debugging and tracing tools, etc. [8]. JSON (JavaScript Object Notation) is an open standard file format and data exchange format which is the best alternative for XML. Android provides four different classes to manipulate JSON data: JSONArray, JSONObject, JSONStringer and JSONTokenizer [9].

AsyncTask (asynchronous task) is designed to enable proper and easy use of the user interface thread. It allows us to run the instructions in the background and then synchronize again with our main thread [10].

The data about the weather in the developed mobile application are taken from online service OpenWeatherMap which provides information through an Application Programming Interface [11].

MOBILE APPLICATION

The mobile application gives up-to-date weather information in a city or town that a user has entered and also provides information about the restaurants in the area specified by the user. When we start the application, on the first page we see 2 buttons below the text, giving information about what each of the buttons does.



Fig. 2. Application activities.

If the user clicks on the right button of the application, a window appears in which the user can enter the name of the city and region where he wants to view the available restaurants, their exact address

and rating for them in google reviews. Also, the user can write the name of the restaurant, or part of the name to see its exact name and exact address.

When we start the application, on the first page we see 2 buttons below the text, giving information about what each of the buttons does (Fig. 3).

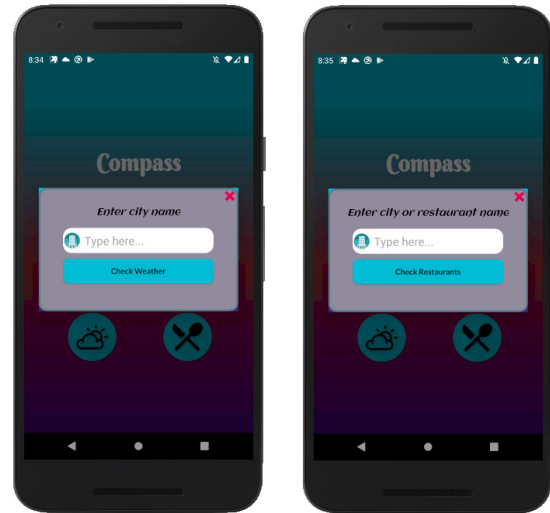


Fig. 3. Search for city and restaurant.

The user can enter the name of a given town or village to check the weather information (Fig. 4). This activity shows the name of the city that enters the user and the country in which the city is located. The weather is also displayed on the screen of the mobile phone, with updated information. Below this information you can see an icon that visualizes the weather and the general description of it at the moment. More important weather information such as the humidity, the air pressure and the exact Celsius temperature is then displayed.

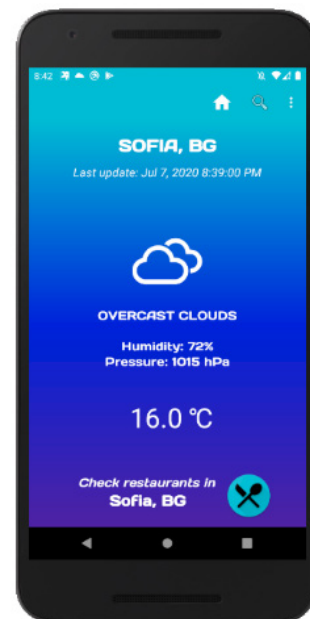


Fig. 4. Activity with weather information.

n activity button has been added showing data on the available restaurants in the city where we are viewing the weather at the moment (Fig. 5).

Fig. 5A shows restaurants in a certain neighborhood in a city. In the specific case, the Elenovo district, Blagoevgrad, Bulgaria, has been set. Fig. 5B shows a list of restaurants containing the keyword Carski. The information displayed for the restaurants is the name of the restaurant, its exact address and the rating from google reviews [12-22]. The limit of the displayed restaurants is twenty. When we enter only the name of the city or the name of the neighborhood in which there are more than twenty restaurants, as a result the application will show a list of the most popular restaurants in the searched place.

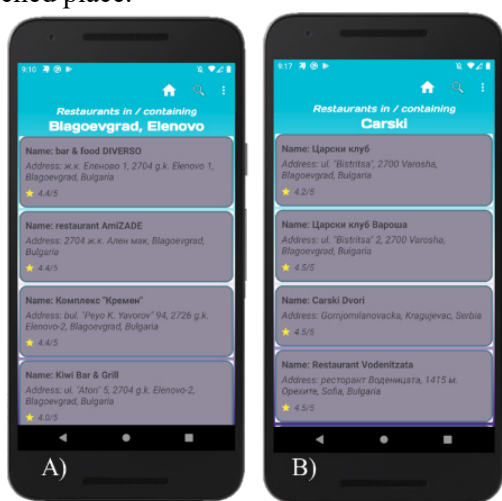


Fig. 5. Activity with information about the restaurants.

CONCLUSIONS

In the last few years Android is one of the leading operating systems in the field of mobile devices, making it the first choice of any user who would like to use such a device. The fact that Android is an open source operating system makes it an ideal platform for creating a wide variety of applications and using all the functionalities offered by the latest technologies.

In the present work a mobile application based on Android has been developed and tested, which permits the user to check in real-time the weather or available restaurants for a given city or a specifically populated place.

Acknowledgement: This paper is partially supported by the Project of the National Science Fund of Bulgaria, BNSF H27/36; National Scientific Program "Information and Communication Technologies for a Single Digital Market in Science, Education and Security (ICTinSES)", financed by the Ministry of Education and Science.

REFERENCES

1. L. Ma, L. Gu, J. Wang, *International Journal of Multimedia and Ubiquitous Engineering*, **9**, 187 (2014).
2. N. Litayem, B. Dhupia, S. Rubab, *International Journal of Advanced Computer Science and Applications IJACSA*, **6 (1)**, 31 (2015).
3. <https://gs.statcounter.com/os-market-share/mobile/worldwide>.
4. <https://source.android.com/>
5. S. Jagtap, D. Hanchate, *International Research Journal of Engineering and Technology (IRJET)*, **4 (7)**, 2248 (2017).
6. Y. Kurniawan, S. Jelatu, N. Adi, V. Kurnila, *Journal of Komodo Science Education*, **1(1)**, 172 (2018).
7. Android: <https://developer.android.com/studio>.
8. VOLLE: <https://developer.android.com/training/volleyYPP>.
9. JSON: https://www.tutorialspoint.com/android/android_son_parser.htm.
10. AsyncTask: https://abhiandroid.com/programming/a_synctask.
11. <https://openweathermap.org/api>.
12. J. Bohacik, *Journal of Information Technologies*, **9(2)**, 1 (2016).
13. F. Sapundzhi, M. Popstoilov, *Bulgarian Chemical Communications*, **50**, Special Issue B, 115 (2018).
14. F. Sapundzhi, *International Journal of Online and Biomedical Engineering*, **15(11)**, 139 (2019).
15. M. Traykov, I. Trenchev. Mathematical models in genetics, *Russian Journal of Genetics*, **52(9)**, 985 (2016).
16. F. Sapundzhi. *International Journal of Online and Biomedical Engineering*, **18(05)**, 147 (2022). <https://doi.org/10.3991/ijoe.v18i05.26949>
17. F. Sapundzhi, *International Journal of Online and Biomedical Engineering*, **15 (12)**, 88 (2019).
18. V. Krалev, R. Krалeva, *IJACR*, **7 (28)**, 1 (2017).
19. F. Sapundzhi, M. Popstoilov, *Bulgarian Chemical Communications*, **52**, 192 (2020).
20. F. Sapundzhi, K. Yordanov, *Bulgarian Chemical Communications*, **52**, 211 (2020).
21. F. Sapundzhi, M. Popstoilov, *Proc. 27th National Conference with International Participation "TELECOM 2019"*, Sofia, Bulgaria, **62** (2019).
22. I. Nedyalkov, G. Georgiev, *EUROCON 2021 - 19th IEEE International Conference on Smart Technologies, Proceedings*, 397 (2021).

Home automation based on Z-wave technology

F. I. Sapundzhi

South-West University "Neofit Rilski", 2700 Blagoevgrad, Bulgaria

Received, November 25, 2021; Accepted: April 08, 2022

With the rapid expansion of the Internet of Things, more devices and objects are network connected. Many people want to have full control over their home communications and this leads to the growth of the smart home automation industry. Z-wave is one of the most popular technologies used to perform smart home and office automation services. It uses a controller to manage and control all devices. The main purpose of the study is to design and investigate a Z-wave home automation system. The smart home built with Z-wave technology is useful for consumers because it will save energy - no lights or AC will be left on when they are not at home.

Keywords: CAD design, Z-wave, Network, Energy efficiency, Dialux, Smart home

INTRODUCTION

In recent times, the Intelligent Home Automation System trend is to control from a distance using a remote control. With the rapid expansion of the Internet of Things (IoT), the most innovative home systems are controlled by smartphones and microcontrollers. Smartphone applications are used to control and monitor home functions using wireless communication techniques [1, 2].

Many people want to have full control over their home communications and this leads to the growth of the home automation industry. Z-wave is one of the most popular technologies used to perform smart home and office automation services. Z-wave is a wireless protocol that essentially focuses on connectivity within the smart home [3, 4].

As the IoT popularity explodes, more connected devices are being added to people's houses. Many sensors, lightbulbs, heating controls, locks, plugs, and the like-pack in Z-wave talk to each other. This technology uses a controller to manage and control all devices. It operates using low-energy radio waves to communicate from device to device [5-7].

Z-wave protocol is a standard based on the ITU G.9959 specification that operates in the industrial, scientific, and medical radio frequency band. It is developed for low bandwidth data communication applications such as security sensors, home automation, alarms, etc. [7-12].

Z-wave transmits on 868.42 MHz (Europe) and 908.42 MHz (United States) frequencies working with FSK and Gaussian Phase Shift Keying (GFSK) modulations [11-16].

The purpose of this article is to present a Z-wave implementation and design of home automation through Cisco Packet Tracer. Through this technology, we can save money on energy bills when

motion detectors are used and the lights are automatically turned off when no motion is detected.

COMPUTER SIMULATIONS AND SYSTEM IMPLEMENTATION

The Z-wave system has three layers - radio, network and an application layer. They work together to create a robust and reliable network that enables numerous nodes and devices to communicate with each other simultaneously. The stack covers Z-wave PHY, MAC, transport, network and application layers (Fig. 1) [11].

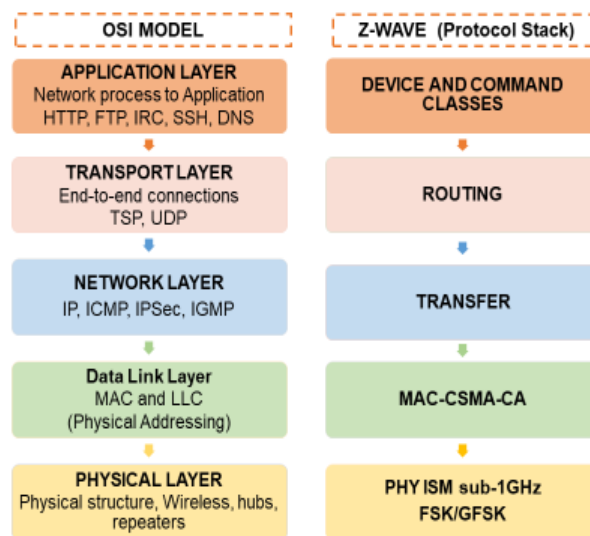


Fig. 1. Diagram of Z-wave protocol stack.

In this technology controlling devices are called controllers (they control other Z-wave devices - remote controls, USB sticks, and IP gateways), and reporting devices are called sensors (they report information by sending a digital or analog signal –

* To whom all correspondence should be sent.
E-mail: sapundzhi@swu.bg

analog and digital sensors) and controlled devices are called actuators (switch digital or analog signals-electrical switches, electrical dimmers, motor control, electrical display, thermostats controls) [13-16].

The software used to perform the computer simulations for the current investigation is as follows

– *AutoCAD* - CAD (computer-aided design) software that architects, engineers, and construction professionals rely on to create precise 2D and 3D drawings. It was used for designing and drawing the electrical installation of the building [18].

– *DIALux evo* - a software for professional lighting design and it was used for computer modeling of the interior, the lighting and 3D visualization of the home [19].

– *Cisco Packet Tracer* was used for network design by connecting different devices to allow for various troubleshooting tests, connectivity and communication testing [20].

The electrical installation interior in the house is designed in AutoCAD which includes electrical wirings details with earthing wire details. Basement, first floor, second floor, attic level, and house plan details are also included in the drawing. It also shows the dimension and circuit flow diagram (Fig. 2) [21]. 2D design of the home automation of the LAN and TV cable in AutoCAD is presented in Fig. 3.

The home automation system consists of three main components: 1) software application through which the user can control the system by computer, smartphone or tablet; 2) transmitter device that connects the software to other devices and 3) peripherals used to execute specified commands. The sensors used in the automation of the building are the most intelligent way to catch all the action happening in the home in real-time. The devices monitor movements, track ambient lighting, keep a tab on indoor temperature and humidity, listen for seismic activity, and protect the home from UV lighting.

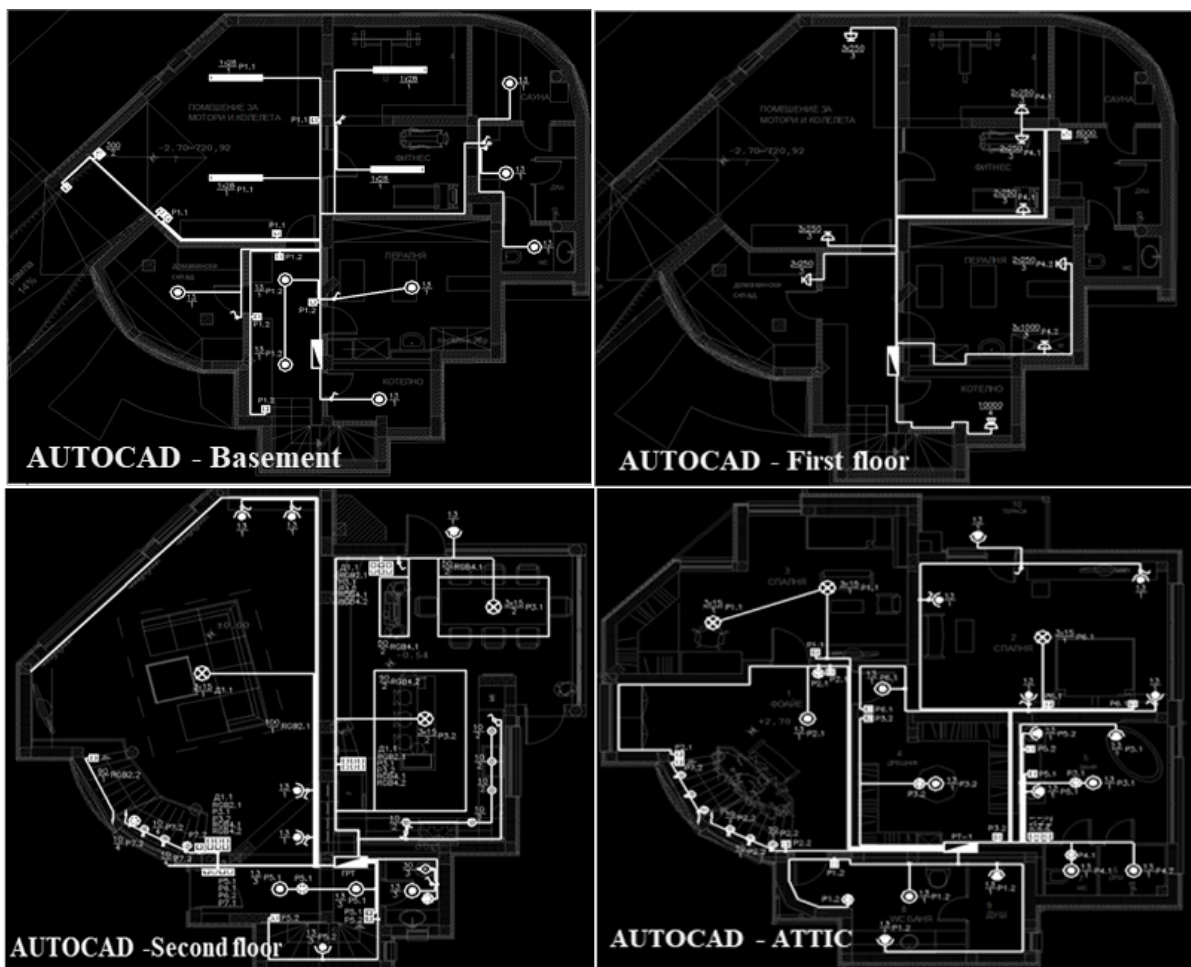


Fig. 2. Design and installation of the current systems of the building realized by AutoCAD.

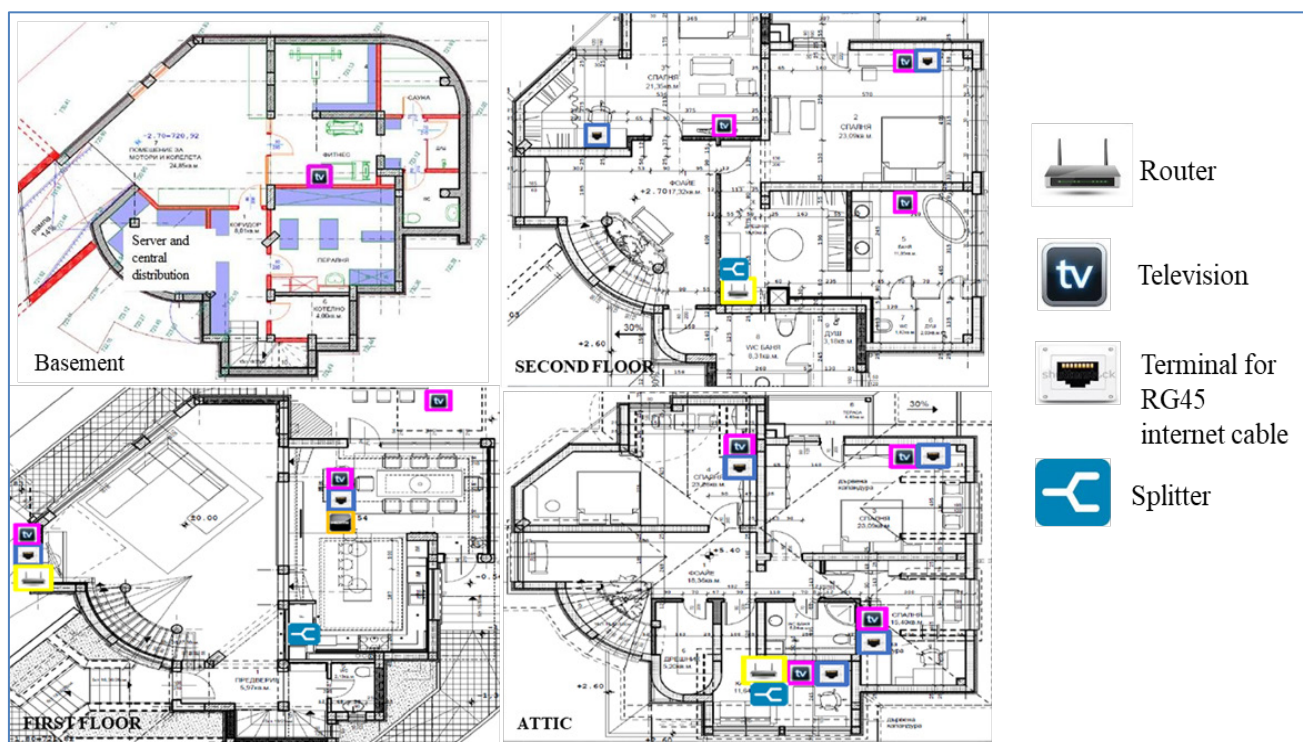


Fig. 3. Design and installation of low-current systems of the building realized by AutoCAD.

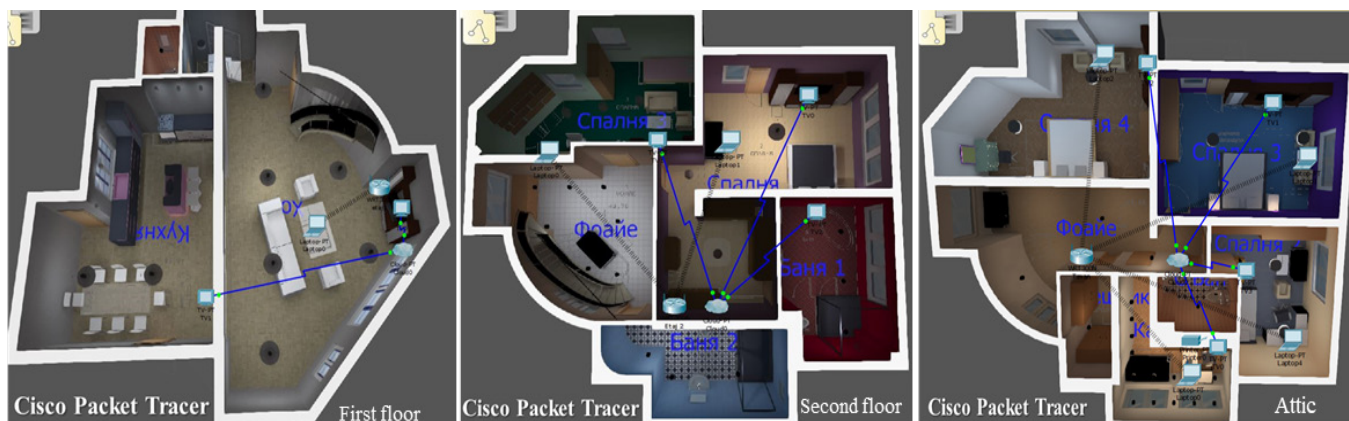


Fig. 4. 3D Design of the building realized on DIALux Evo and Cisco Packet Tracer.

They can be configured to work with the Z-wave controller to receive real-time updates and notifications of building activity. The installed sensors make it possible to monitor home activities in real-time.

3D visualization and lighting design of the building realized on the DIALux Evo program are presented in Fig. 4.

Smart sensors are designed to provide an integrated solution for staying connected with the home, even while we are at work or on a vacation.

The new generations of sensor devices used in home automation have some significant improvements, with sensors now transmitting signals faster and farther.

Motion sensors can be successfully applied in building an intelligent security system. The new sensors feature a range of 5 meters and a field of view of 120°. They capture traffic data and intelligently track every activity in the home. These sensors are used to increase security in the home and to monitor movements, even when we are away from home. They make our home automation system more powerful and smarter.

Z-wave is successfully used to maintain the room temperature, including control of motorized curtains and windows, fans and thermostats. The sensors connected to the Z-wave smart gateway can intelligently control the heating in the home.

Z-wave smart home products can communicate with each other, regardless of brand or building platform, using a central smart hub.

Z-wave is the leading wireless technology behind many of the secure, reliable brands that work to make everyone's home smarter and safer. Z-wave smart home products can communicate with each other, regardless of brand or building platform, using a central smart hub.

A smart hub is used in the automation of the building. The central smart hub ensures that devices in the home are connected to each other and to the user by a simple mobile application for smartphones (tablets). It acts as a central command center for each connected Z-wave device and for connection to the user. Z-wave smart home hubs have a variety of features and capabilities, including Wi-Fi technology that allows remote access to the system [21-28].

There is a smart lighting in the house, which allows remote control of light, on or off, dimming, changing the brightness and color of light and more. The user can create a schedule to turn on the lights at certain hours. Smart lights allow the user to control the energy consumption of the smart home.

CONCLUSIONS

Designing and building of smart homes is related to the necessity of wireless connectivity and Z-wave technology is among the most popular ones for home automation. Bluetooth and Zigbee wireless communication protocols often lack coverage, and Wi-Fi places its limitations on a low-power ecosystem. The Z-wave standard meets the requirements for home automation and Z-wave devices are interoperable - can be easily accessed through the internet or a Z-wave gateway.

We introduced a home automation system based on Z-wave. The smart home built with this technology is useful for consumers as it will save energy, because there will be no lights or AC power left on when they are not at home. In the next project, we will explore the interaction between a Z-wave-based home automation system and control with an Android mobile device.

Acknowledgement: This paper is partially supported by the Project of the National Science Fund of Bulgaria, BNSF 27/36 National Scientific Program "Information and Communication Technologies for a Single Digital Market in Science, Education and Security (ICTinSES)", financed by the Ministry of Education and Science. We also gratefully acknowledge the support by the company

Chikalov EOOD with manager Aleksandar Chikalov.

REFERENCES

1. Ch. Reinisch, W. Kastner, W. Granzer, 5th IEEE International Conference on Industrial Informatics, **2**, 93 (2007).
2. D. Resul, T. Gurkan, T. Ayse, *IJCNA*, **2(6)**, 242 (2015).
3. M. Basma, E. Mohammad, S. Abd El-kader, M. Fakhredinet, *IJAIEEM*, **2(3)**, 413 (2013).
4. F. AlFaris, A. Juaidi, F. Manzano-Agugliaro, *Energy and Buildings*, **153**, 262 (2017).
5. D. Fuller, B. Ramsey Rogue, 40th Local Computer Networks Conference Workshops (LCN Workshops), 734 (2016).
6. Z. Krasniqi, B. Vershevcic, *IC-ISS 2020: 9th International Conference on Information Systems and Security*, Kosovo, 1 (2020).
7. D. Kundu, M. Khallil, T. Das, A. Mamun, A. Musha. *IJSER*, **11(6)**, 697 (2020).
8. O. Taiwo, L. Gabralla, A. Ezugwu, *Computational Science and its Applications – ICCSA 2020*, O. Gervasi et al. (eds.), Springer Nature, Switzerland, 2020.
9. L. Oliveira, J. Rodrigues, S. Kozlov S, R. Rab lo R, V. Albuquerque. *Future Internet*, **11**, 16 (2019).
10. Z-Wave Alliance-Home Management: <https://z-wavealliance.org/home-management/>.
11. <https://www.z-wave.com/>
12. M. Yassein, W. Mardini, A. Khalil, Proceedings of the International Conference on Engineering MIS (ICEMIS), Agadir, Morocco, 1, (2016).
13. IEEE Computer Society. IEEE Standards IEEE 802.15.4-Part 15.4 Wireless MAC and PHY Specifications for Low-Rate Wireless Personal Area Networks LR-WPANs, 2003 edn., The Institute of Electrical and Electronics Engineers Inc., Piscataway, NJ, USA, 2003.
14. IEEE 802.15.6-2012. IEEE Standard for Local and Metropolitan Area Networks Part 15.6: Wireless Body Area Networks; IEEE Standard for Information Technology, IEEE, Piscataway, NJ, USA, **802**, 1 (2012).
15. <https://www.rfwireless-world.com/Tutorials/z-wave-tutorial.html>.
16. <https://www.vesternet.com/pages/how-z-wave-controllers-devices-work>.
17. F. Sapundzhi, M. Popstoilov, *Proc. 27th National Conference with International Participation "TELECOM 2019"*, Sofia, Bulgaria, 62 (2019).
18. AutoCAD: <https://www.autodesk.com/>.
19. Dialux: <https://www.dialux.com/>.
20. Cisco Packet Tracer <https://www.netacad.com/>.
21. F. Sapundzhi, *TEM Journal*, **9** (1), 144 (2020).
22. M. Negnevitsky, *Artificial Intelligence: A Guide to Intelligent Systems*, Addison-Wesley, 2011.
23. F. Sapundzhi, *International Journal of Online and Biomedical Engineering*, **15 (11)**, 139 (2019).

F. I. Sapundzhi: Home automation based on Z-wave technology

24. M. Traykov, I. Trenchev, *Russian Journal of Genetics*, 52(9), 985 (2016).
25. F. Sapundzhi, *International Journal of Online and Biomedical Engineering*, **15 (12)**, 88 (2019).
26. M. Lazarova, K. Kostadinova, *AIP Conference Proceedingsthis*, 2048, 020021 (2018).
27. I. Nedyalkov, G. Georgiev, *EUROCON 2021 - 19th IEEE International Conference on Smart Technologies, Proceedings*, 397 (2021).
28. A. Stoykova, M. Paskaleva, *Springer Proceedings in Business and Economics*, 359 (2021).
29. F. Sapundzhi, M. Popstoilov, *Bulgarian Chemical Communications*, **50**, Special Issue B, 115 (2018).

The importance of biological databases in modeling of structure-activity relationship

F. I. Sapundzhi¹, T. A. Dzimbova^{1,2}

¹South-West University "Neofit Rilski", 2700 Blagoevgrad, Bulgaria

²Institute of Molecular Biology "Roumen Tsanev", Bulgarian Academy of Sciences, Sofia, Bulgaria

Received: November 25, 2021; Accepted: April 15, 2022

Biological databases play a key role in bioinformatics research and applications. Many databases are known that contain different types of information: DNA, sequences of proteins, molecule structures and others. They give researchers access to a large amount of biological data. The aim of the current research is to present a brief overview of major sequence databases and portals currently available and to underline open problems and future trends. The article presents examples for the use of various biological databases for the study of opioid and cannabinoid compounds. This investigation gives a brief description of the importance of biological databases and sequence analysis in bioinformatics research.

Keywords: biological databases, sequences of proteins, bioinformatics, computer modeling, structure-activity relationship

INTRODUCTION

Biological databases play a key role in bioinformatics research. They can be represented as stores of biological information. They contain information from research areas including genomics, proteomics, metabolomics, microarray gene expression, and phylogenetics. The databases give researchers access to a large amount of biological data [1, 2].

Biological data may refer to compounds or information obtained from living organisms and their products. There are many forms of biological data, including sequence data, protein structure, genomic data, and amino acids and the relationships between them [3, 4].

Biological data are connected very closely with bioinformatics, which is an interdisciplinary science that focuses on analyzing and interpreting a huge volume of biological data about DNA, RNA, protein sequences, protein structures, gene expression profiles, and protein interactions [5,6]. Bioinformatics includes two evolving disciplines such as biology and information technology, because solving modern biological problems requires a lot of computational methods such as database management, data modeling, pattern recognition, data extraction, query processing and biological data visualization. The most important task of bioinformatics is the understanding of correlations, structures and patterns in biological data, and next this knowledge can be used in drug discovery, genome analysis and biological control [1]. This science is associated with the development of

databases to store and retrieve biological data; algorithms and statistics for analyzing and determining the relationships in biological data; and statistical tools for data identification and interpretation [7-11].

The aim of the current research is to present a brief overview of major biological databases and portals currently available and to underline open problems and future trends.

Effective management of the huge amount of biological data that is generated on a daily basis is crucial. A challenge for scientists is to integrate and manage these data into existing biological databases. They represent the libraries of biological sciences, collected from scientific experiments, published literature, high-throughput experiment technology, and computational analysis [1-4].

In biological databases, information on gene function, structure, localization, clinical effects of mutations, similarities of biological sequences and structures can be found.

BIOLOGICAL DATABASES

Biological databases can be broadly classified in sequence and design databases. They can be classified in primary, secondary and composite databases (Fig. 1.).

The primary biological databases are well-organized, user-friendly portals to the huge amount of biological data that is produced by researchers around the world.

The first primary databases appeared in the 1980s and 1990s in order to store experimentally determined DNA and protein sequences.

* To whom all correspondence should be sent.
E-mail: sapundzhi@swu.bg

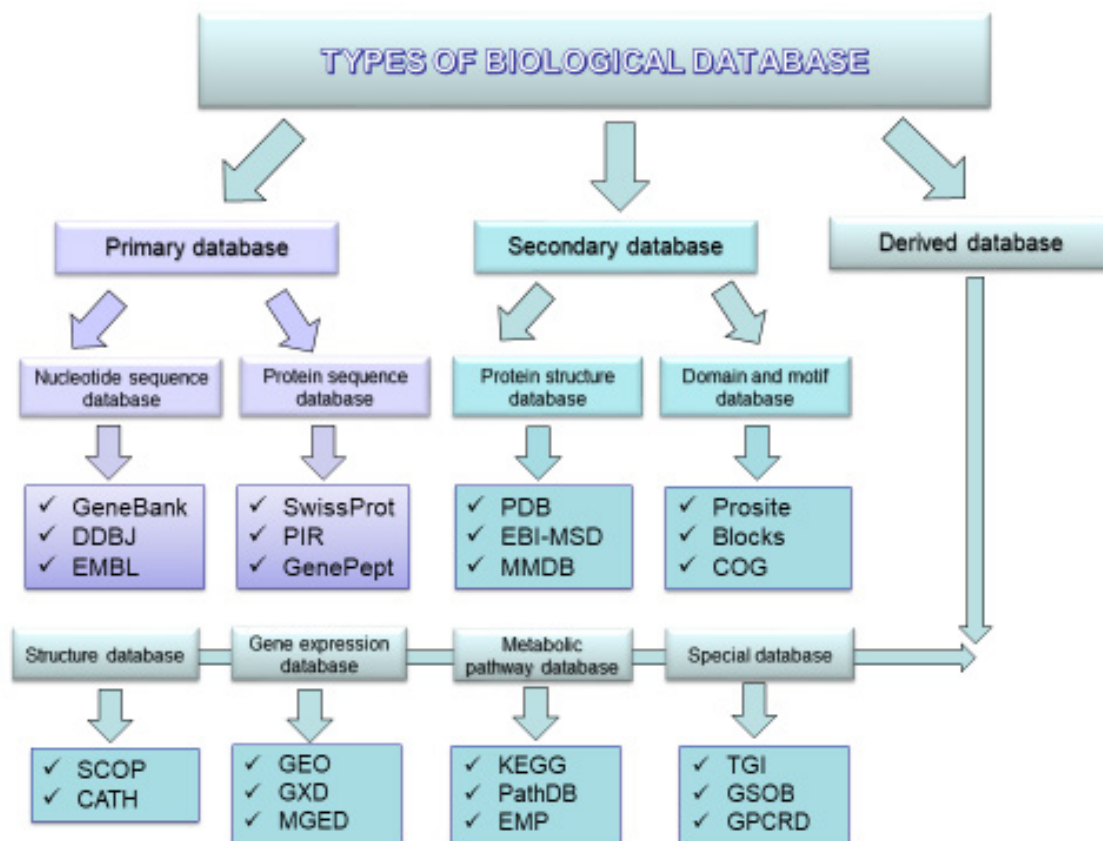


Fig. 1. Types of biological databases.

Today, most protein sequences that can be found in this databases are the product of conceptual translation of genes and genomes determined by DNA sequencing. They contain experimental data such as nucleotide sequences, protein sequences or macromolecular structures, which are submitted directly to the database by the researchers [12]. Examples of the primary databases are the following: GenBank (Genetic Sequence Databank) [13], ENA (European Nucleotide Archive) [14, 15], and DDBJ (DNA Data Bank of Japan) [16], ArrayExpress (Archive of Functional Genomics Data) [17], GEO (Gene Expression Omnibus) [18], PDB (Protein Data Bank) [19]. The nucleotide database was divided into three databases at NCBI: Core Nucleotide database, Expressed Sequence Tag (EST) and Genome Survey Sequence (GSS).

Primary Nucleotide Sequence Database

GenBank (Genetic Sequence Databank) [13]. The GenBank is one of the fastest growing repositories of known nucleotide sequences. The files from it contain data for sequence, access numbers, gene names, phylogenetic classifications, references to published literature, etc. It is developed and maintained at the NCBI. GenBank is a part of International Sequence Database Collaboration (INSDC) which includes ENA database [14], DDBJ

database, and GenBank at NCBI. These organizations exchange data on a daily basis.

EMBL (European Molecular Biology Laboratory) [20]. The EMBL database of DNA and RNA sequences was established in 1980. It contains a collection of scientific literature, which is provided directly by researchers. EMBL is supported by EBI (European Institute of Bioinformatics) and is in close collaboration with GenBank and DDBJ (Fig. 2).

Primary Protein Sequence Databases

There are a large number of protein sequence databases, from simple sequence stores to expertly selected universal databases. The databases that include protein sequences are GenPept, RefSeq, Swiss-Prot, PIR, PRF, and PDB.

SWISS-PROT (Swiss Institute of Bioinformatics, Geneva) [21] - a protein sequence and knowledge database established in 1986. It is a part of UniProt consortium and provides information about the functions of a protein, domain structure and post translational modifications, etc. It is characterized by a minimal level of excess and a high level of integration with other databases.

TrEMBL (translation of EMBL nucleotide sequence database) [22] consists of computer annotated entries derived from the translation of all coding sequences in the nucleotide databases. In this

database, the records are automatically annotated and unreviewed. It is a supplement of Swiss-Port database and contains all translations of EMBL nucleotide sequence entries which are not yet integrated in Swiss-Port.

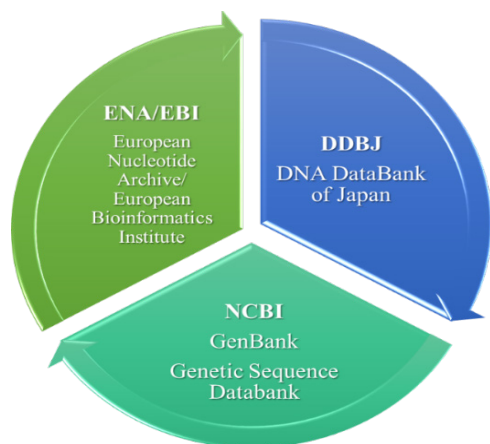


Fig. 2. Nucleotide Sequence Database linkage.

PIR (Protein Information Resource) [23] is a public bioinformatics resource to support genomic and proteomic research and scientific studies. It was established in 1984 by NBRF (National Biomedical Research Foundation) in USA. The database offers a variety of resources to support the distribution and consistency of protein annotations such as PIRSF, ProClass, and ProLINK.

PRF (Protein Research Foundation) [24] is the source of information related to amino acids, peptides and proteins. The information on synthetic compounds, protein sequence data, molecular aspects of proteins, and articles from scientific journals are available in this site.

Secondary Protein Structure Databases

PDB (Protein Data Bank) [19] is the main primary database for 3D structures of biological macromolecules determined by X-ray, crystallography and NMR. It was established in 1971 at Brookhaven National Laboratories. Since 1998 it is now supported by the RCSB (Research Collaboratory for Structural Bioinformatics) [25]. PDB provides tools and resources for studying the structures of biological macromolecules and their relationships and functions with other sequences. It accepts experimental data used to determine the structures and homology models [26, 27].

MSD/EMD (Macromolecular Structure Database) [28]. It is a European project for collection, management and distribution of macromolecular structures integrating current database and IT with a solid core of expertise in structural biology. It works closely with RCSB in the USA and PDB in Japan [29].

EMD (Electron Microscopy Data Base) [30] is part of MSD database [3]. MSD manages, organizes and disseminates data on the structures of biological macromolecules solved by 3D electron microscopy.

MMDB (Molecular Modeling DataBase) [31] is a structural database of NCBI, containing experimentally determined 3D biomolecular structures. The database contains information on the biological function, the mechanisms associated with the function, and the evolutionary history of macromolecules and their relationships [32].

Secondary Domain Motif Database

The Domain Motif Database stores protein sequence motif data which are a set of preserved amino acid residues - important for protein function and located at a certain distance from each other.

PROSITE database [33] stores documentation describing protein domains, families and functional sites, related models and profiles for their identification [34]. Biologically significant sites, models and profiles can be found in it, which will allow the identification of the new sequence to which family of proteins it belongs.

PRINTS [35] is a database for protein fingerprints which are a group of conserved motifs used to characterize a protein family. They can encode protein folds and functionalities more flexibly and powerfully than single motifs [36].

ProDom [37] is a protein domain database automatically generated from the Swiss-Port and TrEMBL sequence database [38,39]. It contains automatic clustering of homologous domains, which is a rational way of organizing protein sequence data.

BLOCKS [40] is a server for sequence analysis at the Fred Hutchinson Cancer Research Center in Seattle, USA. The Blocks Database is a collection of blocks with known protein families that can be used to compare a protein or DNA sequence with documented protein families.

COGs (Clusters of Orthologous Groups of proteins COG) [41,42] is a tool for genome-scale analysis of protein functions and evolution. It is designed to classify proteins from fully sequenced genomes based on the concept of orthology.

3D Structure Databases

SCOP (Structural Classification of Protein database) [43] classifies protein 3D structures in a hierarchical scheme of structure classes. This database contains detailed information on the structural and evolutionary relationships of the proteins from PDB [44].

The **DBAli Database** [45] is related to SCOP which contains pairwise structural alignments generated by different methods [46].

CATH (Class, Architecture, Topology, Homologous) [47] contains a hierarchical classification of protein domains based on their folding patterns. They are obtained from protein structures deposited in PDB [48].

Gene Expression Databases

GEO (Gene Expression Omnibus) [49] - a public functional genomic data repository that accepts data based on arrays and sequences and provides tools to help users search for and download experiments and curated gene expression profiles [50].

GXD (Gene Expression Database) [51] is a community resource with gene expression information for the laboratory mouse. It provides information on which transcripts and proteins are produced by which genes, where and in what amounts their products are expressed and how their expression varies in different murine strains and mutants. GXD is integrated with the Mouse Genome Database (MGD).

MGED (Microarray Gene Expression data) [52] contains microarray data generated by functional genomics and proteomics experiments.

Metabolic Pathway Databases

KEGG PATHWAY database (Kyoto Encyclopedia of Genes and Genomes) [53,54] contains graphical pathway maps for all known metabolic pathways from various organisms. It is a collection of databases dealing with genomes, biological pathways, diseases, drugs, and chemical substances.

EcoCyc [55] a bioinformatics database - *E. coli* database, stores information regarding the genome and biochemical machinery of *E. coli* K-12 MG1655.

LIGAND [56] is a chemical database for enzyme reactions at the Institute for Chemical Research, Kyoto. It is a composite database currently consisting of the COMPOUND, DRUG, GLYCAN, REACTION, RPAIR and ENZYME databases.

PathDB [57] is a relational database that can store detailed and specific metabolic information and visualization methods that aid in the *in silico* detection process. It allows the storage of quantitative information on enzymatic and spontaneous reactions and transport steps.

EMP (Database of enzymes and metabolic pathways) [58] is a public server. It is an encoding of the contents of over 10 000 original publications

on the topics of enzymology and metabolism. This information is transformed into a queryable database. It plays an important role in the interpretation of genetic sequence data.

Special Databases

TGI (TIGR Gene Indices) [59] database uses all publicly available expressed sequence tags (EST) and data known on gene sequence stored in GenBank for each target species.

GPCRdb [60] contains reference data, interactive visualization and experiment design tools for G protein-coupled receptors (GPCRs). It controls the alignment of sequences, structures, and receptor mutations in the literature.

OPEN PROBLEMS AND FUTURE TRENDS

In our work we rely very much on biological databases. The publication of the crystal structures of MOR (mu-opioid receptor), DOR (delta-opioid receptor), CBR1 (cannabinoid receptor type 1) and CBR2 (cannabinoid receptor type 2) helps in the targeted drug design:

- MOR (RCSB, PDBid:4DKL) [61-64];
- DOR (RCSB, PDBid:4e 4) [65-70];
- CBR1 (RCSB, PDBid:5tgz) [71-74];
- CBR2 (RCSB, PDBid:2hff) [75-78].

The possibilities provided by computer methods together with biological databases are related to determining the intimate mechanism of interaction between ligands and receptors, including determining binding sites, binding energies, the presence of specific groups in the structure of ligands that promote their binding to receptor and many others. Determining the relationship between the structure of the ligand and its action using computer methods shortens the time to find potentially active compounds.

CONCLUSIONS

The biological databases are an important tool to help scientists study and explain biological phenomena from the structure of biomolecules to their interaction and to understand the progression of species. The current research presents examples from the use of various biological databases for the study of different compounds. This investigation gives a brief description of the importance of biological databases and sequence analysis in bioinformatics research.

Acknowledgement: This paper is partially supported by Project of the National Science Fund of Bulgaria, BNSF 27/36 National Scientific Program "Information and Communication

F. I. Sapundzhi, T.A. Dzimbova: The importance of biological databases in modeling of structure-activity relationship Technologies for a Single Digital Market in Science, Education and Security (ICTinSES)", financed by the Ministry of Education and Science.

REFERENCES

1. Y. P. P. Chen (ed.), *Bioinformatics technologies*. Springer Science Business Media, 2005.
2. N. Toomula, A. Kumar, S. Kumar, V. Bheemidi, *J. Comput. Sci. Syst. Biol.*, **4**, 87 (2011).
3. D. Jelic, D. Toth, D. Verbanac, *Food Technol. Biotechnol.*, **41**, 269 (2003).
4. J. Dziuba, A. Iwaniak, in: Y Mine, F Shahidi (eds.), *Nutraceutical Proteins and Peptides in Health and Disease*, CRC Press, Boca Raton, 2006, p. 543.
5. J. Wren, A. Bateman, *Bioinformatics*, **24** (19): 2127 (2008).
6. S. Mir, Y. Alhroub, D. Armstrong, J. Berrisford. A. Clark, M. Conroy, J. Dana, M. Deshpande, D. Gupta, A. Gutmanas, P. Haslam, L. Mak, A. Mukhopadhyay, N. Nadzirin, T. Paysan-Lafosse, D. Sehnal, S. Sen, O. Smart, M. Varadi, G. Kleywegt, S. Velankar *Nucleic Acids Research*, **46** (D1), D486 (2018).
7. A. Kin o, G. Bekker, H.Suzuki, Y.Tsuchiya, T. Kawabata, Y. Ikegawa, H. Nakamura, *Nucleic Acids Research*, **45** (D1), D282 (2017).
8. A. Bayat, *BMJ*, **324** (7344), 1018 (2002).
9. K. Herbert, J. Spirollari, J. Wang, W. Piel, J. Westbrook, W. Barker, Z. Hu, C. Wu. *Bioinformatics databases*. Wiley Encyclopedia of Computer Science and Engineering, 2007.
10. M. Traykov, I. Trenchev, *Russian Journal of Genetics*, **52**(9), 985 (2016).
11. M. Arita, I. Karsch-Mizrachi, G. Cochrane, *Nucleic Acids Res.*, **49**(D1), D121 (2021).
12. M. Lazarova, S. Markov, A. Vassilev, *AIP Conference Proceedings*, **2302**, 080004 (2020).
13. GenBank: <http://www.ncbi.nlm.nih.gov/genbank>.
14. G. Hamm, G. Cameron, *Nucleic Acids Research*, **14** (1), 5 (1986).
15. ENA: <https://www.ebi.ac.uk/ena/browser/home>.
16. DDBJ: <https://www.ddb.nig.ac.p>.
17. ArrayExpress: <https://www.ebi.ac.uk/arrayexpress>.
18. GEO: <https://www.ncbi.nlm.nih.gov/geo/>.
19. PDB: <http://www.pdb.org>.
20. EMBL: <http://www.ebi.ac.uk/embl/index.html>.
21. Swiss-Prot: <http://www.expasy.org>.
22. UniProt: <https://www.uniprot.org>.
23. PIR: <https://proteininformationresource.org/>.
24. PRF: <https://www.proteinresearch.net/>.
25. RCSB: <http://www.rcsb.org/pdb/>.
26. H. Berman, J. Westbrook, Z. Feng, G. Gilliland, T. Bhat, H. Weissig, I. Shindyalov, P. Bourne, *Nucl. Acids Res.*, **28**, 235 (2000).
27. O. Ogasawara, Y. Kodama, J. Mashima, T. Kosuge, T. Fu isawa, *Nucleic Acids Res.*, **48**, 45 (2020).
28. MSD: <http://www.ebi.ac.uk/msd/>.
29. PDB : <https://pdb.org/>.
30. EBI: <http://www.ebi.ac.uk/msd/MSDProjects/IIMS3D-EMdep.html>.
31. MMDB: <http://www.ncbi.nlm.nih.gov/Structure/MMDB/mmdb.shtml>.
32. Y. Wang, I. Geer, T. Made , A. Marchler-Bauer, D. Zimmerman, S. Bryant S.H., *Nucl.Acids Res.* **30** (1), 249 (2002).
33. Prosite: <http://us.expasy.org/prosite/>.
34. L. Falquet, M. Pagni, Ph. Bucher, N. Hulo, Ch. Sigrist, K. Hofmann, A. Bairoch, *Nucl. Acids Res.* **30**, 235 (2002).
35. PRINTS: <http://www.bioinf.man.ac.uk/dbbrowser/PRINTS/>.
36. T. Attwood, M. Blythe, D. Flower, A. Gaulton, J. Mabey, N. Maudling, L. McGregor, A. Mitchell, G. Moulton, K. Paine, P. Scordis, *Nucl. Acids Res.*, **30** (1), 239 (2002).
37. Prodom: <http://prodes.toulouse.inra.fr/prodom/2002.1/html/home.php>.
38. F. Servant, C. Bru, S. Carre re, E. Courcelle, J. Gouzy, D. Peyruc, D. Kahn, *Briefings in Bioinformatics*, **3**(3), 246 (2002).
39. F. Corpet F. Servant, J. Gouzy, D. Kahn, *Nucl. Acids Res.*, **28** (1), 267 (2000).
40. Blocks: <http://www.blocks.fhcrc.org/>.
41. COG: <http://www.ncbi.nlm.nih.gov/COG>.
42. R. Tatusov, M. Galperin, D.Natale, E. Kooninet, *Nucleic Acids Research*, **28** (1), 33 (2000).
43. SCOP: <http://scop.mrc-lmb.cam.ac.uk/scop/>.
44. A. Murzin, S. Brenner, T. Hubbard, C. Chothia, *J. Mol. Biol.*, **247**, 536 (1995).
45. D. B. Ali, <http://guitar.rockefeller.edu/DBAli/>.
46. M. Marty-Renome, *Bioinformatics*, **17**, 746 (2001).
47. CATH: <http://www.biochem.ucl.ac.uk/bsm/catnew/index.html>.
48. C. Orengo, A. Martin, G. Hutchinson, S. Jones, D. Jones, A. Michie, M. Swindells, J. Thornton, *Structure*, **5** (8), 1093 (1997).
49. GEO: <https://www.ncbi.nlm.nih.gov/guide/genes-expression/>.
50. R. Edgar, M. Domrachev, A. Lash, *Nucleic Acids Res.*, **30** (1), 207 (2002).
51. <http://www.informatics.ax.org/>.
52. www.mged.org.
53. <https://www.genome.p/kegg/pathway.html>.
54. M. Kanehisa, S. Goto, *Nucleic Acids Res.*, **28** (1) 27 (2000).
55. I. Keseler, J. Collado-Vides, A. Santos-Zavaleta, M. Peralta-Gil, S. Gama-Castro, L. Mu iz-Rascado, C. Bonavides-Martinez, S. Paley, M. Krummenacker, T. Altman, P. Kaipa, A. Spaulding, J. Pacheco, M. Latendresse, C. Fulcher, M. Sarker, A. Shearer, A. Mackie, I. Paulsen, R. Gunsalus, P. Karp. *D.Nucl. Acids Res.*, **39**, 583 (2011).
56. S. Goto Y. Okuno, M. Hattori, T. Nishioka, M. Kanehisa, *Nucleic Acids Res.*, **30**(1), 402 (2002)
57. PathDB: <http://www.ncgr.org/pathdb>.
58. EMP: <http://emp.mcs.anl.gov/>.
59. TIGR: <http://www.tigr.org/tdb/tgi>.
60. GPCRdb: <https://gpcrdb.org>.

61. F. Sapundzhi, T. Dzimbova, N. Pencheva, P. Milanov, *Bulg. Chem. Commun.*, **47**, 613 (2015).
62. T. Dzimbova, F. Sapundzhi, N. Pencheva, P. Milanov, *J. Pept. Sci.*, **18**, (S1) S84, P072, (2012).
63. F. Sapundzhi, T. Dzimbova, N. Pencheva, P. Milanov, *Bulg. Chem. Commun.*, **51**, 569 (2019).
64. F. Sapundzhi, K. Prodanova, M. Lazarova, *AIP Conference Proceedings*, **2172**, 100008 1-6, (2019)
65. F. Sapundzhi, T. Dzimbova, N. Pencheva, P. Milanov, *Der Pharma Chemica*, **8**, 118 (2016).
66. F. Sapundzhi, T. Dzimbova, P. Milanov, N. Pencheva, *Int. J. Bioautomation*, **17** (1), 5 (2013).
67. F. Sapundzhi, T. Dzimbova, N. Pencheva, P. Milanov, *J. Pept. Sci.*, **20** (S1), S294, (2014).
68. F. Sapundzhi, T. Dzimbova, N. Pencheva, P. Milanov. *Bulg. Chem. Commun.*, **49** (E), 23 (2017).
69. F. Sapundzhi, T. Dzimbova, N. Pencheva, P. Milanov. *Bulg. Chem. Commun.*, **49** (E), 768 (2017).
70. F. Sapundzhi, T. Dzimbova, N. Pencheva, P. Milanov, *Bulg. Chem. Commun.*, **50**, Special Issue B, 44 (2018).
71. F. Sapundzhi, T. Dzimbova, *Bulg. Chem. Commun.*, **50**, Special Issue B, 15 (2018).
72. F. Sapundzhi, T. Dzimbova, *J. Chem. Technol.*, **55** (5), 959 (2020).
73. F. Sapundzhi, V. Slavov, *J. Chem. Technol.*, **55** (5), 935 (2020).
74. R. Topalska, T. Dzimbova, *J. Chem. Technol.*, **55** (5), 714 (2020).
75. F. Sapundzhi, T. Dzimbova, *J. Chem. Technol.*, **55** (5), 709 (2020).
76. F. Sapundzhi, T. Dzimbova, *Bulg. Chem. Commun.*, **52** (A), 197 (2020).
77. F. Sapundzhi, *IJOE*, **15** (11), 139 (2019).
78. F. Sapundzhi, T. Dzimbova, *IJOE*, **15** (15), 39 (2019).

Organizational-technological aspects in the construction of construction sites

M. Zafirova^{1*}, D. Kaloshev²

¹*Faculty of Machinery and Construction Technologies in Transport*

²*Department of Transport Construction and Equipment, University of Transport "T. Kableshkov", Sofia, Bulgaria*

Received: November 17, 2021; Accepted: April 29, 2022

The characteristics of the construction builds in the most general form include: (i) volume-compositional solution – the purpose type and character of the facility (or the building) are clarified; (ii) constructive decision - the accepted constructive scheme, the type and constructive features of the elements and of the facility as a whole, some specific constructive requirements are indicated; (iii) technological features – the type of the adopted construction technology, the type and volumes of construction and installation works are defined (including the quantity bill). In organizational and technological solutions, when drawing up the plan for safety and health of the technology, the methods and sequence of execution of all construction and installation works for the overall construction are clarified and proposed.

The purpose of the development is to analyze the impact of different technologies in the construction of a construction site on the organization and operational management in their implementation. For this purpose, it is intended: (i) to consider different technologies in the construction of construction sites; (ii) to trace the impact of the chosen technology on the main resources needed for the construction of the sites.

Keywords: organization, technology, construction sites

INTRODUCTION

The realization of the construction sites is characterized by great dynamics and complexity. The dynamics is dictated by the great variety of the individual sites, as well as the various mechanization, construction materials, the large number of specialists and others. The technology used to realize the finished product is essential.

The stochastic nature of the construction is not to be underestimated due to its strong dependence on climatic conditions. The organization during the implementation of the construction process aims to create the necessary order for interaction between the participants in compliance with the adopted technology [1].

Methods for optimization of labor and financial expenses

The implementation of investment projects in construction can be called a process of mentoring, regulating and managing the construction project from the initial planning phase to its completion. The main goal in their implementation is to meet the expectations of the client (assignor). The project must be both functional and cost-effective. Their implementation is closely linked to the technical characteristics and budget of the project, but also requires good communication between all participants (contracting authorities, contractors, subcontractors, suppliers, institutions and the external environment).

From the point of view of the country executing the project, the organizational and technological aspects of the planning can be both in the stage of preliminary planning of the implementation of the project and in the process of its implementation. The stage of preliminary planning usually represents the process of preparation of the project-budget documentation, collection of offers from subcontractors and suppliers, collection and specification of the projects in parts. In this phase, the aspects that can affect the subsequent implementation include the correct creation of relevant applications (quantitative tables, comparative tables for subcontractors and suppliers, calendar and financial schedules) which, created according to the standard model adopted for the organization, can be easily used by the project implementation team for the subsequent implementation, serving as an organizational package.

The stage of implementation of the project begins with determining the project team and drawing up a schedule of implementation which corresponds to the set start and end dates to the contracting authority. Based on the prepared comparison tables, a schedule for deliveries is prepared and subcontractors are determined for specific construction and installation works. Possible optimizations for the projects by parts are considered, as well as possible risks during the project implementation. In the process of implementation of the site, statistics are kept on workers and work performed (daily activities), as

* To whom all correspondence should be sent.
E-mail: mzafirova@vtu.bg

this could help in planning the next sites. The applications below are a visual aspect of the project implementation, as they guide the team in the implementation of their work and help to reduce errors in the implementation [2, 3].

RESULTS AND DISCUSSION

As an example of optimization in the implementation of the site is considered the

construction of an excavation of a 9-storey residential building divided into 5 blocks with a food supermarket on the ground floor. There are 2 underground levels, the elevation of the bottom excavation is -7.20 m. The dimensions of the excavation are 28 m x 95 m.

The initial project envisages the strengthening of the entire excavation to be completed with the so-called Berlin wall (shown in Fig. 1).

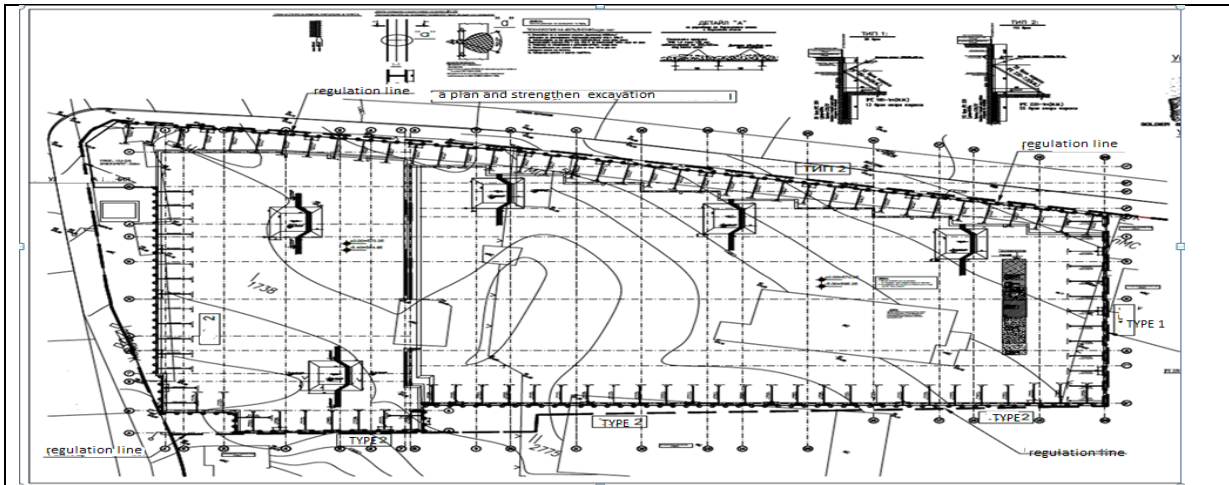


Fig. 1. Excavation plan and strengthening before optimization.



Fig. 2. Leveling of the piles.



Fig. 3. Execution of the trench cladding.

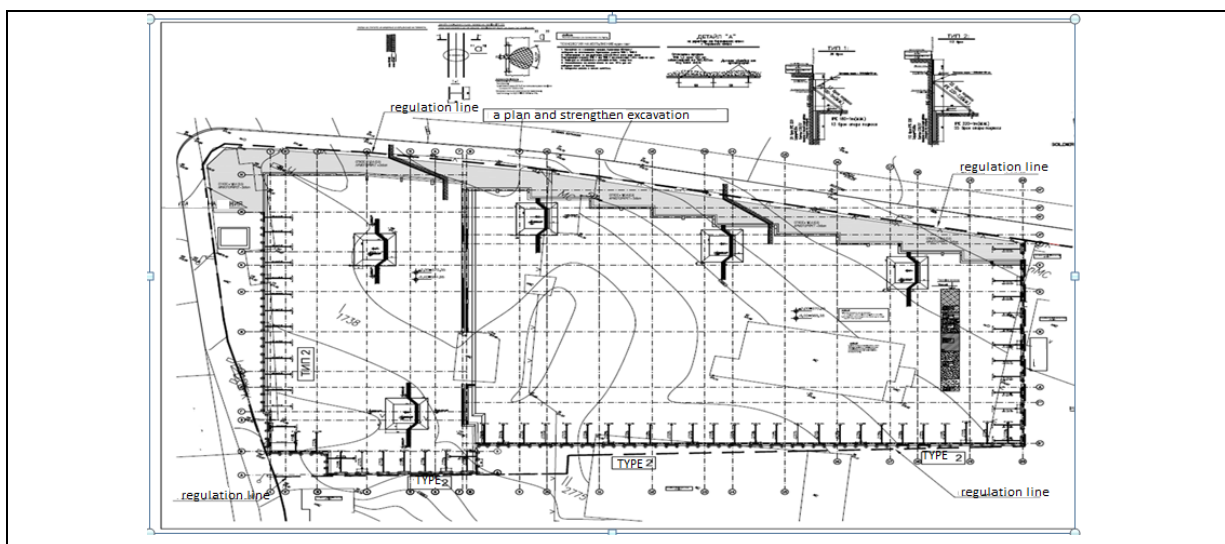


Fig. 4. Excavation plan and strengthening after optimization.

In geotechnical practice, Berlin walls are understood as fortifications made of metal profiles with wooden cladding between them. In the general case they are found in two variants: drilling and driving. In the case of drilling walls, a round drilling is prepared in advance, most often with a diameter d

300 mm. A metal profile is placed in the borehole and concrete is filled to the elevation of the trench. In its second variant, this type of walls is made by nailing the metal profiles. This is done either dynamically by vibrating hammers or by static pressure, for example with an excavator. After the installation of the metal profiles, the excavation begins, and as it progresses, wooden planks are also placed.

In this example, the initial excavation is up to -0.5 m, the depth required for leveling the piles. The excavation is then carried out to the level of the pilot's anchor. Subsequently, the site team decided to reinforce the north wall with shotcreting. (shown in Fig. 4).

Shotcreting is a layering process by spraying a cement mixture, aggregates, water and high pressure additives on various surfaces. Such surfaces can be horizontal, vertical or ceiling areas. (shown in Fig. 5). This decision was accepted because the relief allows the excavation to be filled with a slope on this side. A reinforced mesh 6.5 is laid, Fig. 5.

A new plan is drawn up, which after passing the approval procedures, is implemented on the spot.

In the second option, shotcrete is applied - concrete of 350 sq. m. Its application is more economical. The result is:

- Saving 280 sq.m. of Berlin wall ;
- Saving 25 938 kilograms of structural steel profile IPE220;
- Concreting 55 piles less.

The total value of the saved funds after the optimizations amounts to about BGN 22 000.

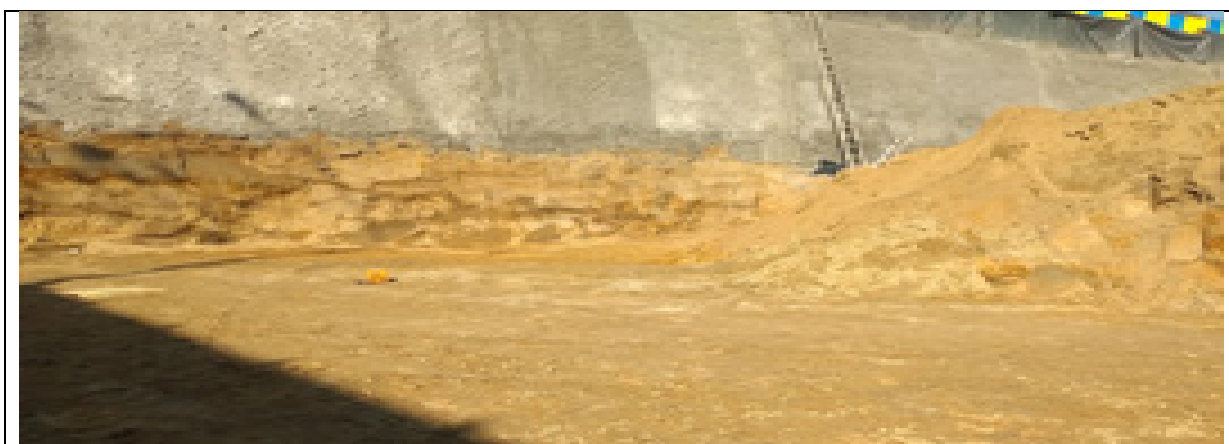


Fig. 5. Strengthening by shotcreting.

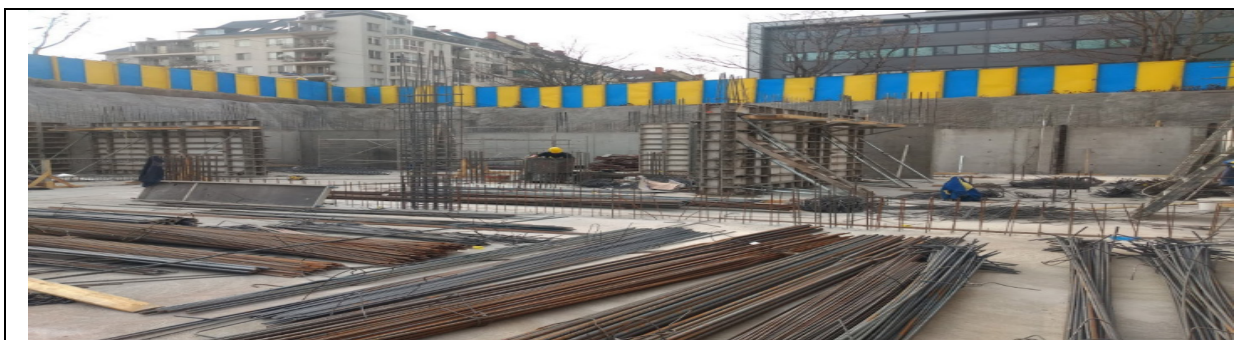


Fig. 6. Final view of the strengthening of the northern side.

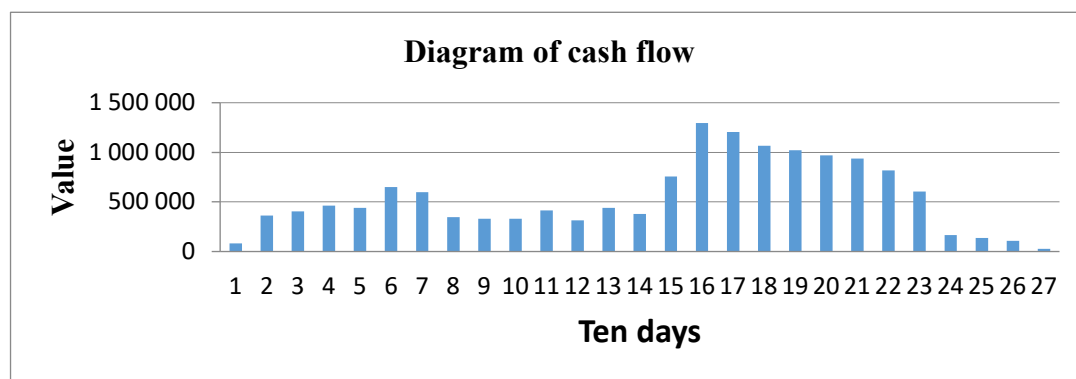


Fig. 7. Diagram of cash flow

Other factors affecting the optimization of performance

The cash flow chart presents the intensity of financial investment in construction. It is a consequence of the payment schedule and the completed stages of the project, having a direct impact on the human and material resources that can be invested in the site for specific periods of time. Drawing up a rational diagram for investing funds will allow the investor to draw up a rational plan for financing and construction of the construction site.

The workforce diagram is compiled on the basis of a calendar plan and is a differential diagram that shows the number of workers needed to complete the project at certain intervals. It is the main factor on which the situation of the site should be created under part of Plan of safety and health, as it is necessary to provide a sufficient area for rest, first aid and storage of accessories for all workers. It is also a major factor in the distribution of human resources in an organization and its possible optimization leads to the implementation of the specific site in a shorter time. It is desirable for the labor diagram to be uniform - to increase gradually with the development of construction, to have a relatively constant level during the period of the most intensive construction and to gradually decrease with the completion of construction.

The diagram of the necessary mechanization for the construction period is a very important attribute in the management of the mechanization of a given organization. Based on the examination of the diagrams of all sites of the organization it can be understood whether the necessary mechanization of the site can be provided without hiring external and if necessary rent of external mechanization - what will be its exact quantity and for what period of time. It is possible to rearrange the individual stages of the implementation of the site so that the respective construction and installation works can enter the time limit in which the organization has its own equipment available. The presence of this type of diagram allows to optimize the use of machines according to certain criteria and on the basis of the diagram to compile route schedules when necessary. The cash flow chart presents the intensity of financial investment in construction. It is a consequence of the payment schedule and the completed stages of the project, having a direct impact on the human and material resources that can be invested in the site for specific periods of time. Drawing up a rational diagram for investing funds will allow the investor to draw up a rational plan for financing and construction of the construction site.

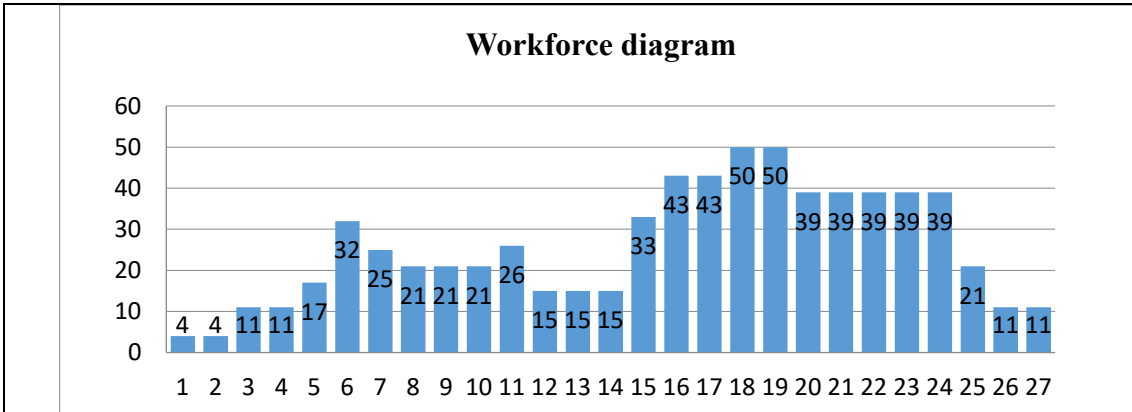


Fig. 8. Workforce diagram

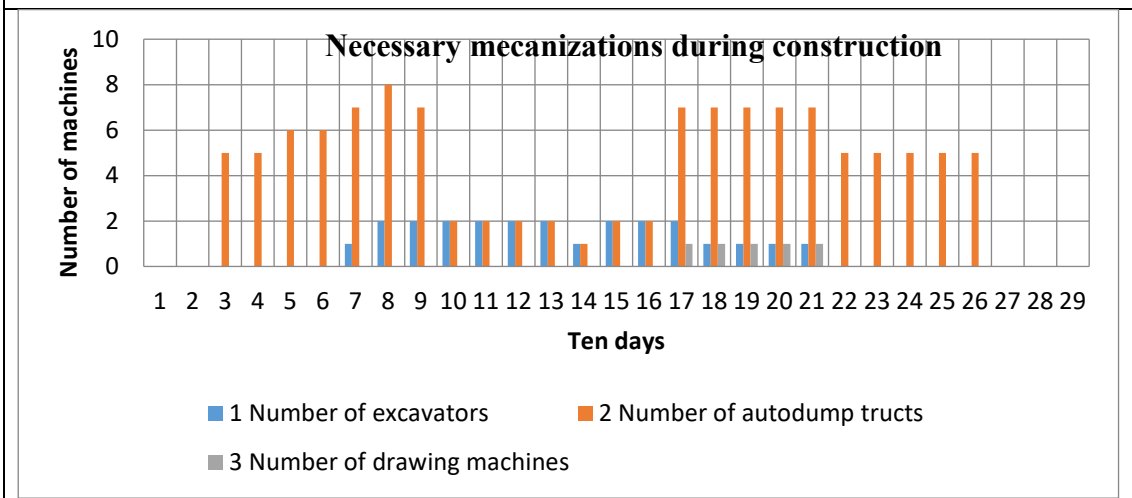


Fig. 9. Diagram of mechanizations

CONCLUSION

When choosing a particular technology, it is necessary to make an in-depth analysis of the technical and economic indicators for the different options. The quantity-value account is the economic indicator for the choice of a given variant. The choice of technology is determined by several indicators such as lead time, choice of equipment, maximum number of workers and others.

REFERENCES

1. I. Sakarev, Organization and management of construction, Sofia, UACG, 1997.
2. A. Apostolov, Fundamentals of project, Sofia, Pro ekta Publishing House, 2014-2004.
3. S. Burton, N. Michael, Project Management, Equilibris Publishing House, 1992.

Section

Methodology in Education

Multimedia technologies in physics teaching

G. Kalpachka¹, V. Kalpachki^{2*}

¹South-West University "Neofit Rilski", 66 Ivan Mihailov Str., 2700 Blagoevgrad, Bulgaria

²Technical University of Sofia, 8 St. Kliment Ohridski Blvd., 1756 Sofia, Bulgaria

Received: October 27, 2021; Accepted: May 25, 2022

The use of multimedia technologies in the secondary school physics teaching is a new, relevant and significant trend in Bulgarian modern education. In the article are presented main methodological possibilities for using multimedia technologies in the educational process in physics in the secondary school. The article gives specific, objective and reasoned answers to the methodological questions: When, where and how can be used multimedia technologies in the physics teaching. The multimedia technologies are innovative educational resources. The use of multimedia technologies complements, expands and diversifies the traditional methods and tools of physics teaching. Their application is related and aimed to increasing the effectiveness of the secondary school physics teaching.

Keywords: Multimedia Technologies, Physics Teaching, Secondary School.

INTRODUCTION

The continuous search for new, non-traditional methods and tools of physics teaching makes the topic of this article current and debatable. On the other hand, the relevance of the article is related to contemporary trends and modernization of the school education in Bulgaria.

Different, but close in meaning definitions of the concept of multimedia technologies are used in the specialised literature. According to the definition formulated in 1988 by the European Commission, which deals with the problems of implementation and use of new technologies, the multimedia technologies have a purpose of creating a product that contains a collection of images, texts and data that are accompanied by sound, video, animation and other visual effects (simulations), which include an interactive interface and other control mechanisms [1]. Over the years, the definition of multimedia technology has evolved, but its meaning remains the same.

The most characteristic feature of multimedia technologies is their interactivity.

The multimedia technologies have applications in various fields of the human activity. They are increasingly used in the education of students in learning the different school subjects.

The use of multimedia technologies in the secondary school physics teaching is a new, relevant and significant trend in Bulgarian modern education.

In the second part of the article are presented the main methodological possibilities for using multimedia technologies in the educational process in physics in the secondary school. They are concretized by the authors of the article on the basis

of the theoretical research in the field of multimedia technologies, the types of multimedia technologies and others. Specific, objective and reasoned answers to the methodological questions When, where and how can be used multimedia technologies in the physics teaching are given in this part of the article.

The main formulated conclusions on the topic are presented in the last part of the article.

MULTIMEDIA TECHNOLOGIES IN THE SECONDARY SCHOOL PHYSICS TEACHING

In the secondary school physics teaching, multimedia technologies can be used in the different physics lessons (for new knowledge, for solving physics problems, for summary, for laboratory exercises, for check and assessment of the students' learning achievements), in the students' extracurricular activity, in conducting e-learning (synchronous and asynchronous), etc.

Various multimedia technologies can be used successfully in the secondary school physics teaching, such as multimedia programs, virtual physics laboratories, electronic multimedia textbooks and aids, multimedia computer presentations and more.

Multimedia programs

Multimedia programs are didactic software products that represent computer models of real physics objects, phenomena or processes, reproducing the real conditions of conducting physics experiments [2].

They provide a qualitatively new type of visualization, because they allow to recreate physics phenomena or processes through computer animation, sound, text, graphics, diagrams,

* To whom all correspondence should be sent:
E-mail: vkalpachki@tu-sofia.bg

numerical values and others and they give opportunities for active intervention in their course by changing the parameters and conditions of the experiments and obtaining concrete results [2].

Multimedia programs can be used in the different physics lessons, in the students' extracurricular activity, in conducting e-learning, etc.

They also can be used when updating, presenting and consolidating the learning content in physics, in checking and assessing of the students' learning achievements, in their independent learning work, in considering the applications of physics knowledge and more.

In the educational process in physics, multimedia programs can be used to:

- illustrate the learning content;
- conduct computer (virtual) interactive physical experiments (demonstration and laboratory, quantitative and qualitative);
- create problem situations and solve learning problems;
- introduce new physical concepts, quantities and units of measurements;
- study and discover causal relationships;
- study and establish functional relationships between physical quantities;
- formulate physical laws;
- solve different types of physical problems (quantitative, graphical, qualitative, experimental, etc.), etc.

Multimedia programs can be used in physics education to:

- create positive motivation in students to learn;
- increase their interest in studying physics;
- form skills and habits for self-acquisition of knowledge;
- diversify traditional teaching aids and methods;

The use of multimedia programs in physics teaching is methodologically appropriate, as everything can be seen at a glance and stimulates the implementation of mental operations - analysis, synthesis, comparison, abstraction, summary and more.

Multimedia physics teaching programs allow conduction of physical experiments that cannot be directly observed or are difficult to perform under natural conditions (experiments at the atomic-molecular level or at the macro level), which are dangerous to the health of students and teachers, but create cognitive interest, which requires a long time or specific and expensive equipment, etc. Through the use of multimedia programs various applications of

physical knowledge in nature, life and human activity can be illustrated.

Multimedia programs are the most commonly used didactic software products in physics teaching in high school, as they provide innovative opportunities to illustrate the studied physical objects, phenomena or processes and to present the learning content in a new, more interesting and attractive way.

Multimedia programs are the basis of virtual physics laboratories, which are also multimedia technologies and are increasingly used in high school physics teaching.

At the moment, a great variety of multimedia physics programs that can be used to study the curriculum in high school, are developed.

When using multimedia programs in physics teaching, students see in practice some of the modern methods and tools (computer modelling and simulation), that are used in science physics to research and study physical objects, phenomena and processes.

Multimedia computer presentations

Multimedia physics teaching programs allow conduction of physical experiments that cannot be directly observed or are difficult to perform under natural conditions (experiments at the atomic-molecular level or at the macro level), which are dangerous to the health of students and teachers, but create cognitive interest, which requires a long time or specific and expensive equipment, etc.

Multimedia computer presentations are modern learning tools that provide innovative opportunities for teaching and learning physics.

They are usually created by using the program MS PowerPoint and they are a series of slides that can include various objects: text, dynamic and static images, sound, etc., as well as animation effects on the objects of a slide or when switching from one slide to another.

They are also a convenient methodological tool for structured presentation of a certain learning content or a certain information in an appropriate and understandable way for students. They can be used in all types of physics lessons, e-learning and more.

Multimedia computer presentations, which are used in physics education in high school, are most often created by teachers in accordance with their views on the structure and content of each lesson. Each presentation usually includes: lesson topic, lesson plan, links to the used didactic software products, control questions and tasks, topics for project work and preparation of messages, reports,

etc. from students in their extracurricular activities, addresses of sites on the Internet with educational resources in physics, etc.

The use of multimedia computer presentations in physics teaching improves the visibility and accessibility of the studied curriculum, attracts the attention of students, creates cognitive interest and positive motivation in them to acquire knowledge in physics.

In multimedia computer presentations, the curriculum in physics can be structured in different ways. They can include a variety of didactic software products such as multimedia programs, video applications, computer animations, electronic visual materials of reference nature, computer interactive programs for solving physics problems and much more. Computer presentations provide opportunities for dosing the amount of information, for its change and repetition according to the interests and abilities of students, available study time and more.

Multimedia computer presentations as innovative learning tools can be used to support one of the most effective methods of teaching physics - problem-based learning. Through the didactic software products included in them, problem situations can be created and learning problems in physics can be solved.

When presenting the curriculum in physics through multimedia computer presentations, the lessons become more various and interesting, the learning process is intensified, the teaching time is reduced, which in turn allows in the lessons to consider more examples and applications, to solve a large number of tasks, to clarify in more detail various theoretical issues and problems, to make discussions, etc.

High school students have sufficient knowledge and skills in information technologies, which can be used to present through multimedia computer presentations with MS PowerPoint prepared by them messages, reports, etc. on certain topics for participation in discussions, seminars, student conferences, various educational programs, competitions, contests, project work, etc.

In the Bulgarian pedagogical literature it is recommended that the duration of a computer presentation should not exceed 25–35 minutes per school hour for students from VII to XI grade.

The use of multimedia computer presentations complements and expands the means and methods of teaching physics, as they allow the learning content to be presented and illustrated in an innovative and different way.

Electronic multimedia textbooks and aids

Electronic multimedia textbooks and aids are modern computer tools for teaching the different subjects studied at school. They are considered in the methodological literature as a new generation of textbooks and aids after the printed ones [3].

Electronic multimedia (interactive) textbooks and aids are structured on the basis of printed, but also include additional educational resources such as multimedia programs, video applications, computer animations, audio recordings, computer interactive tasks and tests, hypertext, dictionaries and many other didactic software products. In addition, a variety of educational and methodological materials for teachers are attached to them.

Electronic multimedia textbooks and aids can be used in physics lessons in high school, in extracurricular activities of students, for e-learning, self-study and more.

The learning content in them is very well illustrated and is accessible for study by students. The way of its presentation provides opportunities for flexibility and variability, for creating problem situations and solving learning problems, for connecting theory with practice, etc.

Electronic multimedia textbooks and aids allow individualization and differentiation of physics education. They are suitable for learning work with students with special educational needs, with students who study according to individual curricula, with outstanding, talented or advanced students, etc.

In electronic multimedia textbooks and aids, the teaching content of physics can be on different levels of difficulty and can be studied in different ways determined by teachers or students.

Electronic multimedia textbooks and aids can be used through various devices (computers, laptops, tablets, smartphones, etc.) both online and offline. Working with them is easy for students and can be done at any time and from any place.

The learning content in the electronic multimedia textbooks and aids can be much easier edited, added and updated, compared to the printed ones.

On the pages of electronic multimedia textbooks and aids you can write, draw, etc., which is not recommended to do when using printed textbooks and aids. The additions and changes made to the electronic versions can be saved or deleted according to user wishes.

In physics teaching, electronic multimedia textbooks and aids can be used to improve visibility, to present and study in dynamics physical objects, phenomena or processes from the micro and macro world, to conduct experiments that require specific

or expensive equipment, to consider various applications of physical knowledge, etc.

The interactive electronic textbooks of the Prosveta publishing group [4] are digital versions of the printed textbooks and are made in the form of FlipBook - leafing books. They are enriched with multimedia materials - tasks, exercises, illustrations, tests, music, videos and more. They fully cover the curriculum of printed textbooks approved by the Ministry of Education and Science. E-textbooks are interactive, entertaining, easy and convenient to work with. Additional interactive resources support the exercises and can be in the form of games, audio, video, 3D visualizations, 360° panoramic images, files, presentations and more [4].

The electronic textbooks of the publishing groups Anubis and Bulvest 2000 [5, 6] are digitized versions of the printed textbooks, enriched with various multimedia educational resources such as: interactive tasks, audio recordings, videos, images, animations, 3D visualizations, virtual simulations, tests, dictionaries, links to specific web pages and online resources, links to .pdf, .doc, .ppt, .pg, .png documents and those created by the platform itself. They allow flexible, interactive and adaptive learning without time, place and access restrictions [5, 6].

Electronic multimedia physics textbooks and aids provide new learning opportunities for students and are increasingly and successfully used in the learning process in high school.

In addition to the presented examples of multimedia technologies applicable in high school physics education, others exist and are used. However, they are not presented due to the limited volume of the article.

The integration of multimedia technologies in the physics teaching in secondary school requires both technical equipment and professional computer and methodological skills of teachers for their use. In traditional (real) physics teaching, the technical equipment includes at least one computer and a multimedia projector or interactive whiteboard for each physics classroom.

Naturally, the question arises: When to use modern educational technologies in physics teaching. Above all, in the cases when they have significant advantages compared to the traditional ones. The use of modern educational technologies is expedient when it leads to positive changes in the content, organization and conduction of the educational process in physics, when it facilitates the acquiring of new knowledge and the formation of skills and relations, when it helps to develop the creative possibilities, the cognitive abilities and

the thinking of the students and when it relieves the teacher's work.

CONCLUSION

The development of science, technology and engineering causes changes in the methods and tools of physics teaching in high school.

Multimedia technologies are innovative educational resources that have a real application in the physics teaching in high school.

In the article are presented examples of multimedia technologies and basic methodological opportunities for their use in the physics teaching process in high school.

The theoretical research on the topic of the article and on the presented methodological possibilities for the application of multimedia technologies in the physics teaching in secondary school show that:

multimedia technologies can be used in various physics lessons, in extracurricular activities of students, to conduct e-learning (synchronous and asynchronous) and others.

many of the problems of physics teaching can be solved in an innovative way through the use of multimedia technologies;

the use of multimedia technologies leads to diversification and enrichment of traditional teaching methods and tools;

multimedia technologies support, rationalize and improve the creative learning activities of teachers with students.

From a methodological point of view, multimedia technologies have a place in every structural part of physics lessons - updating, presenting and consolidating the curriculum in physics, in checking and assessing the learning achievements of students, etc. The use of multimedia technologies expands the methodological opportunities for presentation and visualization, for perception, comprehension, assimilation and application of the curriculum in physics and of the additional information on the topics studied in high school.

The learning content in physics, presented through the use of multimedia technologies, affects various human senses. On this basis, it can be assumed that it is perceived and assimilated more easily by students.

The use of multimedia technologies in the physics teaching in high school contributes to the implementation of interdisciplinary links with the subjects Informatics and Information Technologies, for the acquisition and formation of generalized knowledge, skills and attitudes.

The use of multimedia technologies is one possible methodological option for improving the secondary school physics teaching and for increasing its efficiency.

REFERENCES

1. H. Tuzharov, Multimedia technologies, ,.
2. <http://tu.asenevtsi.com/Media/M28.htm>.
3. G. Kalpachka, Modern educational technologies in physics teaching, Blagoevgrad, University Publishing House Neofit Rilski , 2021, p. 128, ISBN 978-954-00-0261-3.
4. S. Georgieva-Lazarova, Preparation of didactic materials in modern education, 2011, <https://ournals.uni-vt.bg/getarticle.aspx?aid=1017> type .pdf.
5. <https://www.prosveta.bg/>.
6. <https://www.anubis.bg>.
7. <https://www.bulvest.com>.

Investigation of instructional practices in high-school atomic and subatomic physics

K. Ilchev*, I. Kotseva

Sofia University „St. Kliment Ohridski”, Faculty of Physics, Sofia, Bulgaria

Received: November 16, 2021; Revised: March 29, 2022

Education research has illuminated numerous student misconceptions of atomic and subatomic physics. Furthermore, there is evidence that high-school students' engagement is positively correlated with an increase in the variety of applied teaching methods. In this paper, we systematically investigate proposed methods which are likely to improve high-school students' understanding of the microscopic world. This includes specific application of models, cooperative learning, problem-based learning and others. We comment on trends and empirical evaluation within the diverse assortment of proposed activities.

Keywords: physics education, secondary education, instructional practices, atomic physics, nuclear physics, particle physics

INTRODUCTION

Physics at the high-school level covers many conceptually difficult ideas, especially when dealing with phenomena of the microscopic domain. Principles may counter previous student conceptions. Moreover, events are generally not directly visible. Students must develop an adequate model in their mind and relate it to the governing laws of nature.

Several papers document and analyse common high-school student misconceptions in the area of atomic, nuclear and particle physics. For example, Tuz n and Solbes [1] report that while some students have heard about terms such as particle accelerators or the Higgs boson, they still confuse modern with classical physics ideas. The authors empirically show that students may not distinguish the fundamental forces, e.g., when identifying the force responsible for keeping the electron bound to the nucleus. Other reported difficulties relate to the question of how repelling protons can form stable nuclei and which kind of interactions occur when nuclei transform. Another conclusion is that students confuse the hierarchy of microscopic constituents, for instance claiming that nuclei are composed of atoms, etc. These findings point towards the need of instructional practices which establish systematic knowledge and thereby allow students to correctly identify and contextualise scales and fundamental forces.

Another set of misconceptions relates to the atomic and radiation models. Savall-Aleman *et al.* [2] report a multitude of specific difficulties associated with atomic spectra and their interpretation. Students may not account for the quantization of energy levels, grasp photons as being

always absorbed by the atom, confuse the ground state energy, falsely relate high photon intensity with high frequency. Other misconceptions relate to atomic processes where students have claimed that transitions to lower states are always transitions to the ground state, etc. Some statements show that students do not apply energy conservation in the matter-radiation interaction. The authors suggest providing students with more opportunities to use models in order to explain various emission and absorption processes.

When teaching high-school nuclear physics, one will likely encounter student's fear of radiation or radiophobia (Tsuruta *et al.* [3]), probably induced by modern media or past historic events. A lack of knowledge makes it harder for students to grasp radioactivity benefits for society alongside interdisciplinary connections, e.g., to geology, chemistry and biology (de Cicco *et al.* [4]). In addition, teachers may find that experimental activities are not readily available (Bastos *et al.* [5]), either due to the high cost of radiation sources/detectors or safety regulations. Which kind of activities could help students explore the hazards/advantages of radiation, alongside the connection to technology, politics and ethics (Schibuk [6])

Recently, STEM education has gained popularity in research. It aims to prepare students for real, complex problems by increasing their activity in the classroom. The idea is to deepen student thinking, thereby guiding them towards higher cognitive levels. One question of interest is whether a variety of applied teaching methods helps students tackle more difficult problems.

* To whom all correspondence should be sent:
E-mail: konstantin.ilchev@hotmail.com

A statistical correlation of this type has been found within data from TIMSS Advanced 2015. This international study provides results from physics tests and student/teacher questionnaires. It encompasses nine countries and deals with students in their final year of secondary education (ISCED 3). The test consists of three content domains and three cognitive domains - Knowing, Applying and Reasoning (Mullis and Martin [7]). It is possible to analyse TIMSS Advanced data with a web-based data analysis tool called IDE (<https://nces.ed.gov/surveys/international/ide/>). This has allowed us to check the following hypothesis: A variety of applied teaching methods is positively correlated with student results from the Reasoning section of the physics test. IDE has a built-in significance test which confirmed the hypothesis, with $p = 0,05$. (International average; Scale: reasoning (2015); Variable: [PS3BP18M]. For further details, contact the leading author.)

Analysis of TIMSS data has also shown a positive correlation between the variety of teaching methods and minutes spent per week on physics outside of class (which may relate to student motivation).

Research Questions

In view of the aforementioned empirical findings, we formulate the following questions:

- R 1) Which **instructional activities** are suggested in atomic and subatomic high-school physics articles
- R 2) Which kind of **student involvement** is described in these articles
- R 3) Which instructional practices have (empirically) shown to be **effective**

Method of Research

We chose to browse the databases *Scopus*, *ERIC* (and *Google Scholar*) for articles related to questions R 1-3. This section summarizes the steps which led to a set of 32 included articles. The first step was to specify how papers are going to be filtered. We achieved this by applying the following **search string** to all three databases:

(secondary education OR high schools)
AND (instruction OR teaching)
AND (atom* OR nuclear OR particle)

We also checked for recent reviews which are related to our investigation and decided to exclude the term quantum from our search string. The main reason is that such a review has already been published. Kri tenburg-Lewerissa *et al.* [8] included 74 articles (including secondary education) and looked into quantum mechanics misconceptions and

teaching strategies, among other things. The authors conclude that a variety of instructional practices are proposed but there is too little empirical evidence for the effect of these strategies.

Scopus returned 312 hits while ERIC yielded 364 articles. We focused our search by applying the following inclusion criteria: Documents must:

- C1) .be accessible in English;
- C2) .be articles or reviews;
- C3) .be published after 2002;

- C4) .focus on activities for high-school students;
- C5) .provide a description of a practice or student involvement;
- C6) encompass at least one atomic, nuclear or particle physics topic and cannot be limited to teaching quantum physics.

Criteria 1-3 were easily applied because both Scopus and ERIC allow for filtering by language, publication date and document type. This was done first. Scopus yielded **33 hits** (after limiting articles to Physics and Astronomy) while ERIC returned **53 hits** (after limiting to Physics).

Criteria 4-6, however, required looking into the abstract (and usually – the whole text) of the remaining articles. Criterion 4 ensures that the article relates to secondary education. This excludes articles covering undergraduate/pre-service teachers education. Criterion 5 excludes articles dealing either with changes to the curriculum or strategies centred around the teacher explaining specific concepts. Criterion 6 excludes most but not all quantum-related articles as some of these naturally have useful intersections with atomic and subatomic physics. Specifically, some excluded articles focused on topics such as chemical kinetics, bonding; electric/magnetic fields; dark matter, cosmic expansion and other astrophysical concepts without direct relation to particles; special theory of relativity concepts; particle erosion; thermodynamics topics such as the behaviour and motion of particles in gases/liquids/solids. Further details about excluded articles can be provided by the leading author.

We are finally left with 10 (2 extra) 12 Scopus articles and 16 documents from ERIC. We included 4 additional articles from Google Scholar, which sums up to **32 articles to be analysed**.

Note that the 2 extra articles from Scopus were identified during a previous search including the quantum keyword. We decided to keep them because one is related to an experimental activity (photoelectric effect) and the other deals with a very interesting inquiry activity (nanotechnology). We also included 4 articles from G. Scholar, which does

add selection bias. Given our research questions, however, we decided to include the papers because they either give further variety in proposed student activities or provide additional empirical evidence. The included articles can be found in Table 1 of the following section.

RESULTS AND DISCUSSION

Once the 32 articles were selected, we employed the following strategy during our analysis: papers were carefully examined for instructional activities/setup, empirical evaluation and specific student involvement. By student involvement we mean distinct activities students may participate in. While one option is to classify instructional practices as being either model-based, problem-based, design-based, etc., we chose to apply an idea elucidated by Geis [9]. The author suggests that rather than categorizing activities according to utilized methods such as lecture or computer-based, one may want to pursue the critical features of a given activity – attributes which lead to success and may be shared between various methods. The features connections to daily life or receiving feedback, for example, may or may not be included in a lecture, problem-based learning, cooperative learning, etc.

We chose to consider 17 distinct actions students may become involved in during activities. These were adapted from the TIMSS Advanced 2015 and 2019 questionnaires. We also checked whether a given article describes a procedure or TLS (teaching-learning sequence) and whether it includes a quantitative evaluation of the activity. We give more information on the type of empirical evidence provided (see Appendix).

The results of our investigation are summarized in Table 1. It is color-coded and ordered by topic (atomic, nuclear, particle physics, combined/related articles). Note that spotting a feature in a given article (marked with an X in the table) means that it is either explicitly mentioned or (in our opinion) implied by the authors.

The purpose of Table 1 is twofold. Teachers and researchers can browse recent articles very quickly based on specific actions students get involved in. For example, one may be interested in nuclear physics group activities or experiment ideas. We do not suggest comparing articles (i.e., table rows) because some documents are naturally longer than others. They may describe long-term projects which involve students in various ways. On the other hand, some articles focus only on specific aspects of an activity, thereby providing very detailed information. Another way to use the table, however, is to compare table columns. Table 2

shows the frequency of features across all documents. While it may include some bias as mentioned above, it still portrays current trends. As can be seen from Table 2, most articles describe a procedure. Also, most presented activities encourage students to link atomic and subatomic physics ideas to previous content knowledge and to aspects of everyday life. A sizable fraction of papers (63%) focuses on group work and ways of presenting information (66%). More than half (59%) of the papers mention feedback to students. Interestingly, 11 of the papers do not include the use of computers. Despite the modern trend of using simulations, many articles illustrate actual hands-on procedures which deal with or visualize microscopic phenomena in other ways. Moreover, computer use is not central in some of the other papers. 50% of articles refer to experimental procedures while 31% cover experimental design/constructing devices in a real laboratory setting. Less than half of the articles describe classroom discussions, explaining answers and expressing ideas. The lowest percentages are appointed to field work (which is understandable as these are usually long-term activities or international projects) and quantitative evaluations. Another way to concisely present suggested practices is to categorize them (see Table 3).

CONCLUSION

Scopus, ERIC and Google scholar returned articles which cover a variety of instructional activities (Table 3). They allow us to identify and quickly locate specific student involvement (Table 1) and form tendencies (Table 2). The methods presented by the authors generally aim to tackle student misconceptions or relate the topic to student lives. Several papers put an emphasis on scientific literacy, ethics and society. Articles provide creative ideas for constructing and using devices in the classroom, games involving the whole class, working with scientific texts, inquiry-based assignments, university and international collaboration, as well as participation in real, long-term scientific projects. Only some of the practices require computers. Articles generally describe an instructional sequence but rarely (less than 25%) provide quantitative evidence. Authors assess student learning achievement, self-efficacy, conceptions of learning, scientific literacy, attitude and identify misconceptions. The effects reported in articles are mainly positive (see Appendix for details).

Acknowledgement: *This work was supported by the Research Fund of Sofia University under contract number 80-10-142/26.03.2021.*

Table 1. Features of included articles

Article (year)/ description	Quant. eval. ?	Descr. procedures /"TLS"	Class-room disc.	Daily lives	Link knowl.	Expl. answers	Express ideas	Group Work	Computer use	Plan exp./ construct.	Conduct exp.	Interpret data	Present data	Observe phenom.	Use evidence to supp.	Watch demo. of exp.	Field work	Challenging exs.	Give feedback
ATOMIC:																			
Savall-Alem any, F. et al. (2019) PBL atomic spectr.	Y	Y	X	X	X	X	X	X		X	X	X		X	X	X			X
Rodriguez, L. V. et al. (2020) Inquiry quantum.	Y	Y	X	X	X	X	X	X	X			X	X	X	X	X			X
Kontomaris, S. V. et al. (2020) Ionizing vs. non-ion. rad.	N	N		X	X														
Cziprok, C. et al. (2016) Vee heuristic, photoel. eff.	N	Y		X	X			X	X		X	X	X		X				
Cai, S. et al. (2020) AR, photoel. eff.	Y	Y						X	X		X	X		X					X
Woo, Y. et al. (2019) Constr. spectrometer	N	N							X	X			X						
Maffei, G. et al. (2011) Mosaic method, atom. spectra	N	Y	X		X	X		X				X	X	X	X				X
Salazar, R. et al. (2019) Modeling activities	Y	Y	X	X	X	X	X	X	X				X						X
NUCLEAR:																			
Bastos, R. O. et al. (2016) Experiments, low-cost.	N	N		X							X	X							X
Tsuruta, T. et al. (2009) Exp., track detection	N	N		X								X		X		X	X		
De Cicco, F. et al. (2017) Radon exp., School-uni collab.	N	Y		X	X	X		X	X	X	X	X	X	X	X		X	X	X
Schibuk, E. (2015) Activities (Manhattan project)	N	Y	X	X	X	X	X	X	X										X
Sengdala, P. et al. (2014) NOS teaching, Nucl./peace.	N	Y	X	X	X	X	X	X					X						X
Shastri, A. (2007) Constr. Slide-rule comp., nuclear eff.	N	Y	X	X	X	X	X		X	X		X	X		X			X	
Brown, T. (2014) Exp., radioactive dating	N	Y		X	X				X		X	X		X					X
Kapon, S. (2013) Scientific text for students (Einst. $E=mc^2$)	N	Y	X	X	X	X	X	X							X			X	X
KRIŠŤÁK, L. et al. (2013) Multimedia/ DVD activity	Y	Y	X	X	X	X		X	X		X	X			X	X			X
Elbanowska-Ciemuchowska, S. et al. (2011) Many activities	N	Y	X	X	X		X	X	X		X	X	X		X		X	X	X

K. Ilchev, I. Kotseva: Investigation of instructional practices in high-school atomic and subatomic physics

Article/ activity	Quant. eval. ?	Descr. procedures /"TLS"	Class-room disc.	Daily lives	Link knowl.	Expl. answers	Express ideas	Group Work	Computer use	Plan exp./ construct.	Conduct exp.	Interpret data	Present data	Observe phenom.	Use evidence to supp.	Watch demo. of exp.	Field work	Challenging exs.	Give feedback
PARTICLE:																			
Schramek, A. et al. (2019) <u>Research-based teaching, Uni-school. Detectors</u>	N	Y		X	X	X	X	X		X	X	X	X		X	X	X	X	X
Bressan, E. (2011) <u>Research-based teaching, Uni-school, CR detection</u>	N	Y		X					X	X	X	X	X		X		X	X	X
Bardeen, M. et al. (2018) <u>Online tools, QuarkNet</u>	Y	Y	X	X	X	X	X	X	X	X	X	X	X	X	X	X		X	X
van den Berg, E. et al. (2006) <u>Fast feedback, symmetries etc.</u>	N	Y	X		X	X		X										X	X
Kourkoumelis, C. et al. (2014) <u>Online tool, HYPATIA</u>	N	Y	X		X				X			X	X	X	X			X	X
Goldader, J. D. et al. (2010) <u>Constr. cheap CR detec.</u>	N	N							X	X	X		X					X	
Brouwer, W. et al. (2009) <u>Research-based. ALTA proj.</u>	N	Y		X	X	X	X	X	X		X	X	X		X		X	X	
de Souza, V. et al. (2013) (re-) <u>Constr. CR Impact point</u>	N	Y			X					X		X	X		X			X	X
Badalá, A. et al. (2007) <u>Data analysis, Simul. CR data</u>	N	Y	X		X			X	X			X	X					X	
COMBINED /OTHER:																			
Bussani, A. (2020) <u>Dice game, microsc. sys.</u>	N	Y	X		X			X	X			X			X			X	
Kvita, J. et al. (2018) <u>Particle camera for exp.</u>	N	Y		X	X				X		X	X	X	X		X	X	X	
Keegans, J. D. et al. (2021), <u>Outreach, Python, Nucleosynth.</u>	Y	Y			X			X	X			X	X		X			X	X
Planinšič, G. et al. (2008), <u>Constr. AF microscope model, Nano.</u>	N	Y		X	X			X		X	X	X	X		X	X		X	
Laubach, T. A. et al. (2010), <u>Quided inquiry, Nano.</u>	N	Y		X	X	X			X		X	X	X		X			X	

Table 2. Trends

Frequency (out of 32 papers)	Variable		Frequency (out of 32 papers)
Describe procedures/ TLS	84%	Conduct experiment	50%
Link knowledge	81%	Classroom discussion Explain answers	47%
Interpret data	75%	Express ideas	34%
Daily lives	69%	Plan experiment/ construct something Observe phenomenon	31%
Present data, Computer Use	66%	Watch demonstration of an experiment	25%
Group work	63%	uantitative evaluation Field work	22%
Challenging exercises Give feedback Use evidence to support	59%		

Table 3. Summary of proposed activities

<p>Educational games Duhdonium, competitive dice game. Microscopic systems. Bussani, A. (2020)</p> <p>Specific instructional methods Fast feedback method. Particle physics. van den Berg, E. <i>et al.</i> (2006) Modelling method. Atomic models. Salazar, R. <i>et al.</i> (2019) Mosaic (Jigsaw). Atomic spectra. Maftei, G. <i>et al.</i> (2011) Focus on analogies. Ionizing vs. non-ionizing radiation. Kontomaris, S. V. <i>et al.</i> (2020) Guided problem-based learning. Atomic spectra. Savall-Aleman, F. <i>et al.</i> (2019) Many different methods. Nuclear physics. Elbanowska-Ciemuchowska, S. <i>et al.</i> (2011) Reading a scientific text. Class discussions. Einstein's paper on $E = mc^2$. Kapon, S. (2013) Reading articles. NOS teaching. Nuclear physics and peace. Sengdala, P. <i>et al.</i> (2014) Flipped classroom approach. Discussions. Studying the Manhattan project. Schibuk, E. (2015)</p> <p>Experiments => Conduct 4 mystery vials with nano-solutions. Inquiry. Laubach, T. A. <i>et al.</i> (2010) Particle camera MX-10: Particle and nuclear physics. Kvita, J. <i>et al.</i> (2018) Photoelectric effect, using the Vee heuristic. Cziprok, C. <i>et al.</i> (2016) Radioactive dating in the classroom, using Cobalt-60. Brown, T. (2014) Nuclear track detection methods. Tsuruta, T. <i>et al.</i> (2009) Nuclear experiments with low-cost instruments. Nuclear physics. Bastos, R. O. <i>et al.</i> (2016)</p> <p>=> Plan/construct Constructing an atomic force microscope model. Planin, G. <i>et al.</i> (2008) Reconstruction of impact point and arrival direction of a CR particle. de Souza, V. <i>et al.</i> (2013) Constructing a cheap cosmic ray detector. Goldader, J. D. <i>et al.</i> (2010) Constructing detectors at a research center. Research-based teaching. Schramek, A. <i>et al.</i> (2019) Constructing a high-res 3D-printed smartphone spectrometer. Atomic. Woo, Y. <i>et al.</i> (2019) Constructing a slide-rule computer. Effects of nuclear weapons. Shastri, A. (2007)</p> <p>=> Data analysis Extensive air showers of particles. Particle physics. Badal, A. <i>et al.</i> (2007)</p> <p>Online tools/applets/multimedia HYPATIA. (ATLAS event data). Particle physics. Kourkoumelis, C. <i>et al.</i> (2014) Go-Lab activities. Photoelectric effect sequence. Rodriguez, L. V. <i>et al.</i> (2020) Multimedia DVD - nuclear physics. KRIK, K. <i>et al.</i> (2013)</p> <p>Augmented reality (AR) Photoelectric effect experiment using AR in groups. Cai, S. <i>et al.</i> (2020)</p> <p>Outreach/Research program ALTA study of cosmic ray bursts. Hypotheses in student projects. Brouwer, W. <i>et al.</i> (2009) arkNet education program. Research, masterclasses, e-Labs. Bardeen, M. <i>et al.</i> (2018) EEE (Extreme Energy Events) project: Cosmic ray detectors at schools. Bressan, E. (2011) ENVIRAD - Radon measurements at schools and university. De Cicco, F. <i>et al.</i> (2017) ThaiPASS - Data analysis using Python. Astroparticle physics. Keegans, J. D. <i>et al.</i> (2021)</p>
--

REFERENCES

1. P. Tuz n, J. Solbes, *PLoS one*, **11**(6), e0156526 (2016).
2. F. Savall-Alemany, J. L. Dom nech-Blanco, J. Guisasola, J. Mart nez-Torregrosa, *Physics Education Research*, **12**(1), 010132 (2016).
3. T. Tsuruta, S. Hohara, Y. Nakanishi, H. Shimba, *Radiation Measurements*, **44**(9-10), 1036 (2009).
4. F. De Cicco, E. Balzano, B. N. Limata, M. R. Masullo, M. uarto, V. Roca, ... M. Pugliese, *Physics Education*, **52**(6), 065003 (2017).
5. R. O. Bastos, C. A. Boff, F. L. Melquiades, *Physics Education*, **51**(6), 065013 (2016).
6. E. Schibuk, *The Science Teacher*, **82**(7), 27 (2015).
7. I. V. Mullis, M. O. Martin, TIMMS Advanced 2015 Assessment Frameworks, International Association for the Evaluation of Educational Achievement, Herengracht 487, Amsterdam, 1017 BT, The Netherlands, 2014.
8. K. Kri tenburg-Lewerissa, H. J. Pol, A. Brinkman, W. R. Van Joolingen, *Physics Education Research*, **13**(1), 010109 (2017).
9. G. L. Geis, *Canadian Journal of Higher Education*, **14**(2), 91 (1984).
10. A. Schramek, M. . Ol h, Z. Telek, K. Peter, *Canadian Journal of Physics*, **98**(6), 588 (2020).
11. E. Bressan, *Il nuovo cimento C*, **34**(5), 293 (2011).
12. G. Planin i , J. Kova , *Physics Education*, **43**(1), 37 (2008).
13. J. D. Keegans, R. J. Stancliffe, L. E. Bilton, C. R. Cashmore, B. K. Gibson, M. T. Kristensen, ... S. Chongchitnan, *Physics Education*, **56**(3), 035001 (2021).
14. F. Savall-Alemany, J. Guisasola, S. R. Cintas, J. Mart nez-Torregrosa, *Physics Education Research*, **15**(2), 020138 (2019).
15. L. V. Rodriguez, J. T. van der Veen, A. An ewierden, E. van den Berg, T. de Jong, *Physics Education*, **55**(6), 065026 (2020).
16. S. V. Kontomaris, A. Malamou, G. Balogiannis, N. Antonopoulou, *Physics Education*, **55**(2), 025007 (2019).
17. C. Cziprok, F. F. Popescu, *Romanian Reports in Physics*, **68**(2), 879 (2016).
18. T. A. Laubach, L. A. Elizondo, P. J. McCann, S. Gilani, *The Physics Teacher*, **48**(3), 186 (2010).
19. A. Bussani, *The Physics Teacher*, **58**(3), 167 (2020).
20. J. Kvita, B. erm kov , N. Matulov , J. Po tulka, D. Stan k, *Physics Education*, **54**(2), 025011 (2019).
21. P. Sengdala, C. Yuenyong, *European Journal of Science and Mathematics Education*, **2**(2), 119 (2014).
22. M. Bardeen, M. Wayne, M. J. Young, *Education Sciences*, **8**(1), 17 (2018).
23. E. van den Berg, D. Hoekzema, *Physics Education*, **41**(1), 47 (2006).
24. S. Cai, C. Liu, T. Wang, E. Liu, J. C. Liang, *British Journal of Educational Technology*, **52**(1), 235 (2021).
25. C. Kourkoumelis, S. Vourakis, *Physics Education*, **49**(1), 21 (2014).
26. A. Shastri, *The Physics Teacher*, **45**(9), 559 (2007).
27. T. Brown, *The Physics Teacher*, **52**(2), 115 (2014).
28. Y. Woo, Y. G. Ju, *Physics Education*, **54**(1), 015010 (2018).
29. J. D. Goldader, S. Choi, *The Physics Teacher*, **48**(9), 594 (2010).
30. W. Brouwer, J. Pinfeld, R. Soluk, B. McDonough, V. Pasek, Z. Bao shan, *The Physics Teacher*, **47**(8), 494 (2009).
31. V. de Souza, M. A. Barros, E. C. Marques Filho, C. R. Garbelotti, H. A. Jo o, *Physics Education*, **48**(2), 238 (2013).
32. S. Kapon, *Physics Education*, **48**(1), 90 (2013).
33. A. Badal , F. Blanco, P. La Rocca, G. S. Pappalardo, A. Pulvirenti, F. Riggi, *European Journal of Physics*, **28**(5), 903 (2007).
34. G. Maftai, M. Maftai, *Procedia-Social and Behavioral Sciences*, **15**, 1605 (2011).
35. . Kri k, J. Stebila, Z. Danihelov , *Scientia in Educatione*, **4**(1) (2013).
36. S. Elbanowska-Ciemuchowska, M. A. Giembicka, How to Stimulate Students Interest in Nuclear Physics Online Submission, (2011).
37. R. Salazar, Evaluating a Didactic Strategy to Promote Atomic Models Learning in High School Students through Hake s Method, Online Submission, **7**(5), 293 (2019).

APPENDIX: OVERVIEW OF EMPIRICAL EVALUATION

Article (Year)	Context of study/sample	Control group	Pre-test	Post-test	Statistical analysis	Results
Savali-Alemany, F. et al. (2019) PBL atomic spectr.	Assess learning achievement and identify student misconceptions. Experimental group (PBL): total of 74 students, 2 high schools. Control group (lectures+problem solving): total of 67 students. Teachers – over 10 year experience, incl. PBL.	Yes	Yes. No correct answers - exp. Or ctrl. group.	Yes. Included in appendix. Open-ended answers to three questions. Classification of student answers. High inter-rater reliability. 5 students who performed very well additionally interviewed to check knowledge.	Yes. Chi-square test. Fisher's p. Cohen's h.	Experimental group performed stat. signif. better in all 3 questions. Cohen's h suggests a large effect size. Discussion of observed student misconceptions.
Rodriguez, L. V. et al. (2020) Inquiry quantum.	Assess learning outcomes and identify student misconceptions. 114 students from four high schools.	No	No	Data collection through digital environment. MCQ and open-ended questions.	Correct answers reported as a %.	Majority of students understand critical concepts related to the photoelectric effect. Less successful in answering certain open-ended questions.
Cal S. et al. (2020) Augmented reality, photoel. eff.	Assess student self-efficacy and conceptions of learning. Experimental group (AR): total of 49 students. Control group (flash-based): total of 49 students from one high school.	Yes	Yes. No significant difference.	Yes. SEOLP questionnaire, COLP questionnaire.	Yes. t-test analysis. ANCOVA.	AR group achieved significantly higher scores on physics learning self-efficacy compared to the Flash group. (4 out of 6 aspects showed improvement, namely conceptual understanding, higher-order thinking skills, practical work and social communication.) AR group scored higher in applying, understanding and seeing in a new way. (higher-level conception) They scored lower in memorizing and calculating (lower-level conception).
Salazar, R. et al. (2019) Modeling activities	Assess learning outcomes (Hake's gain score). 20 students from one school.	No	Yes	Yes. Included in appendix.	Yes. Hake's normalized gain.	Most answers show a high conceptual gain ($g > 0.7$). Only three questions still trouble students ($g < 0.3$). Average gain for the 20 questions is high ($g = 0.72$). Authors report student answers to activities.
KRIŠTÁK, L. et al. (2013) Multimedia/DVD activity	Assess learning gains in area of: remembering, understanding, transfer of specific and non-specific knowledge (analysis, synthesis etc.). Experimental group (Multimedia DVD): 104 students. Control group ("traditional" teaching): 101 students. Students are from four high schools. Same teacher taught the students (for each school).	Yes	No	Yes. Included in appendix. Open-ended/MCQ.	Yes. F-test and t-test. Normal distribution verified for both groups.	Students using DVD multimedia scored significantly higher than students using "traditional" methods, in all three categories: specific and non-specific transfer, remembering and understanding.
Bardeen, M. et al. (2018) Online tools, QuarkNet	Assess increase in scientific literacy of students. Masterclass effectiveness - knowledge and attitude. 582 students.	No	Yes. Conceptual maps. Masterclass: Yes.	Yes. Conceptual maps. Masterclass: Yes.	Yes. However, analysis of effect sizes and differences only mentioned; no details included in paper.	Post-maps show a more sophisticated or scientifically literate understanding of the scientific process. Improvements for students with higher and with lower pre-program maps. Masterclasses: Positive attitude towards physics: 4.0 average out of 5. Increase student knowledge and skills.
Keegans, J. D. et al. (2021), Outreach, Python, Nucleosynthesis	Assess student attitude and skills. 60 students from 30 schools	No	No (2018 event). Yes (2019 event).	Yes. Questionnaire included in appendix.	No, however all student responses clearly shown on histogram.	(2018) Largely positive attitude towards the summer school. (2019) Self-assessment shows that students believe their programming and computer science skills have increased. Most students would pursue a STEM career. Perceived usefulness of Python, interest in nuclear astrophysics and STEM-career interest have increased (pre- to post-test).

Application of the project method in physics education in classes with intensive studying of English

G. Malchev*

Peyo Kracholov Yavorov Profiled High School, Petrich, Bulgaria

Received: November 27, 2021; Revised: May 24, 2022

The article is dedicated to project-based learning as a way to create an interactive educational environment that stimulates students' cognitive activity. It dwells on the essence of the project method and the preliminary stages the preparation of a training project goes through. Emphasis is placed on the application of this method in physics education. The article also presents an option, a feasible one in common pedagogical practice, of including project-based physics education in the school curriculum of 9th graders with intensive study of English in junior high.

Keywords: physics education, project method, English language, information technology, interdisciplinary relations

INTRODUCTION

Contemporary pedagogical reality has made physics education a real challenge bearing in mind the diminished interest on the part of students in this academic subject. The latter often consider physics hard to learn because it requires much greater effort and logical thinking to understand the various processes and phenomena that are studied at school. However, in the course of achieving a goal even the hardest obstacles can easily be overcome at a certain point provided the right approach has been found. In this particular case this means selecting and combining different methods and means aiming at boosting students' cognitive capabilities and motivation to study. In and out of school, ways should be found to inspire students to become explorers and obtain knowledge on their own through various activities. There is no doubt, far more efficient a form of education is for students not just to study and re-produce what they have learned but to think, come up with ideas, discuss issues, review and summarize solutions to pressing problems of science, technics, nature, outer space. The analytical perception of the physical matter is definitely a way to bring science closer to students so that they can understand it better. That is why contemporary teachers should not just teach and make students learn what they have been taught, they need to trigger students' thinking through intellectual interaction. Such interactive ambience relying on a multitude of methods and the application of various approaches can be founded on project-based education. Pedagogical practice has shown that using projects in physics education has universal appeal among students. Project work makes students braver and more confident in their studies. Besides, they come

up with creative ideas and ways of implementing them. Thus they come to realize physics is not that hard a subject to master.

THE ESSENCE OF THE PROJECT METHOD

The project method is not entirely new – it first appeared at the beginning of the 20th century in the USA. It is also known as 'the problem method' and was initiated by John Dewey and his student William Killpatrick who made use of the ideas of the humanistic stream of philosophy and pedagogy. The method was pretty successful and was introduced to American schools due to its rational combination of theoretical knowledge and its practical application for the solution of particular everyday problems. During the first decade of the last century it got the attention of some Russian pedagogues but it was not until the 30s that it became common practice in the ex-USSR [1].

"All that I learn I know what I need for and where and how I will be using it" – this somehow summarizes what the project is all about in contemporary context.

The term 'project' is what project-based education is really based on. Translated literally from Latin it means 'thrown forward'. It is often used in different fields of human life denoting a plan, an intention. Didactics views it as a "topic for research (survey) in the context of the didactic tasks (without opposing it to or eliminating the subject curriculum requirements), the successful development of which presupposes both theoretical background and practical implementation" [2]. An activity the content of which is document-certified leading to the accomplishment of set goals over a certain period of time' is yet another definition in terms of the activity approach.

* To whom all correspondence should be sent:

E-mail: gmalchev@abv.bg

Participation in project work promotes students' thinking for themselves and thinking creatively, finding and solving problems. That is usually achieved by integrating knowledge from different scientific fields, which in its turn leads to the development of certain skills like foreseeing the results and possible consequences of the decisions students have made [3]. Central to the realization of the project method is students' work – individual, pair or group work, which aims at solving a problem. The result of their activity – the final material product should be presented in public in due form. Thus the school project is an all-round cognitive activity comprised of a goal, topic, planned activities and results.

Work on the project starts with defining unambiguously the topic [4]. Then it is open for discussion among the participants who work out the details and plan the activities. The planning can be done within the school or it may involve the coordinated efforts of several schools. The teacher should emphasize certain parts of the project work so that the students can gradually get a full grasp of it. Initially the teacher should act the part of a leader. Then, as the working process progresses and should any obstacles appear he/she should be a consultant, a mentor figure [5]. The more aware of the imperatives and the final results the students are, the greater their interest. In fact, project work at school is quite a challenge for students to demonstrate their personal qualities and skills.

Working out the school project goes through the following stages [6]:

Stage 1. Research – that involves selection of the topic, brief analysis of the problem, formulating a hypothesis, discussion of the research methods to use, forming groups and giving them assignments.

Stage 2. Analysis – it has to do with analysis of the available information and searching for up-to-date approaches to accomplish the goal of the project, as well as working out a plan of the activities.

Stage 3. Realization of the planned activities.

Stage 4. Presentation – reviewing and presenting the results.

Stage 5. Control – analysis of the results and assessing the fortes and weaknesses of the project.

Project-based learning goes far beyond the limitations of the authoritarian and reproductive methods. It entails a self-centred, interactive and brilliantly concocted mixture of methods and means. It also provides the chance for the teacher to take the students' strengths into consideration and act upon them. That, in its turn, stimulates and updates the already accumulated knowledge and

skills, which is the perfect foundation for future individual cognitive work.

PROJECT-BASED EDUCATION IN PHYSICS

The project method combined with the traditional lesson planning in physics classes adds to and enriches the teaching process thus making it interesting and innovative. Such an addition follows the trend in worldwide educational theory and practice of re-locating the functions and individual work of the students in class. That makes education more personal and makes the most of the students' skills acquired in various fields of science.

In general, for students to be able to gain good and long-lasting knowledge of physics, we should bear in mind two important factors:

- *the way the teacher schedules and works out the content of the coursebook;*
- *the character of the cognitive activity performed by the students.*

These factors determine to a large extent the level of mastering the forms of logical reasoning like analysis, synthesis, comparison, systematization, abstraction, review, providing specific examples. These factors are of crucial importance in project-based education. Without them knowledge acquisition would be impossible. The reason for that is simply because knowledge should first be understood and then acquired. Then again understanding depends on the way scientific information is perceived by the students and the level of formation of the abovementioned logical operations [7].

By applying the project method students actually learn to develop expedient and diverse mental activity, which leads to easier and better acquisition of the complex concepts and phenomena of physics and provokes higher cognitive interest.

Practice and experience in the field has made it evident that the project method emphasizes the following [8, 9]:

- it promotes individual cognitive work during which the students solve problems they themselves consider important in the field of physics and its application in different spheres of life;
- the teacher gets in the shoes of an adviser and a partner who monitors students in the process of studying physics;
- there is constant teacher-student feedback, which helps in determining the fortes and weaknesses of the project activities, as well as in finding solutions to difficult issues;
- it entails a reflection on the personal cognitive activity of the students which is a sign of

self-governed development as concerns the synergic ideas of self-organizing in the complex nonlinear structures.

A PROPOSITION FOR PROJECT-BASED PHYSICS EDUCATION IN CLASSES WITH INTENSIVE STUDYING OF ENGLISH IN JUNIOR HIGH

The end of the autumn term of 2018/2019 marked the initiation of project-based learning in Peyo Yavorov Highschool in the 9th grade – a class profiled “Software and hardware science” with intensive learning of English. The topic of the project was “Heat Engines and the Environment” as was the title of one of the scheduled lessons for discussion in the 9th grade on the curriculum with students studying English intensively in junior high. Within a month three teams of students, two members each, were given the assignment to prepare three presentations of the project in Bulgarian, to translate them into English and present their papers in English on the day of the open-door lesson. For the purpose of the project task the students were expected to integrate knowledge and skills they had acquired in physics and astronomy, IT and English. In IT at that level

of education making a presentation is considered the basics whereas the intensive learning of English in that particular class, especially in the 8th grade presupposes a good command of the language. That is why, the real challenge turned out to be the physics part, namely the teams’ research work on the three topics: “The role of heat engines in the development of the technological revolution”, “Heat engines and the pollution of the environment”, “Ways of reducing the pollution of the environment”. The first topic was assigned to Hristina Avramova and Andrey Manchev, Ilian Svechev and Ilian Karamfilov were given the second, the third went to Raya Pavlova, Theodora Chuchurova. Apart from that, the physics teacher Georgi Malchev prepared his own presentation for the open-door lesson dwelling on the description of heat engines and quotes from the students’ work (Fig. 1). Another student – Antonina Borunsuzova was engaged to do simultaneous translation during the lesson. The selection of students was predetermined mainly by their fluency in English after a consultation with their English teacher Donika Dimitrova.



Fig. 1. The first slides of the presentations of the teacher and his students.

At the first meeting the students were given directions as to the goal of the project. They were specifically instructed to research the topic on their own and then to inform the rest of the class about the significance of heat engines in the development of the technological revolution and the harm they bring to the environment. The teacher consulted each team separately about the kind of information and photos their presentation should contain. He also highlighted the stages the project was supposed to undergo in the course of the following four weeks as well as the deadlines they had to make:

Stage 1. *Searching the net for information relevant to the three topics of presentation (deadline: two weeks for making the presentation, including consulting the teacher):*

1. *The role of heat engines in the development of the technological revolution:*

- Historical background.
- James Watt and his contribution to the development of the steam engine.
- When did internal combustion engines first appear? What advantages do they have over steam engines?
- How do jet engines operate? Where can they be applied?

2. *Heat engines and the pollution of the environment – one of the most pressing problems of our time:*

- What are the reasons for the incomplete using up of thermal energy and its dispersion into the environment on the premises of thermo-electric and nuclear-power stations?
- How does water heating in water basins affect the organisms that live in them?
- What exactly is the 'greenhouse effect' that leads to warmer temperatures and climate change round the globe?

3. *Ways of reducing the pollution of the environment and solving urgent ecological issues:*

- What new engines are being developed to limit the pollution of the environment?
- Are there any advances in the usage of solar energy and its transformation into electricity?
- What new technologies are being developed for the reduction of thermal pollution?
- How does the installation of a centralized heating system prevent pollution?

Stage 2. *Handing in the presentations to the teacher of physics, final proofreading, correction and editing the photos (deadline: the last day of Stage 1.) as well as English translation of the presentations and the lines of the teacher of physics*

intended for the open-door lesson (deadline: a week). Final consultations of the three teams were appointed with the teacher of physics and of the translator with the teacher of English. On the latter's advice some minor corrections were made in the English version of the text and plan of the lesson.

Stage 3. *Rehearsal of the presentations in the presence of the teachers of physics and English (deadline: a week). There were two rehearsals altogether aiming at coordinating the work of the three teams and emphasizing the specific pronunciation of some complex English terms.*

Stage 4. *Open-door lesson on the topic of the project.* The lesson was done in Bulgarian and English in front of the class and some formally invited visiting teachers (deadline: the last day of Stage 3.). At the beginning the teacher of physics delivered a brief lecture on the nature of heat engines and the three engine types – steam engine, internal combustion engine, jet engine. Every line on the part of the teacher was duly translated on the spot by the student in charge of translation (Fig. 2). After that the topics of the three teams were announced – one after another. In the same fashion the students made their presentations in English (Fig. 3). Then the teacher reviewed their performance and drew some conclusions about the effect of heat engines on the environment.

Stage 5. *Analyzing and evaluating the project by the teacher.* He commented on students' participation and gave them excellent marks for their diligence at the end of the lesson.

CONCLUSION

The realized school project managed to create specific educational environment, which made it easier for the students to learn about the ecological consequences of the work of heat engines. The project was based on their skills to research scientific information, analyze it, visualize and present it in the language they study intensively. The approach was rather different from the traditional one, but it definitely made the participants interested in similar linguistic presentations of other themes and topics of physics. That is why such presentations of three other topics in the next part of the coursebook were given to students as home assignments. It is obvious that the laws and phenomena of physics seem to impress students more when they think of them in terms of a foreign language.



Fig. 2. The participants in the project and their teacher of physics before and during the open-door lesson.



Fig. 3. Presentation in front of the class and some visiting teachers.

Combining physics with English and IT is definitely a working mechanism for establishing inter-subject relations. The project was carried out successfully because the students' learning of physics was supported by their linguistic and IT skills. This triple collaboration made them feel worthier, they viewed the project in highly positive terms and participated eagerly in all activities. Besides, they put a great deal of effort into their

work demonstrating great responsibility, creativity and knack for research and exploration.

Over the last couple of years, project-based learning has triggered greater interest among students and teachers. One of the reasons is the contemporary trend of establishing a connection between theory and practice, education and production/scientific research. Another reason for the appeal of the method is the opportunity it gives

for the appointed tasks and activities to be performed online. This was of crucial importance last year considering the distant education schools had to switch to as a result of the global COVID-pandemic.

In general, project-based learning shows students the subject of physics in an entirely different light. Assuming the part of young researchers, they soon realize it is not just a theory but something accessible once they have reached the scientific truth through hard and active learning. This way they perceive more deeply and thoroughly the fundamental scientific explanation of the processes and phenomena in the whole material world. And that, as we all know, is the ultimate mission of every teacher of physics.

REFERENCES

1. P. Radev, Brief Didactics, FastPrintBooks, Plovdiv, 2016.
2. M. Andreev, The Process of Education. Didactics, St. Kliment Ohridski University Press, Sofia, 1996.
3. D. Mitova, Project-oriented technological education, Neofit Rilski South-West University Press, Blagoevgrad, 2006.
4. M. Ivanova, in: Developing teamwork skills and inspiring creative thinking in making school projects (Proc. 4th Nat. Conf. Education in a Society of Information, Plovdiv, 2011), Development of an Informational Society Association, Plovdiv, 2011, p. 239.
5. K. Marulevska, *Pedagogy*, **2**, 6 (2008).
6. K. Marulevska, Project-based Learning in Primary Schools, Neofit Rilski South-West University Press, Blagoevgrad, 2009.
7. R. Vassileva, *Bulgarian Chemical Communications*, **47**, Special Issue B, 498 (2015).
8. M. Delinesheva, *Pedagogy*, **3**, 11 (2006).
9. A. Muzzarelli, Master's report, Michigan Technological University, Michigan, 2007. <https://digitalcommons.mtu.edu/cgi/viewcontent.cgi?article=1527&context=etds>.

Special session

"Low-carbon energy for transport and household"

Basic mathematical modeling and experimental validation of electrochemical hydrogen compressor

G. Borisov*, N. Borisov, E. Slavcheva

“Acad. Evgeni Budevski” Institute of Electrochemistry and Energy Systems, Bulgarian Academy of Sciences, 1113 Sofia, Bulgaria

Received: November 29, 2021; Revised: April 19, 2022

A mathematical modeling of electrochemical hydrogen compression process is presented. The model is based on theoretical thermodynamic functions and kinetic equations. The calculations are performed using free Scilab 6.0 software at varying input parameters such as current density, temperature and pressure. The developed model allows determination of polarization U/j characteristics, ohmic drop and energy efficiency of the compressor. It is validated using real experimental data from a laboratory prototype of electrochemical compressor in a single mode operation. The prototype system works with a membrane electrode assembly containing magnetron sputtered Pt catalysts on both electrodes ($0.25 \text{ mgPt}\cdot\text{cm}^{-2}$ loading) and Nafion 117 polymer electrolyte membrane. The model is further developed to predict the behavior of the compressor at high differential pressure and elevated temperature.

Keywords: Electrochemical hydrogen compressor, differential pressure, energy efficiency, temperature dependency, mathematical modeling

INTRODUCTION

Hydrogen economy is a rapidly growing industry, which is expected to contribute essentially in reducing the energy consumption and harmful air pollutions, as well as in stimulating the global economic growth. Hydrogen is a flexible energy carrier, capable to address the grid balancing issues and energy delivery in remote places. It is a sustainable alternative to fossil fuels, however, it suffers from a low volumetric energy density [1-3]. The most technically challenging barrier in regard to hydrogen economy is the development of safe, compact, and cost-effective hydrogen storage technology [4]. Hydrogen can be stored in a gaseous or liquid form, in metals, glass micro spheres, carbon nanotubes, etc. For efficient storage, each of the listed approaches requires medium to high pressure [5]. The electrochemical hydrogen compression (EHC) is highly efficient, low-maintenance and silent technology, considered as a potentially viable and cost-competitive alternative to the mechanical piston compression [6-8]. Over the time the EHC systems have been significantly improved in regard to energy efficiency, size, weight, level of compression, etc. The key element in these systems is the membrane electrode assembly where, in similarity to the PEM FC, the electrochemical conversion takes place [9-11]. The working principle of the EHC is presented schematically in Fig. 1.

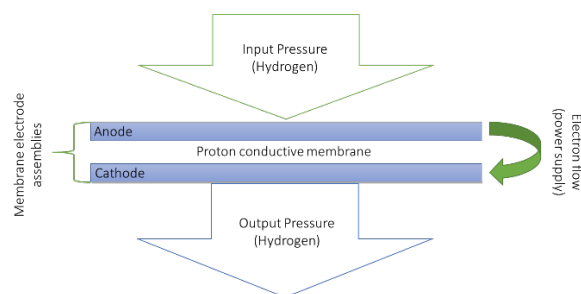
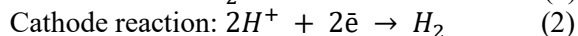
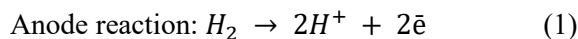


Fig. 1. Principle scheme of electrochemical hydrogen compressor in a single-mode operation.

The electrochemical hydrogen compression cell, in similarity to the fuel and electrolysis cell, consists of two chambers, one for each partial reaction. The hydrogen gas is delivered in the anode chamber of the system where the hydrogen molecules are split to protons and electrons (eq. 1). The protons move through the proton-conductive membrane to the cathode side where the reverse hydrogen evolution reaction takes place (eq. 2) and the obtained H_2 is accumulated and pressurized.



The total cell voltage U_{EHC} required for the overall process (eq. 3) is a sum of the Nernst potential, E_{Nernst} , the activation energy, E_{act} , and the ohmic losses, E_{ohmic} (eq. 4):

$$U_{EHC} = E_{Nernst} + E_{ohmic} + E_{act} \quad (4)$$

* To whom all correspondence should be sent.
E-mail: gal.rusev@iecs.bas.bg

Due to the low activation energy of the process the assumption in eq. 5 is accepted:

$$U_{EHC} = E_{Nernst} + E_{ohmic} \quad (5)$$

The Nernst potential, E_{Nernst} , is determined by eq. 6:

$$E_{Nernst} = E^0 + \frac{RT}{nF} \ln\left(\frac{a_{oxid}}{a_{red}}\right) \quad (6)$$

where R is the universal gas constant, T is the temperature, n - the number of electrons, F - the Faraday constant. In case of electrochemical hydrogen compression, the electrolyte is a solid proton conductive membrane and using eq. 7, eq. 6 is transformed in eq. 8:

$$\ln\left(\frac{a_{oxid}}{a_{red}}\right) = \ln\left(\frac{P_{an}}{P_{cath}}\right) \quad (7)$$

$$E_{Nernst} = E^0 + \frac{RT}{nF} \ln\left(\frac{P_{an}}{P_{cath}}\right) \quad (8)$$

where, P_{cath} is the output pressure of the compressor (at the cathode side) and P_{an} is the input pressure (at the anode side). The ohmic potential of a reversible electrochemical process with fast kinetics such as the one in (eq. 3) can be determined modeled by eq. 9:

$$E_{ohmic} = \left(\frac{\delta}{\sigma}\right) i \quad (9)$$

where, δ is the membrane thickness (cm), σ is the cell conductivity ($S \cdot cm^{-1}$), and i is the operating current density. The membrane conductivity is a function of the temperature and it is estimated using eq. 10:

$$\rho = 0.0007t + 0.0574 \quad (10)$$

where, t is temperature in °C. The differential pressure between both cell chambers is given by eq. 11:

$$P_{diff} = P_{cath} - P_{anode} \quad (11)$$

The most important operating parameter of the electrochemical hydrogen compression is the energy efficiency, also called voltage efficiency (eq. 12). It expresses the hydrogen conversion efficiency from which the electrical losses are subtracted.

$$E_{ef} = \frac{E_{Nernst}}{U_{EHC}} 100 \quad (12)$$

The operation at open-circuit voltage would yield 100% voltage efficiency. However, at open-circuit voltage no compression would be accomplished.

In this paper a simple modeling of an electrochemical hydrogen compressor is presented based on its working principle (Fig. 1), the corresponding electrochemical reactions (eqs. 1-3), the thermodynamic formulas (eqs. 4-8), and the assumptions (eqs. 9-12). The goal was to calculate the energy requirements of the electrochemical hydrogen conversion at different

input operating parameters. The results were validated using the experimental data from real tests performed in a laboratory prototype of electrochemical compressor in a single-mode of operation.

Mathematical model

The basic mathematical modeling was carried out using free Scilab 6.0 software. The eqs. 4-12 were applied as a programmable code directly in the Scinote part of the software. After validation, the obtained data were used to predict the behavior of the EHC at 2 operational regimes: *i*) regime “filter” (differential pressure 0 bar) which can be used to separate hydrogen from gaseous mixtures and obtain highly clean hydrogen; and *ii*) regime “hydrogen pump” (at 10 bars differential pressure) used for compression. The variables used in the developed model are summarized in Table 1:

Table 1. Nomenclature of variables

Symbol	Parameter	Dimension	Value
U_{EHC}	Cell voltage	[V]	-
E_{Nernst}	Nernst potential	[V]	-
E_{ohmic}	Ohmic potential	[V]	-
i	Current density	[A.cm ⁻²]	0-0.14
n	Number of electrons	-	2
F	Faraday constant	[C/mol]	96.485
R	Universal gas constant	[J K ⁻¹ mol ⁻¹]	8.314
T	Temperature	[K]	293 - 353
P_{anod}	Pressure in the anode chamber (input)	[Bar]	1
P_{cathod}	Pressure in the cathode chamber (output)	[Bar]	1-11
P_{diff}	Differential pressure	[Bar]	10
E_f	Voltage efficiency	%	-

EXPERIMENTAL

The developed mathematical model was validated using a laboratory developed electrochemical hydrogen compressor with a single membrane electrode assembly (MEA) capable to operate in the temperature range up to 120°C and pressure up to 160 bar. A picture of the device is presented in Fig. 2.

The membrane electrode assembly (MEA) is the active element of the device where the electrochemical reactions proceed (HOR at the anode and HER on the cathode). It also separates both chambers of the compressor. The geometric area of the MEA under study was 7 cm². The

polymer membrane used was a proton-conductive Nafion 117.



Fig. 2. Picture of the self-developed electrochemical hydrogen compressor.

Both electrodes had identical structure. The gas diffusion layer was a commercially available Freudenberg H2315 C2 covered by sputtered Pt catalytic film with loading of $0.25 \text{ mg}_{\text{Pt}} \cdot \text{cm}^{-2}$. The MEA preparation procedure was described in details elsewhere [12]. The input hydrogen was supplied from a bottle with precisely controlled output pressure in the range from 1 to 5 bars. The electrochemical performance was investigated using Potentiostat / galvanostat Gamry model 1010E.

RESULTS AND DISCUSSION

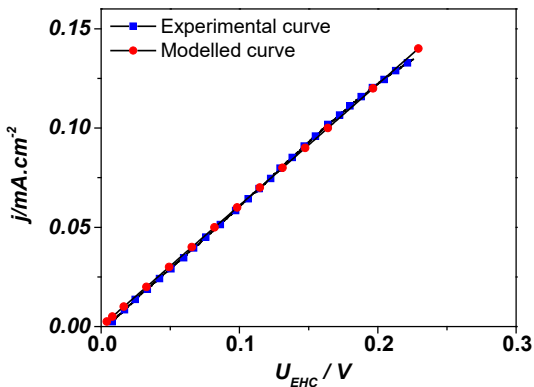


Fig. 3. Model and experimental voltampere characteristics of EHC at operating temperature 20°C and 0 bar differential pressure (regime “filter”); potential scan rate $1 \text{ mV} \cdot \text{s}^{-1}$.

The electrochemical performance of EHC is characterized by its voltampere characteristics (also called polarization curves and voltammograms) illustrating the dependency between the cell voltage and the density of the passing current at different operating conditions such as pressure, temperature, etc. Voltammograms gained from the mathematical

model and those obtained experimentally are compared in Fig. 3.

Both polarization curves show a linear increase of current density with the increasing cell voltage and identical slopes which evidences the feasibility of the developed model.

To predict the behavior of the EHC at higher temperatures and differential pressures, the model was further developed. In Fig. 4 are shown the obtained results at a differential pressure varying in the range 0 – 10 bar and temperature 20°C .

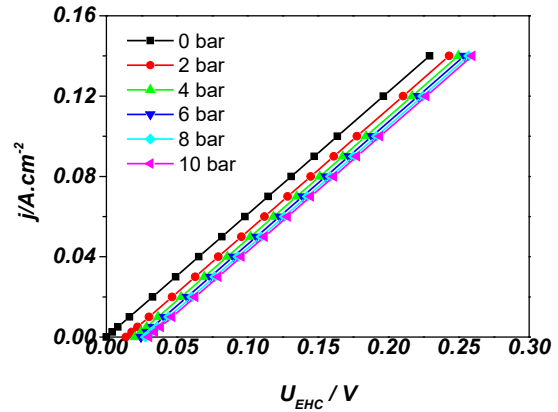


Fig. 4. Model voltampere characteristics of EHC at temperature 20°C and varying differential pressure in the range of 0 - 10 bars; potential scan rate $1 \text{ mV} \cdot \text{s}^{-1}$.

As already discussed, the differential pressure is the difference between the pressure in the cathode and anode chambers of the cell (eq. 11). According to the model, the varying differential pressure has several distinct effects on the EHC operating characteristics. First of all, as it is seen from the curves in Fig. 4, the increase of P_{diff} leads to a shift of the open circuit potential (U at $j = 0$) in positive direction. Secondly, with the increasing differential pressure all curves demonstrate linearity but the slope for each curve is slightly different and decreases with the increase of the pressure. Finally, the cell voltage at a given current density increases with the increasing P_{diff} . The higher differential pressure means higher concentration of hydrogen in the cathodic chamber of EHC which in turn, leads to transport limitations since the removal of hydrogen molecules produced on the cathode slows down. As a result, the HER overpotential and the cell voltage increase as well, meaning that more energy is required to convert hydrogen and thus, the efficiency of the EHC decreases.

Further simulations were performed to investigate the behavior of the system under varying operating temperature (up to 80°C) in both “filter” and “pump” regimes. The obtained results are presented in Figs. 5 and 6, respectively.

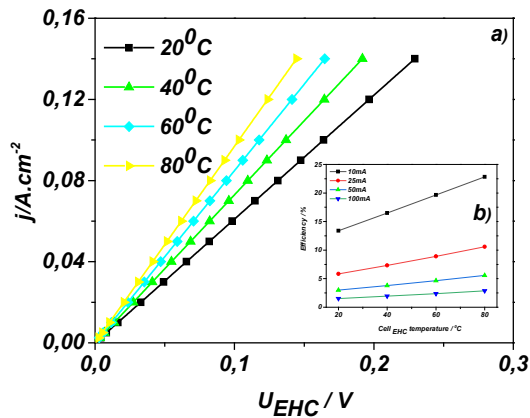


Fig. 5. Model voltampere characteristics in “filter” regime of EHC at varying temperature (a) and voltage efficiency at different current densities (b).

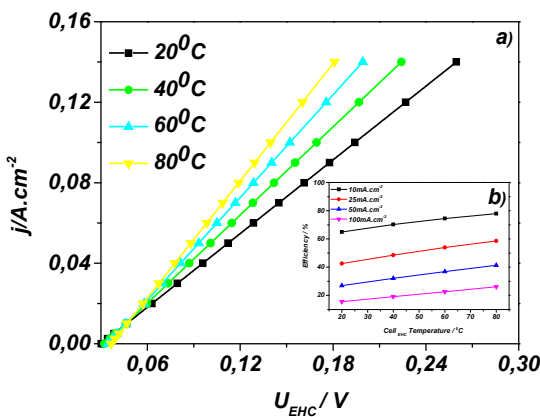


Fig. 6. Model voltampere characteristics in “hydrogen pump” regime of EHC at varying temperature (a) and voltage efficiency at different current densities (b).

At zero differential pressure (regime “filter”) the open circuit potential does not change with the increase of temperature, while the cell voltage essentially decreases. At a fixed current density of 140 mA.cm⁻² the decrease is with 40 mV per each 20°C. The voltage efficiency of EHC is also strongly temperature-dependent. The inset in Figure 5 shows the values of the efficiency calculated by eq. 12 at different current densities. It is seen that with the increasing temperature the EHC voltage efficiency increases, while the increase in the current density has an opposite effect. The highest efficiency value of 22% was calculated at 10 mA.cm⁻² and 80°C.

The calculations performed at differential pressure of up to 10 bar (regime “hydrogen pump”) demonstrate a similar behavior of the compressor. The cell voltage at 140 mA.cm⁻² drops with the increasing temperature with approximate 50-60 mV per each 20°C, the current density has the opposite effect, while the energy efficiency increases reaching a

maximum value of nearly 80% at 10 mA.cm⁻² and 80°C.

CONCLUSIONS

The developed mathematical model based on fundamental thermodynamics and electrochemical relationships describes the influence of different operating parameters of the electrochemical hydrogen compressor on its U/j characteristics and energy efficiency. The model was validated by real experimental data and applied to predict the working characteristics of the compressor in “filter” and “pump” regime at varying operative temperatures.

Acknowledgements: The authors acknowledge the support of the project BG05M2OP001-1.002-0014 „Center of competence HITMOBIL - Technologies and systems for generation, storage and consumption of clean energy”, funded by Operational Program “Science and education for smart growth” 2014-2020, co-funded by the EU from European Regional Development Fund as well as ‘Young Scientists and Postdoctoral candidates’, funded by the Ministry of Education and Science.

REFERENCES

1. P. Falcone, M. Sapio, *Current Opinion in Green and Sustainable Chemistry*, **31**, 100506 (2021).
2. L. Zhao, F. Xu, C. Zhang, Z. Wang, H. Ju, X. Gao, X. Zhang, L. Sun, Z. Liu, *Progress in Natural Science: Materials International*, **31**, 165 (2021).
3. Y. Kojima, *International Journal of Hydrogen Energy*, **44**, 18179 (2019).
4. S. Singla, N. Shetti, S. Basu, K. Mondal, T. Aminabhavi, *Journal of Environmental Management*, **302**, 113963 (2022).
5. A. Abdalla, S. Hossain, O. Nisfindy, A. Azad, M. Dawood, A. Azad, *Energy Conversion and Management*, **165**, 602 (2018).
6. G. Durmus, C. Colpan, Y. Devrim, *Journal of Power Sources*, **494**, 229743 (2021).
7. S. Toghyani, E. Afshari, E. Baniyadi, *Journal of Energy Storage*, **30**, 101469 (2020).
8. S. Toghyani, E. Baniyadi, E. Afshari, *International Journal of Hydrogen Energy*, **46**, 24271 (2021).
9. J. Zou, Y. Jin, Z. Wen, S. Xing, N. Han, K. Yao, Z. Zhao, M. Chen, J. Fan, H. Li, H. Wang, *Journal of Power Sources*, **484**, 229249 (2021).
10. A. Chouhan, B. Bahar, A. Prasad, *International Journal of Hydrogen Energy*, **45**, 10991 (2020).
11. S. Grigoriev, I. Shtatny, P. Millet, V. Poremsky, V. Fateev, *International Journal of Hydrogen Energy*, **36**, 4148 (2011).
12. E. Slavcheva, I. Radev, S. Bliznakov, G. Topalov, P. Andreev, E. Budevski, *Electrochimica Acta*, **52**, 3889 (2007).

Electrocatalytic activity of Ni- and Co-modified graphitized paper towards hydrogen evolution reaction in neutral electrolyte

E. Chorbadzhiyska^{1,2*}, G. Borisov³, D. Apostolova¹, E. Slavcheva³, M. Mitov^{1,2}, Y. Hubenova^{3,4}

¹Department of Chemistry, South-West University, Blagoevgrad, Bulgaria

²Innovative Centre for Eco Energy Technologies, South-West University "Neofit Rilski", Blagoevgrad, Bulgaria

³Institute of Electrochemistry and Energy Systems "Academician Evgeny Budevski", Bulgarian Academy of Sciences (IEES-BAS), Sofia, Bulgaria

⁴Department of Biochemistry and Microbiology, Plovdiv University, Plovdiv, Bulgaria

Received: March 08, 2022; Revised: May 05, 2022

The choice of highly effective cathode materials for microbial electrolysis cell (MEC) is the main challenge for the practical implementation of this innovative technology for hydrogen generation. In this study, nickel and cobalt catalysts, synthesized by direct selective grafting from acetylacetonate precursors, were deposited on graphitized paper with microspores sublayer (GP with MPL). The electrocatalytic activity of the produced modified electrodes towards hydrogen evolution reaction (HER) in neutral electrolyte was examined by linear voltammetry, chronoamperometry, and electrochemical impedance spectroscopy. Both types of modified materials exhibit much higher electrocatalytic activity towards HER than the unmodified graphitized paper. The highest electrocatalytic activity was achieved with 0.5 mg.cm⁻² loading of nickel and cobalt catalysts.

Keywords: Ni- and Co-modified graphitized paper; hydrogen evolution reaction, electrocatalytic activity, cathodes, microbial electrolysis cells.

INTRODUCTION

The opinion of most scientists is that the hydrogen will be the main energy source in the near future [1-4]. Currently, about 95% of the industrial hydrogen production worldwide is based on steam reforming of natural gas and other light hydrocarbons, partial oxidation of heavier hydrocarbons, and coal gasification, which is not perspective in terms of the recently proclaimed "circular" economy. In this regard, new alternative methods for hydrogen production have been intensively researched and developed in recent decades. One of the newest methods in this direction is the microbial electrolysis cell (MEC) - an electrochemical device that uses microorganisms to oxidize organic substrates at the anode and generate hydrogen at the cathode. The use of exoelectrogenic microorganisms requires mild experimental conditions such as neutral medium and ambient temperature [5].

The main challenge for the practical implementation of MEC for hydrogen production is the choice of effective cathode electrocatalysts with high electrocatalytic activity in neutral medium. Platinum is the best catalyst for the electrochemical generation of hydrogen by water electrolysis. It possesses high electrocatalytic activity and low hydrogen overpotential [6], but its high cost, scarcity and propensity to poisoning limit the wide

application in MEC [7]. The development of efficient and cost-effective cathodes as an alternative to Pt has provoked intensive research over the last decade. Partial replacement or reduction of the platinum load are among the main strategies applied [8-10]. Kye *et al.* [11] showed that Pt-Au electrocatalysts have a larger active surface area than Pt nanoparticles alone. Palladium, with its high electrical conductivity and excellent catalytic properties, is closest to platinum. Huang *et al.* [12] reported that deposited palladium nanoparticles on carbon cloth are 50 times more efficient than platinum catalyst. In our previous studies [13-15], it was established that the electrocatalytic activity of Pd-Au co-deposits for HER increases with the augmentation of the gold content. Nickel is widely used as electrode material in industry due to its low cost and good catalytic properties in highly advanced alkaline water electrolysis [16]. To enhance the catalytic activity of Ni-based materials, various methods have been applied, such as alloying with other metals, incorporation of particles, as well as production of electrodes with a well-developed, rough or porous surface. For example, the alloying of nickel with transition metals (Fe, Mo, W, Co), as well as with P significantly improves the catalytic activity for HER compared to that of the pure metals [17]. Selembo *et al.* [18] deposited nickel oxide on a thin layer of metal and thus obtained an effective cathode for MEC. Hu *et al.* [19] demonstrated

* To whom all correspondence should be sent.
E-mail: elli_e1@abv.bg

comparable MEC performances in terms of hydrogen production rate using NiMo and NiW catalysts electrodeposited on carbon cloth with those achieved with Pt cathodes. Investigating NiW and NiMo electrodeposited on Ni-foam as cathodes in MEC, Mitov *et al.* [20] achieved a hydrogen production rate in the range from $0.04 \div 0.14 \text{ m}^3(\text{H}_2) \text{ m}^{-3} \text{ d}^{-1}$ at an applied voltage of 0.6 V. Cobalt-based composites have also shown relatively high catalytic activity for HER [21] and other related reactions [22, 23] with practical importance.

Despite the high cathodic efficiency achieved with some of the materials studied in MEC, their productivity is still relatively low and has not been confirmed in large-scale reactors. This necessitates the creation and research of new highly efficient catalysts as one of the priority tasks for turning MEC into a technology of industrial importance.

In this study, nickel and cobalt catalysts dispersed over non-stoichiometric titanium oxides, synthesized by direct selective grafting from acetylacetonate precursors, were deposited on graphitized paper (GP) and the electrocatalytic activity of the produced modified electrodes towards HER in neutral electrolyte was examined. The results obtained with different electrodes were compared and discussed.

MATERIALS AND METHODS

Nickel and cobalt catalysts were synthesized from an acetylacetonate precursor ($\text{M}[(\text{C}_5\text{H}_7\text{O}_2)_n]_m$, $\text{M} = \text{Ni}, \text{Co}$) by direct selective grafting following the procedure previously described by Maksimova *et al.* [24]. Magneli-phase titanium sub-oxide (MPT) powder with particle size of 60 to 100 nm was used as a catalytic carrier for the samples. The metallic part in each of the catalysts was 40 wt.%, denoted Ni40/MPT and Co40/MPT. The prepared catalysts were deposited on round-shaped samples of graphitized paper (GP provided by Freudenberg, Germany (H2315)) with geometric area of 1.0 cm^2 by airbrush technique with purified air gas carrier. The catalytic loading of all developed electrodes varies in the range of 0.25 to $1 \text{ mg}\cdot\text{cm}^{-2}$. The modified electrodes were dried at room temperature for 6 h before electrochemical characterization.

The phase composition, surface morphology and structure of the catalysts were studied by scanning electron microscopy (SEM) and X-ray diffraction (XRD). The XRD patterns were recorded on a X-ray diffractometer Philips APD15 with $\text{Cu K}\alpha$ radiation at constant rate of 0.02° over an angle range $2\theta = 10 \div 90^\circ$.

The electrochemical performance of the produced electrodes in neutral phosphate buffer

solution (PBS) was investigated by linear voltammetry (LV), chronoamperometry (CA) and electrochemical impedance spectroscopy (EIS).

LV was performed with a scan rate of 0.01 V/s over the potential range from 0 to -2.0 V (*vs.* Ag/AgCl) in 67 mM PBS (pH 7.0). The evaluation of the performance was based on the voltage needed to initiate hydrogen production (V_e) and the slope (V_h) of the first linear region in the voltammogram.

Chronoamperometric measurements were carried out in the same electrolyte at -0.9 ; -1.0 and -1.2 V (*vs.* Ag/AgCl) for 10 min at each potential. The quantity of the produced hydrogen was calculated by integration of the areas under the obtained chronoamperograms and applying Faraday's law.

The EIS measurements were performed at applied AC with an amplitude of the signal of 0.01 V and $E_{dc} = -1.2 \text{ V}$ (*vs.* Ag/AgCl) in the frequency range from 100 kHz to 0.1 Hz.

All electrochemical experiments were carried out in a three-electrode cell with an electrolyte volume of 30 cm^3 by using a potentiostat-galvanostat AUTOLAB PGSTAT 204. The electrode samples were connected as a working electrode and a platinum wire was used as counter electrode, the potential was measured against Ag/AgCl (3.5 M KCl) reference electrode.

RESULTS AND DISCUSSION

The phase composition of the MPT support and of the monometallic catalysts was studied by XRD. The diffraction patterns are presented in Fig. 1. The reflections show that both Ni and Co are in the crystal state and the crystallographic orientation of Ni particles is mainly in (111) and (200), while the Co particles are in (100) and (002) crystallographic planes. The calculated crystallite average size by Sherrer equation [25] is 22 nm for Ni40/MPT and 26 nm for the Co40/MPT.

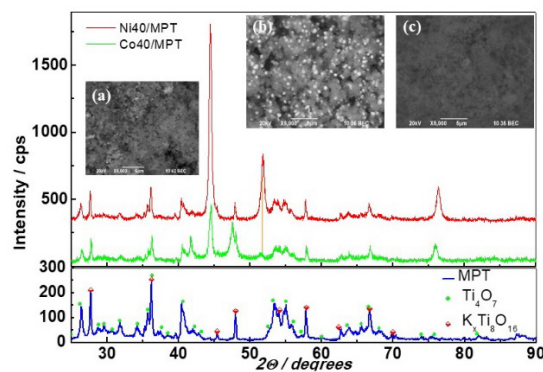


Fig. 1. XRD patterns of the MPT support and the Ni40/MPT and Co40/MPT catalysts; SEM images of the MPT (a) support, Co40/MPT (b), and Ni40/MPT (c).

In addition, the SEM images, presented in Fig. 1 b, c show fine dispersion of the catalytic particles over the whole surface of the support (a).

Linear voltammograms obtained with the newly produced Ni and Co modified GP with different loading of catalysts and non-modified GP are compared in Fig. 2. The LVs indicated that by sweeping the potential more negative than -0.3 V (vs. Ag/AgCl) for Ni modified materials and -0.6 V (vs. Ag/AgCl) for Co modified materials, respectively, the cathodic current for all modified GP electrodes gradually increased. The values of current density at -2.0 V (vs. Ag/AgCl) are given in Table 1. The obtained values are by an order of magnitude higher than those reported for PdAu electrodeposits [15] and those for NiFeCoP/carbon felt examined under the same conditions [26]. In addition, the estimated values of the voltage needed to initiate hydrogen production, V_e , and the slope in the voltammogram, V_h , which corresponds to the rate of the HER are also presented in Table 1. The minimum voltage needed to initiate substantial current (V_e) was in the range between -0.3 ÷ -0.7 V vs. Ag/AgCl (-0.1 ÷ -0.5 V vs. SHE) for all studied electrodes, which is comparable to that reported for Pt/carbon cloth in PBS [21]. The obtained results indicate that the bare GP possesses a higher overpotential ($V_e = -0.82$ V vs. Ag/AgCl) in respect to HER than the modified electrodes. V_e for Ni-modified electrodes is about two times lower than bare GP. The values of the V_h of the Ni modified materials are twice higher than GP and for the Co-modified materials – four times, respectively. The combination of lowest overpotential and highest hydrogen production rate determines 0.50 mg.cm⁻² Co/GP and 0.50 mg.cm⁻² Ni/GP as the best electrocatalysts for HER among all modified materials. Probably, the increasing of the catalyst loading on the GP clogs the electrode material and reduces its electrocatalytic properties.

A deeper insight into the electrochemical kinetics of the electrodes was obtained by electrochemical impedance spectroscopy (EIS). Nyquist plots of the graphitized paper and modified materials recorded at -1.2 V (vs. Ag/AgCl) are presented in Fig. 3. The obtained results show that the polarization resistance of all modified electrode materials is with an order of magnitude lower than that of the non-modified graphitized paper. The lowest polarization resistance for both types of catalysts is exhibited by the samples with catalytic loading of 0.5 mg.cm⁻², which explains their highest electrocatalytic activity.

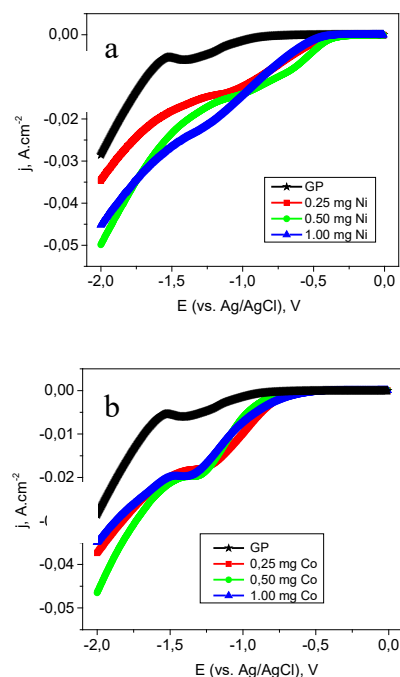


Fig. 2. Linear voltammetry obtained with non-modified GP and modified GP with: a) nickel catalyst/GP; b) cobalt catalyst/GP

Table 1. Summarized table of the estimated values of the voltage needed to initiate hydrogen production, V_e , and the slope in the voltammogram, V_h , which corresponds to the rate of HER.

Material	$j(-2.0V)$, A.cm ⁻²	V_e , V (vs. Ag/AgCl)	V_h , A/V
GP	0.029	-0.82	0.011
0.25 Ni	0.035	-0.35	0.020
0.50 Ni	0.050	-0.31	0.024
1.00 Ni	0.045	-0.40	0.027
0.25 Co	0.037	-0.65	0.032
0.50 Co	0.046	-0.67	0.041
1.00 Co	0.035	-0.57	0.028

Chronoamperograms obtained with non-modified GP and with the investigated materials at -1.2 V (vs. Ag/AgCl) in PBS are presented in Fig. 4 a, b.

The newly produced materials exhibit higher electrocatalytic activity than non-modified GP. The quantities of evolved hydrogen, estimated from chronoamperometric measurements, are compared in Fig. 3c. The hydrogen evolution rates achieved with modified materials are several times higher than those obtained with GP.

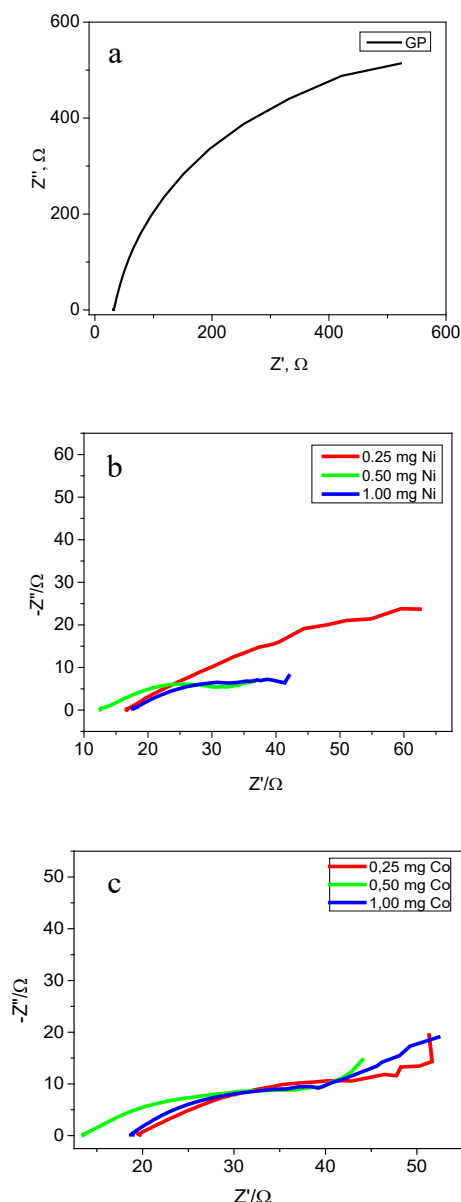


Fig. 3. Nyquist plots of the EIS of the: a) Graphitized paper; b) Nickel catalysts/GP; c) Cobalt catalyst/GP

CONCLUSIONS

Nickel and cobalt catalysts were deposited on graphitized paper (GP). The electrocatalytic activity of the newly synthesized materials towards HER was investigated in neutral phosphate buffer solution with respect to their potential application as cathodes in microbial electrolysis cells. Despite different catalyst loadings, the estimated current production rates indicate that the developed Ni- and Co-modified electrodes exhibit much higher electrocatalytic activity compared to the non-modified GP. The obtained electrochemical results determined as optimal the catalytic loading of 0.50 mg.cm⁻².

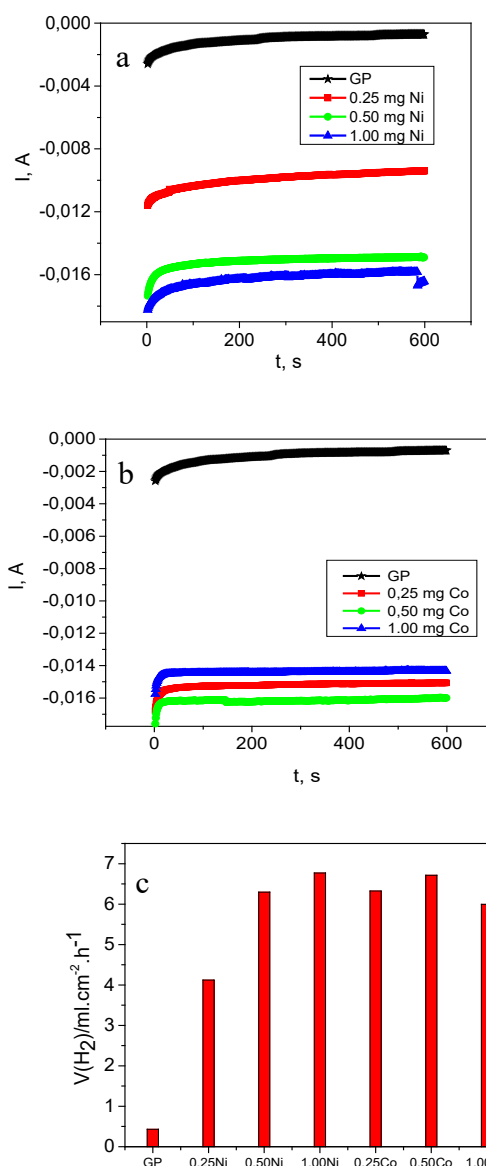


Fig. 4. Chronoamperometric curves obtained at a potential of -1.2V with investigated materials: a) Ni/GP; b) Co/GP; c) Quantity of the produced hydrogen, calculated by integration of areas under chronoamperometric curves obtained at a potential of -1.2V.

The highest current density of 0.05A.cm⁻² (at -2.0V vs. Ag/AgCl) was achieved with 0.50 mg Ni/GP. The obtained values of the quantities of the produced hydrogen, calculated by integration of areas under the chronoamperometric curves obtained at potential -1.2V (vs. Ag/AgCl), for the examined materials are ranged in 6.0 ÷ 6.8 ml.cm⁻².h⁻¹, except for 0.25 mg Ni/GP – 4.1 ml.cm⁻².h⁻¹. Further evaluation of the produced materials as cathodes in MEC is in progress.

Acknowledgements: This study was supported by the Bulgarian National Science Fund through contract KP-06-H29/8/2018. The authors kindly acknowledge the financial support to project BG05M2OP001-1.002-0014 Center of Competence HITMOBIL - Technologies and systems for generation, storage and consumption of clean energy, funded by Operational Programme "Science and Education or Smart Growth 2014-2020, co-funded by the EU from European Regional Development Fund.

REFERENCES

1. V. Goltsov, T. Veziroglu, *Int. J. Hydrogen Energy*, **26**, 909 (2001).
2. T. Veziroglu, *Int. J. Hydrogen Energy*, **27**, 715 (2002).
3. L. Barreto, A. Makihira, K. Riahi, *Int. J. Hydrogen Energy*, **28**, 267 (2003).
4. K. Chaea, M. Choia, J. Leea, F. Ajayia, S. Kim, *Int. J. Hydrogen Energy*, **33**, 5184 (2008).
5. L.D.S. Munoz, B. Erable, L. Etcheverry, J. Riess, R. Bass'eguy, *Electrochem. Commun.*, **12**, 183 (2010).
6. J. Ambler, B. Logan, *Int. J. Hydrogen Energy*, **36**, 160 (2011).
7. R. Rozendal, M. Hamelers, J. Molenkamp, N. Buisman, *Water Res.*, **41**, 1984 (2007).
8. J. Pettersson, B. Ramsey, D. Harrison, *J. Power Sources*, **157**, 28 (2006).
9. Y. Fan, E. Sharbrough, H. Liu, *Environ. Sci. Technol.*, **42**, 8101 (2008).
10. J. Kye, M. Shin, B. Lim, J. Jang, I. Oh, S. Hwang, *ACS Nano.*, **7**, 6017 (2013).
11. Y. Huang, X. Liu, X. Sun, G. Sheng, Y. Zhang, G. Yan, S. Wang, A. Xu, H. Yu, *Int. J. Hydrogen Energy*, **36**, 2773 (2011).
12. E. Chorbadzhiyska, M. Mitov, G. Hristov, N. Dimcheva, L. Nalbandian, A. Evdou, Y. Hubenova, *Int. J. of Electrochem.*, **2014**, 1 (2014).
13. E. Chorbadzhiyska, Y. Hubenova, G. Hristov, L. Nalbandian, M. Mitov, *Bulg. Chem. Commun.*, **47**, 1002 (2015).
14. E. Chorbadzhiyska, M. Mitov, L. Nalbandian, Y. Hubenova, *Int. J. Hydrogen Energy*, **40**, 7329 (2015).
15. S. De, J. Zhang, R. Luque, N. Yan, *Energy Environ. Sci.*, **9**, 3314 (2016).
- A. Chaurasia, P. Mondal, *Chemosphere*, **286**, 131728 (2022).
16. P. Selembo, M. Merrill, B. Logan, *J. Power Sources*, **190**, 271 (2009).
17. H. Hu, Y. Fan, H. Liu, *Int. J. Hydrogen Energy*, **35**, 3227 (2010).
18. M. Mitov, E. Chorbadzhiyska, L. Nalbandian, Y. Hubenova, *J. Power Sources*, **356**, 467 (2017).
19. Y. Zhang, M. Merrill, B. Logan, *Int. J. Hydrogen Energy*, **35**, 12020 (2010).
20. M. Mitov, R. Rashkov, N. Atanassov, A. Zielonka, *J. Mater. Sci.*, **42**, 3367 (2007).
21. M. Mitov, G. Hristov, E. Hristova, R. Rashkov, M. Arnaudova, A. Zielonka, *Environmental Chemistry Letters*, **7**, 249 (2009).
22. K. Maksimova, E. Lefterova, S. Atanasova – Vladimirova, E. Slavcheva, *Bulgarian Chemical Communications*, **48 B**, 85 (2016).
23. J. Langford, A. Wilson, *Journal of Applied Crystallography*, **11**, 102 (1978).
24. M. Mitov, E. Chorbadzhiyska, R. Rashkov, Y. Hubenova, *Int. J. Hydrogen Energy*, **37**, 16522 (2012).

BULGARIAN CHEMICAL COMMUNICATIONS

Instructions about Preparation of Manuscripts

General remarks: Manuscripts are submitted in English by e-mail or by mail (in duplicate). The text must be typed double-spaced, on A4 format paper using Times New Roman font size 12, normal character spacing. The manuscript should not exceed 15 pages (about 3500 words), including photographs, tables, drawings, formulae, etc. Authors are requested to use margins of 3 cm on all sides. For mail submission hard copies, made by a clearly legible duplication process, are requested. Manuscripts should be subdivided into labelled sections, e.g. **Introduction, Experimental, Results and Discussion**, etc.

The title page comprises headline, author's names and affiliations, abstract and key words.

Attention is drawn to the following:

a) **The title** of the manuscript should reflect concisely the purpose and findings of the work. Abbreviations, symbols, chemical formulas, references and footnotes should be avoided. If indispensable, abbreviations and formulas should be given in parentheses immediately after the respective full form.

b) **The author's** first and middle name initials, and family name in full should be given, followed by the address (or addresses) of the contributing laboratory (laboratories). **The affiliation** of the author(s) should be listed in detail (no abbreviations!). The author to whom correspondence and/or inquiries should be sent should be indicated by asterisk (*).

The abstract should be self-explanatory and intelligible without any references to the text and containing not more than 250 words. It should be followed by key words (not more than six).

References should be numbered sequentially in the order, in which they are cited in the text. The numbers in the text should be enclosed in brackets [2], [5, 6], [9–12], etc., set on the text line. References, typed with double spacing, are to be listed in numerical order on a separate sheet. All references are to be given in Latin letters. The names of the authors are given without inversion. Titles of journals must be abbreviated according to Chemical Abstracts and given in italics, the volume is typed in bold, the initial page is given and the year in parentheses. Attention is drawn to the following conventions:

a) The names of all authors of a certain publications should be given. The use of "*et al.*" in

the list of references is not acceptable.

b) Only the initials of the first and middle names should be given.

In the manuscripts, the reference to author(s) of cited works should be made without giving initials, e.g. "Bush and Smith [7] pioneered...". If the reference carries the names of three or more authors it should be quoted as "Bush *et al.* [7]", if Bush is the first author, or as "Bush and co-workers [7]", if Bush is the senior author.

Footnotes should be reduced to a minimum. Each footnote should be typed double-spaced at the bottom of the page, on which its subject is first mentioned.

Tables are numbered with Arabic numerals on the left-hand top. Each table should be referred to in the text. Column headings should be as short as possible but they must define units unambiguously. The units are to be separated from the preceding symbols by a comma or brackets.

Note: The following format should be used when figures, equations, etc. are referred to the text (followed by the respective numbers): Fig., Eqns., Table, Scheme.

Schemes and figures. Each manuscript (hard copy) should contain or be accompanied by the respective illustrative material as well as by the respective figure captions in a separate file (sheet). As far as presentation of units is concerned, SI units are to be used. However, some non-SI units are also acceptable, such as °C, ml, l, etc.

The author(s) name(s), the title of the manuscript, the number of drawings, photographs, diagrams, etc., should be written in black pencil on the back of the illustrative material (hard copies) in accordance with the list enclosed. Avoid using more than 6 (12 for reviews, respectively) figures in the manuscript. Since most of the illustrative materials are to be presented as 8-cm wide pictures, attention should be paid that all axis titles, numerals, legend(s) and texts are legible.

The authors are asked to submit **the final text** (after the manuscript has been accepted for publication) in electronic form either by e-mail or mail on a 3.5" diskette (CD) using a PC Word-processor. The main text, list of references, tables and figure captions should be saved in separate files (as *.rtf or *.doc) with clearly identifiable file names. It is essential that the name and version of

the word-processing program and the format of the text files is clearly indicated. It is recommended that the pictures are presented in *.tif, *.jpg, *.cdr or *.bmp format, the equations are written using "Equation Editor" and chemical reaction schemes are written using ISIS Draw or ChemDraw programme.

The authors are required to submit the final text with a list of three individuals and their e-mail addresses that can be considered by the Editors as potential reviewers. Please, note that the reviewers should be outside the authors' own institution or organization. The Editorial Board of the journal is not obliged to accept these proposals.

EXAMPLES FOR PRESENTATION OF REFERENCES

REFERENCES

1. D. S. Newsome, *Catal. Rev.–Sci. Eng.*, **21**, 275 (1980).
2. C.-H. Lin, C.-Y. Hsu, *J. Chem. Soc. Chem. Commun.*, 1479 (1992).
3. R. G. Parr, W. Yang, *Density Functional Theory of Atoms and Molecules*, Oxford Univ. Press, New York, 1989.
4. V. Ponec, G. C. Bond, *Catalysis by Metals and Alloys* (Stud. Surf. Sci. Catal., vol. 95), Elsevier, Amsterdam, 1995.
5. G. Kadinov, S. Todorova, A. Palazov, in: *New Frontiers in Catalysis* (Proc. 10th Int. Congr. Catal., Budapest, 1992), L. Guzzi, F. Solymosi, P. Tetenyi (eds.), Akademiai Kiado, Budapest, 1993, Part C, p. 2817.
6. G. L. C. Maire, F. Garin, in: *Catalysis. Science and Technology*, J. R. Anderson, M. Boudart (eds), vol. 6, Springer-Verlag, Berlin, 1984, p. 161.
7. D. Pocknell, *GB Patent 2 207 355* (1949).
8. G. Angelov, PhD Thesis, UCTM, Sofia, 2001.
9. JCPDS International Center for Diffraction Data, Power Diffraction File, Swarthmore, PA, 1991.
10. *CA* **127**, 184 762q (1998).
11. P. Hou, H. Wise, *J. Catal.*, in press.
12. M. Sinev, private communication.
13. <http://www.chemweb.com/alchem/articles/1051611477211.html>.

CONTENTS

*Ninth International Conference of FMNS (FMNS-2021) "Modern Trends in Science",
Blagoevgrad, Bulgaria, September 15-19, 2021*

<i>Editorial – FMNS-2021</i>	5
<i>Section Chemistry</i>	
<i>N. O. Appazov, B. M. Diyarova, B. M. Bazarbayev, B. Zh. Dzhiembaev, O. Lygina, Obtaining granular activated carbon using a binder gelatin in the joint processing of rice and oil waste</i>	9
<i>A. G. Chapkanov, T. G. Dzimbova, Factors influencing the tautomeric form stabilization and spectral characteristics of 1-phenyl substituted pyrazol-5-ones</i>	13
<i>T. Dzimbova, A. Chapkanov, Combined action of His-Leu analogues on angiotensin converting enzyme (ACE) and angiotensin receptor (AR)</i>	18
<i>Ch. Girginov, St. Kozhukharov, B. Tzaneva, Durability of porous anodic alumina layers on AA1050 modified by incorporation of Cu, Ni and Cu/Ni</i>	21
<i>S. Minkova, I. Vlaeva, Kr. Nikolova, N. Petkova, G. Gentscheva, Ch. Tzvetkova, Assessment of the elemental composition, antioxidant activity, and optical properties of non-traditional Bulgarian fruit wines</i>	26
<i>A. Aleksandrova, M. Matrakova, P. Nikolov, Influence of electrolyte additives on the performance of the positive plates of lead batteries</i>	31
<i>Chr. B. Boyadjiev, P. G. Popova-Krumova, B. Chr. Boyadjiev, Absorption-adsorption method for waste-free decontamination of gases from SO₂</i>	37
<i>Section Physics</i>	
<i>A. V. Grigorov, T. Yovcheva, I. Iliev, I. Vlaeva, A. Viraneva, Impact of physical and chemical modification on the immobilization of β-galactosidase in poly-lactic acid multilayer structures</i>	47
<i>N. A. Ispulov, A. Zh. Zhumabekov, K. R. Dossumbekov, A. K. Bektazinova, On matrices of coefficients of electromagnetic and elastic waves propagating in anisotropic media</i>	53
<i>R. K. Kasarov, S. N. Kasarova, N. G. Sultanova, Material and optomechanical characteristics of polymers in optical design</i>	58
<i>S. Milenkova, B. Pilicheva, N. Zahariev, B. Shivachev, R. Ivanov Rusev, T. Yovcheva, M. Marudova, Milk protein-based formulations as controlled delivery systems for tolfenamic acid</i>	64
<i>A. Stoyanova-Ivanova, S. Kolev, V. Petrova, O. Petkov, L. M. Tran, M. Babij, A. Zaleski, V. Mikli, D. Kovacheva, Physicochemical study of bulk Dy-123 doped with nano-Fe₃O₄</i>	71
<i>N. Shuyushbayeva, A. Kaliyeva, N. Tanasheva, G. Altayeva, M. Talpakova Opportunities of ecologization of physics course</i>	77
<i>R. Stanoeva, A. A. Zaitsev, P. I. Zarubin, Possibility of measuring the angular characteristics of the primary and secondary tracks of relativistic nuclear fragmentation by the nuclear track emulsion method</i>	81
<i>Section Technical Sciences</i>	
<i>F. I. Sapundzhi, M. D. Mladenov, An Android-based mobile application giving information for weather in real-time</i>	89
<i>F. I. Sapundzhi, Home automation based on Z-wave technology</i>	92
<i>F. I. Sapundzhi, T. A. Dzimbova, The importance of biological databases in modeling of structure-activity relationship</i>	97
<i>M. Zafirova, D. Kaloshev, Organizational-technological aspects in the construction of construction sites</i>	103
<i>Section Methodology of Education</i>	
<i>G. Kalpachka, V. Kalpachki, Multimedia technologies in physics teaching</i>	111
<i>K. Ilchev, I. Kotseva, Investigation of instructional practices in high-school atomic and subatomic physics</i>	116
<i>G. Malchev, Application of the project method in physics education in classes with intensive studying of English</i>	124

Special session Low-carbon energy for transport and household

<i>G. Borisov, N. Borisov, E. Slavcheva, Basic mathematical modeling and experimental validation of electrochemical hydrogen compressor.....</i>	133
<i>E. Chorbadzhiyska, G. Borisov, D. Apostolova, E. Slavcheva, M. Mitov, Y. Hubenova, Electrocatalytic activity of Ni- and Co-modified graphitized paper towards hydrogen evolution reaction in neutral electrolyte.....</i>	137
<i>INSTRUCTIONS TO AUTHORS.....</i>	143